UNIVERSITÀ DEGLI STUDI DI PAVIA

DOTTORATO IN SCIENZE CHIMICHE E FARMACEUTICHE E INNOVAZIONE INDUSTRIALE
(XXXVI Ciclo)

Coordinatore: Chiar.mo Prof. Giorgio Colombo

Novel approaches toward sp^2-sp^3 medicinal chemistry relevant scaffolds

Tesi di Dottorato di
Eugenio Roà

AA 2022/2023

Tutor
Chiar.mo Prof. David Sarlah

Table of contents:

0.0.0.0 - Preface

0.1.0.0 - Preface

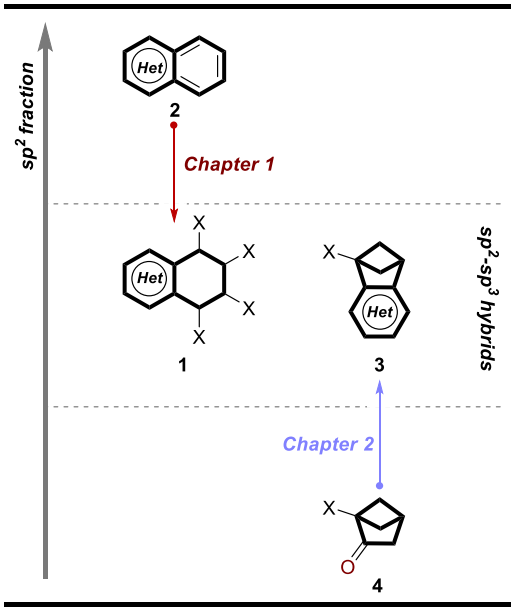

Scheme 1. Two approaches to sp2-sp3 hybrids of biological active small molecules: Chapter 1: Dearomative approach to (amino)cyclitols. The dearomatization decrease the sp^2-fraction of polyarenes. Chapter 2: Synthesis of (hetero)aromatics-bicyclo[2.1.1]hexanes building blocks. The aromatization of (hetero)aromatics increases the sp2-fraction of the saturated bicyclic motif.

In recent years, sp^2-sp^3 hybrids are emerging as medicinal chemistry relevant building blocks.[1–3] In this thesis two different strategies to reach sp^2-sp^3 hybrids will be discussed. In **Chapter 1** the development of a dearomative platform for the synthesis of (amino)cyclitols-aryls sp^2-sp^3 hybrids (**1**) will be illustrated. This approach allows to reduce the sp^2-fraction of polynuclear aryls and (hetero)aryls (**2**), setting the desired cyclohexanes rings. In **Chapter 2** a series of (hetero)aryls-bicyclo[2.1.1]hexanes sp^2-sp^3 hybrids (**3**) have been developed increasing the sp^2-fraction of bicyclic ketones (**4**). Both the chapters are divided in an introduction focused on synthetic chemistry, a discussion of the main results with the conclusions, and a detailed experimental section.

0.2.0.0 - References:

(1) Tomohiro, D.; Hiroki, Y.; Takahiro, N. α, β-UNSATURATED AMIDE COMPOUND, December 27, 2018. https://patentscope.wipo.int/search/en/detail.jsf?docId=WO2018235926 (accessed 2023-08-12).

(2) Janda, K. D.; Dickerson, T. J. Nicotine Immunoconjugates. WO2009120954A2, October 1, 2009. https://patents.google.com/patent/WO2009120954A2/en/en17 (accessed 2023-08-12).

(3) Graceffa, R.; Kaller, M.; La, D.; Lopez, P.; Patel, V. F.; Zhong, W. Substituted Pyrano [2,3-b] Pyridinamine Compounds as Beta-Secretase Modulators and Methods of Use. US20100120774A1, May 13, 2010. https://patents.google.com/patent/US20100120774/en (accessed 2023-08-12).

1.0.0.0 - Chapter 1: Diversification of Simple Arenes into Complex (Amino)cyclitols

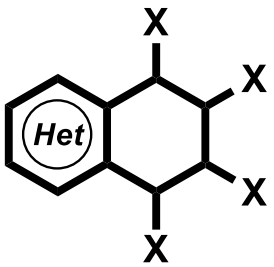

1.1.0.0 - Introduction

1.1.1.0 - Classic dearomatizations

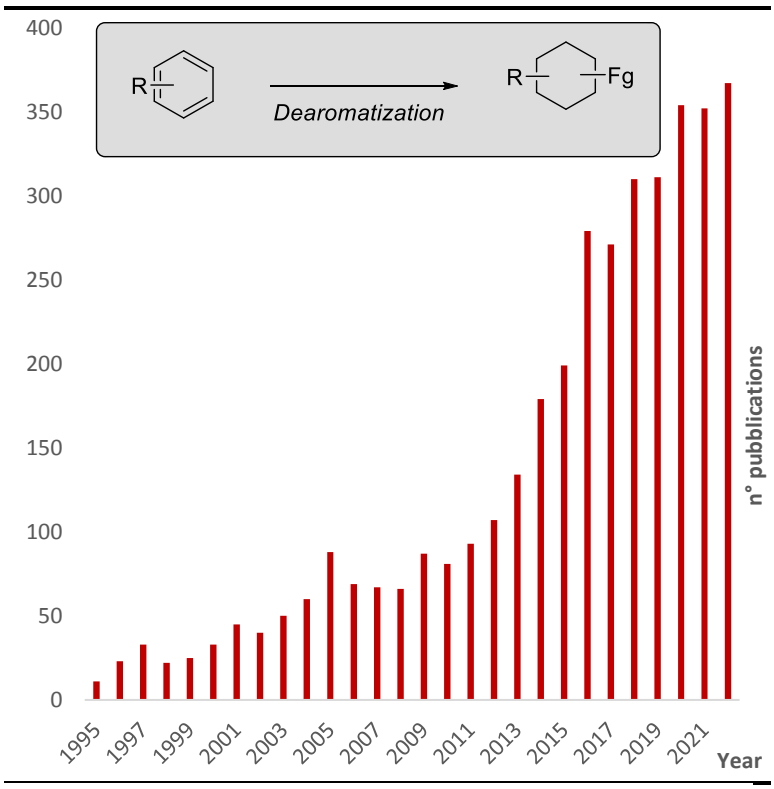

Figure 1. Number of publications containing the term "dearomatization'' in the abstract in the time frame between 1995 and 2022 (source SciFinde^{n}).

It is estimated that the petrochemical and coal industries produce around 100 million tons of aromatic compounds every year, most of which are employed in the production of polymers, solvents, and fuels contributing to the modern lifestyle. Their stability and their abundance make the arenes one of the most inexpensive, handy, and ready-to-use sources of carbon available for the organic chemists.[1]

The electronic stabilization that characterizes this class of compounds gives them extraordinary stability over a wide range of reaction conditions, yet also features them with a chemistry orthogonal to the reactivity of most of the functional groups. Not surprisingly, the reactivity of arenes has been well studied in the past centuries.[1,2] The dearomatizations are reactions which are able to remove the aromaticity of

arenes getting aliphatic compounds characterized by high C-sp^3 content, often desired in biologically active compounds,[3] and a completely different chemistry.[4] As shown in **Figure 1** the number of publications that use the term "dearomatization" in

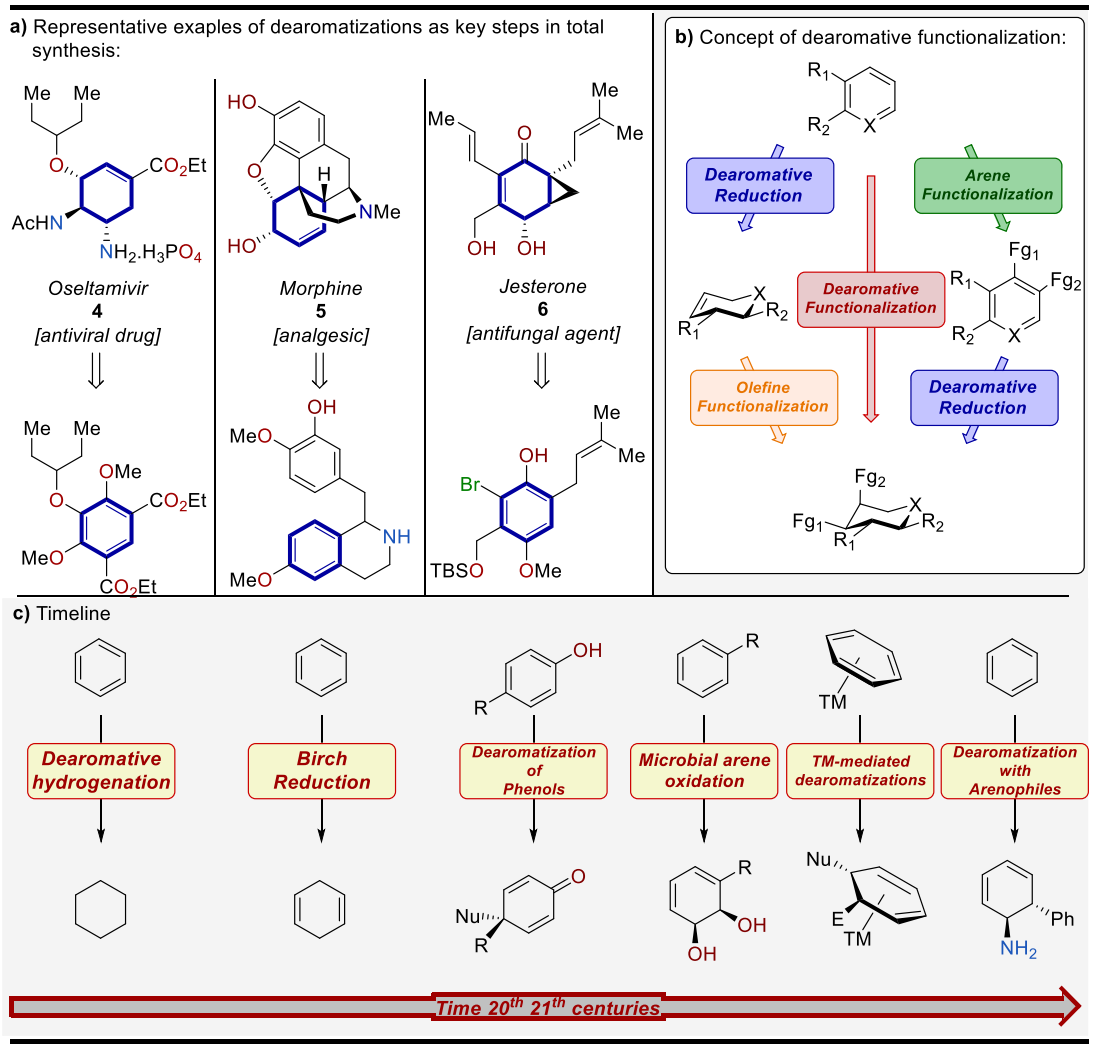

Scheme 2. a) Selected examples of dearomatizations applied in total synthesis. **b)** Concept of dearomative functionalization. **c)** Timeline in the development of dearomative technologies.

their abstract constantly increased in the timeframe between 1995 and 2022 as the interest in these powerful transformations.

Historically, these processes had a great impact on the discipline of organic synthesis (**Scheme 2**).[4] Between the most common and first discovered dearomatization we can name the dearomative hydrogenations, one of the most useful synthetic tools, applied in the synthesis of several bioactive compounds such as the antiviral drug Oseltamivir **4**. Another dearomative transformation is the metal-dissolved Birch reduction, which involves a single electron reduction and is employed in several synthesis including the well-known analgesic Morphine **5**. The oxidative dearomatization of phenols is a well-established transformation, widely applied in synthesis as in the antifungal Jesterone **6**. More modern methods often employ microbial arene oxidations, transition metals mediated dearomatizations, and arenophiles to get intermediates of significant synthetic value. These methodologies are having a great impact on the discipline of organic synthesis, giving access to new disconnections (**Scheme 2c**). A limitation of the classical dearomative transformations is the lack of functional groups introduced, often added before the dearomatization exploiting the arene chemistry, or on the dearomatized building blocks employing, for example, olefine functionalizations (**Scheme 2b**). An ideal transformation would remove the aromaticity and simultaneously introduce new functional groups, increasing the complexity of the chemical species accessible. Transformations like these are called: “Dearomative functionalizations” and had proved to be a demanding task for organic chemists. Functionalized products with a desirable degree of complexity are often obtained using stoichiometric amounts of

transition-metal complexes of Os, Ru, Re, Cr, and Mn. However, this approach raises concerns about the toxicity of these metals, where an alternative option is represented by the arenophile dearomatizations.

1.1.2.0 - Disconnection guidelines in dearomative chemistry

Recently, a review that covers the applications of the dearomative logic in total synthesis has been published by Huck *et al.*[4] This detailed work takes into account the years between 2011 and 2022, and collects more than 400 articles. The authors divide the dearomative strategies adopted into four categories (**Scheme 3**):

1. **Transform-based:** The dearomatization can be used as a simplifying transformation, as in the case when the reaction is associated with a C-C or C-X bond disconnection or with the introduction of functional groups that can be used to increase the system's complexity. Two examples of this strategy are found in the synthesis of α-cedrene **7** by Wender *et al.*[5] where a *meta*-photocycloaddition is used to greatly simplify the synthetic approach and in the synthesis of Penicillone A **8** by Liao *et al.*[6] where an oxidative phenol dearomatization is used to introduce a cyclohexanone, exploited to reach the target molecule.
2. **Structure goal strategy:** Densely functionalized tridimensional structures can be traced back to simple planar aromatic structures by dearomatization. A well-explanatory example of this strategy is offered by the synthesis of

Sertraline **9** reported by Sarlah group,[7] here the desired functionalities have been set on the cheap and readily available naphthalene through a dearomative *syn*-1,4-carbammination.

3. **Topological guided analysis:** In the case of complex caged and polycyclic molecules, network analysis often suggests strategic disconnections. In this context, dearomatizations can furnish unique transformations, leading to greatly simplified cycles. Sarpong's synthesis of Arcutinidine **10** serves to illustrate this approach.[8]

4. **Stereochemical based:** Dearomatizations can offer a way to establish both relative and absolute stereochemistry. The former has been well exploited in the hydrogenation of poly substituted benzenes obtaining all *cis* cyclohexanes, while a good example of the latter is furnished by the Lewis' synthesis of Zelenol **11** where the absolute stereochemistry was introduced with microbial arene oxidation.[9]

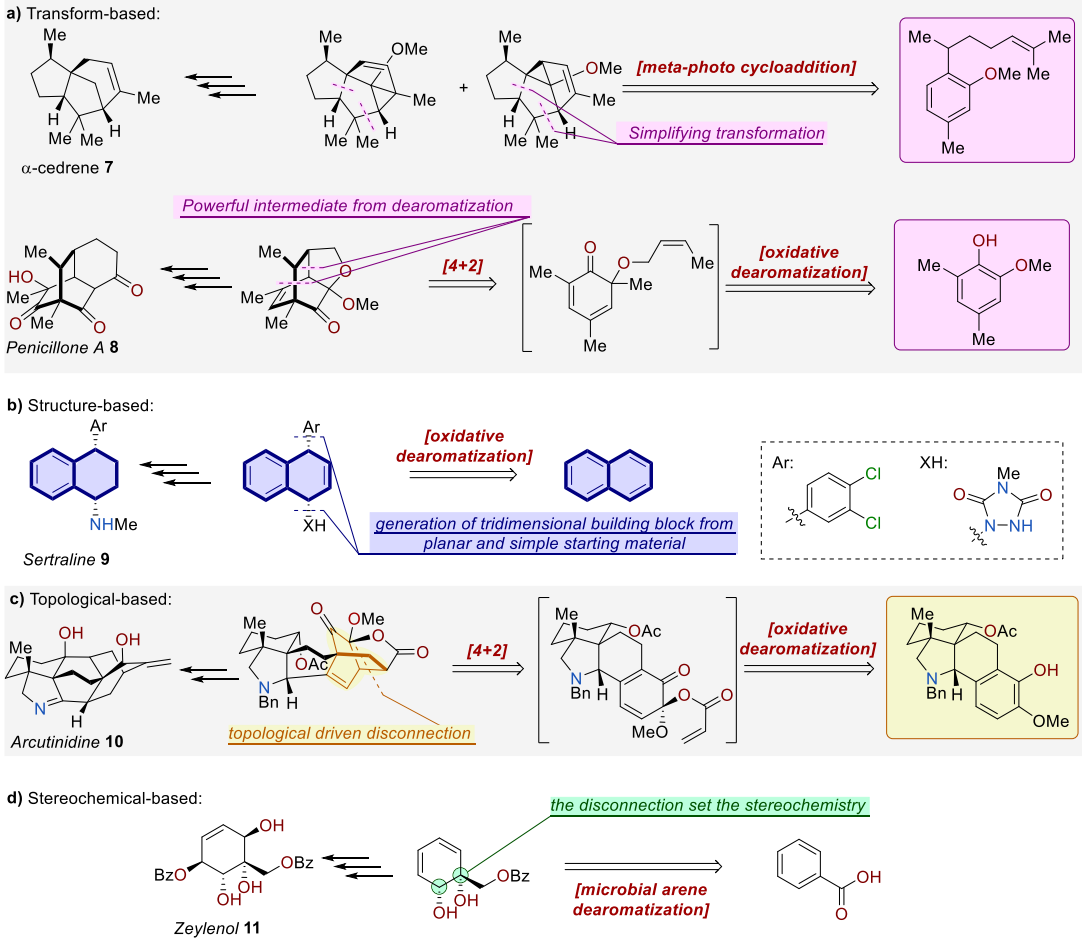

Scheme 3. Selected examples of application of dearomative logic in natural products synthesis **a)** transform-based approach, **b)** Structure-based approach, **c)** Topological-based approach, and **d)** Stereochemical-based approach.

In general, the dearomative synthetic strategies can be divided into three phases (**Scheme 4**).[4] The first phase includes all the post dearomative transformations that can produce a fully or partially dearomatized intermedium. Here, the aliphatic and olefinic chemistry can be used to pursue synthetically strategic C-C and C-X disconnections. The second stage is the dearomatization itself, where several dearomative processes are possible depending on the retron generated in the first phase. For the nature of the dearomative chemistry, this phase bridges the gap

between the aliphatic chemistry to the aromatic chemistry, tracing back a more saturated intermediate to an aromatic retron. In the third phase, aromatic chemistry can be used for those disconnections that are difficult for aliphatic compounds but accessible for the arenes. As a result, aliphatic and aromatic chemistries are interconnected by dearomatization, benefitting the retrosynthetic analysis.

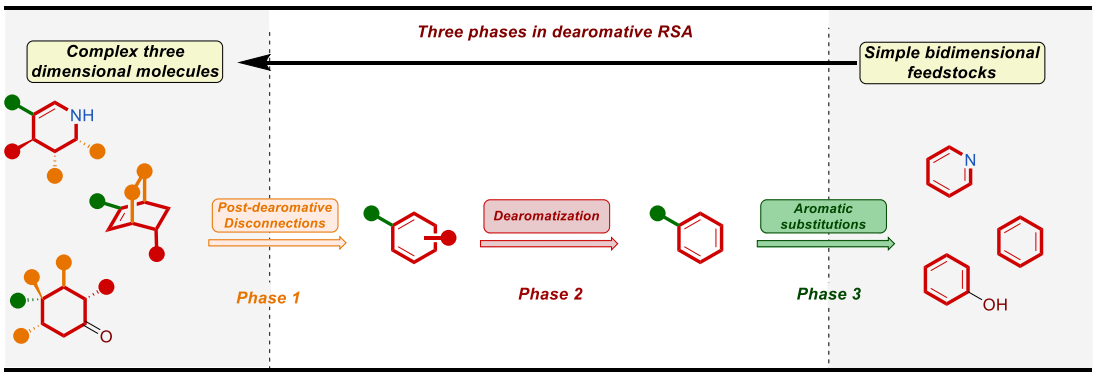

Scheme 4. Dearomative retrosynthetic logic in three phases.

1.1.3.0 - Arenophile-mediated dearomatizations

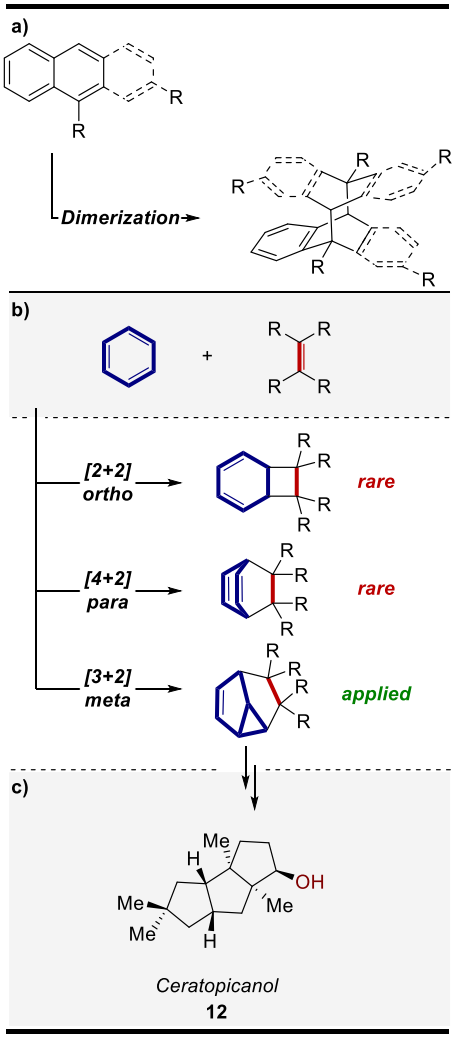

Scheme 5. Cycloadditions allows from the photoexcitation of arenes, **a)** dimerization of polyaromatics, **b)** alkene-arene photocycloadditions, **c)** application of the alkene-arene meta-photocycloaddition in the total synthesis of Cerapicanol **12**.

Aromatic compounds are known for their inertness; nevertheless, remarkable reactivity can arise from their photoexcitation, allowing for cycloadditions and dimerizations.[1,4,10] This reactivity is accessed by using energetic UV lamps that excite the relatively high π,π^*- singlet state of the arenes. Two examples are the dimerization of polyaromatics (**Scheme 5a**)[11–17] and the alkene-arene *meta*-photocycloaddition(**Scheme 5b**),[18,19] that has been widely documented and employed in several syntheses, such as in the synthesis of Ceratopicanol **12** (**Scheme 5c**).[20] The *ortho*- and the *para*-photocycloadditions are possible, but they are relatively rare and have few application, often confined to academic curiosity (**Scheme 5b**).[2] A conceptually similar *para*-cycloaddition is possible between arenes and small molecules named arenophiles. The arenophiles react with arene in a cycloaddition producing a cycloadduct characterized by the presence of olefines, amenable to further derivatizations (**Scheme 6**). This powerful transformation represents a

relatively new field and had caught the attention of our group. In 1984 Sheridan and coworkers report a light promoted cycloaddition between naphthalene **13** and N-

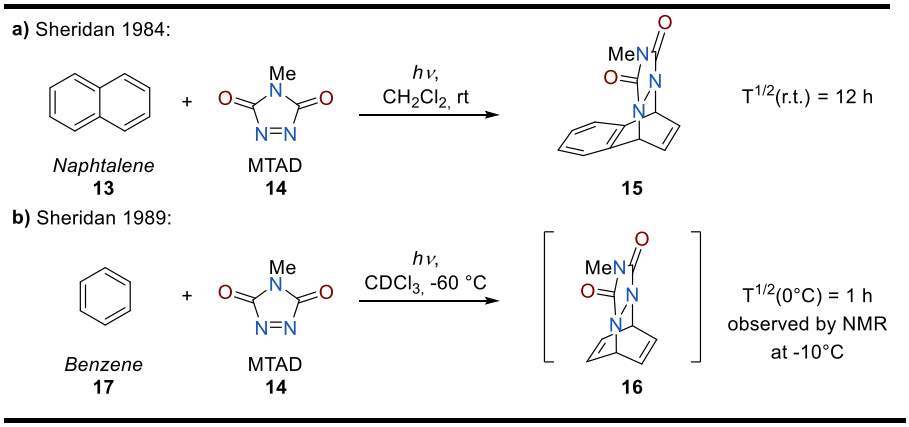

Scheme 6. Earlier experiments reported by Sheridan *et al.*[21,22] in MTAD-mediated dearomative chemistry, **a)** dearomatization of naphthalene **13**. **b)** dearomatization of benzene **16**.

methyl-1,2,4-triazoline-3,5-dione (MTAD, **14**) obtaining a dearomatized naphthalene-MTAD *para*-cycloadduct **15**.[21] The bicyclic compound was isolated with a good yield (40%) resulting in relatively stable with a half-life of 12 hours at room temperature. Typically, the cycloadducts between MTAD and monoaromatics are much less stable. However, despite this, the same group was able to observe the formation of the benzene-MTAD cycloadduct **16** using low-temperature NMR a few years later.[22] The half-life of this cycloadduct was calculated to be 1 hour at 0 °C, its instability impedes the isolation but not the possibility of reacting it. Up to that time, MTAD **14** was known and studied in thermal cycloadditions.[23] In the years after Sheridan tried to elucidate the mechanism of this transformation with Quantum data yields experiments[24,25]. These studies indicate that both the singlet and the triplet states of MTAD can undergo photoaddition with benzene **17** and naphthalene **13**.

The authors also suggest that the mechanism is most likely concerted. The thermodynamics of the process is different for benzene **17** and naphthalene **13**: in fact, the electron transfer between singlet excited MTAD **14** (^{1}MTAD*) and naphthalene **13** is an exergonic process, while the same process with benzene **17** is endergonic. This suggests that there may be different mechanisms for mononuclear arenes and polynuclear arenes. Later, Breton and coworkers conducted a series of reports to investigate the reversible cycloaddition between MTAD and several naphthalene.[26] Although the mechanism of this cycloaddition remains ambiguous, the most reliable mechanistic hypothesis, based on these reports,[24–26] includes a light-induced electron transfer or a charge transfer (**Scheme 7a**). These paths pass respectively through an excited charge-separated intimate ion radical pair (Exciplex I) or a three-electron stabilize exciplex (Exciplex II) (**Scheme 7a**), both of which are prone to formal cycloadditions. In the first case (estimated by the Rehm-Weller model, **Scheme 7b**),[27] the arenophile is the only specie excited by the visible radiation in virtue of its narrower LUMO-HOMO gap. The excited arenophile forms the Exciplex I by transferring an electron from the higher-energy HOMO of the arene, to the SOMO of the arenophile. The exciplex, therefore, collapses in the arene-arenophile adduct. A restrictive mechanistic requirement for the electron transfer pathway is that the HOMO of the arene is within the HOMO-LUMO range of the arenophile (**Scheme 7b**). In order to identify other possible arenophiles, our group had performed a frontier molecular orbital analysis of several arenophile candidates using

benzene **17** (HOMO = -9.9 eV) and naphthalene **13** (HOMO = -8.4 eV) as arenes benchmarks.[10]

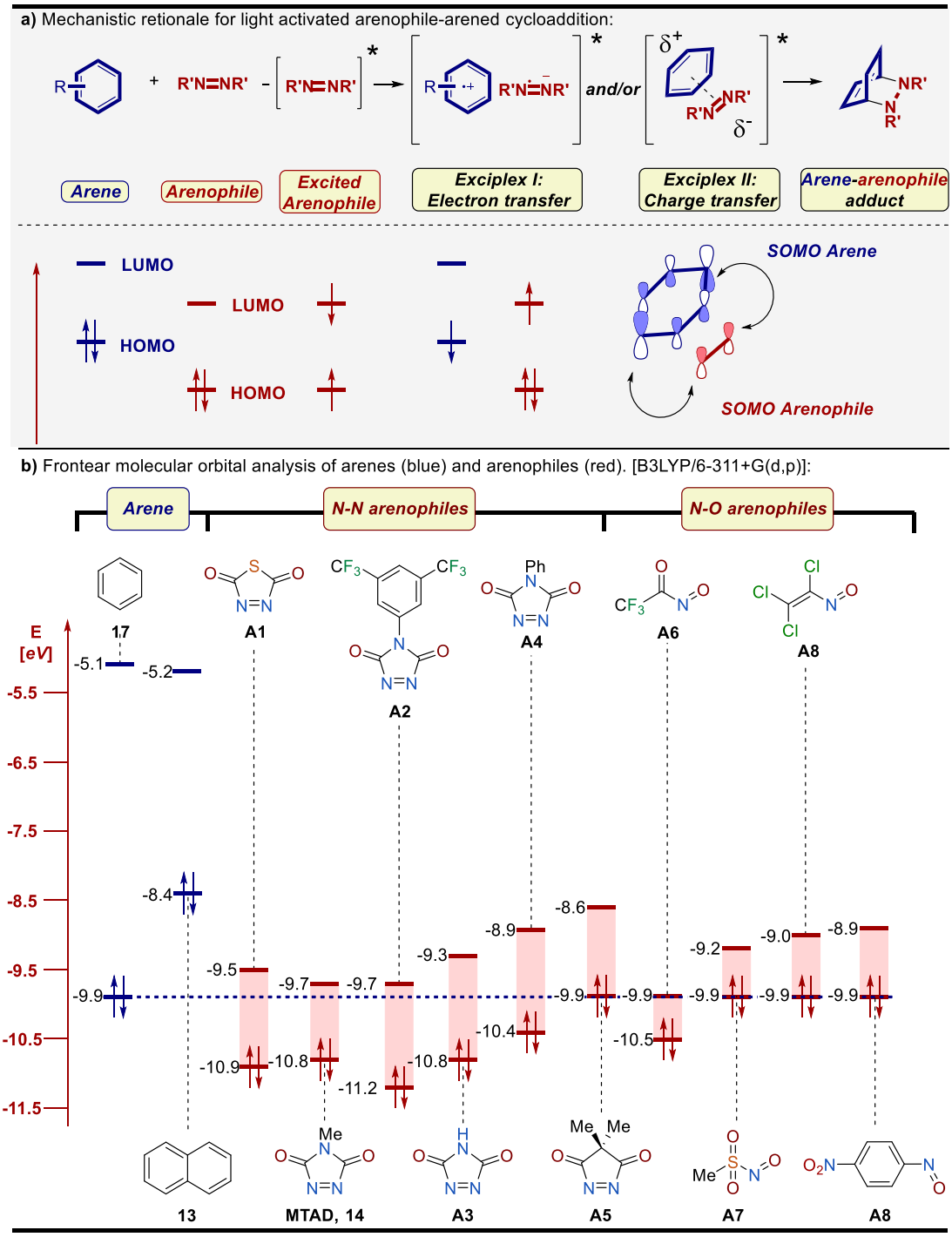

Scheme 7. a) Mechanistic hypothesis, **b)** Computational-assisted discovery of arenophiles by comparison of the frontier molecular orbitals energies of arenophiles and arenes.

The HOMO and LUMO of a series of N-N arenophiles and N-O arenophiles have been calculated and compared with the arenes HOMOs. In **Scheme 7b** several 1,2,4-triazoline-3,5-diones and symmetric cyclic (Z)-diazo-compounds containing electron deficient groups that match the desired electronic properties for reacting with benzene are reported (**A1**, **A2**, **A3** and **A6**); those compounds could be an alternative to MTAD **14**. From the computational study, it also emerges that several electron deficient nitroso compounds (**A6**, **A7**, **A8** and **A9**) meet the desired electronic criteria. Those compounds could give access to 1,4-*syn*-hydroxyamination dearomatized equivalents. A second hypothesis considers the formation of a charge transfer complex. Even this path has shown to be productive for the formation of the cycloadduct, as proven by the decreasing E_{CT}(MTAD) (energies of the charge absorption bands between MTAD and benzenes derivatives) with decreasing E_{pa} (peak potential determined by cyclic voltammetry).[25,27]

Our research group has a long-standing experience in the development of MTAD-based dearomative methods. We have experienced four practical observations (**Scheme 8**): 1) The MTAD **14** solutions are characterized by a strong pink coloration that disappears when MTAD **14** is completely consumed. Therefore, the conversion of MTAD can be monitored colorimetrically.

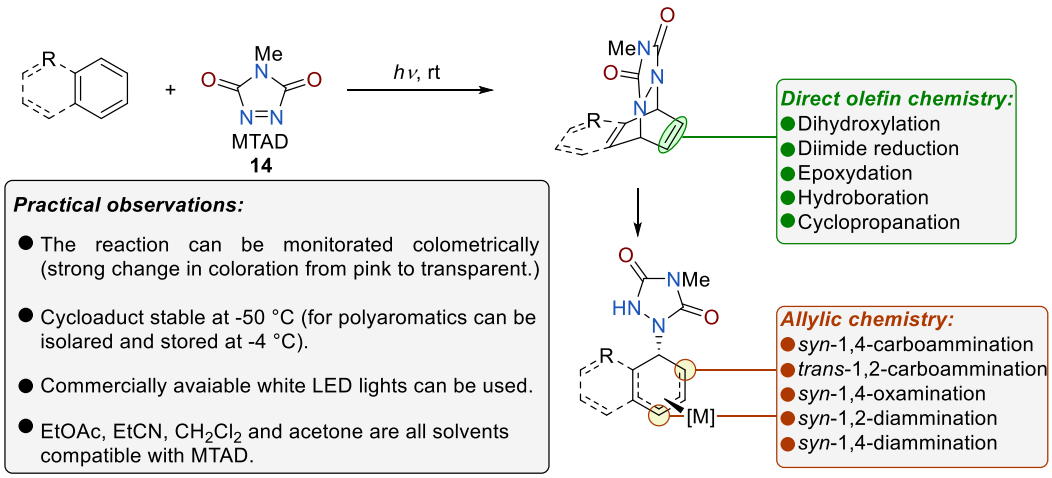

Scheme 8. Classification of the dearomative methodologies developed by our group divided in those that exploit the olefinic chemistry (green box) and those that rely on allylic chemistry (brown box). Important practical observations are grouped in the grey box.

2) Despite the original paper by Sheridan reporting the MTAD-arenes cycloadducts as stable at -10 °C, in our experience, they slowly undergo cycloreversion to MTAD **14** and benzene **17** at temperatures between -40 °C and -30 °C. For temperatures higher than -20 °C the *retro* [4+2] process is rapid. The stability of the MTAD-polyaromatics cycloadducts is much higher and they can be purified by chromatography and stored at -4 °C even for months. 3) Commercially available white LEDs lights are strong enough to quantitatively dearomatize and produce the cycloadducts in a few hours on a small scale and in a few days on a gram scale. 4) A variety of solvents is compatible with MTAD **14** chemistry, including dichloromethane, ethyl acetate, propionitrile, and acetone.

The cold solutions of MATD-arene cycloadducts are stable enough to be synthetically useful, obtaining bench-stable products. Several methodologies have been developed and classified into two classes (**Scheme 8**).[7,10,28–35]

1. Methodologies that directly exploit the olefine chemistry intercepting the newly formed double bond. This class includes reactions such as dearomative dihydroxylation, diimide reduction, epoxidation, hydroboration, and cyclopropanation.
2. Methodologies that are based on allylic substitution, where the allylic N-C bond is cleaved by a catalyst and substituted with several nucleophiles. This class includes the *syn*-1,4-carboammination, the *trans*-1,2-carboammination, the syn-1,4-oxamination, the *syn*-1,2-diammination, and the *syn*-1,4-diammination.

These methodologies have proven to be synthetically very useful, giving access to molecules and intermediates relevant for medicinal chemistry and total synthesis. One of the strongest limitations of this chemistry is given by the elevated stability of the urazole residue present in the arenes-MTAD cycloadducts. The hydrolysis of the urazole is necessary to deliver advanced intermediates but has proven to be a challenging task: in our research several specific procedures had been successfully developed.

In **Schemes 9, 10,** and **11** the MTAD-based methods are reported in chronological order. In 2016 we report the first method, a dearomative dihydroxylation (**Schemes 9**).[10] Here the cycloadduct was intercepted by OsO_4 in an Upjohn dihydroxylation delivering a diol characterized by the presence of the

bridging urazole **18**. In the monoaromatics the bridging urazole was hydrolyzed using KOH and ^{i}PrOH getting a bridging hydrazine. This hydrazine can be oxidized in *situ* to form a bridging azocompound that undergoes a *retro* [4+2] collapsing at dienes dienes **19**. The urazole of the MTAD-polyaromatics diols had proved to be more stable, requiring harsher conditions (neat hydrazine at 100 °C) to produce the bridging hydrazine. A protocol to produce the protected *syn*-1,4-diamides **20** was developed bis-benzoylating the bridging hydrazines and cleaving the N-N bond employing SmI_2. The dearomative dihydroxylation had proved to be a powerful synthetic tool for the synthesis of bioactive compounds allowing the synthesis of the glycosidase inhibitor Conduramine A **21**. Alongside the Upjohn dihydroxylation, the modified Narasaka–Sharpless protocol has also been successfully implemented for monoaromatics, allowing the rapid construction of boronic esters **22**. The synthetic applicability of these intermediates was exemplified by the collective total synthesis of the natural products[21] Lycoricidine **23** and Narciclasine **24**.[36]

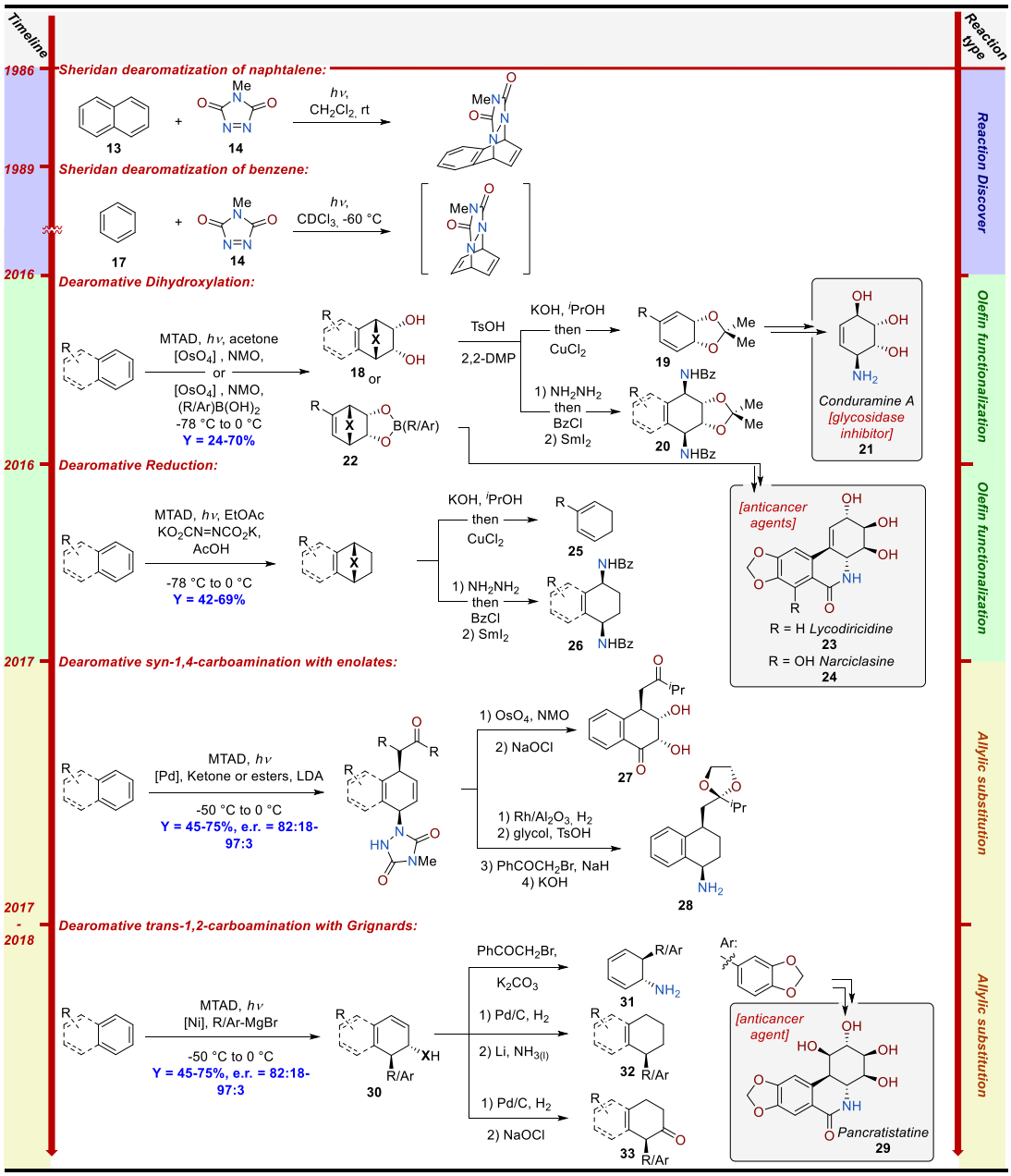

Scheme 9. Timeline of the development of MTAD chemistry from 1986 to 2018.

A second olefine-based method was reported in the same year, using the diimide to reduce the newly formed double bond of the cycloadduct (**Schemes 9**).[28] Similar to the dihydroxylation, urazole was used to get dienes **25** and *syn*-1,4-diamides **26**. The first example of an allylic-based strategy was the dearomative *syn*-1,4-

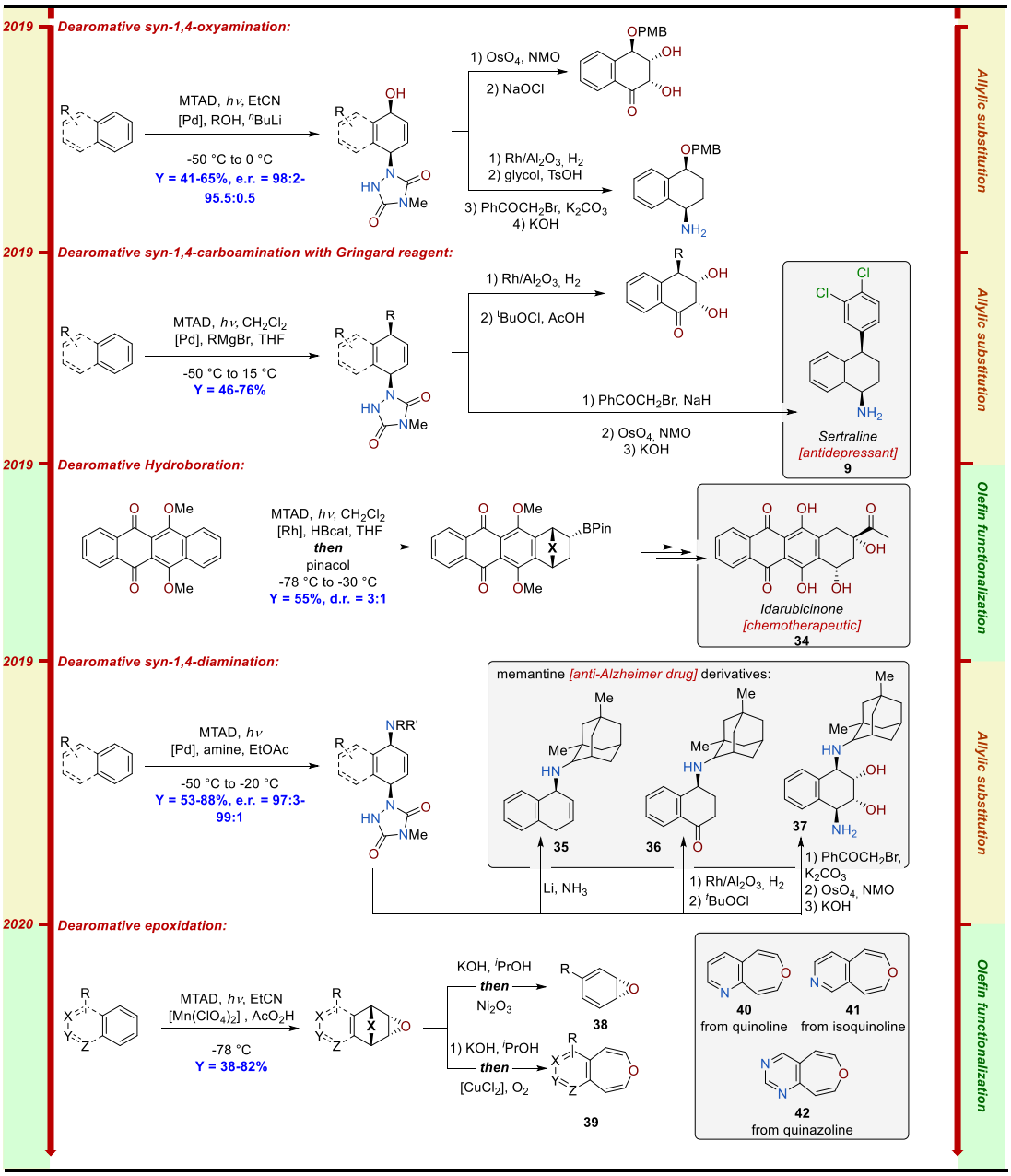

Scheme 10. Timeline of the development of MTAD chemistry from 2019 to 2020.

carboammination (**Scheme 9**).[37] In this method a Pd catalyst was used to get the allylic intermediate, intercepted with enolates. The newly formed double bond had proved to be susceptible to hydrogenation and dihydroxylation, while the benzylic urazole proved to be prone to oxidation to ketone **27**. The delivery of the free amine

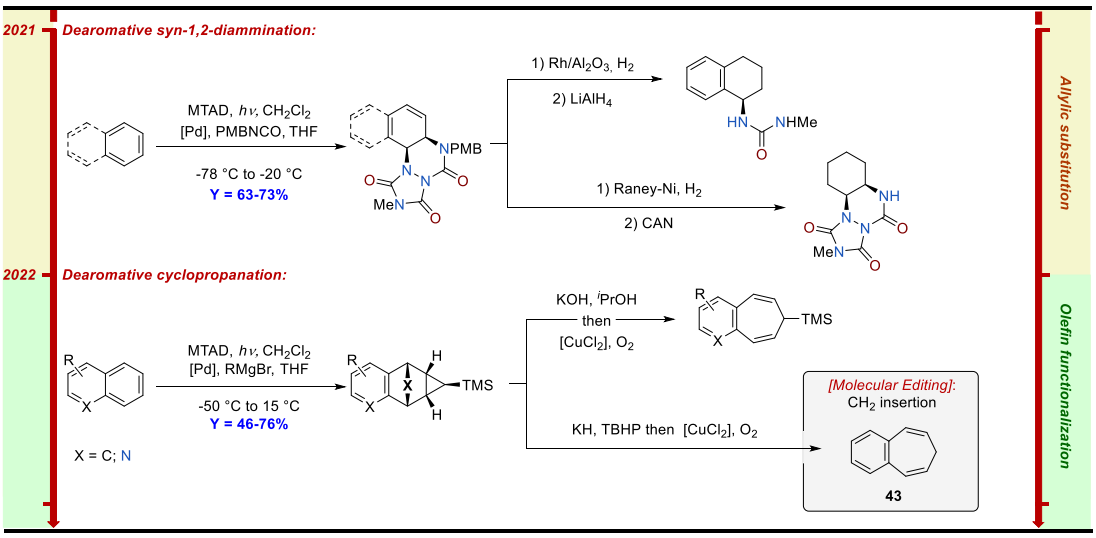

Scheme 11. Timeline of the development of MTAD chemistry from 2021 to 2022.

28 from the urazole was possible by alkylating the free nitrogen with α-bromoacetophenone and subsequent KOH hydrolysis. In 2017, the total synthesis of Pancratistatine **29** was reported (**Scheme 9**),[38] which involve as the first step the enantioselective Ni-catalyzed *trans*-1,2-carboammination of benzene **17**. The following year, the method was published, expanding the scope to include benzene and naphthalene derivatives and using aryl and vinyl Grignard as C sources.[29] The 1,2-carboammination intermediates **30** have shown adaptability in the synthesis of amines **31**, saturated compounds **32** and ketones **33**. In 2019, the toolbox of dearomative transformation was significantly expanded, the *syn*-1,4-oxyamination[31] and the Pd-catalyzed *syn*-1,4-carboammination[7] with Grignard were published (**Scheme 10**). Interestingly, the regioselectivity of this last transformation is complementary to the Ni-catalyzed carboammination and the reaction was used for the synthesis of the antidepressant agent Sertraline **9** from naphthalene **13**. A

dearomative hydroboration was developed in the context of the total synthesis of the Idarubicinone **34** (**Scheme 10**),[39] the anthracyclinone of the idarubicin, a type II polyketide with chemotherapeutic activity. A highly enantioselective *syn*-1,4-diamination was developed in the same year (**Scheme 10**).[32] Interestingly, three analogs of the FDA-approved anti-Alzheimer drug memantine (**35**-**37**) were rapidly synthesized, showing the utility of this methods in the diversification and structural elaboration of medicinal chemistry-relevant compounds. In 2020, the family of olefin-based transformations was enlarged, including the dearomative epoxidation (**Scheme 10**).[33] In this case, after the hydrolysis of the urazole to hydrazine and its oxidation, arene oxides **38** and benzoxepines **39** were obtained, respectively, from monocyclic arenes and polycyclic arenes. This unique transformation gave rapid access to azabenzoxepines (**40**-**42**), an unexplored class of heterocycles, starting from quinoline, isoquinoline, quinazoline and their derivates. In 2021, a preliminary work on the 1,2-*syn*-diammination was published, but with a limited scope that include only benzene **17** and naphthalene **13** (**Scheme 11**).[34] More recently, the dearomative cyclopropanation was reported (**Scheme 11**).[35] The urazole can be cleaved from the products through cycloreversion, obtaining benzocycloheptanes **43**. This method represents a unique way for arenes ring expansion and the first practical example of CH_2 arenes insertion in the 2,3-position of polyaromatics.

The toolbox offered by the arenophile-mediated dearomatization is very flexible, allowing unique disconnections and the rapid construction of synthetically

useful building blocks and bioactive molecules. The synthetic potential offered by these techniques is not only limited to the multistep synthesis of complex molecules, but also to molecular editing and the divergent synthesis of small bioactive molecules. In fact, the unique disconnections offered are well-suited for the modular diversification of fixed scaffolds. In **Section 1.2.0.0,** we will discuss the development of a platform for the diversification of aminocyclitols, a class of antibiotics.

1.1.4.0 - Biological activity and structure of (amino)cyclitols

Highly functionalized carbocycles are prevalent in biological-active compounds.[40] This class of compounds includes (amino)cyclitols, 5- or 6- member ring carbocycles characterized by the presence of at least one amino group and three pendant hydroxy functions (**Scheme 12a**).[41,42] Several (amino)cyclitol-conjugate

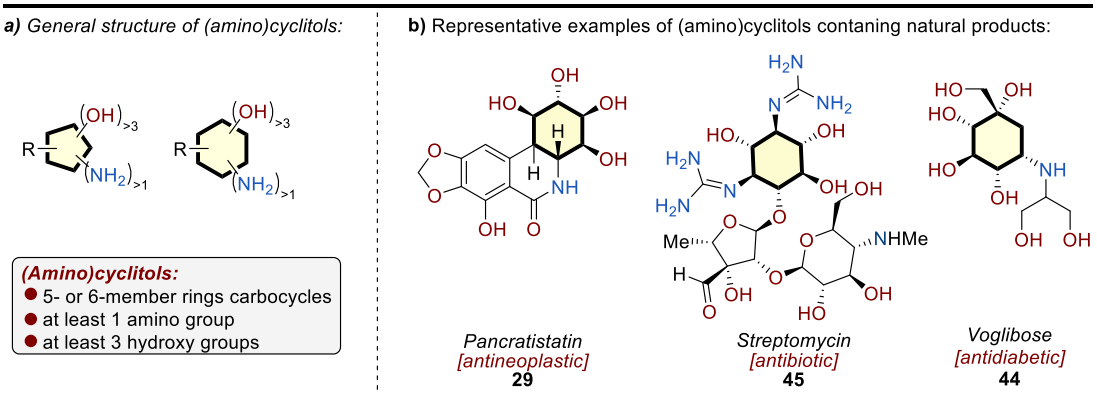

Scheme 12. a) General structural features of the (amino)cyclitos. **b)** Representative examples of (amino)cyclitols containing bioactive molecules.

molecules have important medical applications (**Scheme 12b**); an example is the α-glucosidase inhibitor Viglibose **44**, a C7 (amino)cyclitol used in the treatment of diabetes.[43] They also represent the aglycone moiety of the (amino)glycosides, a class of biological active molecules characterized by the presence of an (amino)cyclitol decorated with one or more aminosugars; an example is the broad-spectrum antibiotic Streptomycin **45**.[44] The (amino)cyclitol scaffold is found in natural products with important biological activity, exemplified by the *Amarilladaceae* alkaloid Pancratistatin **29,** known for its potent antineoplastic activity.[45]

The mode of action of (amino)glycoside antibiotics has been studied and relies on the suppression of the protein expression binding the ribosomal RNA.[40,46]

Medicinal chemistry studies on this class of highly decorated molecules are often limited by the diversity of synthesizable compounds. The development of new synthetic methods would bring a breakthrough contribution in this field.

1.1.5.0 - Synthetic approaches to (amino)cyclitols

As we saw in the previous **Section 1.1.4.0,** the (amino)cyclitol scaffold plays a relevant role in drug design. Not surprisingly, several successful synthetic campaigns have taken place over the decades.[41,42] The synthetic approaches can be grouped into two main categories (**Scheme 13**): those that exploit the chiral pool by taking advantage of preinstalled functionalities (e.g. Quinic acid **46**,[47] Vibo-quercitol **47**[48] or D-glucose **48**[48]), and those that construct decorated carbocycles through cyclizations,[49] annulations,[50] and dearomatizations.[51–53] In this section, these strategies will be discussed in more detail.

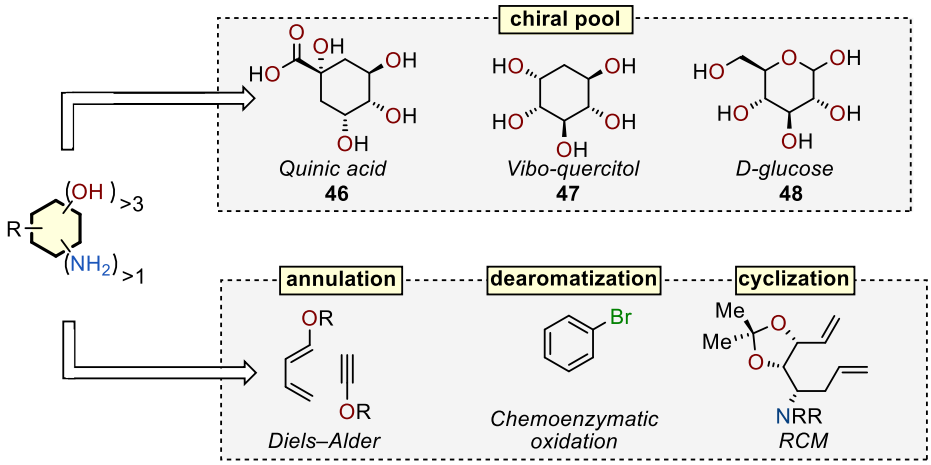

Scheme 13. Common retrosynthetic approaches to (amino)cyclitols. Upper box: chiral pool-based approaches. Lower box: fully synthetic approaches.

1.1.5.1 - Chiral pool-based approaches to (amino)cyclitols

Readily available molecules with pre-installed functionality are popular heteroatom-rich sources. The chiral pool strategy bypasses the need to install heteroatoms and, often, set the stereochemistry. Molecules like Quinoic acid **46** and

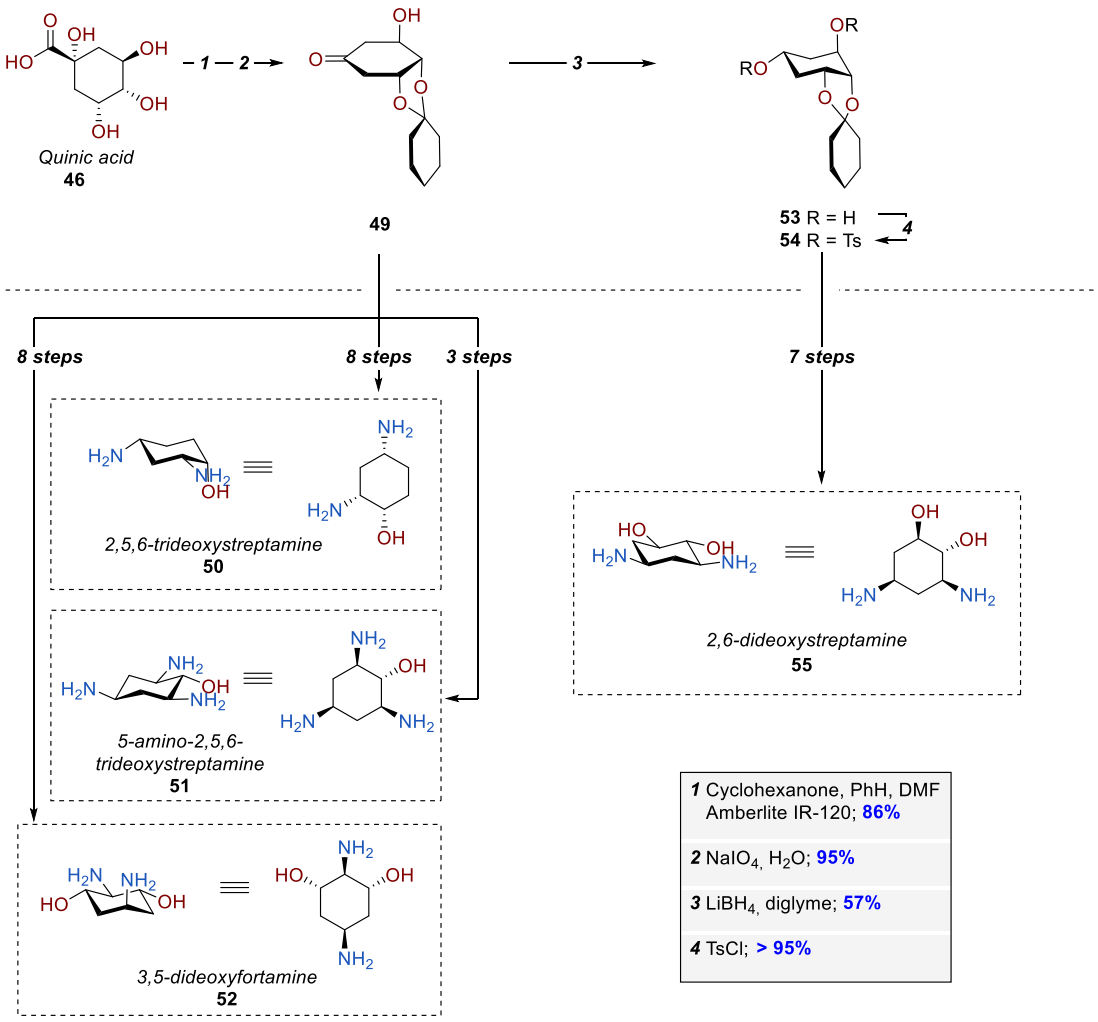

Scheme 14. Synthesis of streptamine and fortamine analogs from Quinic acid **46**.

Vibo-quercitol **47** can act as templates for the 6-member carbocyclic rings. An example of this strategy was furnished by Sepulchre *et al* in 1980 (**Scheme 14**).[47] In this work, Quinoic acid **46** was converted in the ketone **49** by protecting the *syn*-diol as a cyclohexylidene acetal and oxidating the tertiary alcohol with sodium metaperiodate. The ketone **49** was exploited to reach the Streptamine analogs 2,5,6-trideoxystreptamine **50** and 5-amino-2,5,6-trideoxystreptamine **51** respectively in eight and three steps. Also, a fortamine analog, the 3,5-dideoxyfortamine **52**, was

synthesized in eight steps from **49**. The reduction of **49** with $LiBH_4$ yields the free diol **53**, which, after tosylation, offers 2,6-dideoxystreptamine **55**. Even though several

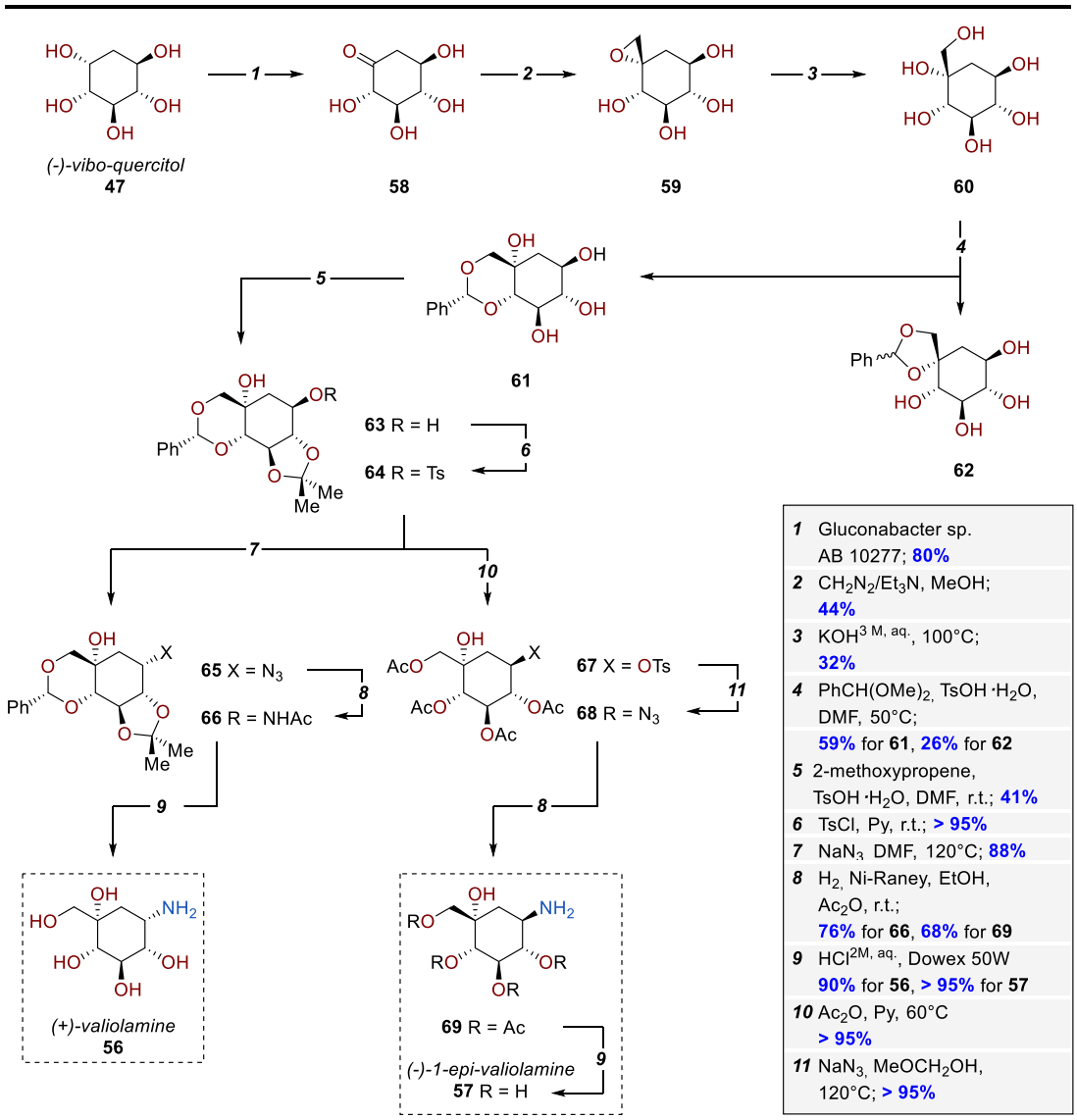

Scheme 15. Synthesis of Valiolamine **56** and (-)-*epi*-valiolamine **57** from (-)-*vibo*-quercitol **46**.

steps were needed; this pioneering work offers a good example of how the chiral pool can be exploited to reach highly decorated species.

Korenaga *et al.*[54] have reported the synthesis of Valiolamine **56** and its 1-epimer **57**, starting from (-)-*vibo*-quercitol **47**, a cyclitol readily available from *myo*-inositol through bio-deoxygenation (**Scheme 15**). The selective oxidation of the hydroxide on carbon 5 was accomplished biochemically by obtaining the ketone **58**. Diazomethane was used to introduce the hexacyclic carbon as spiroepoxide **59**. Under basic conditions, methylene hydroxide is formed on **60**. The benzylidenation of **60** produces acetal **61** along with spiro derivative **62**, convertible in **61,** regenerating **60**. A 2-methoxypropene and TFA were employed to protect the trans diol on carbons 2 and 3, yielding the key intermediate **63**, where all the alcohols are chemically distinguishable. The secondary alcohol of **63** was tosylate delivering **64,** that represents the branching point of the synthetic pathway. A direct substitution was accomplished by treating **64** with NaN_3 in DMF, giving the azide **65**. The natural product (+)-valiolamine **56** was obtained through a sequence of hydrogenation to **66** and overall deprotection. To obtain the 1-epimer of Valiolamine **57,** a Walden-inversion was applied. The protecting group of **64** was exchanged to obtain the tetra-acetyl tosylate **67**; a stereoritentive azide substitution was achieved using NaN_3 through the intermediacy of an acetoxonium ion with the acetyl group on carbon 4. As before, the hydrogenation/deprotection sequence was used to deliver (-)-1-*epi*-valiolamine **57**.

The sugars represent the most exploited class of naturally occurring chiral molecules in the context of (amino)cyclitol synthesis. Several cyclizations have been adopted to establish the carbocycles, including ring closing metathesis (RCM), radical

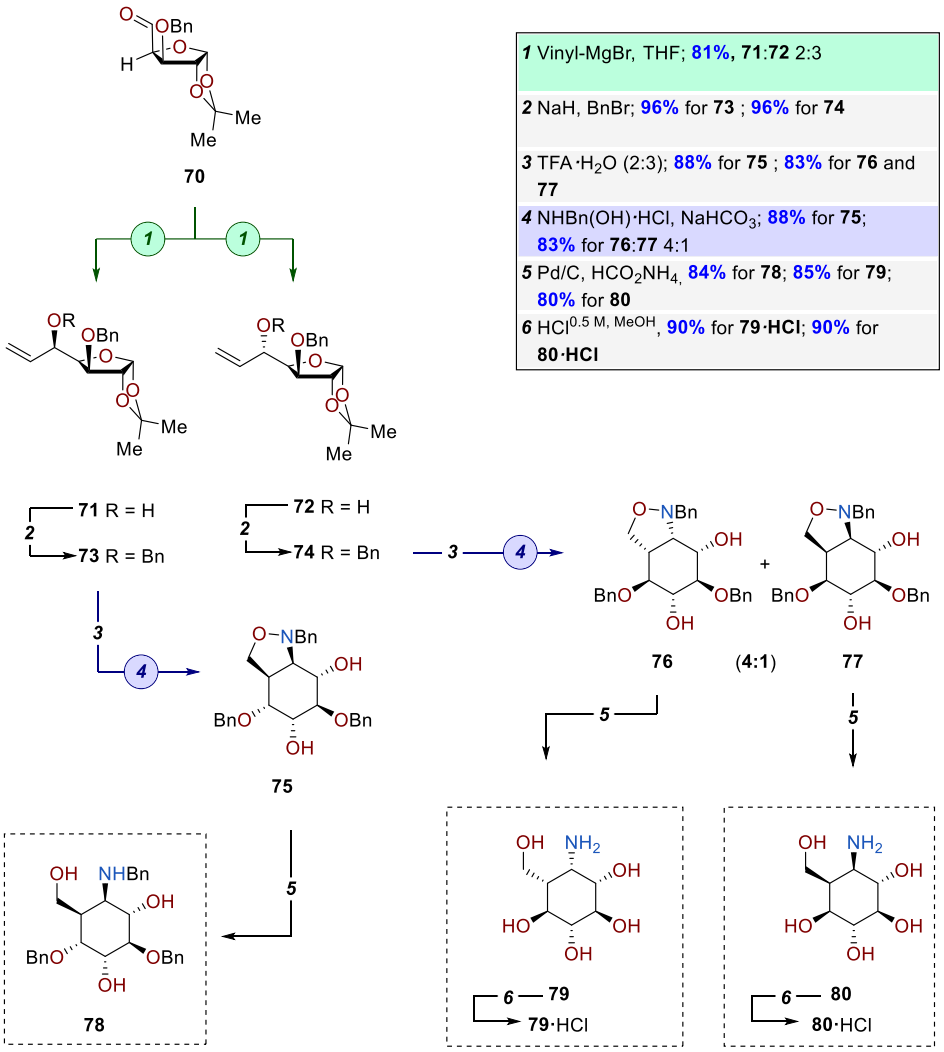

Scheme 16. Selected example of intramolecular nitrone-olefine cycloadditions (INOC) used for the synthesis of (amino)cyclitols form a sugar derivative.

cyclizations, McMurry coupling, and intramolecular nitrone-olefine cycloadditions (INOC).[41,42] A good example of the latter has been provided by Chakraborty *et al.*[55] (**Scheme 16**). A series of validamine analogs was obtained starting from 3-*O*-benzyl-

1,2-*xylo*-pentodialdose. The vinylation of the aldehyde **70**, accessible from the sugar, yields the two diasteroisomers **71** and **72**. The benzylation of the allylic alcohols and acetal deprotection prepare the substrates for the INOC cyclizations. In the case of **73**, a regioselective cyclization was observed giving **75**; while, for **74,** the cyclization yields both the diasteroisomers **76** and **77** in a 4:1 ratio. Clevadge of the N-O bond and simultaneous debenzylations offer the three diasteroisomers **78**, **79** and **80**.

The most applied reaction for sugar cyclization is RCM. A selective route for valienamine **81** was described by Jung *et al.* (**Scheme 17a**).[48] The linear precursor **82,** accessible from D-glucose **48,** underwent TBDPS deprotection, Swern oxidation, and vinyl Grignard addition delivering the allylic alcohol **83**. RCM yielded both the diasteroisomers **84** and **85**, with the mixture subsequently converted to the sole **84** through an oxidation/stereoselective reduction sequence. The alcohol **84** was benzylated and treated with chlorosulfonyl isocyanate to obtain Cbz amine **86** through a stereoselective S_Ni mechanism. The amine **86** was subjected to boron trichloride in dichloromethane to deprotect all functionalities and delivering *(+)*-valienamine **81**.

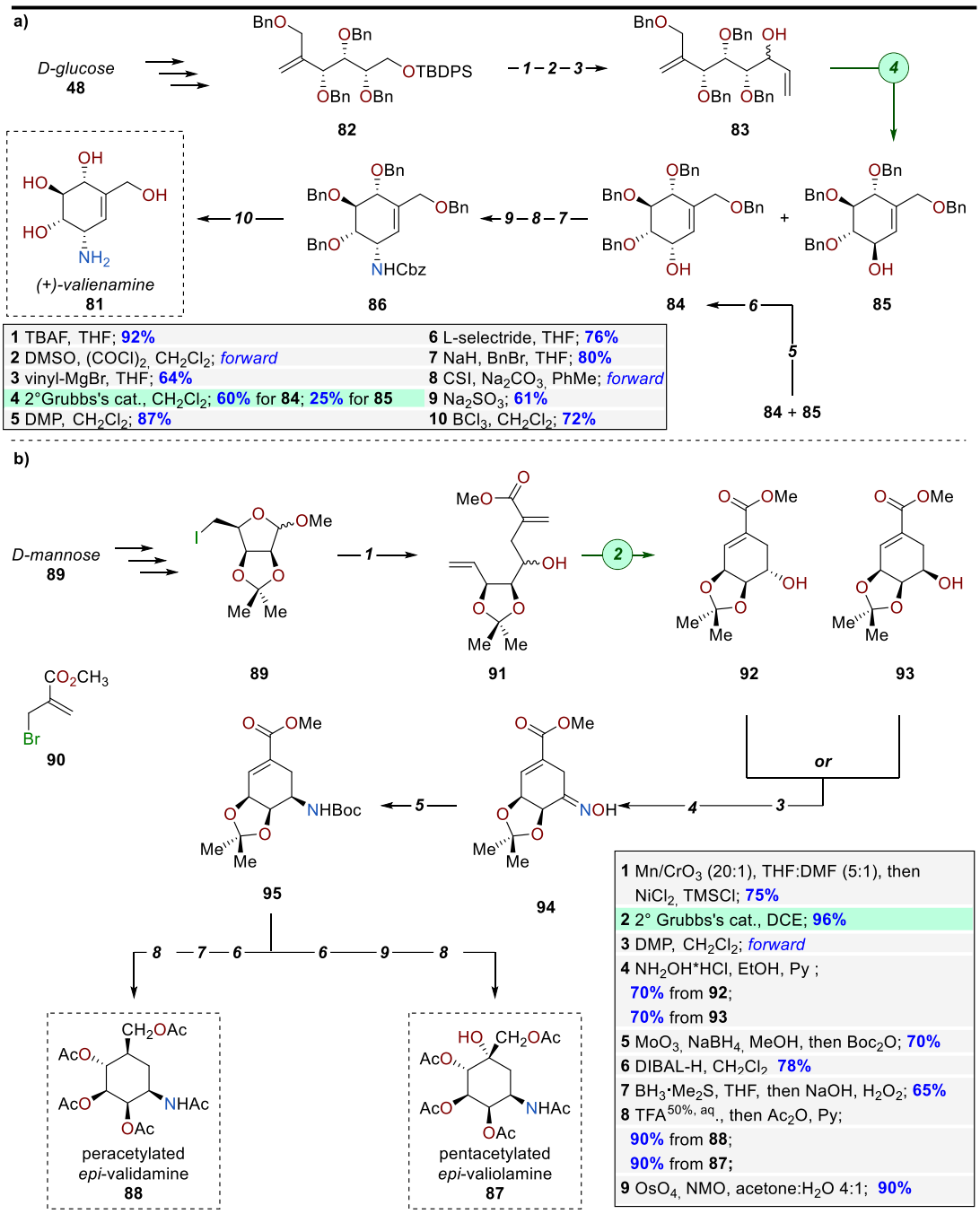

Scheme 17. Selected examples of RCM adopted to cyclize sugars in C7 (amino)cyclitols synthesis **a)** Synthesis of *(+)*-valielamine **81** from *D*-glucose **48**. b) Synthesis of validamine analogs from *D*-mannose **89**.

Rao and co-workers have developed the synthesis of peracetylated *epi*-validamine **87** and peracetylated *epi*-valiolamine **88** from *D*-mannose **89** (**Scheme 17b**). A non-

stereoselective Nozaki-Hiyama-Kishi reaction was conducted to transform the iodo compound **89** into the diasteromeric mixture of 1,6-diolephines **91**. An RCM establishes the cyclohexane yielding both diateroisomers **92** and **93**. Dess-Martin oxidation of **92** and **93,** followed by a treatment with hydroxylamine hydrochloride offered the oxime **94,** which was suitable for a stereoselective reduction/protection sequence to yield the Boc amine **95**. Compound **95** was exposed to a series of tranformations, including DIBALH reduction, hydroboration/oxidation, and protection group exchange, resulting in the Validamine analog **88**. A sequence of DIBALH reduction, dihydroxylation, global deprotection, and acetylation was used to accede the Valiolamine analog **87** from **95**.

Several interesting examples of RCM sugars cyclizations have been employed in the synthesis of C6 (amino)cyclitols. A Synthesis of (-)-conduramine F-4 **96** was reported by Ramesh and co-workers (**Scheme 18a**).[56] The tri-*O*-benzyl-*D*-glucal **97** was converted in the linear precursor **98** through a step sequence. The diol **98** was treated with Swern oxidation and Wittig olefination obtaining the 1,6-diolefine **99**. A second-generation Grubb's catalyst was used for the cyclization obtaining **100.** Finally, a series of protecting group manipulations was necessary to obtain the final natural product **96**. Batchu and co-workers have exploited the D-mannitol derivative **102** to obtain Conduramine F and E analogs (**Scheme 18b**).[57] The diol **103** was submitted to Malaprade fragmentation and vinylation, obtaining two allylic alcohols **104** and **105,** with a diastereomeric ratio of 1:1.3. A selective primary acetal

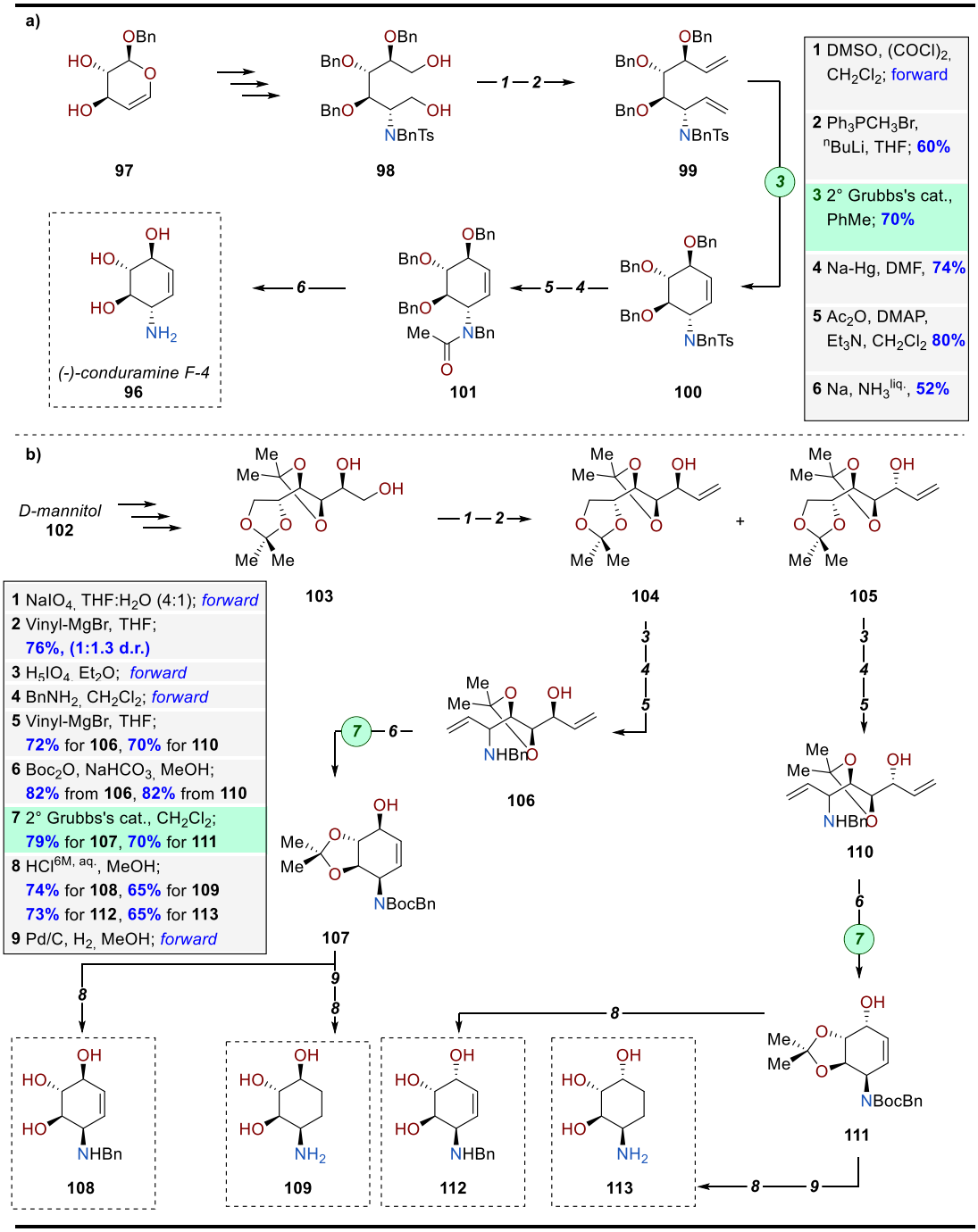

Scheme 18. Selected examples of RCM adopted to cyclize sugars in C6 (amino)cyclitols synthesis **a)** Synthesis of (-)-conduramine F-4 **96**. **b)** Synthesis of conduramine E analogs **108** and **109** and of conduramine F analogs **112** and **113** from *D*-mannitol **102**.

deprotection followed by diol cleavage with periodic acid, aldimine formation, and nucleophilic addition was used to convert **104** in the benzylamine **106**. Once the 1,6-

diene was installed, a sequence involving Boc protection and RCM was employed to yield the cyclohexene **107**. Acid conditions were utilized to simultaneously deprotect the trans-diol and the Boc amine, resulting in the formation of the Conduramine F analog **108**. Hydrogenations of the olefine **107**, followed by deprotection, led to the Conduramine F analog **109**. Starting from the diastereoisomer **105,** the same sequence was used to access the Conduramine E analogs **112** and **113**.

1.1.5.2 - Fully synthetic approaches to (amino)cyclitols

As we have seen, the chiral pool has proven to be a valuable source of (amino)cyclitol precursors. However, the defined structures used can impose limitations to the diversity and control of accessible structure. For these reasons, several fully synthetic approaches to (amino)cyclitols have been developed over the years. A very relevant example of this has been furnished by Riera *et al.* (**Scheme 19**).[49] In this work, full control of the stereocenters in Conduramine analogs was obtained by Sharpless epoxidation, Mitzunobu inversion, organometallic addition and *cis*-dihydroxylation (**Scheme 19**, box). A completely regioselective nucleophilic opening of the enantiomerically enriched epoxide obtained from **114,** followed by Boc and TBDPS protections, was used to yield the Boc amine **115**, which represents the first branch point of the stereodivergent synthesis. TBDPS deprotection and acetal protection were used to yield *cis*-**116,** while a Mitzunobu inversion of the secondary alcohol **115** and subsequent protection group manipulations deliver the *trans*-**116**. Swern oxidation was used to oxidize the primary alcohol and

organometallic addition, followed by acetylation to deliver the four diasteroisomers: *cis-anti*-**117**, *cis-syn*-**117**, *trans-anti*-**117**, and *trans-syn*-**117**. A late-stage RCM was used to cyclize the linear precursor, obtaining the relative cyclohexenes (**118-121**).

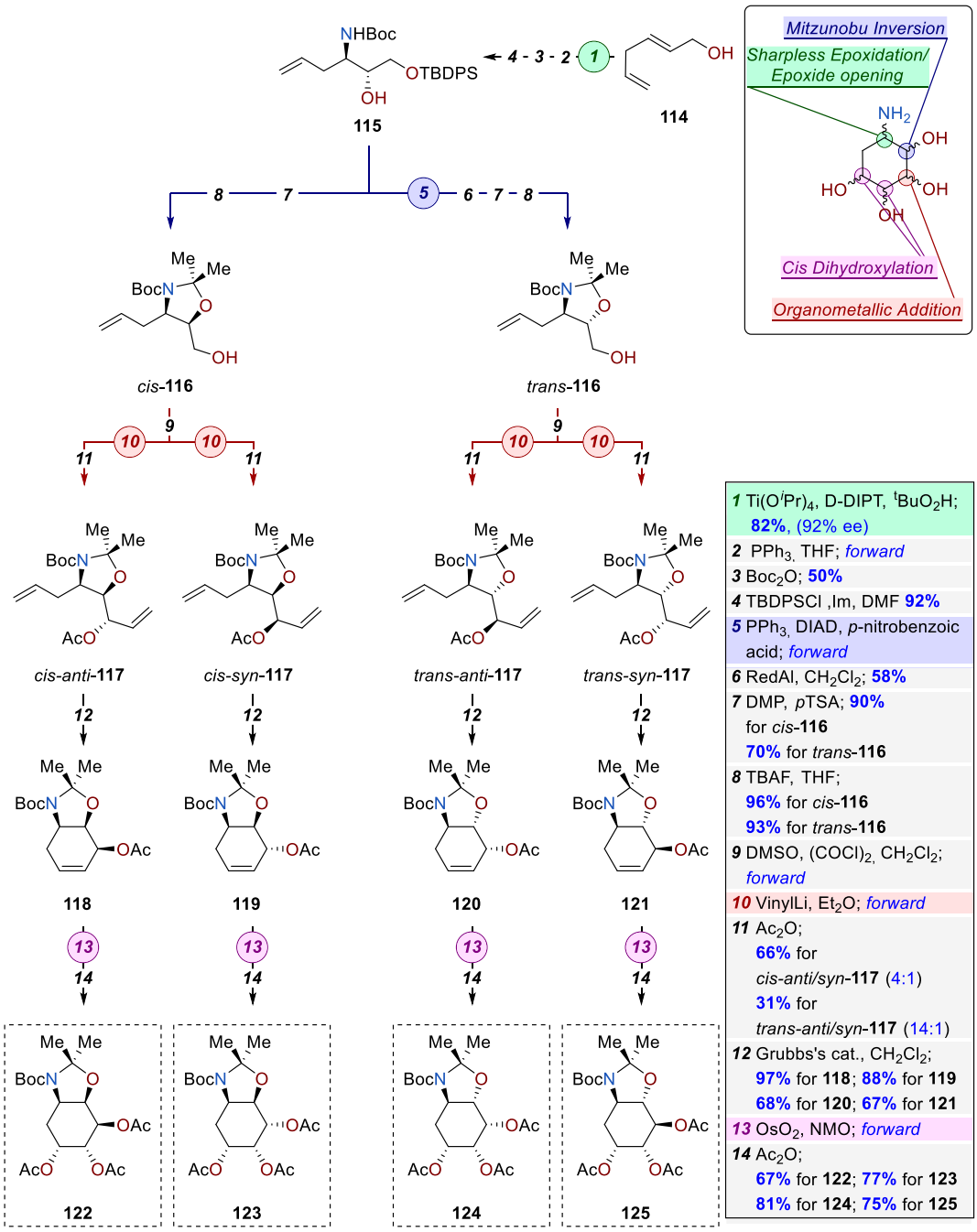

Scheme19. Selected example of RCM annulation for the synthesis of four conduramine analogs.

Finally, a sequence of Upjohn *cis*-dihydroxylation and acetylation was used to acquire the four protected Conduramine analogs **122**, **123**, **124**, and **125**.

In 2016, Nishida and co-workers reported a fully synthetic approach based on annulation (**Scheme 20**).[58] Here, an asymmetric ytterbium catalyzed Diels-Alder reaction between the Danishefsky diene **126** and the dienophiles **127** was used to

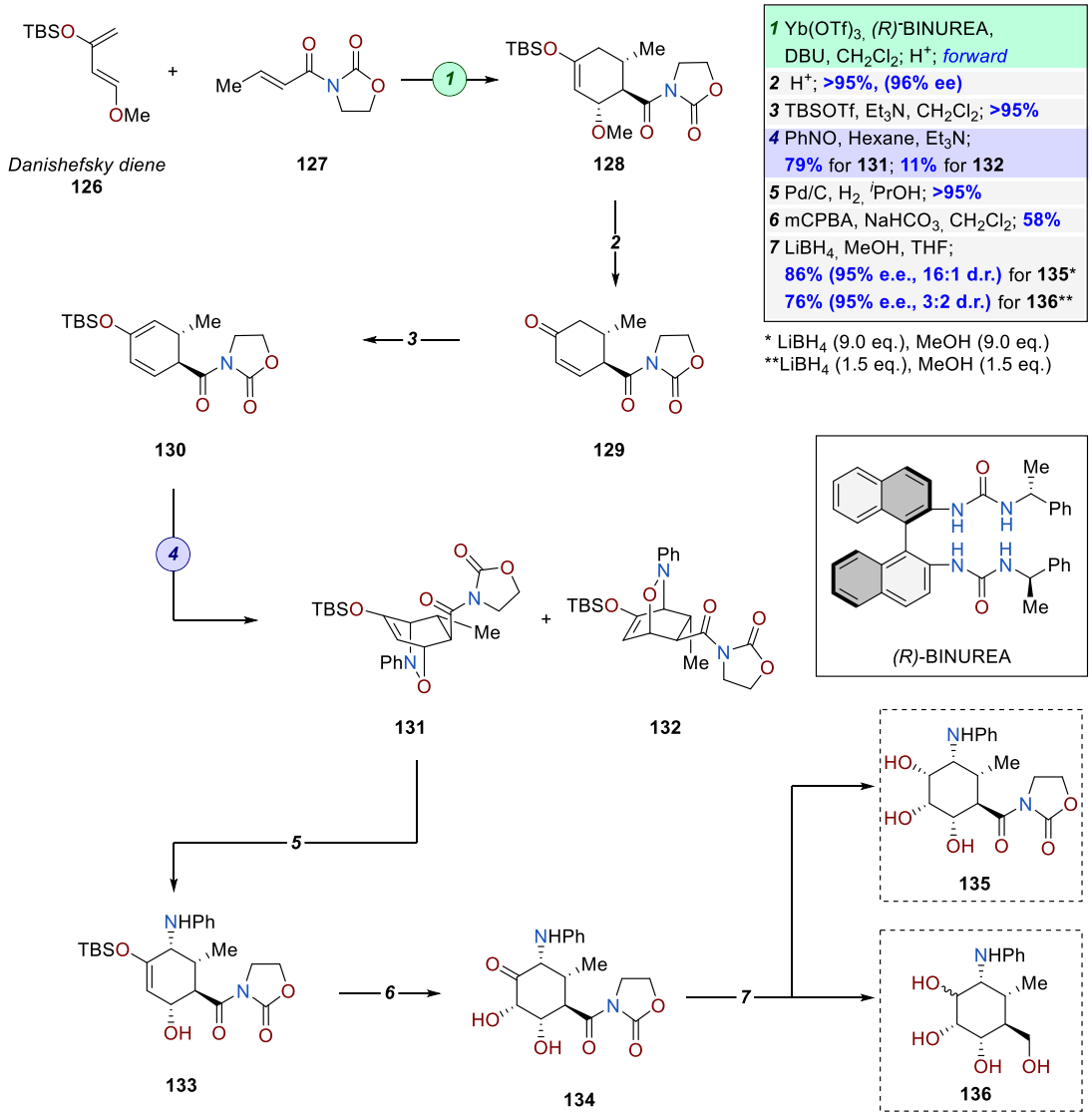

Scheme 20. Selected example of Diels-Alder annulation for the synthesis of C7 (amino)cyclitols.

install the hexacyclic carbocycle **128**. Acid conditions deliver the α,β-unsaturated ketone **129**, which is then converted in the diene **130** through TBS deprotection, amenable for the facial selective nitroso Diels-Alder with nitrosobenzene to **131** and **132**.

The hydrogenation of the N-O bond delivers the *syn*-1,4-aminol **131,** which was converted into the α-hydroxyketone **134** through Rubottom oxidation. $LiBH_4$ reduction yields the C7 (amino)cyclitol **135,** with the oxazolidinone still installed. However, increasing the equivalents of $LiBH_4$ leads to the complete reduction of the oxazolidinone, but decreases the selectivity in the carbonyl reduction, resulting in the diastereomeric mixture **136**.

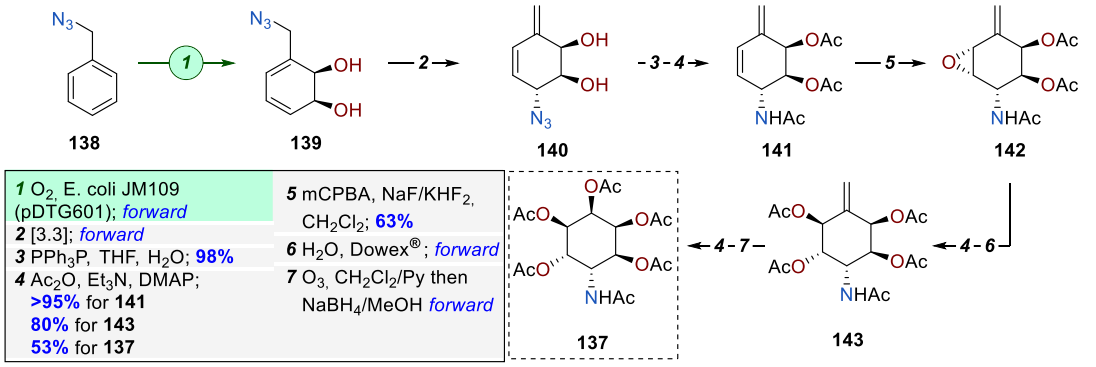

Scheme 21. Stereoselective dearomative synthesis of (amino)cyclitol starting from benzyl azide.

Arenes represent the ideal precursors for (amino)cyclitols, being largely available and having the carbocyclic structure already installed. The direct synthesis of decorated cyclohexanes through chemoenzymatic deraomatization of arenes represents a promising strategy, even if few examples are present in the literature.

In 2016, Carrera *et al.*[51] reported the first enantioselective synthesis of (amino)cyclitol **137,** starting from benzyl azide **138** (**Scheme 21**). The key transformation was the enzymatic dearomative dihydroxylation, which was employed to convert benzyl azide into allylic azide **139,** that spontaneously undergoes a sigmatropic [3.3] rearrangement, yielding the diene **140**. Staudinger reaction between azide **140** and triphenylphosphine was used to introduce an allylic amine, subsequently acetylated to **141**. Next, the olefin **141** was epoxidized to **142,** followed by a consequent acid epoxide opening/acetylation used to obtain the penta acetylated tetraol **143**. Finally, the fully decorated cyclohexane **137** was established *via* ozonolysis and acetylation.

More recently, Banwell and co-workers reported the synthesis of the C7 (amino)cyclitol analog 4-*epi*-kirkamide **144** through the dearomatization of bromo benzene **145** (**Scheme 22b**).[52,58] The enantiopure diol **146** was converted into the corresponding acetal, and the reaction with N-bromoacetamide (NBA) in the presence of tin bromide yielded the allylic amine **147**. The acylazirideine **148** was generated *in situ* by treating **147** with potassium hexamethyldisilazide (KMDS) in the presence of tetra *n*-butylammonium bromide (TBAB), followed by a spontaneous Heine-type reaction, resulting in the oxazoline **149**. Acid conditions deliver the vinyl bromide **150,** which was then converted into the corresponding vinyl iodide. The iodo compound underwent Pd-catalyzed carboxyamination using carbon monoxide and methoxy(methyl)amine, installing a Weinreb amide in compound **151**. The aldehyde

152 was obtained after the DIBALH reduction of **151** and the TBS protection of the secondary alcohol. The final product **144,** was acquired via aldehyde reduction in Luche conditions and acetal deprotection.

Gonzalez and colleagues have reported the shortest synthesis of the (amino)cyclitolic moiety found in the antibiotic Hygromicine **153**, using a dearomative approach.[53] Starting with the catechol **146**, which is accessible through chemoenzymatic dearomatization of bromobenzene **145**,[58] it was acetalized and then epoxidized to **154**. Exposure to lithium chloride and ethyl acetoacetate, followed by the reaction with NaN_3, converted **154** into allylic azide **155**. A one-pot dihydroxylation/reduction yielded the (azido)cyclitol **156**. The hydroxy groups in **156** were benzylated, and the methylenedioxy acetal was installed in **157** through a transacetalization with dimethoxymethane (DMM). Subsequent hydrogenolysis of the benzyl ethers, reduction of the azide and then a treatment with NaOH provided the natural (amino)cyclitol **153**.

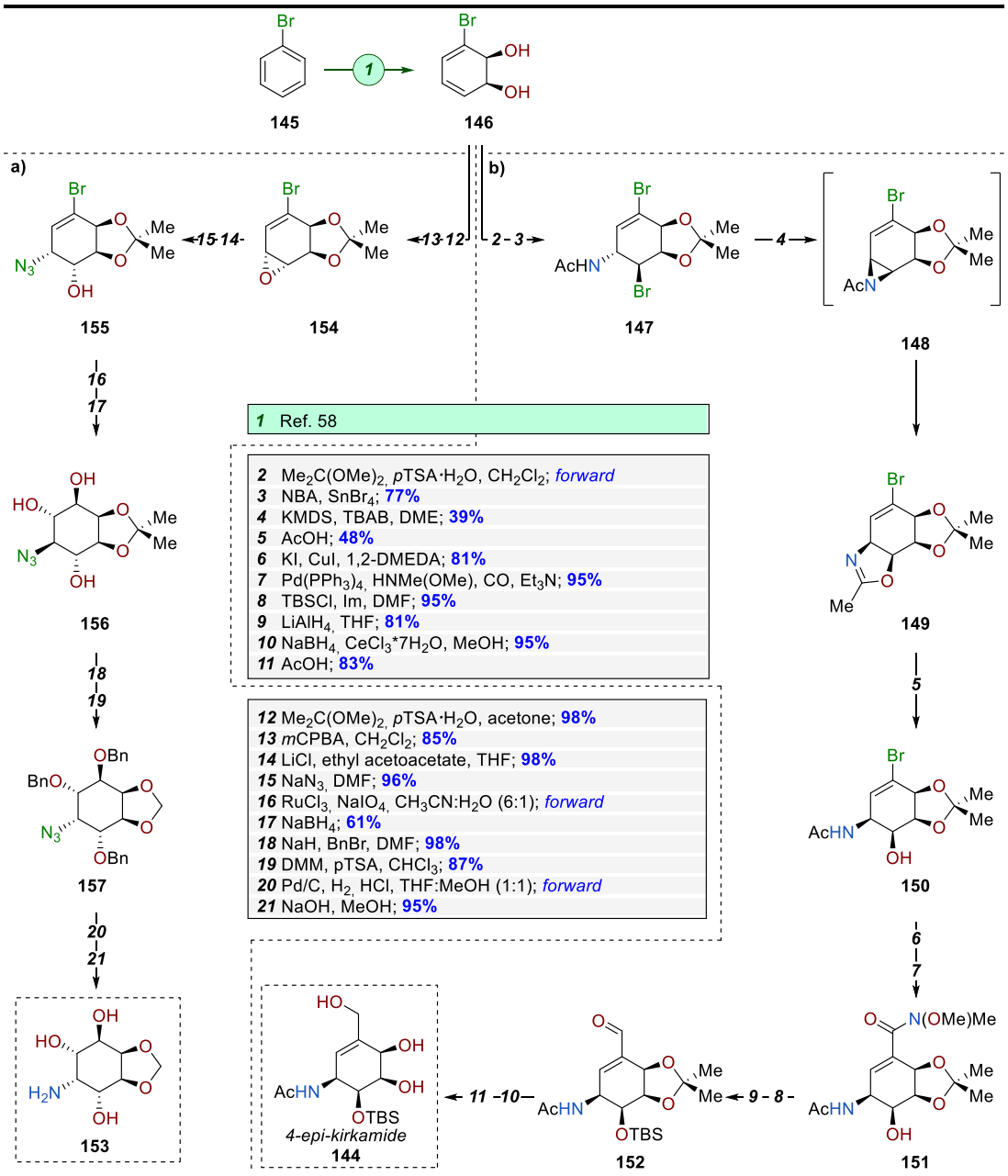

Scheme 22. Selected examples of dearomative enzymatic oxidation for the synthesis of (amino)cyclitols from bromobenzene **145**. **a)** Synthesis of the (amino)cyclitolic moiety of Hydromicine. **153** **b)** Synthesis of 4-*epi*-kirkamide **144**.

1.2.0.0 - Aim of the project

As we have seen in the previous chapter, several successful (amino)cyclitol syntheses have been achieved. Nevertheless, the manipulation of heteroatoms-rich intermediates often complicates synthetic pathways, necessitating multiple protection group manipulations and demanding a linear construction of precursors. The primary consequence of these constraints is that the size of the accessible (amino)cyclitol library is generally small, with only a few compounds obtained after cumbersome synthesis.

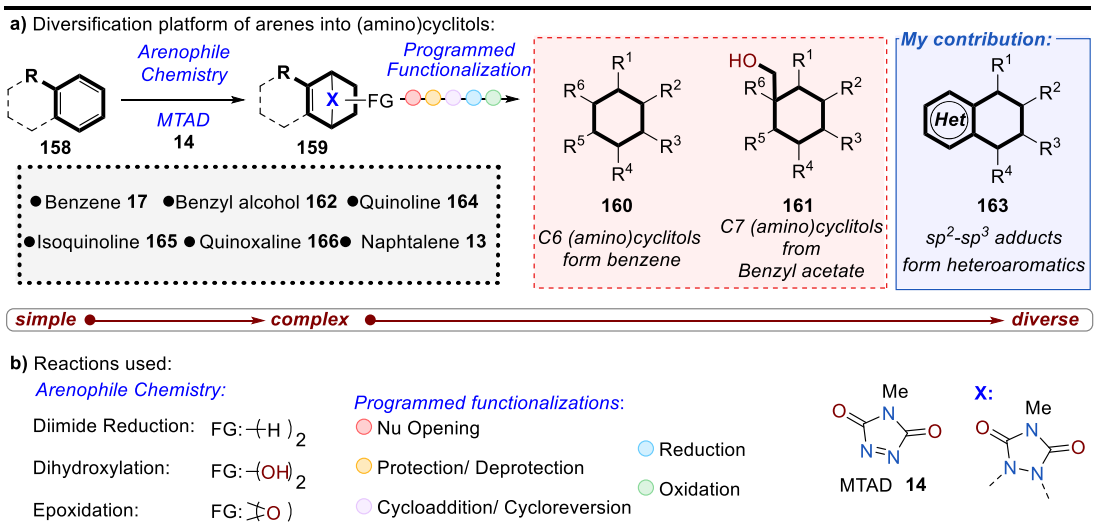

Scheme 23. a) Diversification platform for the diversification of arenes into (amino)cyclitols. The platform relies on areophile chemistry to convert arenes into dearomatized cycloadducts amenable for programmed transformations to decorated cyclohexanes. Three classes of analogs have been obtained: C6 (amino)cyclitols, C7 (amino)cyclitols, and sp^2-sp^3 hybrids (discussed in detail in this thesis). **b)** Reaction used for the dearomatization and diversification.

The construction of decorated six-membered rings can greatly benefit of dearomative transformations, which enable convenient structure-based disconnections, tracing back complex carbocycles to simple and readily available arenes. As shown in **Schemes 20** and **21,** several multistep target syntheses of

(amino)cyclitols employ these disconnections. However, dearomative reactions have not been used in divergent strategies. We envision that the arenophile chemistry reported by our group (**Section 1.1.3.0**) could furnish an ideal platform for (amino)cyclitol diversification; accordingly, a variety of simple arenes and (hetero)arenes have been used as templates to achieve a wide range of structures in a systematic and iterative synthetic approach (**Scheme 23a**). The simple arenes **158** are thus converted into the more complex [2.2.2]-bicyclic systems **159**, amenable for the diversification into decorated hexanes exploiting a series of programmed functionalization (**Scheme 23b**). The arenophile's urazolic subunit residue from the dearomatization can serve as either an amine or diene surrogate, allowing the introduction of heteroatoms in a regio- and stereocontrolled manner. Depending on the arene used as a template, the analogs obtained can be divided into three classes: the C6 (amino)cyclitols **160** derived from benzene **17**, the C7 (amino)cyclitols **161** obtained from benzyl acetate **162**, and the medicinal chemistry relevant sp^2- sp^3 hybrids (amino)cyclitols **163** produced starting from polyaromatics. My main contribution to this project has been in the synthesis of the sp^2-sp^3 hybrids by dearomatizing naphthalene **13**, quinoline **164**, isoquinoline **165** and quinoxaline **166.** For the purpose of this essay, this part of the project will be discussed in detail in **Section 1.3.2.0** and in the experimental part (**Section 1.6.0.0**). The next section will cover the approach to the C6 and C7 analogs for completeness.

1.3.0.0 - Results and discussion

1.3.1.0 - Diversification of monoaromatics into C6 and C7 (amino)cyclitols

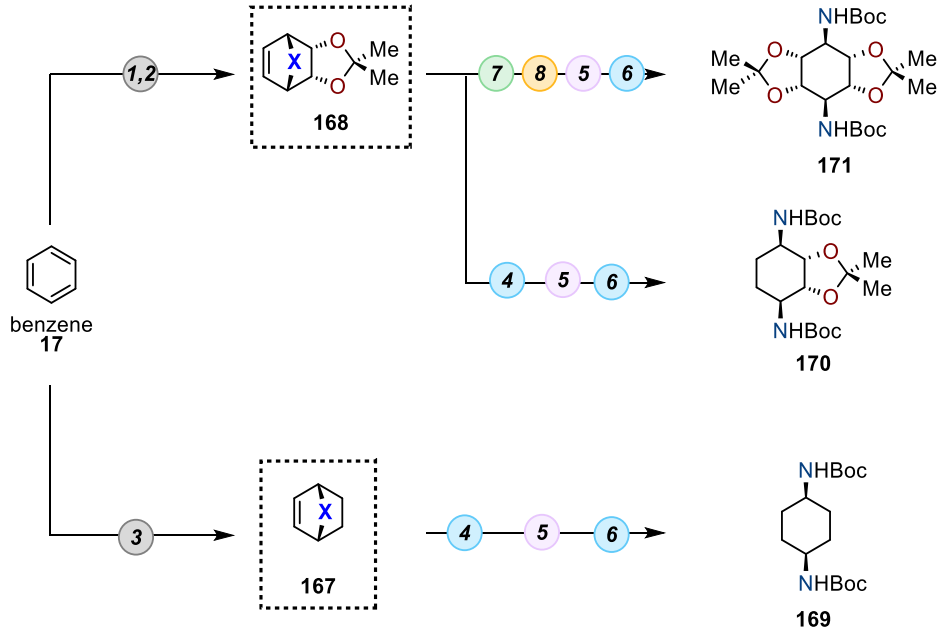

1 MTAD, *hν then* OsO_4, NMO, acetone;	***5*** KOH, *i*PrOH, *then* $CuCl_2$; to **7** **93%**; to **9** **54%**; to **10** **68%**;
2 *p*TSA, DMP, CH_2Cl_2;	***6*** H_2, Ni-Raney, EtOH,*then* Boc_2O; to **7** **53%**; to **9** **88%**; to **10** **70%**;
3 MTAD, *hν then* $KO_2C{=}CO_2K$, AcOH, EtOAc	***7*** OsO_4, NMO, H_2O, acetone; **78%**;
4 H_2, Pd/C, MeOH; to **7** **99%**; to **9** **66%**;	***8*** *p*TsOH, 2,2-DMP, DCM; **82%**.

Scheme 24. Diversification of benzene **17** into *syn*-1,4-diamines.

The first application of our strategy exploits the bridging urazole as masked *syn*-1,4-diamine. Both dearomative diimide reduction and dearomative dihydroxylation were employed to give the cycloadduct **167** and the acetal **168** (**Scheme 24**). Subsequently, both olefins **167** and **168** were exposed to a three-step sequence, including hydrogenation, hydrolysis of the urazole with subsequent oxidation to diazine, and hydrogenation. The two diamines **169** and **170** were isolated as Boc protected. A similar reaction sequence has been adopted to convert **168** in the protected tetraol **171.** Here, the olefin in **168** was dehydroxylated and protected as

an acetonide before proceeding with the previously described sequence. Overall, this synthetic pathway furnishes C6 (amino)cyclitols characterized by the presence of *syn*-1,4-diamines and different levels of oxidation on carbons 2, 3, 5, and 6.

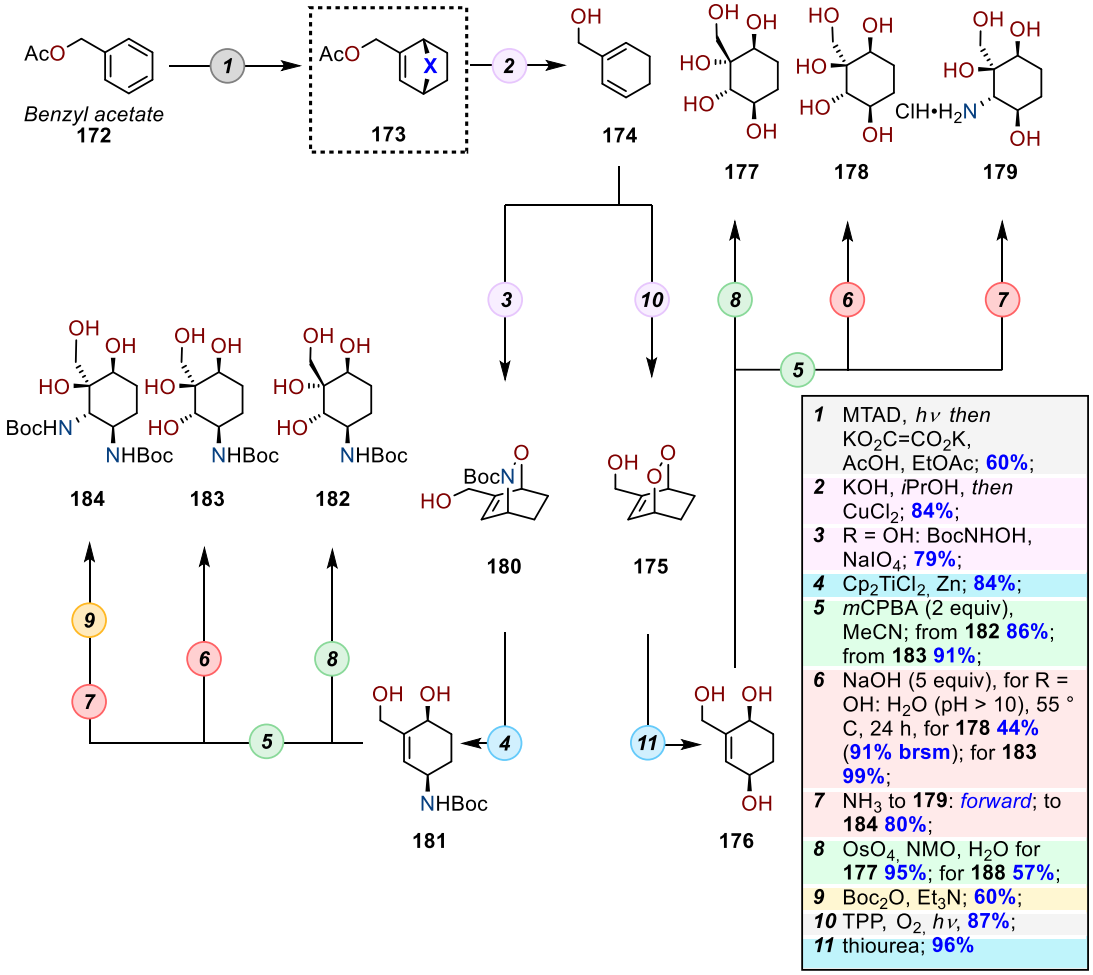

Scheme 25. Diversification of benzyl acetate **172** into *syn*-1,4-aminols and *syn*-1,4-diols through dearomative diimide reduction.

After the introduction of diamines, we move to the installation of diols and aminols in the carbocycles. For this purpose, the urazole has been used as a diene surrogate amenable for hetero-Diels-Alder reactions with either nitroso compounds or singlet oxygen (**Scheme 25**). To obtain a library of C7 (amino)cyclitols, the diimide-

reduced product **173** was exposed to one pot urazole hydrolysis and oxidation to form a diazine that spontaneously cycloreverted, giving the diene **174**. The cycloaddition of diene **174** with singlet oxygen produced the endoperoxide **175**, which was then converted in the *syn*-1,4-diol **176** through a mild reductive cleavage of the O-O bond with thiourea. Accordingly, **176** was diversified into pentanols **177** and **178**, and in the amino tetraol **179** by means of dihydroxylation and epoxidation/nucleophilic openings. The regioselective nitroso-Diels Alder between the diene **174** and nitroso-Boc gives access to the cycloadduct **180**. The reductive cleavage of the N-O bond delivers the aminol **181,** which is prone to the same diversification pathway used for *syn*-1,4-diol **176**, furnishing the amino tetraols **182** and **183**, as well as diamino triol **184**.

The products of dearomative dihydroxylation of benzene **17** and benzyl acetate **172** were used to obtain *syn*-1,4-diols (**Scheme 26**) and *syn*-1,4-aminols (**Scheme 27a**). Both **186** and **187** were engaged in a singlet oxygen-Diels-Alder to the adducts **188** and **189** (**Scheme 26**). Iterating the diversification steps used before, the dienes were transformed in the diols **190** and **191** that furnish a branch point to the cyclohexanes **192**, **193**, **194**, and **195**. Analog results were obtained from the introduction of *syn*-1,4-aminols into the acetal dienes **186** and **187** (**Scheme 27a**). The

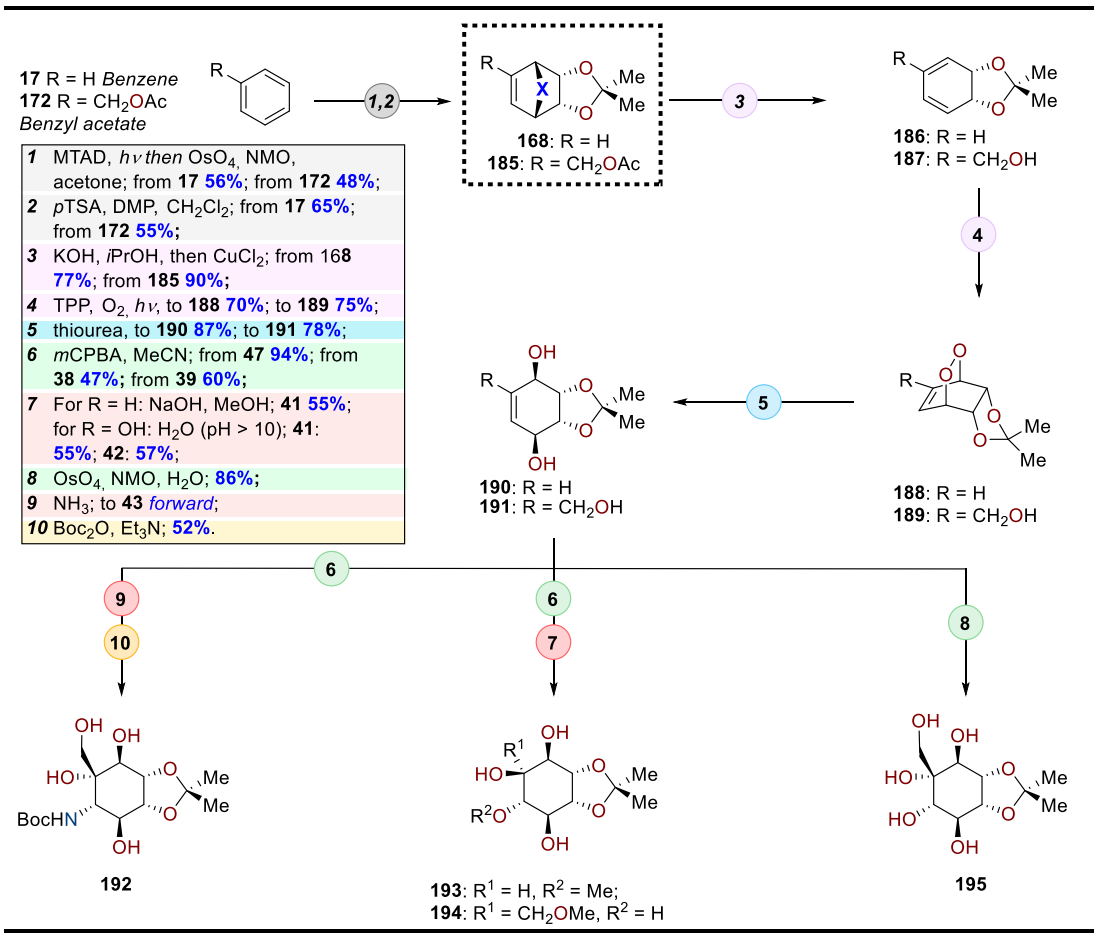

Scheme 26. Diversification of benzene **17** and benzyl acetate **172** into *syn*-1,4-diols through dearomative diimide dihydroxylation.

aminols **198** and **199** were set *via* nitroso-Diel-Alder/reductive cleavage and diversified by means of olefin chemistry into the corresponding C6 and C7 (amino)cyclitol **200**, **201**, **202**, **203**, and **204**.

Finally, to prove the utility of our platform in target synthesis, the naturally occurring (amino)cyclitol Valienamine **81** was conveniently synthesized from trimethyl orthobenzoate **205** (**Scheme 27b**). The route began with the dearomatized-epoxidated cycloadduct **206**, which was then subjected to one pot cycloreversion to form the labile arenoxide, trapped in an acyl nitroso-Diels-Alder to yield the epoxide **207**. A sequence of DIBALH reduction, reductive N-O bond cleavage, and TBS protection of the primary alcohol, led to the *syn*-1,4-aminol motif in **208**. The *trans*-2,3-diol was introduced through a Boc-assisted intramolecular epoxide opening to the carbamate **209**. Once all the heteroatoms were set with the correct regio- and stereochemistry, Valienamine **81** was delivered by the simultaneous carbamate hydrolysis and TBS deprotection.

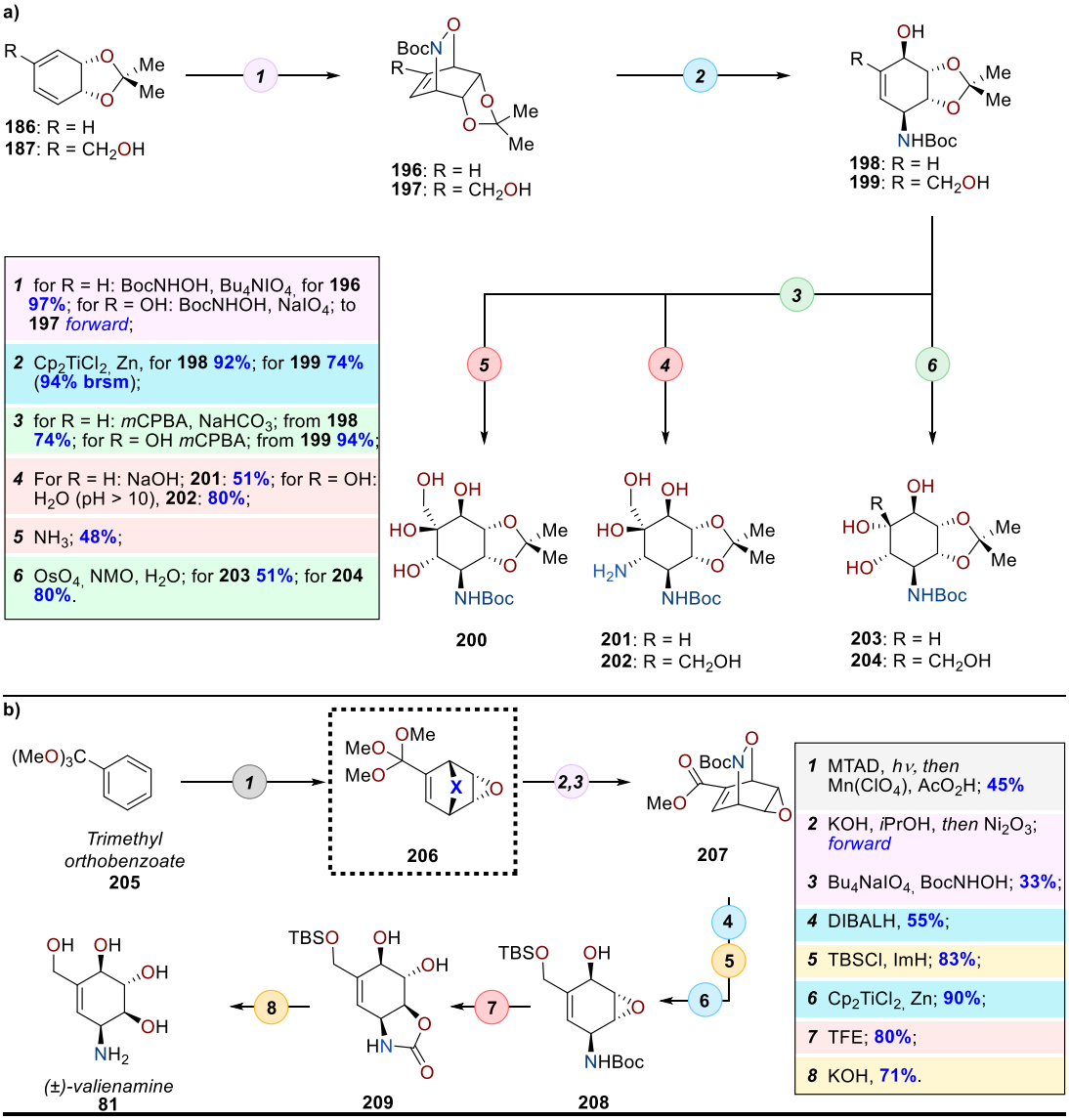

Scheme 27. a) Diversification of the dienes **186** and **187** into syn-1,4-aminols. **b)** Total synthesis of the naturally occurring C7 (amino)cyclitol (±)-valienamine **81**.

1.3.2.0 - Diversification of polyaromatics into sp^2-sp^3 hybrids (amino)cyclitol analogs

The synthetic campaign toward the sp^2-sp^3 hybrids began by establishing a reliable synthetic throughput of dearomatized cycloadducts (**Scheme 28**).

a) Dearomative diimide reduction:

SM	*Yield (%)*	*Scale (g)*	*Notes*
(*2*)	**56**	3.0	*not reported*
(*3*)	**54**	3.0	*not reported*
(*4*)	**56**	3.0	*reported (Ref. 10)*

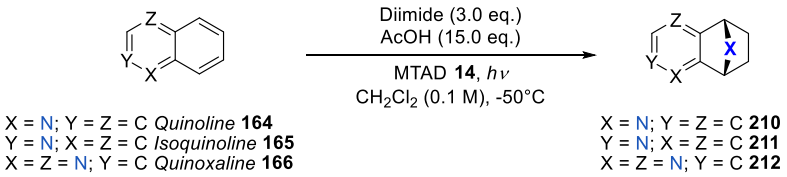

b) Dearomative dihydroxylation:

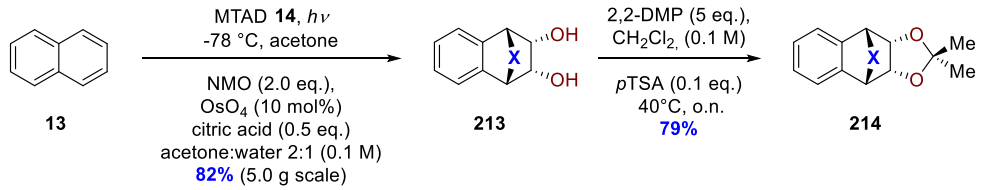

Scheme 28. Synthetic throughput of the dearomatized products from polyaromatics **a)** Dearomative diimide reduction, **b)** dearomative dihydroxylation.

Accordingly, the scope of dearomative diimide reduction was expanded to include previously unreported quinoline **164** and isoquinoline **165**. The already reported quinoxaline **166** was also chosen as a substrate.[28] The dearomative dihydroxylation is reported for naphthalene **13**,[10] the diol **213** was protected to yield acetal **214**. Unfortunately, attempts to achieve dearomatized diols were unsuccessful, possibly due to the tendency of these compounds to poison catalysts. All the dearomatizations were run smoothly on a multigram scale, furnishing the desired intermediates in a useful amount.

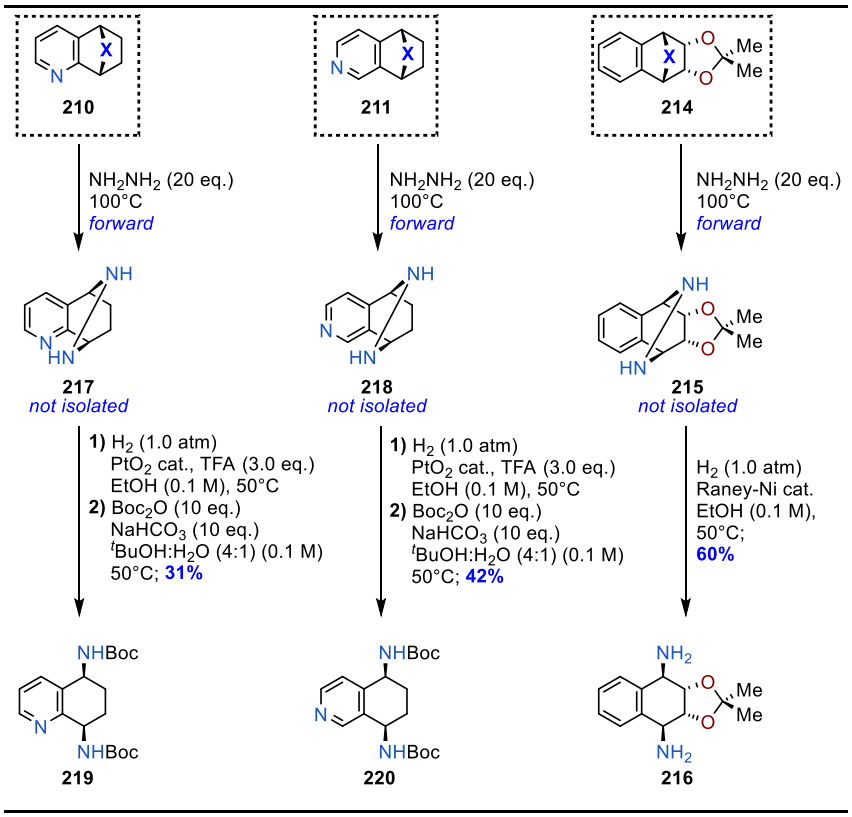

Scheme 29. Synthesis of syn-1,4-diamines from Quinoline, Isoquinoline, and Naphthalene derivatives.

As for the monoaromatics, the first aim was to deliver the *syn*-1,4-diamines using the bridging urazole as a diamine surrogate (**Scheme 29**). For this purpose, the naphthalene-derived diol **214** was treated with hydrazine, resulting in the hydrolysis of the bridging urazole residue from MTAD to form bridging hydrazine **215**; direct hydrogenation of the N-N bond produced diamine **216**. The same procedure was applied to the reduced adducts of quinoline **210** and isoquinoline **211**, obtaining two regioisomers characterized by a pyridinic ring condensed to the carbocycle. Their isolation, and characterization was strongly simplified by Boc protection, getting the protected diamines **219** and **220**.

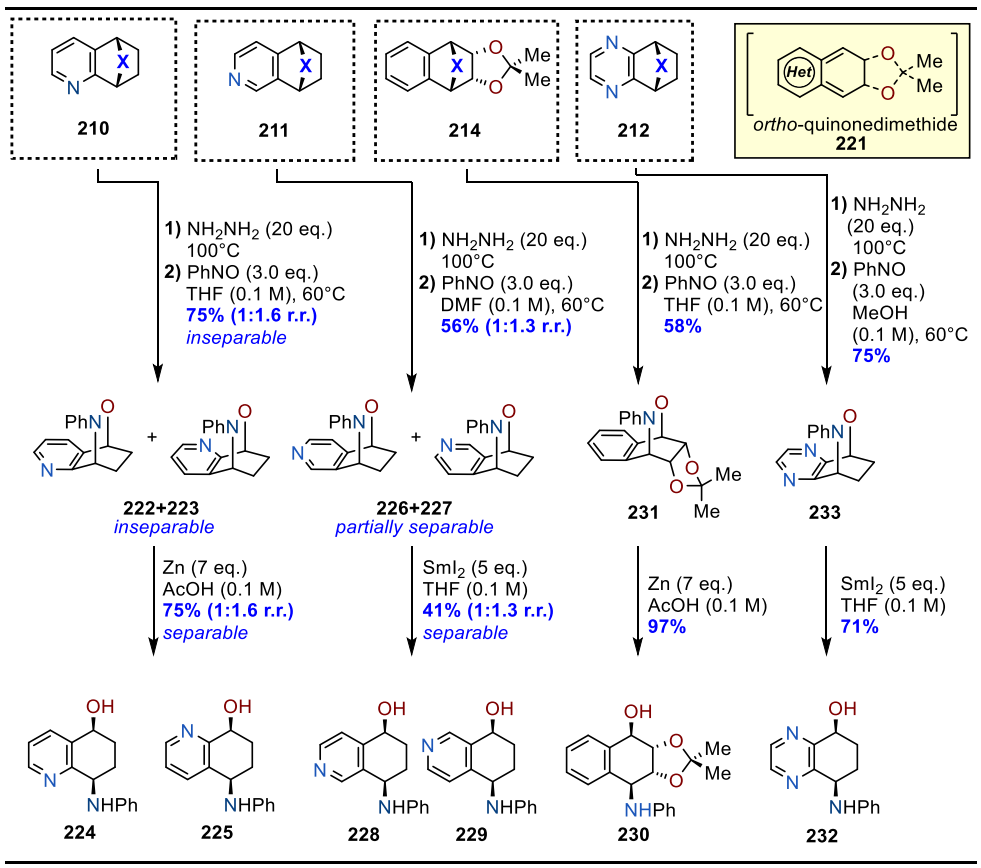

Scheme 30. Synthesis of *syn*-1,4-aminols from Quinoline, Isoquinoline, Quinoxaline, and Naphthalene derivatives.

Once the diamines were established, we moved to the introduction of *syn*-1,4-aminols (**Scheme 30**). Unlike the monoaromatics where dienes were delivered and isolated, urazole was used as a surrogate for labile *ortho*-quinodimethides **221** (**Scheme 30**, yellow box). Accordingly, the urazoles of the dearomative reduction products **210**, **211**, and **212,** and of the acetal **214** were hydrolyzed with hydrazine,

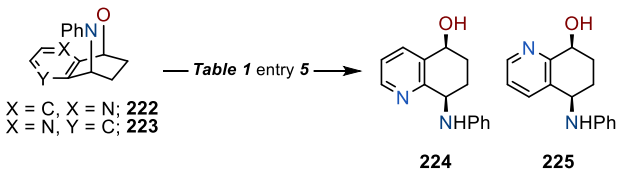

Table 1:

entry	*scale*	*conditions*	*notes*
1	20 mg	CuCl **(1.0 eq.)**, MeOH **(0.1 M)**, 80°C	degradation
2	20 mg	$TiCl_2Cp_2$ **(2.5 eq.)**, Zn **(5.0 eq.)**, CH_2Cl_2 **(0.1 M)**	degradation
3	20 mg	Ni-Raney, H_2 **(1 atm)**, EtOH **(0.1 M)**	no conversion
4	20 mg	Zn **(3.0 eq.)**, AcOH **(0.1 M)**	**Y = 70%**
5	500 mg	Zn **(3.0 eq.)**, AcOH **(0.1 M)**	**Y = 75% (1:1.16)**

Scheme 31. Optimization of the N-O cleavage of the mixture of cycloadducts **222** and **223**. **Table 1:** conditions used.

giving the bridging hydrazines, which were oxidized to diazines using nitroso benzene. The diazines spontaneously cyclorevert to the highly reactive *ortho*-quinodimethides **221**, which are later trapped in a nitroso-Diels-Alder by an excess of nitroso benzene. The reaction proved to be solvent-sensitive, with the best results obtained when the reaction was conducted in tetrahydrofuran for the quinoline and naphthalene derivates **210** and **214**, in dimethylformamide for the isoquinoline cycloadduct **211**, and methanol for the product of dearomative reduction of quinoxaline **212**. When the cycloadduct **210** was exposed to these conditions an inseparable mixture of the two cycloadducts **222** and **223** in a 1:1.6 ratio. A condition screening was necessary to identify the best ones for the N-O bond cleavage (**Scheme 31**). The reductive N-O bond opening with titanocene, which was previously applied for the monoaromatics, only lead to a complex mixture of dehydration and aniline elimination products (**Scheme 31**, Table 1, entry 2). The same disappointing result was obtained using coppler(I) chloride as a reducing agent, while the attempt at hydrogenative cleavage led to the recovery of the starting material. The delivering of aminols **224** and **225** was finally accomplished using zinc in acetic acid This reaction proved to be scalable, with practical scale up to 500 mg. Aminols **224** and **225** were easily separable chromatographically. Similarly, in the case of isoquinoline **165**, the nitroso-Diel-Alder did not result to be regioselective, giving a mixture of cycloadducts **226** and **227** Even in this case, the N-O bond opening has showed to be problematic (**Scheme 32**). The zinc in acetic acid protocol led only to the degradation of the

starting material (**Scheme 32**, Table 3 entry 1). Traces of the product were obtained through hydrogenation with nickel-Raney (**Scheme 32**, Table 1 entry 1), and a condition screening for hydrogenations resulted in no conversions (**Scheme 32**, Table 2 entries 2 and 4) or degradation (**Scheme 32**, Table 2 entries 3 and 5) of the starting material. Metal-based protocols were attempted, and a promising result was obtained using copper (I) chloride in methanol. However, the reaction scale-up affected dramatically the yield (**Scheme 32**, Table 3 entries 3 and 4). No conversion was observed after exposing the substrates to molybdenum carbonyl (**Scheme 32**, Table 3 entry 5). Finally, good results were obtained with samarium iodine (**Scheme 32**, Table 3 entry 6). The reaction led to the desired products with a yield above 50%

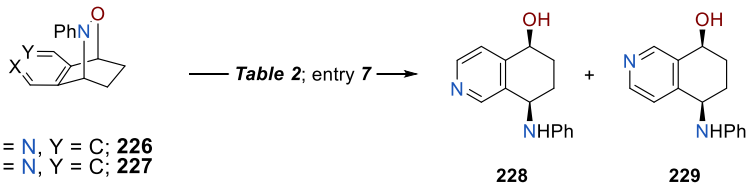

Table 2 Hydrogenations:

Entry	*Scale (mg)*	*Cat. (%m/m)*	*Solvent*	*Additive*	*T (°C)*	*Notes*
1	50 mg	Raney-Ni (10 %)	EtOH (0.2 M)	TFA (4.0 eq.)	r.t.; o.n.	C = 12%Traces of product
2	20 mg	Pd/C (10 %)	EtOH (0.2 M)	TFA (4.0 eq.)	r.t.; o.n.	no conversion
3	20 mg	Pd/C (10 %)	EtOH (0.2 M)	TFA (4.0 eq.)	50°C; o.n.	degradation
4	20 mg	PtO_2 (10 %)	MeOH (0.2 M)	-	r.t.; o.n.	C = 17%, degr.
5	20 mg	PtO_2 (10 %)	MeOH (0.2 M)	TFA (1.5 eq.)	r.t.; o.n.	degradation

Table 3 Metals reductions:

Entry	*Scale (mg)*	*Reagents*	*Solvent*	*T (°C)*	*Notes*
1	10 mg	Zn (3.0 eq.)	AcOH (0.1 M)	r.t., 4h	degradation
2	10 mg	Zn (1.5 eq.), HCl (40 eq.)	MeOH (0.05 M)	r.t., o.n.	degradation
3	10 mg	CuCl (1.0 eq.)	MeOH (0. 2 M)	70°C, o.n.	**Y = 35%**
4	50 mg	CuCl (1.0 eq.)	MeOH (0.2 M)	70°C, o.n.	degradation
5	10 mg	$Mo(CO)_6$ (1.5 eq.)	CH_3CN wet (0.1 M)	80°C, o.n.	no conversion
6	10 mg	$SmI_2^{0.1\ M,THF}$ (5.0 eq.)	THF (0.1 M)	-78°C to r.t., o.n.	**Y = 56%**
7	500 mg	$SmI_2^{0.1\ M,THF}$ (5.0 eq.)	THF (0.1 M)	-78°C to r.t., o.n.	**Y = 41%; (1:1.2)**

Scheme 32. Optimization of the N-O cleavage of the mixture of cycloadduts **226** and **227**. **Table 2:** Hydrogenations tested. **Table 3:** Metals reductions used.

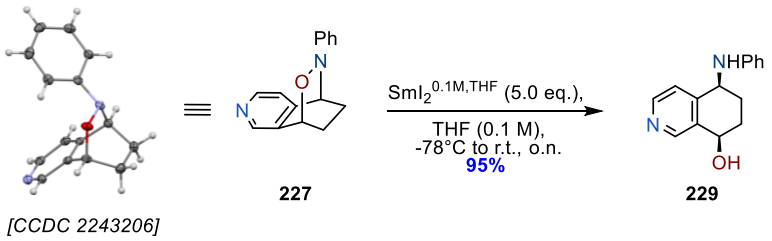

Scheme 33. Crystal structure of **227**. I's N-O opening deliver **229** demonstrating its structure.

on the screening scale, resulting to be scalable with only a minimal yield decrease.

The regioisomer **227** was partially crystallized from the mixture with **226**, obtaining its crystal structure (**Scheme 33**). Exposure of **227** to samarium iodine delivered the *syn*-1,4-aminol **229**, confirming its structure as previously attributed by 2D-NMRs. From quinoline **164** and isoquinoline **165**, a library of sp^2-sp^3 adducts characterized by the presence of condensed pyridinic rings was obtained. The benzene condensed cyclohexane **230** was yielded from the nitroso-naphthalene cycloadduct **231** using zinc in acetic acid, while the pyrazine-containing hybrid **232** was delivered in good yield only when samarium iodine was employed (**Scheme 30**).

1.4.0.0 - Conclusions

In summary, a diversification platform has been developed exploiting the arenophile chemistry to achieve decorated cyclohexanes, utilizing simple and abundant arenes as templates. The dearomatized intermediates were diversified through strategic and iterative olefin transformations, permitting a rapid expansion of the explored chemical space. More than 30 natural and non-natural (amino)cyclitols have been obtained, including C6 and C7 (amino)aminocyclitols. Furthermore, a library of medicinal chemistry-relevant sp^2-sp^3 arenes-cyclohexanes hybrids was synthesized from naphthalene, quinoline, isoquinoline, and quinoxaline. Overall, the platform makes accessible a wide breath of chemical space, which includes regions of interest and/or relatively unexplored in drug discovery (see Principal Moment of Inertia analysis **Section 1.6.4.0**). This platform could facilitate chemical biology studies on (amino)cyclitols fragments as well as the synthesis of natural products containing heavily decorated cyclohexanes.

1.5.0.0 - References

(1) Huck, C. J. Shaping Molecular Landscapes: Recent Advances, Opportunities, and Challenges in Dearomatization. *Shap. Mol. Landsc. Recent Adv. Oppor. Chall. Dearomatization* **2020**, *6*, 1589–1603. https://doi.org/10.1016/j.chempr.2020.06.015.

(2) Wertjes, W. C. Recent Advances in Chemical Dearomatization of Nonactivated Arenes. *Chem Soc Rev* **2018**.

(3) Lovering, F.; Bikker, J.; Humblet, C. Escape from Flatland: Increasing Saturation as an Approach to Improving Clinical Success. *J. Med. Chem.* **2009**, *52* (21), 6752–6756. https://doi.org/10.1021/jm901241e.

(4) Huck, C. J. Dearomative Logic in Natural Product Total Synthesis. *Nat. Prod. Rep.* **2022**.

(5) Wender, P. A.; Howbert, J. J. Synthetic Studies on Arene-Olefin Cycloadditions: Total Synthesis of (.+-.)-.Alpha.-Cedrene. *J. Am. Chem. Soc.* **1981**, *103* (3), 688–690. https://doi.org/10.1021/ja00393a041.

(6) Hsu, D.-S.; Liao, C.-C. First Total Syntheses of (±)-Penicillones A and B. *Org. Lett.* **2007**, *9* (22), 4563–4565. https://doi.org/10.1021/ol702062p.

(7) Tang, C.; Okumura, M.; Zhu, Y.; Hooper, A. R.; Zhou, Y.; Lee, Y.-H.; Sarlah, D. Palladium-Catalyzed Dearomative Syn-1,4-Carboamination with Grignard Reagents. *Angew Chem Int Ed* **2019**, 5.

(8) Owens, K. R.; McCowen, S. V.; Blackford, K. A.; Ueno, S.; Hirooka, Y.; Weber, M.; Sarpong, R. Total Synthesis of the Diterpenoid Alkaloid Arcutinidine Using a Strategy Inspired by Chemical Network Analysis. *J. Am. Chem. Soc.* **2019**, *141* (35), 13713–13717. https://doi.org/10.1021/jacs.9b05815.

(9) Palframan, M. J.; Kociok-Köhn, G.; Lewis, S. E. Photooxygenation of a Microbial Arene Oxidation Product and Regioselective Kornblum–DeLaMare Rearrangement: Total Synthesis of Zeylenols and Zeylenones. *Chem. – Eur. J.* **2012**, *18* (15), 4766–4774. https://doi.org/10.1002/chem.201104035.

(10) Southgate, E. H. Dearomative Dihydroxylation with Arenophiles. *Nat. Chem.* **2016**, *8*.

(11) Greene, F. D.; Misrock, S. L.; Wolfe, J. R. The Structure of Anthracene Photodimers. *J. Am. Chem. Soc.* **1955**, *77* (14), 3852–3855. https://doi.org/10.1021/ja01619a051.

(12) Albini, A.; Giannantonio, L. Photochemical Dimerization and Cross Cycloaddition of 2-Naphthalenecarbonitrile. *J. Org. Chem.* **1984**, *49* (20), 3862–3863. https://doi.org/10.1021/jo00194a049.

(13) Breton, G. W.; Vang, X. Photodimerization of Anthracene. *J. Chem. Educ.* **1998**, *75* (1), 81. https://doi.org/10.1021/ed075p81.

(14) Bouas-Laurent, H.; Castellan, A.; Desvergne, J.-P.; Lapouyade, R. Photodimerization of Anthracenes in Fluid Solution:Structural Aspects. *Chem. Soc. Rev.* **2000**, *29* (1), 43–55. https://doi.org/10.1039/A801821I.
(15) Islangulov, R. R.; Castellano, F. N. Photochemical Upconversion: Anthracene Dimerization Sensitized to Visible Light by a RuII Chromophore. *Angew. Chem.* **2006**, *118* (36), 6103–6105. https://doi.org/10.1002/ange.200601615.
(16) Zouev, I.; Cao, D.-K.; Sreevidya, T. V.; Telzhensky, M.; Botoshansky, M.; Kaftory, M. Photodimerization of Anthracene Derivatives in Their Neat Solid State and in Solid Molecular Compounds. *CrystEngComm* **2011**, *13* (13), 4376–4381. https://doi.org/10.1039/C0CE00739K.
(17) Salzillo, T.; Venuti, E.; Femoni, C.; Della Valle, R. G.; Tarroni, R.; Brillante, A. Crystal Structure of the 9-Anthracene–Carboxylic Acid Photochemical Dimer and Its Solvates by X-Ray Diffraction and Raman Microscopy. *Cryst. Growth Des.* **2017**, *17* (6), 3361–3370. https://doi.org/10.1021/acs.cgd.7b00333.
(18) Remy, R.; Bochet, C. G. Arene–Alkene Cycloaddition. *Chem. Rev.* **2016**, *116* (17), 9816–9849. https://doi.org/10.1021/acs.chemrev.6b00005.
(19) Streit, U.; Bochet, C. G. The Arene–Alkene Photocycloaddition. *Beilstein J Org Chem* **2011**.
(20) Baralotto, C.; Chanon, M.; Julliard, M. Total Synthesis of the Tricyclic Sesquiterpene (±)-Ceratopicanol. An Illustration of the Holosynthon Concept. *J. Org. Chem.* **1996**, *61* (11), 3576–3577. https://doi.org/10.1021/jo960382k.
(21) Kjell, D. P.; Sheridan, R. S. Photochemical Cycloaddition of N-Methyltriazolinedione to Naphthalene. *J. Am. Chem. Soc.* **1984**, *106* (18), 5368–5370. https://doi.org/10.1021/ja00330a065.
(22) Hamrock, S. J.; Sheridan, R. S. Para Photoaddition of N-Methyltriazolinedione to Benzene. Synthesis of Energy-Rich Azo Compounds Comprising Benzene + Nitrogen. *J. Am. Chem. Soc.* **1989**, *111* (26), 9247–9249. https://doi.org/10.1021/ja00208a028.
(23) De Bruycker, K.; Billiet, S.; Houck, H. A.; Chattopadhyay, S.; Winne, J. M.; Du Prez, F. E. Triazolinediones as Highly Enabling Synthetic Tools. *Chem. Rev.* **2016**, *116* (6), 3919–3974. https://doi.org/10.1021/acs.chemrev.5b00599.
(24) Kjell, D. P.; Sheridan, R. S. A Photochemical Diels—Alder Reaction of N-Methyltriazolinedione. *J. Photochem.* **1985**, *28* (2), 205–214. https://doi.org/10.1016/0047-2670(85)87032-5.
(25) Hamrock, S. J.; Sheridan, R. S. Photochemical Diels-Alder Addition of N-Methyltriazolinedione to Phenanthrene. *Tetrahedron Lett.* **1988**, *29* (43), 5509–5512. https://doi.org/10.1016/S0040-4039(00)80799-6.
(26) Breton, G. W.; Newton, K. A. Further Studies of the Thermal and Photochemical Diels−Alder Reactions of *N* -Methyl-1,2,4-Triazoline-3,5-Dione (MeTAD) with Naphthalene and Some Substituted Naphthalenes. *J. Org. Chem.* **2000**, *65* (10), 2863–2869. https://doi.org/10.1021/jo9906429.

(27) Breton, G. W.; Hoke, K. R. Application of Radical Cation Spin Density Maps toward the Prediction of Photochemical Reactivity between *N* -Methyl-1,2,4-Triazoline-3,5-Dione and Substituted Benzenes. *J. Org. Chem.* **2013**, *78* (10), 4697–4707. https://doi.org/10.1021/jo4001417.
(28) Mikiko Okumura. Arenophile-Mediated Dearomative Reduction. *Angew. Chem. Int. Ed.*
(29) Hernandez, L. W.; Klöckner, U.; Pospech, J.; Hauss, L.; Sarlah, D. Nickel-Catalyzed Dearomative *Trans* -1,2-Carboamination. *J. Am. Chem. Soc.* **2018**, *140* (13), 4503–4507. https://doi.org/10.1021/jacs.8b01726.
(30) Okumura, M.; Nakamata Huynh, S. M.; Pospech, J.; Sarlah, D. Arenophile-Mediated Dearomative Reduction. *Angew. Chem. Int. Ed.* **2016**, *55* (51), 15910–15914. https://doi.org/10.1002/anie.201609686.
(31) Tang, C.; Okumura, M.; Deng, H.; Sarlah, D. Palladium-Catalyzed Dearomative Syn-1,4-Oxyamination. *Angew Chem* **2019**, 5.
(32) Wertjes, W. C.; Okumura, M.; Sarlah, D. Palladium-Catalyzed Dearomative *Syn* -1,4-Diamination. *J. Am. Chem. Soc.* **2019**, *141* (1), 163–167. https://doi.org/10.1021/jacs.8b13030.
(33) Siddiqi, Z.; Wertjes, W. C.; Sarlah, D. Chemical Equivalent of Arene Monooxygenases: Dearomative Synthesis of Arene Oxides and Oxepines. *J. Am. Chem. Soc.* **2020**, *142* (22), 10125–10131. https://doi.org/10.1021/jacs.0c02724.
(34) Davis, C. W.; Bingham, T. W.; Okumura, M.; Sarlah, D. Dearomative Syn-1,2-Diamination of Benzene and Naphthalene. *Synthesis* **2021**, *53* (22), 4290–4296. https://doi.org/10.1055/s-0040-1719842.
(35) Piacentini, P.; Bingham, T. W.; Sarlah, D. Dearomative Ring Expansion of Polycyclic Arenes. *Angew. Chem. Int. Ed.* **2022**, *61* (36), e202208014. https://doi.org/10.1002/anie.202208014.
(36) Southgate, E. H.; Holycross, D. R.; Sarlah, D. Total Synthesis of Lycoricidine and Narciclasine by Chemical Dearomatization of Bromobenzene. *Angew. Chem. Int. Ed.* **2017**, *56* (47), 15049–15052. https://doi.org/10.1002/anie.201709712.
(37) Okumura, M.; Shved, A. S.; Sarlah, D. Palladium-Catalyzed Dearomative *Syn* -1,4-Carboamination. *J. Am. Chem. Soc.* **2017**, *139* (49), 17787–17790. https://doi.org/10.1021/jacs.7b11663.
(38) Hernandez, L. W.; Pospech, J.; Klöckner, U.; Bingham, T. W.; Sarlah, D. Synthesis of (+)-Pancratistatins via Catalytic Desymmetrization of Benzene. *J. Am. Chem. Soc.* **2017**, *139* (44), 15656–15659. https://doi.org/10.1021/jacs.7b10351.
(39) Dennis, D. G.; Okumura, M.; Sarlah, D. Synthesis of (±)-Idarubicinone via Global Functionalization of Tetracene. *J. Am. Chem. Soc.* **2019**, *141* (26), 10193–10198. https://doi.org/10.1021/jacs.9b05370.
(40) L., D.; A., D. Medicinal Chemistry of Aminocyclitols. *Curr. Med. Chem.* **2010**, *17* (22), 2393–2418.

(41) Delgado, A. Recent Advances in the Chemistry of Aminocyclitols. *Eur. J. Org. Chem.* **2008**, *2008* (23), 3893–3906. https://doi.org/10.1002/ejoc.200800238.
(42) Salamci, E. Recent Developments Concerned with the Synthesis of Aminocyclitols. *Tetrahedron Lett.* **2020**, *61* (15), 151728. https://doi.org/10.1016/j.tetlet.2020.151728.
(43) Chen, X.; Zheng, Y.; Shen, Y. Voglibose (Basen®, AO-128), One of the Most Important α-Glucosidase Inhibitors. *Curr. Med. Chem.* **2006**, *13* (1), 109–116. https://doi.org/10.2174/092986706789803035.
(44) Becker, B.; Cooper, M. A. Aminoglycoside Antibiotics in the 21st Century. *ACS Chem. Biol.* **2013**, *8* (1), 105–115. https://doi.org/10.1021/cb3005116.
(45) Pettit, G. R.; Gaddamidi, V.; Cragg, G. M. Antineoplastic Agents, 105. Zephyranthes Grandiflora. *J. Nat. Prod.* **1984**, *47* (6), 1018–1020. https://doi.org/10.1021/np50036a020.
(46) Davies, J.; Wright, G. D. Bacterial Resistance to Aminoglycoside Antibiotics. *Trends Microbiol.* **1997**, *5* (6), 234–240. https://doi.org/10.1016/S0966-842X(97)01033-0.
(47) Castellanos, L.; Cléophax, J.; Colas, C.; Gero, S. D.; Leboul, J.; Mercier, D.; Olesker, A.; Rolland, A.; Quiclet-Sire, B.; Sepulchre, A.-M. Synthesis of Aminocyclitols from L-Quinic Acid. *Carbohydr. Res.* **1980**, *82* (2), 283–301. https://doi.org/10.1016/S0008-6215(00)85704-3.
(48) Li, Q. R.; Kim, S. I.; Park, S. J.; Yang, H. R.; Baek, A. R.; Kim, I. S.; Jung, Y. H. Total Synthesis of (þ)-Valienamine and (À)-1-Epi-Valienamine via a Highly Diastereoselective Allylic Amination of Cyclic Polybenzyl Ether Using Chlorosulfonyl Isocyanate. **2013**.
(49) Alegret, C.; Benet-Buchholz, J.; Riera, A. Stereodivergent Syntheses of Conduramines and Aminocyclitols. *Org. Lett.* **2006**, *8* (14), 3069–3072. https://doi.org/10.1021/ol061022e.
(50) Harada, S.; Li, K.; Kino, R.; Takeda, T.; Wu, C.-H.; Hiraoka, S.; Nishida, A. Construction of Optically Active Isotwistanes and Aminocyclitols Using Chiral Cyclohexadiene as a Common Intermediate. *Chem. Pharm. Bull. (Tokyo)* **2016**, *64* (10), 1474–1483. https://doi.org/10.1248/cpb.c16-00431.
(51) de la Sovera, V.; Garay, P.; Thevenet, N.; Macías, M. A.; González, D.; Seoane, G.; Carrera, I. Novel Chemoenzymatic Synthesis of an Enantiopure Allo-Inosamine Hexaacetate from Benzyl Azide. *Tetrahedron Lett.* **2016**, *57* (23), 2484–2487. https://doi.org/10.1016/j.tetlet.2016.04.072.
(52) Dlugosch, M.; Ma, X.; Yang, S.; Banwell, M. G.; Ma, C.; Ward, J. S.; Carr, P. Syntheses of Structurally and Stereochemically Varied Forms of C_7N Aminocyclitol Derivatives from Enzymatically Derived and Homochiral *Cis* -1,2-Dihydrocatechols. *Org. Lett.* **2018**, *20* (22), 7225–7228. https://doi.org/10.1021/acs.orglett.8b03149.

(53) Carrau, G.; Bellomo, A. I.; Suescun, L.; Gonzalez, D. Chemoenzymatic Synthesis of Hygromycin Aminocyclitol Moiety and Its C2 Epimer. *Eur. J. Org. Chem.* **2019**, *2019* (4), 788–802. https://doi.org/10.1002/ejoc.201801424.
(54) Chakraborty, C.; Vyavahare, V. P.; Dhavale, D. D. Intra-Molecular Nitrone–Olefin Cycloaddition of D-Glucose Derived Allylic Alcohol: Synthesis of New Aminocyclohexitols. **2007**.
(55) Kumar, B. S. Synthesis of Some Carbahexopyranoses Using Mn/CrCl3 Mediated Domino Reactions and Ring Closing Metathesis. **2016**.
(56) Harit, V. K.; Ramesh, N. G. A Chiron Approach to Diversity-Oriented Synthesis of Aminocyclitols, (−)-Conduramine F-4 and Polyhydroxyaminoazepanes from a Common Precursor. *J. Org. Chem.* **2016**, *81* (23), 11574–11586. https://doi.org/10.1021/acs.joc.6b01790.
(57) Katakam, R. Stereoselective Synthesis of N-Benzyl Conduramine F-1, N-Benzyl Ent-Conduramine E-1, Dihydroconduramine F-1 and Ent-Dihydroconduramine E-1. *Tetrahedron Lett.* **2017**.
(58) Taher, E. S.; Banwell, M. G.; Buckler, J. N.; Yan, Q.; Lan, P. The Exploitation of Enzymatically-Derived Cis-1,2-Dihydrocatechols and Related Compounds in the Synthesis of Biologically Active Natural Products. *Chem. Rec.* **2018**, *18* (2), 239–264. https://doi.org/10.1002/tcr.201700064.

1.6.0.0 - Experimental section

1.6.1.0 - Material and methods

1.6.1.1 - General procedures

Unless otherwise noted, all reactions were carried out under an ambient atmosphere. All chemicals were purchased from commercial suppliers and used as received. *N*-Methyl-1,2,4-triazoline-3,5-dione (MTAD) was prepared based on the literature procedure[1] and was resublimed before use. Raney®-Nickel was bought from Sigma Aldrich. Dry dichloromethane (CH_2Cl_2), ethyl acetate (EtOAc) and tetrahydrofuran (THF) were obtained by passing commercially available anhydrous, oxygen-free HPLC-grade solvents through activated alumina columns. Analytical thin-layer chromatography was performed on Merck silica gel 60 F254 aluminum plates. Visualization was accomplished with UV light and/or potassium permanganate ($KMnO_4$). Retention factor (R_f) values reported were measured using a 5 × 2 cm TLC plate in a developing chamber containing the solvent system described. Flash column chromatography was performed using Silicycle SiliaFlash® P60 (SiO_2, 40-63 µm particle size, 230-400 mesh). ^{1}H and ^{13}C NMR spectra were recorded on Bruker 400 (400 MHz, ^{1}H; 101 MHz, ^{13}C), Bruker 500 (500 MHz, ^{1}H; 126 MHz, ^{13}C), Varian Unity Inova 500 (500 MHz, ^{1}H; 126 MHz, ^{13}C), or Varian 600 (600 MHz, ^{1}H; 151 MHz, ^{13}C) spectrometers. Spectra are referenced to residual chloroform (δ = 7.26 ppm, ^{1}H;

[1] Siddiqi Z. *et al., Org. Process Res. Dev.* **2020**, 24, *12*, 2953–2959.

77.16 ppm, ^{13}C), residual methanol (δ = 3.31 ppm, ^{1}H; 49.00 ppm, ^{13}C), residual benzene (δ = 7.16 ppm, ^{1}H; 128.06 ppm, ^{13}C), residual H_2O (δ = 4.76 ppm, ^{1}H) or residual dimethyl sulfoxide (δ = 2.50 ppm, ^{1}H; 39.5 ppm, ^{13}C). Chemical shifts are reported in parts per million (ppm). Multiplicities are indicated by s (singlet), d (doublet), t (triplet), q (quartet), m (multiplet), and br (broad). Coupling constants J are reported in Hertz (Hz). Mass spectrometry (MS) was performed either by the University of Illinois Mass Spectrometry Laboratory or at the University of Pavia. Electrospray ionization (ESI+) spectra were performed using a time-of-flight (TOF) mass analyzer. Data are reported in the form of m/z (intensity relative to the base peak = 100). Infrared spectra were measured neat on either a Perkin-Elmer spectrum BX FT-IR spectrometer or Agilent Cary 630 FTIR with ATR. Peaks are reported in cm^{-1} with indicated relative intensities: s (strong, 0–33% T); m (medium, 34–66% T), w (weak, 67–100% T), and br (broad). Visible-light spectrum of LED was recorded using an Avantes Sensline Avaspec-ULS TEC Spectrometer. Melting points of solids, compounds that solidified after chromatography, were measured on a Buchi B-540 melting point apparatus and are uncorrected. The x-ray diffraction experiments were conducted using Bruker D8 Venture/Photon 100 diffractometer or Bruker APEX-II CCD diffractometer. Using Olex the structure was solved with ShelXT7 structure solution program using Intrinsic Phasing solution method, and the XL8 refinement package using Least Squares minimization.

1.6.1.2 - Abbreviations

MTAD = 4-Methyl-1,2,4-triazoline-3,5-dione, THF = tetrahydrofuran, DMF = *N*,*N*-Dimethylformamide, DMSO = Dimethylsulfoxide, *m*CPBA = *meta*-3-chloroperbenzoic acid, TBSCl = *tert*-butyldimethylsilyl chloride, 2,2-DMP = 2,2-dimethoxypropane, DMAP = 4-dimethylaminopyridine.

1.6.1.3 - Photochemical Set-Up

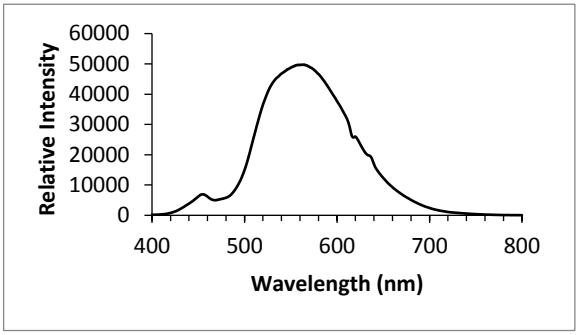

Figure S2. Spectrum of LED bulb used.

LED light source: Generic cool white light LED corn bulbs were used for the photochemical experiments. These can be obtained from several manufactures over amazon.com and proved to give consistent results as well as identical visible spectra. Detailed info:

Socket: G4

LED Chip: 48 LEDs SMD 2835

Consume wattage: 4W

Input voltage: AC / DC 12V

Beam degree: 360 degrees

Color temperature: 6500K (Cool White)

Initial Lumens (lm): 290

Figure S3. LED bulb used.

1.6.1.4 - Photochemical set-up for small scale reactions (up to 2.0 mmol scale)

Five 4 W LED corn bulbs (12V, cool white light 6500K) were wired to a suitable 12V power supply, then sealed into test tubes and capped with septa (Picture S1). Lights and reaction tubes were arranged in a carrousel fashion for maximal exposure of each reaction vessel to light source and were submerged in a −78°C bath. Generally, up to four 0.2-2.0 mmol scale reactions can be run in the same bath using five 4 W lamps.

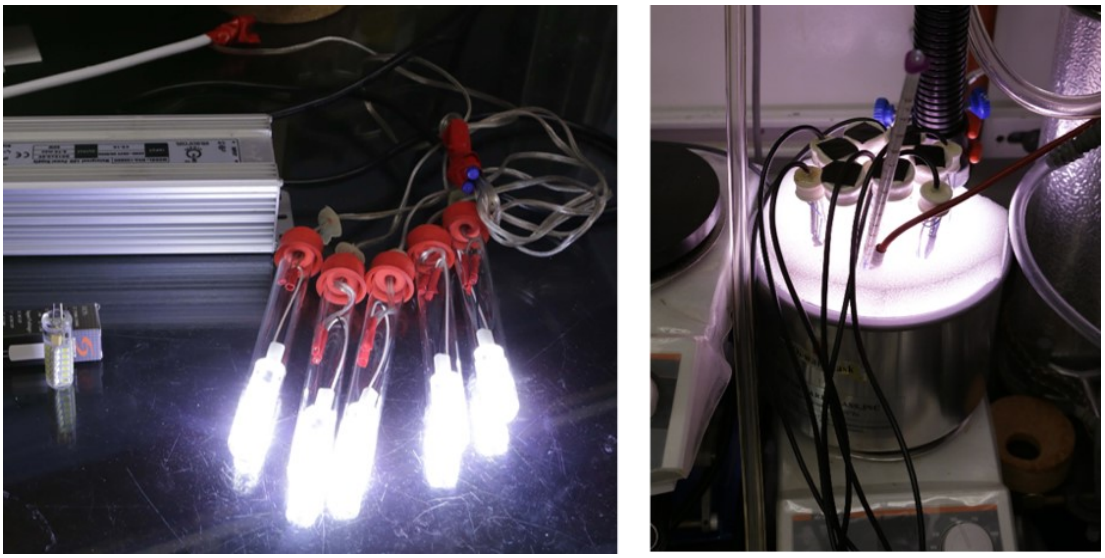

Picture 1. Assembly of LED bulbs for small-scale photochemical reactions.

1.6.1.5 - Photochemical set-up for medium scale reactions (up to 25 mmol scale)

Eight 4 W LED corn bulbs (12V, cool white light 6500K) were wired to a suitable 12V power supply, then sealed into test tubes and capped with septa. Lights were arranged in a carrousel fashion around a 500 mL Schlenk flask. The whole set-up was kept submerged in a −78°C bath during the photochemical reaction.

1.6.2.0 - Procedures

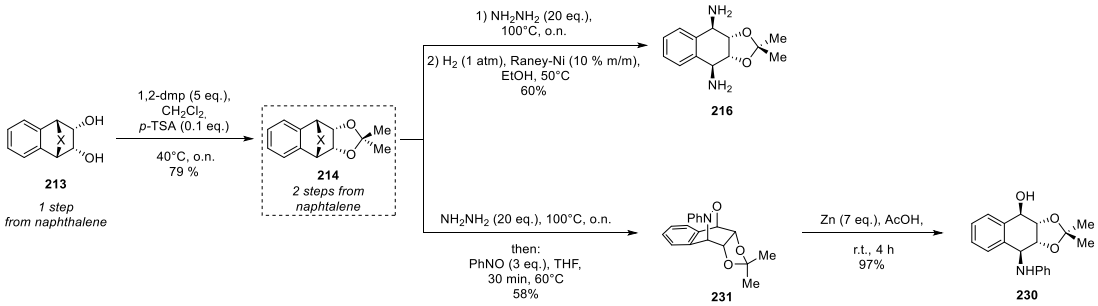

Scheme S1. Conversion of intermediate **214** to **216** and **230.**

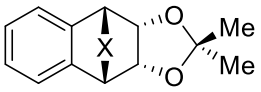

214

1.6.2.1 - Acetonide 214. To a solution of diol **213** (3.0 g, 11.0 mmol, 1.0 eq.)[1] in CH_2Cl_2 (44.0 mL, 0.25 M) was added 2,2-dimethoxypropane (6.7 mL, 54.0 mmol, 5.0 eq.) and *p*-toluenesulfonic acid monohydrate (210.0 mg, 1.1 mmol, 0.1 eq.). The reaction mixture was heated and stirred at 40°C under a nitrogen atmosphere overnight. The reaction was cooled, diluted with CH_2Cl_2 and washed with aqueous NaOH (0.2 M, 2 × 30 mL) and the combined aqueous layers were extracted with CH_2Cl_2 (3 × 100 mL). The combined organic layers were dried with anhydrous $MgSO_4$, filtered, and concentrated *in vacuo*. The crude organics were purified *via* column chromatography (SiO_2, 10:1 – 7:3 *n*-hexane:EtOAc mixture) to afford **214** (3.0 g, 9.5 mmol, 87%) as a white solid.

R_f 0.3 (*n*-hexane:EtOAc = 10:1, UV).

^{1}H NMR (500 MHz, $CDCl_3$) δ 7.40 (m, 4H), 5.41 (s, 2H), 4.80 (s, 2H), 2.87 (s, 3H), 1.27 (s, 3H), 0.60 (s, 3H).

^{13}C NMR (101 MHz, $CDCl_3$) δ 156.6, 131.4, 129.3, 126.5, 112.4, 74.1, 56.2, 25.7, 25.5, 25.4.

[1] Sarlah D. *et al., Nature Chem,* **2016**, *8*, 922–928.

IR (ATR, neat, cm^{-1}): 3009 (w), 2980 (w), 2932 (w), 1769 (m), 1700 (s), 1453 (s), 1375 (s), 1212 (s) 1075 (s), 862 (m), 750 (s), 556 (s).

HRMS (EI+/TOF, m/z) calcd. For $C_{16}H_{18}N_3O_4^+$ $[M+H]^+$ calc.: 316.1297; found: 316.1296.

m.p. 235 – 236°C.

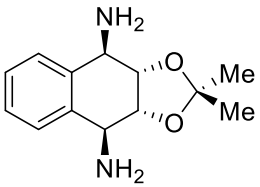

216

1.6.2.2 - Diamine 216. The experimental procedure was adjusted from a reported protocol.[1] A mixture of the acetonide protected cycloadduct **214** (200 mg, 0.8 mmol, 1.0 eq.) and anhydrous hydrazine (0.520 mL, 16.4 mmol, 20 eq.) was stirred at 100°C until full conversion of the cycloadduct was observed (around 16 h). The reaction was allowed to cool to 50°C and volatiles were removed *in vacuo*. Ethanol (4.1 mL, 0.2 M) was added under a hydrogen atmosphere (balloon) followed by Raney®-Nickel (400 μL, W.R. Grace and Co. Raney® 2400, slurry, in H_2O). The resulting mixture was stirred under a hydrogen atmosphere at 50°C for 8 h, then filtered through a plug of celite. The resulting crude material purified purified *via* column chromatography (SiO_2; 5% - 40% MeOH in CH_2Cl_2) to provide the title compound **216** (89.8 mg, 60%) as a colorless foam.

R_f 0.2 (*n*-hexane:EtOAc = 3:7, UV, $KMnO_4$).

^{1}H NMR (500 MHz, MeOD) δ 7.40 (ddd, *J* = 45.3, 5.5, 3.3 Hz, 4H), 4.12 (dd, *J* = 4.6, 1.8 Hz, 2H), 3.95 (dd, *J* = 4.7, 1.9 Hz, 2H), 1.38 (s, 3H), 1.37 (s, 3H).

[1] Sarlah D. *et al., Nature Chem,* **2016**, *8*, 922–928.

^{13}C NMR (126 MHz, MeOD) δ 137.9, 128.6, 126.0, 111.0, 81.4, 55.0, 27.2, 24.6.

IR (ATR, neat, cm^{-1}): 3359 (m), 3293 (m), 2985 (m), 2893 (m), 1666 (m), 1599 (w), 1373 (m), 1208 (s), 1162 (m), 1047 (s), 874 (w), 824 (w), 747 (s), 519 (m).

HRMS (EI+/TOF, m/z) calcd. For $C_{13}H_{19}N_2O_2^+$ $[M+H]^+$ calc.: 235.1447; found: 235.1447.

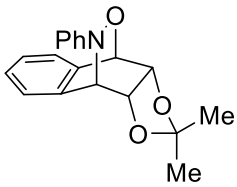

231

1.6.2.3 - Cycloadduct 231. The procedure was adjusted from a reported protocol.[1] The acetonide **214** (500 mg, 1.59 mmol, 1.0 eq.) was refluxed in hydrazine (1.54 mL,31.7 mmol, 20 eq.) at 100°C until full conversion of the cycloadduct was observed (around 16 h). Volatiles were removed *in vacuo*[2] and the residue was dissolved in dry tetrahydrofuran (7.9 mL). Nitrosobenzene (510 mg, 4.76 mmol, 3.0 eq.) was added and the reaction mixture was stirred at 60°C for 30 min. The crude product was purified by flash chromatography (SiO_2, 10:1-7:3 hexane:EtOAc) to provide the title compound **231** (285 mg, 58%) as a white solid.

R_f 0.3 (*n*-hexane:EtOAc = 10:1, UV).

^{1}H NMR (500 MHz, $CDCl_3$) δ 7.33 (m, 2H), 7.24 (m, 1H), 7.1 (m, 2H), 7.04 (dd, J = 7.37, 1.1 Hz, 1H), 6.85 (m,3H), 5.33 (d, J = 4.55 Hz, 2H), 4.96 (m, 2H), 4.85 (dd, J = 6.62, 4.6 Hz, 1H), 1.28 (s, 3H), 0.62 (s, 3H).

---

[1] Okumura M. *et al. Angew. Chem. Int. Ed.* **2016**, *55*,15910–15914.

[2] *It has been observed that elimination of hydrazine became difficult on scales larger than 500 mg. Residual hydrazine can consume nitrosobenzene, so multiple azeotropic evaporations with toluene are recommended.*

^{13}C NMR (126 MHz, $CDCl_3$) δ 150.7, 133.9, 131.6, 128.6, 128.1, 126.8, 125.8, 123.0, 117.7, 110.9, 73.8, 74.0, 73.6, 25.5, 25.6.

IR (ATR, neat, cm^{-1}): 3076 (w), 3035 (w), 2932 (m), 1582 (m), 1486 (s), 1374 (s), 1260 (s), 1064 (s), 751 (s), 688 (s), 630 (m), 576 (s), 524 (s).

HRMS (EI+/TOF, m/z) calcd. For $C_{19}H_{20}NO_3^+$ $[M+H]^+$ calc.: 310.1443; found: 310.1439.

m.p. 167 – 168°C.

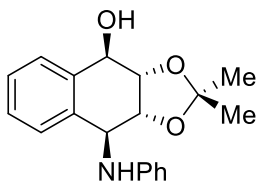

230

1.6.2.4 - Alcohol 230. To a solution of the benzene condensed cycloadduct **231** (93.2 mg 0.30 mmol, 1.00 eq.) in glacial acetic acid (1.0 mL, 0.3 M) activated zinc powder (237.3 mg, 2.1 mmol, 7.00 eq.) was added. The reaction mixture was stirred at room temperature until full conversion was observed by TLC (around 4 h). The reaction mixture was diluted in toluene, filtered through celite, and concentrated under reduced pressure. The title compound **230** was isolated flash chromatography (SiO_2, 10:1-7:3 *n*-hexane:EtOAc) as a white solid (98.0 mg, 97%).

R_f 0.3 (*n*-hexane:EtOAc = 8:2, UV, $KMnO_4$).

^{1}H NMR (500 MHz, $CDCl_3$) δ 7.55 (d, J = 7.4 Hz, 1H), 7.40 – 7.28 (m, 3H), 7.20 (dd, J = 8.6, 7.3 Hz, 2H), 6.79 (tt, J = 7.3, 1.1 Hz, 1H), 6.74 – 6.68 (m, 2H), 4.87 (d, J = 5.7 Hz, 1H), 4.46 – 4.40 (m, 2H), 4.36 (td, J = 5.7, 2.3 Hz, 1H), 1.56 (s, 2H), 1.37 (d, J = 5.0 Hz, 6H).

^{13}C NMR (126 MHz, $CDCl_3$) δ 147.2, 136.5, 135.1, 129.4, 128.2, 128.1, 127.1, 125.7, 118.9, 114.5, 110.3, 79.7, 72.0, 57.2, 26.9, 24.6.

IR (ATR, neat, cm^{-1}): 3469 (s), 3357 (s), 3034 (w), 2982 (w), 2923 (w), 1602 (m), 1519 (m), 1380 (m), 1268 (m), 1204 (m), 1125 (m), 1048 (s), 832 (m), 755 (s), 697 (s), 529 (m).

HRMS (EI+/TOF, m/z) calcd. For $C_{19}H_{22}NO_3^+$ $[M+H]^+$ calc.: 312.1600; found: 312.1599.

m.p. 155 – 157°C.

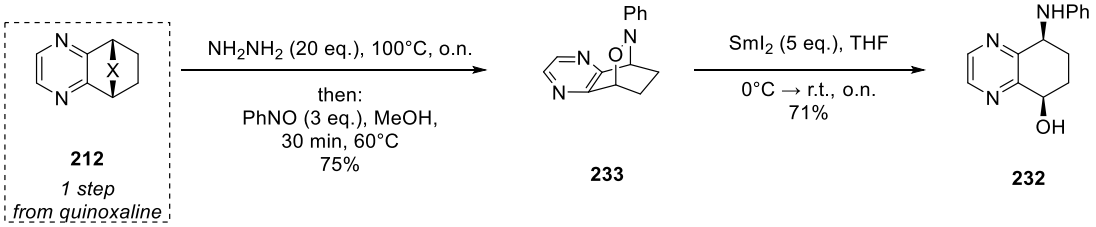

Scheme S2. Conversion of intermediate **212** to **232.**

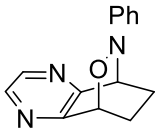

233

1.6.2.5 - Pyrazine fused cycloadduct 233. The procedure was adjusted from a reported protocol.[1] The urazole containing cycloadduct **212** (500 mg, 2.05 mmol, 1.0 eq.) was refluxed in hydrazine (1.31 mL, 41.0 mmol, 20 eq.) at 100°C until full conversion of the cycloadduct was observed (around 16 h). Volatiles were removed *in vacuo*[2] and the residue was dissolved in methanol (10.2 mL). Nitrosobenzene (660 mg, 6.15 mmol, 3.0 eq.) was added and the reaction mixture was stirred at 60°C for 30 min. The crude product was purified by flash chromatography (SiO_2, 10:1-7:3 *n*-hexane:EtOAc) to provide the title compound **233** (366 mg, 75%) as a brown solid.

R_f 0.4 (*n*-hexane:EtOAc = 3:7, UV).

^{1}H NMR (500 MHz, MeOD) δ 8.43 (dd, J = 41.5, 2.9 Hz, 2H), 7.08 (dd, J = 8.8, 7.2 Hz, 2H), 6.90 – 6.75 (m, 3H), 5.45 – 5.35 (m, 1H), 5.11 (t, J =

[1] Okumura M. *et al. Angew. Chem. Int. Ed.* **2016**, *55*,15910–15914.

[2] *It has been observed that elimination of hydrazine became difficult on scales larger than 500 mg. Residual hydrazine can consume nitrosobenzene, so multiple azeotropic evaporations with toluene are recommended.*

3.1 Hz, 1H), 2.66 – 2.42 (m, 2H), 1.94 – 1.76 (m, 1H), 1.68 – 1.44 (m, 1H).

^{13}C NMR (126 MHz, MeOD) δ 153.0, 152.2, 151.7, 145.5, 145.2, 129.6, 124.1, 118.2, 75.6, 62.8, 24.8, 22.4.

IR (ATR, neat, cm^{-1}): 3058 (w), 2990 (w), 2973 (s), 2937 (w), 1590 (m), 1481 (m), 1402 (m), 1348 (m), 949 (m), 854 (m), 768 (s),704 (s) 514 (m).

HRMS (EI+/TOF, m/z) calcd. For $C_{14}H_{14}N_3O^+$ $[M+H]^+$ calc.: 240.1137; found: 240.1134.

m.p. 134 – 135°C.

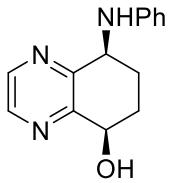

232

1.6.2.6 - Pyrazine fused alcohol 232. The cycloadduct **233** (100.0 mg, 0.418 mmol, 1.00 eq.) was placed in a flame dried round bottom flask with a stir bar under nitrogen atmosphere. Dry SPS grade THF (4.2 mL, 0.1 M) was added to the flask, the suspension was cooled in an ice bath for 10 min. A freshly prepared solution of SmI_2 (21.0 mL, 0.1 M in THF, 5.0 eq.) was added to the reaction mixture dropwise and resulting deep blue solution was heated at room temperature overnight. When complete conversion was observed by TLC, the excess of SmI_2 was quenched with a saturated solution of $NaHCO_3$ (15 mL), diluted with EtOAc (25 mL), and the organic layer was separated. The aqueous layer was extracted with EtOAc (3 x 50 mL), the combined organic layers were dried over anhydrous $MgSO_4$, and the solvent was removed *in vacuo*. The crude material was purified by flash chromatography (SiO_2, 7:3-1:9 *n*-hexane:EtOAc) to obtain **232** as a brown foam (71.4 mg, 71%).

R_f 0.3 (*n*-hexane:EtOAc = 3:7, UV, $KMnO_4$).

^{1}H NMR (600 MHz, MeOD) δ 8.54 (m, 2H), 7.13 (m, 2H), 6.77 (m, 2H), 6.65 (m, 1H), 4.80 (m, 1H), 4.64 (m, 1H), 2.21 – 2.07 (m, 4H).

^{13}C NMR (151 MHz, MeOD) δ 155.2, 154.4, 149.4, 144.8, 144.7, 130.1, 118.5, 114.7, 69.4, 54.6, 28.8, 25.4.

IR (ATR, neat, cm^{-1}): 3356 (s), 3049 (m), 2927 (s), 1649 (m), 1600 (s), 1497 (s), 1071 (s), 747 (s), 693 (s).

HRMS (EI+/TOF, m/z) calcd. For $C_{14}H_{16}N_3O^+$ $[M+H]^+$ calc.: 242.1293; found: 242.1293.

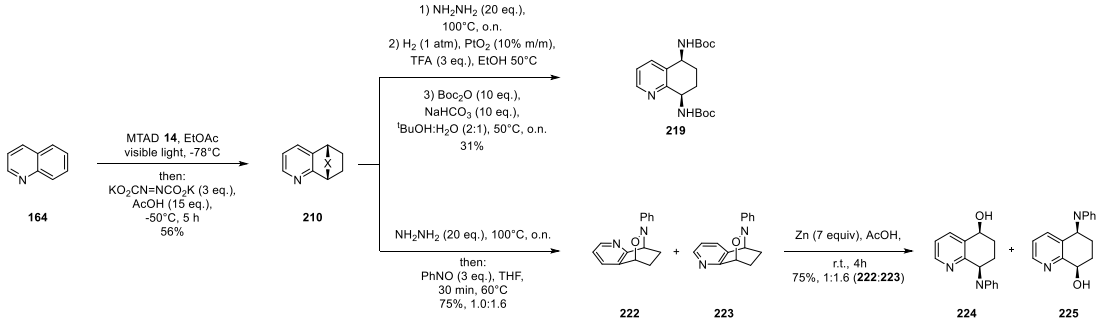

Scheme S3. Conversion of intermediate quinoline **164** to **219**, **224**, and **225**.

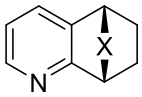

210

1.6.2.7 - Pyridine fused cycloadduct 210. The protocol was adjusted from the reported procedure.[1] MTAD **14** (3.0 g, 26.5 mmol, 1.0 eq.) was placed in 500 mL round bottom flask equipped with a large stir bar. Ethyl acetate (265 mL, 0.1 M) was added to the flask at −78°C, followed by the addition of quinoline **164** (6.2 mL, 53.1 mmol, 2.0 eq.). The mixture was then stirred under irradiation with LED lights at −78°C until full decolorization of the reaction mixture was observed (*pink to colorless solution, usually 36 hours*). After turning the lights off, potassium azodicarboxylate (15.5 g, 79.6 mmol, 3.0 eq.) was added in one portion,

[1] Okumura M. *et al. Angew. Chem. Int. Ed.* **2016**, *55*,15910–15914.

followed by the addition of acetic acid (22.8 mL, 398.0 mmol, 15 eq.) in ethyl acetate (240.0 mL) at −78°C. After stirring the resulting suspension at −50°C for 5 h, the reaction was warmed up to rt in a water bath, then quenched with water (120.0 mL). Saturated aqueous sodium bicarbonate solution (400 mL) was added, and then the organic phase was separated. The aqueous phase was extracted with ethyl acetate (3 × 100 mL). The combined organic layer was washed with saturated aqueous sodium chloride solution (90 mL), dried over anhydrous MgSO4, and concentrated *in vacuo*. The crude mixture was purified by flash column chromatography (SiO_2, 10:1 – 3:7 hexane:EtOAc) to provide compound **210** (3.6 g, 15.0 mmol, 56 %) as a white solid.

R_f	0.3 (*n*-hexane:EtOAc = 3:7, UV).
^{1}H NMR	(600 MHz, DMSO-d_6) δ 8.50 – 8.49 (m, 1H), 8.48 (s, 1H), 7.84 – 7.81 (m, 1H), 7.42 (dd, J = 7.5, 5.0 Hz, 1H), 5.48 (t, J = 2.8 Hz, 1H), 5.28 (t, J = 2.8 Hz, 1H), 2.72 (s, 3H), 2.37 – 2.23 (m, 2H), 1.79 – 1.56 (m, 2H).
^{13}C NMR	(151 MHz, DMSO-d_6) δ 156.4, 156.3, 154.2, 149.1, 131.6, 129.9, 124.2, 55.2, 52.7, 25.0, 22.7, 22.2.
IR	(ATR, neat, cm^{-1}): 3073 (w), 2973 (w), 1765 (m), 1696 (s), 1458 (s), 1395 (m), 1058 (s), 835 (s) 542 (m).
HRMS	(EI+/TOF, m/z) calcd. For $C_{12}H_{13}N_4O_2^+$ $[M+H]^+$ calc.: 245.1039; found: 245.1039.
m.p.	166 – 167°C.

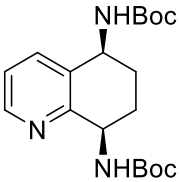

219

1.6.2.8 - Boc protected diamine 219. The experimental procedure was adjusted from the reported protocol.[1] The urazole containing cycloadduct **164** (500 mg, 2.05 mmol, 1.0 eq.) was placed in a flame dried round bottom flask along with a stir bar and anhydrous hydrazine (1.31 mL, 40.9 mmol, 20 eq.). The flask was purged with nitrogen and stirred at 100°C for 16 h. The reaction was allowed to cool down to 50°C and volatiles were removed *in vacuo*. The crude reaction mixture was dissolved in ethanol (10.2 mL, 0.2 M) and Adams' catalyst (50.0 mg, 10 $\%^{m/m}$) along with trifluoroacetic acid (470 μL, 6.14 mmol, 3.0 eq.) the reactor was purged with nitrogen and then with H_2. The reaction mixture was stirred under an atmosphere of H_2 (balloon) at 50°C for 8 h then filtered through a plug of Celite. The resulting crude material was dissolved in a 2:1 mixture of ^tBuOH:H_2O (4.1 mL, 0.5 M) then Boc_2O (4.7 mL, 20.5 mmol, 10 eq.) and $NaHCO_3$ (1.72 g, 20.5 mmol, 10 eq.) were added. The reaction mixture was stirred ad 50°C overnight, cooled at room temperature, diluted with water (15 mL) and extracted with ethyl acetate (3 × 150 mL). The combined organic phases were dried on anhydrous $MgSO_4$, filtered and purified by flash chromatography (SiO_2; 10:1-1:1 *n*-hexanes:EtOAc) to provide the title compound **219** (234 mg, 31%) as a light brown solid.

R_f 0.3 (*n*-hexane:EtOAc = 1:1, UV, $KMnO_4$).

m.p. 178 – 180°C.

[1] Okumura M. *et al. Angew. Chem. Int. Ed.* **2016**, *55*,15910–15914.

^{1}H NMR (500 MHz, MeOD) δ 8.41 (dd, *J* = 5.0, 1.8 Hz, 1H), 7.75 (d, *J* = 7.9 Hz, 1H), 7.33 (dd, *J* = 7.9, 4.7 Hz, 1H), 4.71 (dd, *J* = 8.5, 5.3 Hz, 1H), 4.66 (t, *J* = 5.1 Hz, 1H), 2.17 – 1.80 (m, 4H), 1.48 (d, *J* = 5.2 Hz, 18H).

^{13}C NMR (126 MHz, MeOD) δ 158.1, 157.7, 156.3, 149.2, 138.2, 136.2, 124.5, 80.5, 80.3, 51.6, 49.3,[1] 28.8, 28.76, 28.2, 26.9.

IR (ATR, neat, cm^{-1}): 3275 (m), 2970 (m), 2941 (m), 1700 (s), 1675 (s), 1525 (s), 1309 (m), 1249 (m), 1160 (s), 1086 (m), 967 (w), 653 (w).

HRMS (EI+/TOF, m/z) calcd. For $C_{19}H_{30}N_3O_4^+$ $[M+H]^+$ calc.: 364.2236; found: 364.2230.

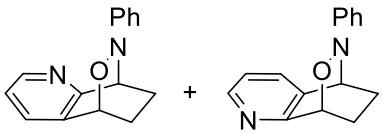

222 **223**

1.6.2.8 - Pyridine fused cycloadducts 222 and 223. The procedure was adjusted from the reported protocol.[2] The pyridine fused cycloadduct **210** (500 mg, 2.05 mmol, 1.0 eq.) was refluxed in hydrazine (1.31 mL, 41.0 mmol, 20 eq.) at 100°C until full conversion of the cycloadduct was observed (around 16 h). Volatiles were removed *in vacuo*[3] and the residue was dissolved in dry tetrahydrofuran (10.2 mL). Nitrosobenzene (660 mg, 6.15 mmol, 3.0 eq.) was added and the reaction mixture was stirred at 60°C for 30 min. The crude product was purified by flash chromatography (SiO_2, 10:1-3:7 hexane:EtOAc) to provide the title compounds **222** and **223** as an inseparable mixture of regioisomers (368 mg, 75 %, 1.0:1.6).

R_f 0.3 (*n*-hexane:EtOAc = 3:7, UV).

---

[1] *Covered by the MeOD but well visible from the HSQC.*
[2] Okumura M. *et al. Angew. Chem. Int. Ed.* **2016**, *55*,15910–15914.
[3] *It has been observed that elimination of hydrazine became difficult on scales larger than 500 mg. Residual hydrazine can consume nitrosobenzene, so multiple azeotropic evaporations with toluene are recommended.*

^{1}H NMR (500 MHz, MeOD) δ 8.39 (dd, *J* = 5.2, 1.5 Hz, 1H), 8.29 (dd, *J* = 5.1, 1.5 Hz, 1H), 7.82 (dd, *J* = 7.7, 1.6 Hz, 1H), 7.48 (dd, *J* = 7.5, 1.6 Hz, 1H), 7.34 (dd, *J* = 7.5, 5.2 Hz, 1H), 7.27 (dd, *J* = 7.5, 5.1 Hz, 1H), 7.07 (td, *J* = 8.7, 7.1 Hz, 3H), 6.92 – 6.78 (m, 5H), 5.41 (dd, *J* = 4.2, 1.4 Hz, 1H), 5.26 (d, *J* = 3.2 Hz, 1H), 5.06 (t, *J* = 2.8 Hz, 1H), 4.97 (t, *J* = 3.1 Hz, 1H), 2.62 – 2.37 (m, 4H), 1.92 – 1.69 (m, 2H), 1.66 – 1.41 (m, 2H).

^{13}C NMR (126 MHz, MeOD) δ 157.7, 155.7, 152.6, 152.5, 149.1, 148.8, 134.5, 134.2, 132.8, 132.3, 129.5, 129.5, 125.2, 124.9, 123.9, 123.8, 118.4, 118.3, 75.3, 73.8, 62.8, 61.0, 25.6, 24.9, 23.2, 22.6.

IR (ATR, neat, cm^{-1}): 3054 (w), 2966 (m), 2932 (m), 1730 (m), 1586 (m), 1468 (m), 1431 (m), 1265 (m), 959 (m), 854 (m), 827 (s), 734 (s), 695 (s).

HRMS (EI+/TOF, m/z) calcd. For $C_{15}H_{15}N_2O^+$ $[M+H]^+$ calc.: 239.1184; found: 239.1182.

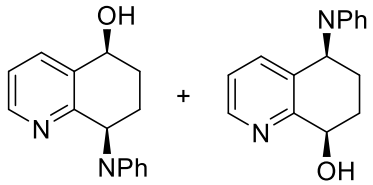

224 **225**

1.6.2.9 - Pyridine fused alcohols 224 and 225. To a 1.0:1.6 mixture of the cycloadducts **222** and **223** (200.0 mg 0.839 mmol, 1.0 eq.) in glacial acetic acid (2.8 mL, 3 M) zinc in powder (384.0 mg, 5.88 mmol, 7.0 eq.) was added. The reaction mixture was stirred at room temperature until full conversion was observed by TLC (around 4 h). The reaction mixture was diluted in toluene, filtered through celite and concentrated under reduced pressure. The title compounds were isolated by reverse Biotage® Isolera™ One (AQ C18 column Spherical; 20 – 35µm; 100A; 20 g, 20%-55% MeCN in H2O, detection at λ = 275 nm) getting **224** and **225**, both as a brown foam (151 mg, 0.629 mmol, combined yield 75%, 1.0:1.6).

224:

R_f 0.3 (*n*-hexane:EtOAc = 6:4, UV, $KMnO_4$).

^{1}H NMR (500 MHz, MeOD) δ 8.43 (dd, J = 4.8, 1.7 Hz, 1H), 7.98 (dd, J = 7.1, 1.5 Hz, 0H), 7.35 l(dd, J = 7.9, 4.7 Hz, 1H), 7.12 (dd, J = 8.6, 7.2 Hz, 1H), 6.74 (d, J = 7.5 Hz, 1H), 6.63 (dd, J = 7.9, 6.7 Hz, 0H), 4.74 (dd, J = 7.7, 5.0 Hz, 1H), 4.56 (t, J = 4.5 Hz, 1H), 2.32 – 1.82 (m, 2H).

^{13}C NMR (101 MHz, MeOD): δ 157.3, 149.3, 149.2, 138.1, 137.9, 130.1, 124.25, 118.1, 114.4, 68.3, 53.9, 29.0, 25.7.

IR (ATR, neat, cm^{-1}): 3360 (s), 3258 (s), 3047 (w), 2948 (s), 2862 (w), 1738 (w), 1602 (m), 1497 (m), 1322 (m), 966 (m), 912 (m), 807 (m), 743 (s), 866 (s), 692 (s), 505 (s).

HRMS (EI+/TOF, m/z) calcd.. For $C_{15}H_{16}N_2O^+$ $[M+H]^+$ calc.: 241.1341; found: 241.1342.

225:

R_f 0.3 (*n*-hexane:EtOAc = 6:4, UV, $KmnO_4$).

^{1}H NMR ^{1}H NMR (500 MHz, MeOD) δ 8.45 – 8.43 (m, 1H), 7.89 (d, *J* = 7.8 Hz, 1H), 7.28 (dd, *J* = 7.9, 4.7 Hz, 1H), 7.11 (dd, *J* = 8.6, 7.3 Hz, 2H), 6.75 – 6.64 (m, 2H), 6.62 (tt, *J* = 7.4, 1.1 Hz, 1H), 4.73 (m, 1H), 4.67 – 4.57 (m, 1H), 2.13 – 1.95 (m, 4H).

^{13}C NMR (126 MHz, MeOD) δ 158.2, 149.4, 148.9, 138.4, 136.9, 130.2, 124.5, 118.1, 114.2, 69.2, 52.3, 30.0, 25.4.

IR (ATR, neat, cm^{-1}): 3326 (m), 3219 (m), 2939 (m), 2890 (m), 2401 (m), 1597 (s), 1494 (s), 1435 (m), 964 (m), 767 (s), 721 (s).

HRMS (EI+/TOF, m/z) calcd. For $C_{15}H_{16}N_2O^+$ $[M+H]^+$ calc.: 241.1341; found: 241.1341.

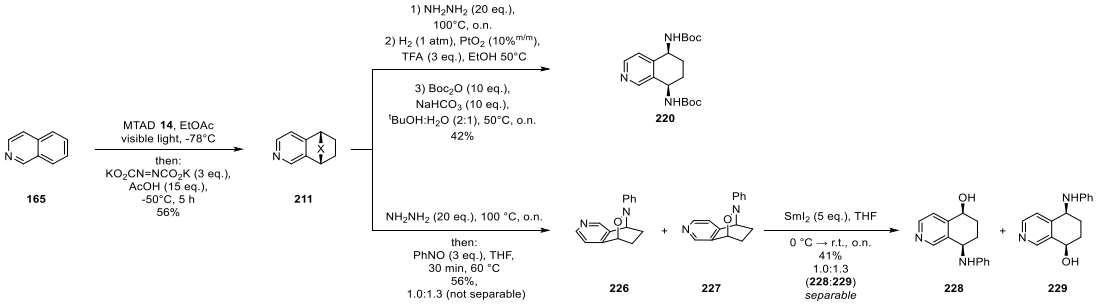

Scheme S4. Conversion of intermediate isoquinoline **165** to **220**, **228**, and **229**.

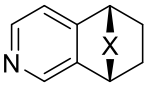

211

1.6.2.10 - Pyridine fused cycloadduct 211. The protocol was adjusted from the reported procedure.[128] MTAD **14** (3.0 g, 26.5 mmol, 1.0 eq.) was placed in a 500 mL round bottom flask. Ethyl acetate (265 mL, 0.1 M) was added to the flask at −78°C, followed by the addition of isoquinoline **165** (6.2 mL, 53.1 mmol, 2.0 eq.). The mixture was then stirred under the irradiation with LED lights at −78°C until full decolorization of the reaction mixture was observed (*pink to colorless solution, usually about 36 hours*). After turning the lights off, potassium azodicarboxylate (15.5 g, 79.6 mmol, 3.0 eq.) was added in one portion, followed by the addition of acetic acid (22.8 mL, 398.0 mmol, 15 eq.) in ethyl acetate (240.0 mL) at −78°C. After stirring the resulting suspension at −50°C for 5 h, the reaction was warmed up to r.t. in water bath, then quenched with water (120.0 mL). Saturated aqueous sodium bicarbonate solution (400 mL) was added, and then the organic phase was separated. The aqueous phase was extracted with ethyl acetate (3 × 100 mL). The combined organic layer was washed with saturated aqueous sodium

[1] Okumura M. *et al. Angew. Chem. Int. Ed.* **2016**, *55*,15910–15914.

chloride solution (90 mL), dried over anhydrous MgSO4, and concentrated *in vacuo*. The crude mixture was purified by flash column chromatography (SiO_2, 10:1 – 3:7 hexane:EtOAc mixture) to provide compound **211** (3.6 g, 15.0 mmol, 56%) as a light brown solid.

R_f 0.2 (*n*-hexane:EtOAc = 3:7, UV).

m.p. 176 – 177°C.

^{1}H NMR (600 MHz, DMSO-d_6) δ 8.62 (d, J = 4.6 Hz, 1H), 8.59 (s, 1H), 7.44 (d, J = 4.8 Hz, 1H), 5.46 (s, 1H), 5.42 (s, 1H), 2.71 (s, 3H), 2.38 – 2.23 (m, 2H), 1.64 (d, J = 8.8 Hz, 2H).

^{13}C NMR (151 MHz, DMSO-d_6) δ 156.5, 156.4, 150.3, 143.8, 142.9, 130.6, 118.4, 52.0, 50.8, 25.0, 22.7, 22.0.

IR (ATR, neat, cm^{-1}): 3001 (w), 2946 (w), 1764 (m), 1701 (s), 1456 (s), 1207 (m), 1033 (m), 763 (s), 599 (s), 542 (s).

HRMS (EI+/TOF, m/z) calcd. For $C_{12}H_{13}N_4O_2^+$ $[M+H]^+$ calc.: 245.1039; found: 245.1043.

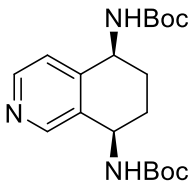

220

1.6.2.11 - Boc protected diamine 220. The experimental procedure was adjusted from the reported protocol.[1] The urazole containing cycloadduct **211** (500 mg, 2.05 mmol, 1.0 eq.) was placed in a flame dried round bottom flask along with a stir bar and anhydrous hydrazine (1.31 mL, 40.9 mmol, 20 eq.). The flask was purged with nitrogen and stirred at 100°C for 16 h. The reaction was allowed to cool down to 50°C and volatiles were removed *in vacuo*. The crude reaction mixture was dissolved in ethanol (10.2

[1] Okumura M. *et al., Angew. Chem. Int. Ed.* **2016**, *55*,15910–15914.

mL, 0.2 M) and Adams' catalyst (50.0 mg, 10%$^{m/m}$) along with trifluoroacetic acid (470 μL, 6.14 mmol, 3.0 eq.) the reactor was purged with nitrogen and then with H_2. The reaction mixture was stirred under an atmosphere of H_2 (balloon) at 50°C for 8 h then filtered through a plug of celite. The resulting crude material was dissolved in a 2:1 mixture of ^{t}BuOH:H_2O (4.1 mL, 0.5 M) then Boc_2O (4.7 mL, 20.5 mmol, 10 eq.) and $NaHCO_3$ (1.72 g, 20.5 mmol, 10 eq.) were added. The reaction mixture was stirred ad 50°C overnight, cooled at room temperature, diluted with water (15 mL), and extracted with ethyl acetate (3 x 150 mL). The combined organic phases were dried on anhydrous $MgSO_4$, filtered and purified by flash chromatography (SiO_2; 10:1-1:1 *n*-hexanes:EtOAc) to provide the title compound **220** (314 mg, 42%) as a bright yellow solid. From the NMR the compound result to be a mixture of conformers.

R_f 0.2 (*n*-hexane:EtOAc = 3:7, UV, $KMnO_4$).

^{1}H NMR (500 MHz, $CDCl_3$)[1] δ 8.62 – 8.11 (m, 2H), 7.56 – 6.91 (m, 2H), 4.79 – 4.63 (m, 1H), 4.59 - 4.55 (m, 1H), 3.33 (s, 1H), 2.11 – 1.65 (m, 4H), 1.43 (m, 18H).

^{13}C NMR (126 MHz, $CDCl_3$)[1] δ 155.8, 155.8, 155.7, 155.5, 155.5, 155.2, 155.1, 149.5, 149.3, 148.9, 148.8, 147.9, 147.8, 147.7, 147.5, 147.3, 147.1, 134.3, 133.7, 121.6, 121.6, 121.3, 78.2, 78.1, 78.1, 47.9, 47.8, 46.9, 46.8, 46.6, 46.5, 45.1, 45.0, 28.2, 26.6, 25.4.

IR (ATR, neat, cm^{-1}): 3323 (m), 2976 (m), 2931 (m), 1683 (s), 1513 (s), 1244 (s), 1160 (s), 1045 (w), 841 (w), 620 (w).

HRMS (EI+/TOF, m/z) calcd. For $C_{19}H_{30}N_3O_4^+$ $[M+H]^+$ calc.: 364.2236; found: 364.2234.

m.p. 178 – 179°C.

[1] *Mixture of rotamers confirmed by VT NMR.*

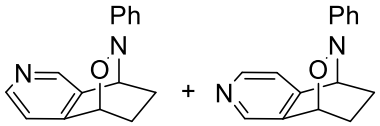

226 **227**

1.6.2.12 - Pyridine fused cycloadducts 226 and 227. The procedure was adjusted from the reported protocol.[1] The pyridine fused cycloadduct **211** (500 mg, 2.05 mmol, 1.0 eq.) was refluxed in hydrazine (1.31 mL, 41.0 mmol, 20 eq.) at 100°C until full conversion of the cycloadduct was observed (around 16 h). Volatiles were removed *in vacuo*[2] and the residue was dissolved in dimethylformamide (10.2 mL, 0.2 M). Nitrosobenzene (660 mg, 6.15 mmol, 3.0 eq.) was added and the reaction mixture was stirred at 60°C for 30 min. The reaction mixture was diluted with water (10 mL) and extracted with ethyl acetate (3 × 50 mL). The organic phases were washed with a saturated solution of brine three times (50 mL), dried over anhydrous $MgSO_4$ and the solvent was removed under reduced pressure. The crude product was purified by flash chromatography (SiO_2, 7:3-1:9 *n*-hexane:EtOAc) to provide the title compounds **226** and **227** (275 mg, 56 %, 1.0:1.3) as a complex mixture of the two regioisomers along with products of degradation of the nitrosobenzene. The mixture was crystallized in ethanol two times getting 31.0 mg of the minority regioisomer **227** as colorless crystals. The ethanol phase was evaporated recovering the rest of the material (240 mg) that was purified

[1] Okumura M. *et al., Angew. Chem. Int. Ed.* **2016**, *55*,15910–15914.
[2] *It has been observed that elimination of hydrazine became difficult on scales larger than 500 mg. Residual hydrazine can consume nitrosobenzene, so multiple azeotropic evaporations with toluene are recommended.*

by preparative TLC (SiO_2, 2:8 hexane:EtOAc) getting a clean mixture of the two regioisomers (236 mg, 1.0:2.1) as a reddish brown foam.

226 + 227

R_f 0.3 (*n*-hexane:EtOAc = 1:9, UV).

^{1}H NMR (500 MHz, $CDCl_3$) δ 8.60 – 8.53 (m, 1H), 8.48 (d, *J* = 4.82 Hz, 0.3H), 8.25 (s, 0.7H), 7.26 (m, 0.6H),[1] 7.14 – 7.03 (m, 2H), 6.92 (d, *J* = 4.85 Hz, 0.3H), 6.88 – 6.76 (m, 3H), 5.31 (dd, *J* = 4.2, 1.5 Hz, 0.3H), 5.20 (dd, *J* = 4.3, 1.5 Hz, 0.7H), 4.82 (t, *J* = 3.0 Hz, 0.7H), 4.76 (t, *J* = 3.0 Hz, 0.3H), 2.68 – 2.45 (m, 2.1H), 1.73 (ddq, *J* = 15.7, 9.3, 3.1 Hz, 1H), 1.50 (dddt, *J* = 13.5, 12.1, 3.4, 1.6 Hz, 1H).

^{13}C NMR (126 MHz, $CDCl_3$) δ 151.2, 149.8, 143.5, 143.4, 133.5, 128.7, 122.9, 119.3, 117.2, 70.4, 59.7, 24.8, 22.1.

IR (ATR, neat, cm^{-1}): 3031 (w), 2994 (w), 2936 (w), 1738 (w), 1480 (m), 962 (s), 851 (s), 761 (s), 695 (s).

HRMS (ESI-TOF, m/z) calcd. For $C_{15}H_{15}N_2O^+$ $[M+H]^+$ calc.: 239.1184; found: 239.1184.

m.p. 182 – 183°C.

47

R_f 0.3 (*n*-hexane:EtOAc = 1:9, UV).

^{1}H NMR (500 MHz, $CDCl_3$) δ 8.57 (s, 1H), 8.48 (d, *J* = 4.9 Hz, 1H), 7.17 – 6.99 (m, 2H), 6.91 (d, *J* = 4.8 Hz, 1H), 6.87 – 6.69 (m, 3H), 5.40 – 5.23 (m, 1H), 4.76 (t, *J* = 3.0 Hz, 1H), 2.71 – 2.43 (m, 2H), 1.74 (tt, *J* = 12.4, 3.0 Hz, 1H), 1.59 – 1.37 (m, 1H).

^{13}C NMR (126 MHz, $CDCl_3$) δ 151.2, 149.8, 143.5, 143.4, 133.5, 128.7, 122.9, 119.3, 117.2, 70.4, 59.7, 24.8, 22.1.

---

[1] *Partially covered by $CDCl_3$, visible from the HSQC.*

IR (ATR, neat, cm^{-1}): 3158 (m), 2968 (m), 2935 (s), 1595 (s), 1486 (s), 1421 (m), 1184 (m), 962 (m), 835 (s), 760 (s), 696 (s).

HRMS (ESI-TOF, m/z) calcd. For $C_{15}H_{15}N_2O^+$ $[M+H]^+$ calc.: 239.1184; found: 239.1182.

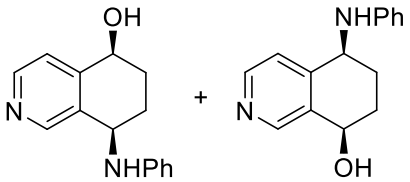

228 **229**

1.6.2.13 - Pyridine fused alcohols 228 and 229. A 2.1:1.0 mixture of the pyridine condensed cycloadducts **226** and **227** (100.0 mg, 0.420 mmol, 1.0 eq.) was placed in a flame dried round bottom flask with a stir bar under nitrogen atmosphere. Dry SPS grade THF (4.2 mL, 0.1 M) was added to the flask, the suspension was cooled in an ice bath for around 10 min. A freshly prepared solution of SmI_2 (21.0 mL, 0.1 M in THF, 5.0 eq.) was added to the reaction mixture dropwise getting a deep blue solution. The mixture was heated at room temperature overnight, when complete conversion was observed by TLC the excess of SmI_2 was quenched with a statured solution of $NaHCO_3$ (15 mL), diluted with EtOAc (25 mL) and the organic layer was separated. The aqueous layer was extracted with EtOAc (3 × 50 mL), the combined organic layers were dried over anhydrous $MgSO_4$ and the solvent was removed *in vacuo*. The titled compounds were isolated from the crude by reverse Biotage® Isolera™ One (AQ C18 column Spherical; 20 – 35µm; 100A; 20 g, 20%-55% MeCN in H_2O, detection at λ = 275 nm) to afford

228 and **229**, both as brown foams (41.2 mg, 0.172 mmol, combined yield 41% 1.2:1.0).[1]

228:

R_f 0.3 (*n*-hexane:EtOAc = 3:7, UV, $KMnO_4$).

^{1}H NMR (500 MHz, MeOD) δ 8.51 (s, 1H), 8.40 (s, 1H), 7.56 (d, *J* = 5.2 Hz, 1H), 7.13 (dd, *J* = 8.7, 7.2 Hz, 1H), 6.79 – 6.68 (m, 2H), 6.64 (t, *J* = 7.3, 1H), 4.68 (m, 2H), 2.16 – 1.88 (m, 4H).

^{13}C NMR (126 MHz, MeOD)[2] δ 151.6, 150.6, 149.1, 148.0, 130.2, 123.4[3], 118.2, 114.2, 67.8, 49.3[4], 29.1, 25.9.

IR (ATR, neat, cm^{-1}): 3334 (w), 2928 (w), 1601 (s), 1498 (s), 1413 (m),1311 (w), 1072 (w), 750 (m), 694 (m).

HRMS (EI+/TOF, m/z) calcd. For $C_{15}H_{17}N_2O^+$ $[M+H]^+$ calc.: 241.1341; found: 241.1342.

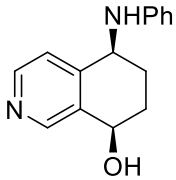

229

1.6.2.14 - Alcohol 229. The cycloadduct **227** (100.0 mg, 0.420 mmol, 1.0 eq.) was placed in a flame dried round bottom flask with a stir bar under nitrogen atmosphere. Dry SPS grade THF (4.2 mL, 0.1 M) was added to the flask, the suspension was cooled in an ice bath for around 10 min.. A freshly prepared 0.1 M solution in THF of SmI_2 (21.0 mL, 0.1 M in THF, 5.0 eq.) was added to the reaction mixture dropwise getting a deep blue solution. The mixture was heated at room temperature overnight. When complete

[1] *While we take a 2.1:1.0 ratio of 226:227 forward, we observe a 1:1 ratio of 228:229 following chromatography. We believe that this ratio diminishment may be due to either the decomposition of 228 (product of 226) during column chromatography or low reactivity of 226 in comparison to 227.*
[2] *One quaternary carbon is not ^{13}C NMR active.*
[3] *Slightly visible from ^{13}C, well visible from HSQC.*
[4] *Covered by MeOD, well visible from HSQC.*

conversion was observed by TLC the excess of SmI_2 was quenched with a saturated solution of $NaHCO_3$ (15 mL), diluted with EtOAc (25 mL) and the organic layer was separated. The aqueous layer was extracted with EtOAc (3 x 50 mL), the combined organic layers were dried over anhydrous $MgSO_4$, and the solvent was removed *in vacuo*. The crude material was purified by flash chromatography (SiO_2, 7:3-1:9 *n*-hexane:EtOAc) to afford **229** as a light brown foam (95.5 mg, 95%).

R_f 0.3 (*n*-hexane:EtOAc = 3:7, UV, $KMnO_4$).

^{1}H NMR (600 MHz, MeOD) δ 8.58 (s, 1H), 8.34 (d, *J* = 5.3 Hz, 1H), 7.48 (d, *J* = 5.3 Hz, 1H), 7.12 (dd, *J* = 8.6, 7.3 Hz, 2H), 6.71 (dt, *J* = 7.7, 1.1 Hz, 2H), 6.63 (tt, *J* = 7.3, 1.1 Hz, 1H), 4.82 (m, 1H), 4.57 (t, *J* = 5.4 Hz, 1H), 2.34 – 1.78 (m, 4H).

^{13}C NMR (151 MHz, MeOD) δ 151.1, 150.7, 149.4, 148.5, 137.0, 130.2, 124.0, 118.2, 114.2, 65.9, 52.0, 30.5, 25.3.

IR (ATR, neat, cm^{-1}): 3293 (s), 3108 (s), 2944 (m), 2852 (m), 1600 (s), 1493 (s), 1292 (m), 1251 (m), 1088 (m), 1049 (m), 968 (s), 830 (m), 748 (s), 695 (s).

HRMS (EI+/TOF, m/z) calcd. For $C_{15}H_{17}N_2O^+$ $[M+H]^+$ calc.: 241.1341; found: 241.1345.

1.6.3.0 - Crystallographic Data

Single crystals of $C_{15}H_{14}N_2O$ **227** were recrystallized from ethanol. A suitable crystal was selected and [Mounted using Paratone-N oil (Exxon) on a cryo-loop (Hampton) with (-2 3 5) face roughly perpendicular to the spindle axis] on a Bruker APEX-II CCD diffractometer. The crystal was kept at 100.00°K during data collection. Using Olex2,[1] the structure was solved with the XT[2] structure solution program using Intrinsic Phasing and refined with the XL[34] refinement package using Least Squares minimization.

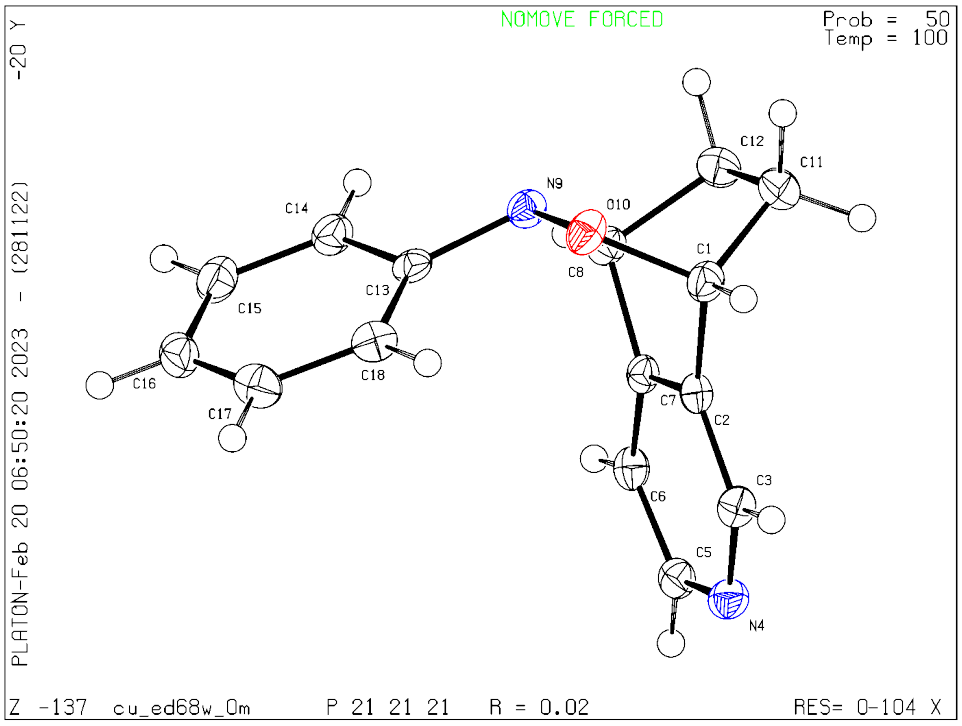

[1]Chang Y. K. *et al. J., Org. Chem*. **2005**, *70* (8), 3299–3302.
[2] Dolomanov O. V. *et al., J. Appl. Cryst.* **2009,** *42*, 339-341.
[3] Sheldrick G. M., *Acta Cryst*. **2015**, *A71*, 3-8.
[4] Sheldrick G. M., *Acta Cryst*. **2008,** *A64*, 112-122.

Table S1. Crystal data and structure refinement for **227.**

Identification code	cu_ed68w_0m
Empirical formula	$C_{15}H_{14}N_2O$
Formula weight	238.28
Temperature/K	100.00
Crystal system	orthorhombic
Space group	$P2_12_12_1$
a/Å	9.3242(4)
b/Å	9.9190(5)
c/Å	12.8658(6)
α/°	90
β/°	90
γ/°	90
Volume/Å^3	1189.92(10)
Z	4
ρ_{calc}g/cm^3	1.330
μ/mm^{-1}	0.675
F(000)	504.0
Crystal size/mm^3	0.482 × 0.481 × 0.126
Radiation	MoKα (λ = 1.54178)
2Θ range for data collection/°	11.264 to 136.454
Index ranges	$-11 \leq h \leq 11$, $-11 \leq k \leq 11$, $-15 \leq l \leq 15$
Reflections collected	16020
Independent reflections	2182 [R_{int} = 0.0232, R_{sigma} = 0.0140]
Data/restraints/parameters	2182/0/165
Goodness-of-fit on F^2	1.056
Final R indexes [I>=2σ (I)]	R_1 = 0.0243, wR_2 = 0.0632
Final R indexes [all data]	R_1 = 0.0244, wR_2 = 0.0633
Largest diff. peak/hole / e Å^{-3}	0.17/-0.12
Flack parameter	0.4(3)

1.6.4.0 - Principal Moment of Inertia analysis (PMI)

A Principal Moment of Inertia (PMI) (**Figure S1**) analysis has been used to represent the chemical space explored in this survey. In **Figure S1a** the (poly)aromatic-series is compared with the FDA-approved drugs (grey dots), while in **Figure S1b** the benzyl acetate-series is shown. Unsurprisingly, the analogs obtained from polyaromatics contain a higher sp^2 fraction and are more crowded in the well-explored region between 1D and 2D (**Figure S1a**). On the other hand, those obtained from acetyl benzoate are more spread toward the less explored 3D region, with the dearomative products between the 1D and 2D region (**Figure S1b** red circles), while the opened C7 (amino)cyclitols analogs are in the 3D region (**Figure S1b** yellow circles). This representation well shown the breath of the structural diversity that can be achieved with our platform, ranging from well explored areas to the least exploited ones.

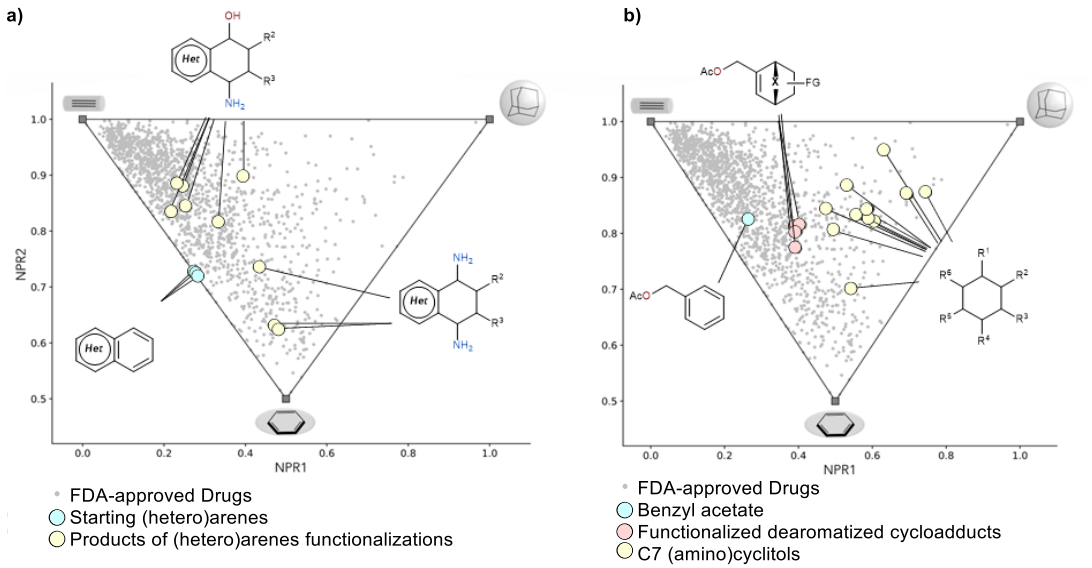

Figure S1. Principal moment of inertia (PMI) comparison between FDA-approved drugs and (amino)cyclitol analogs. **a)** Comparison with sp^2-sp^3 hybrids series, **b)** comparison with benzyl acetate derivatives series.

1.6.5.0 - NMR spectra

1.6.5.1 ^{1}H NMR and ^{13}C NMR of cycloadduct 210

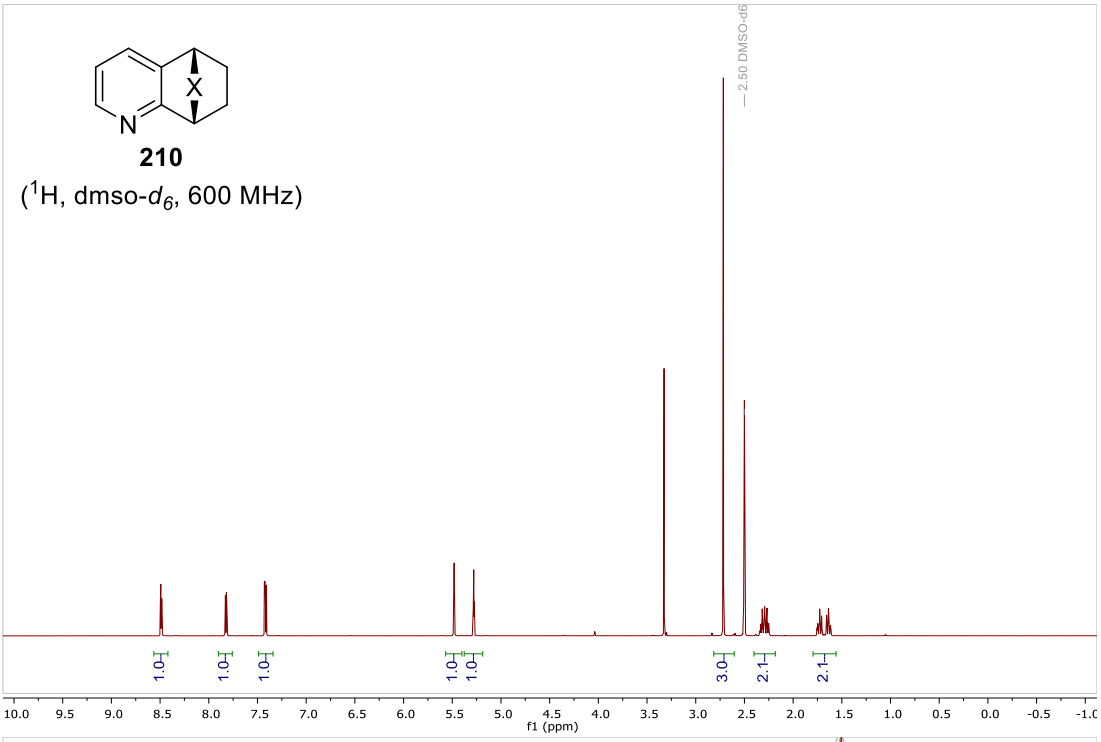

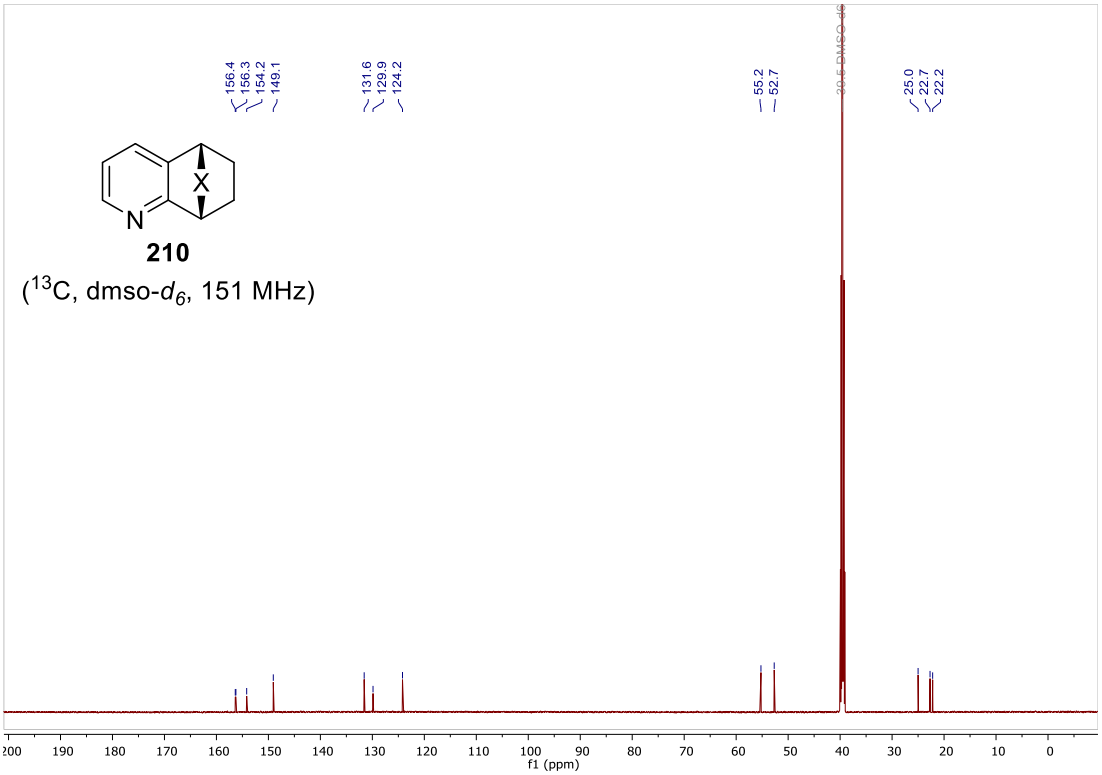

1.6.5.2 - ^{1}H NMR and ^{13}C NMR of cycloadduct 211

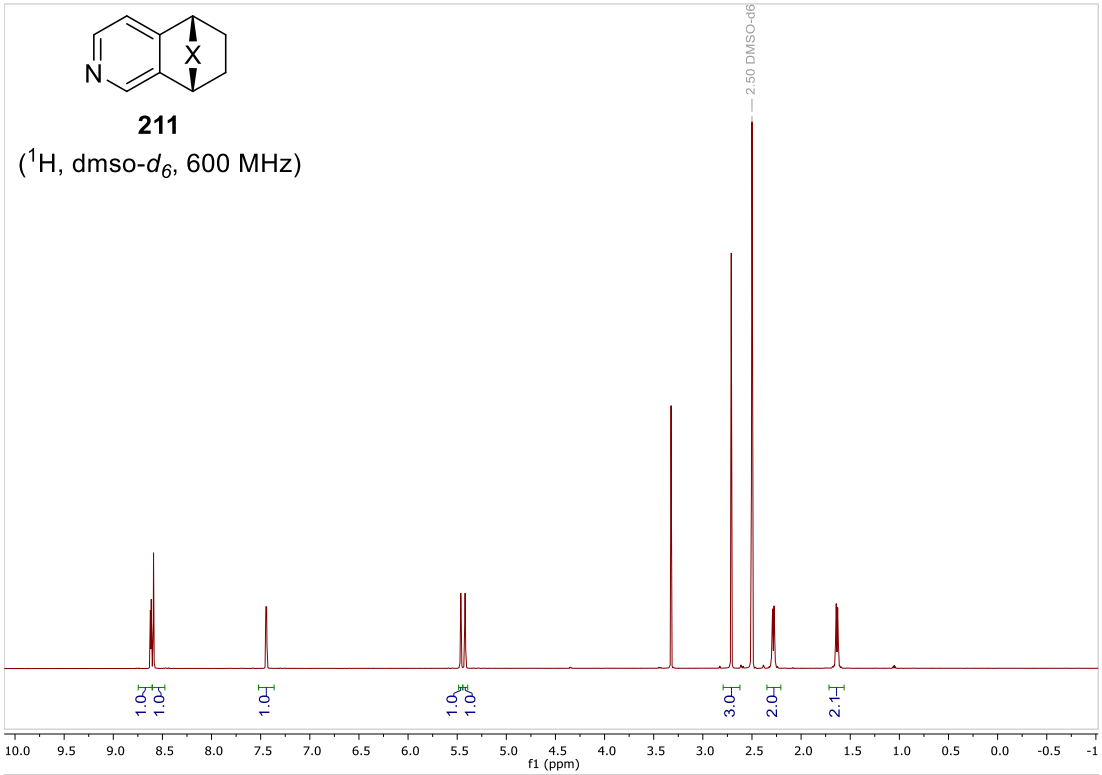

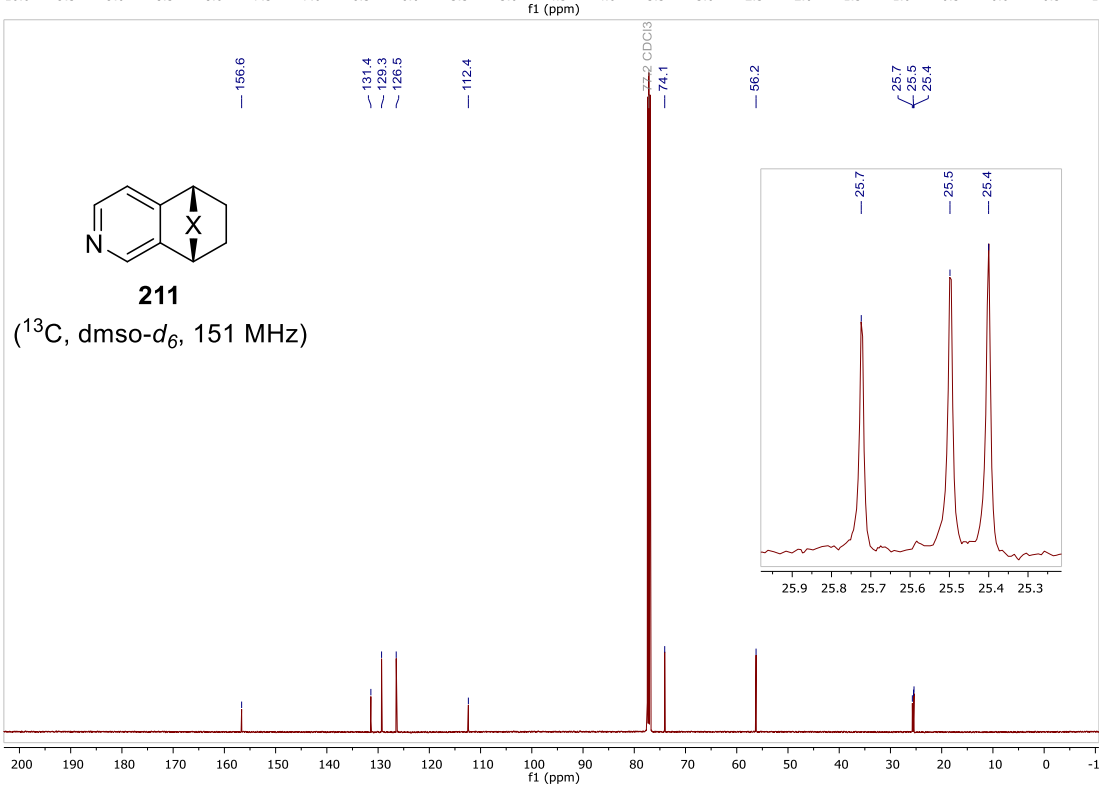

1.6.5.3 - ^{1}H NMR and ^{13}C NMR of cycloadduct 214

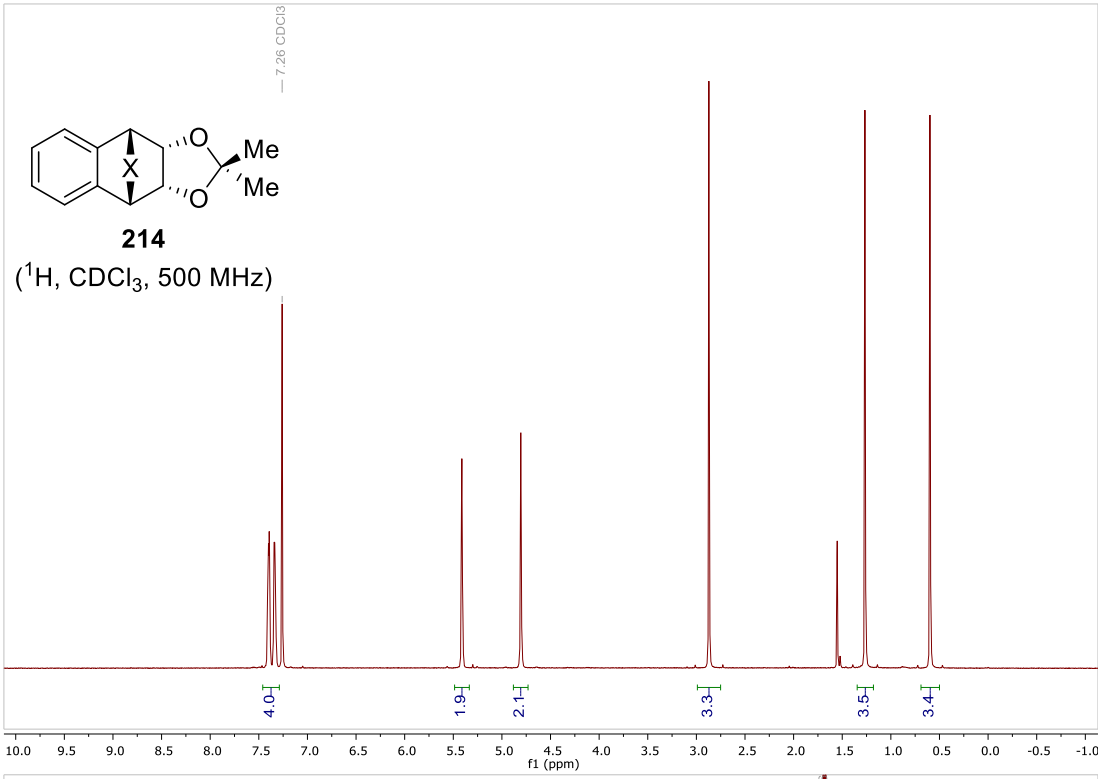

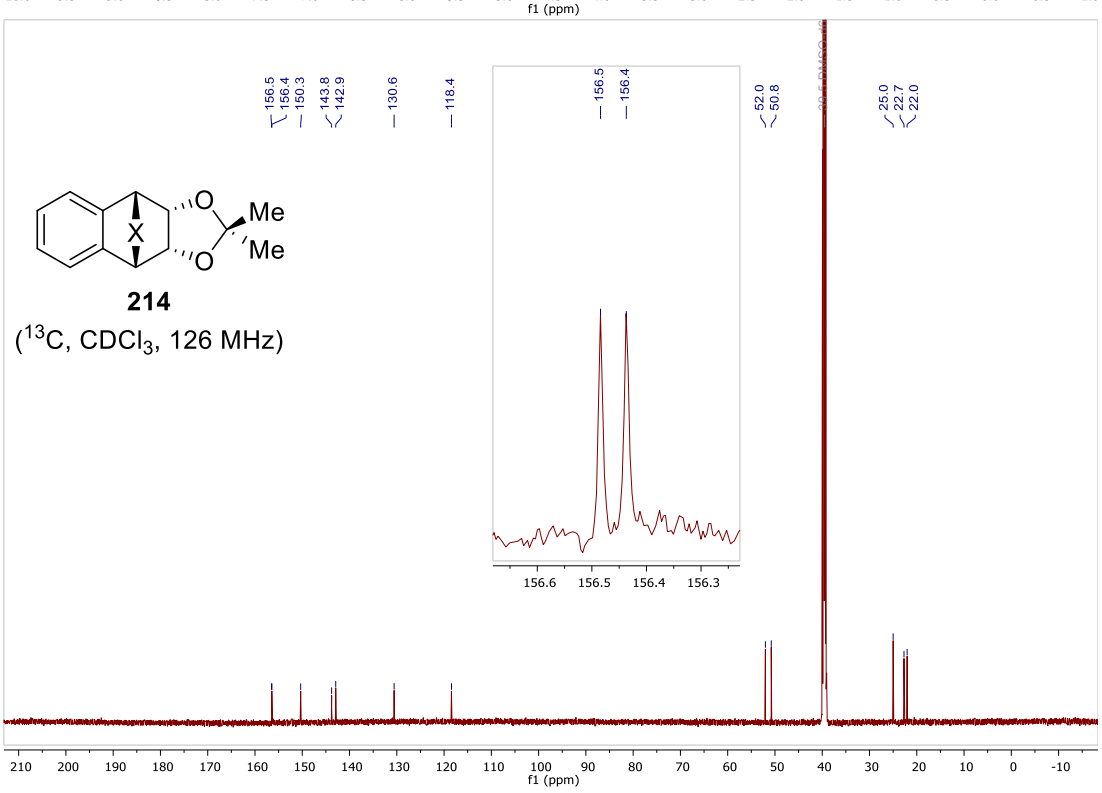

1.6.5.4 - ^{1}H NMR and ^{13}C NMR of benzene condensed *syn*-1,4-diamine 216

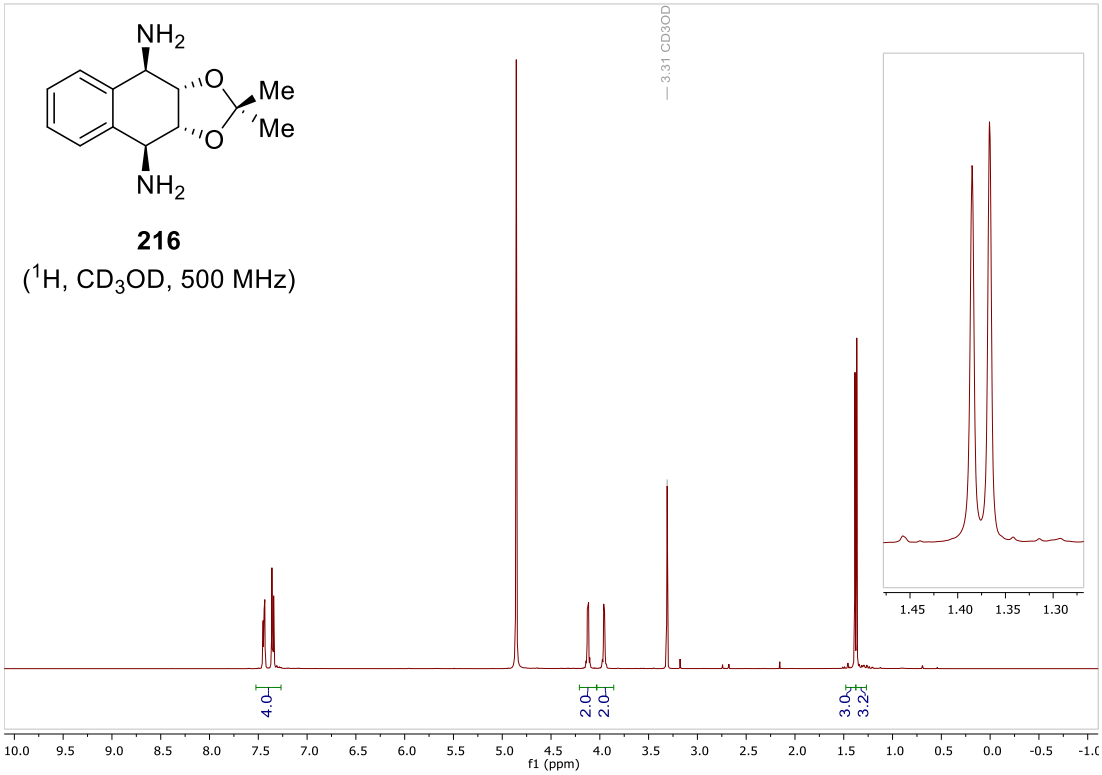

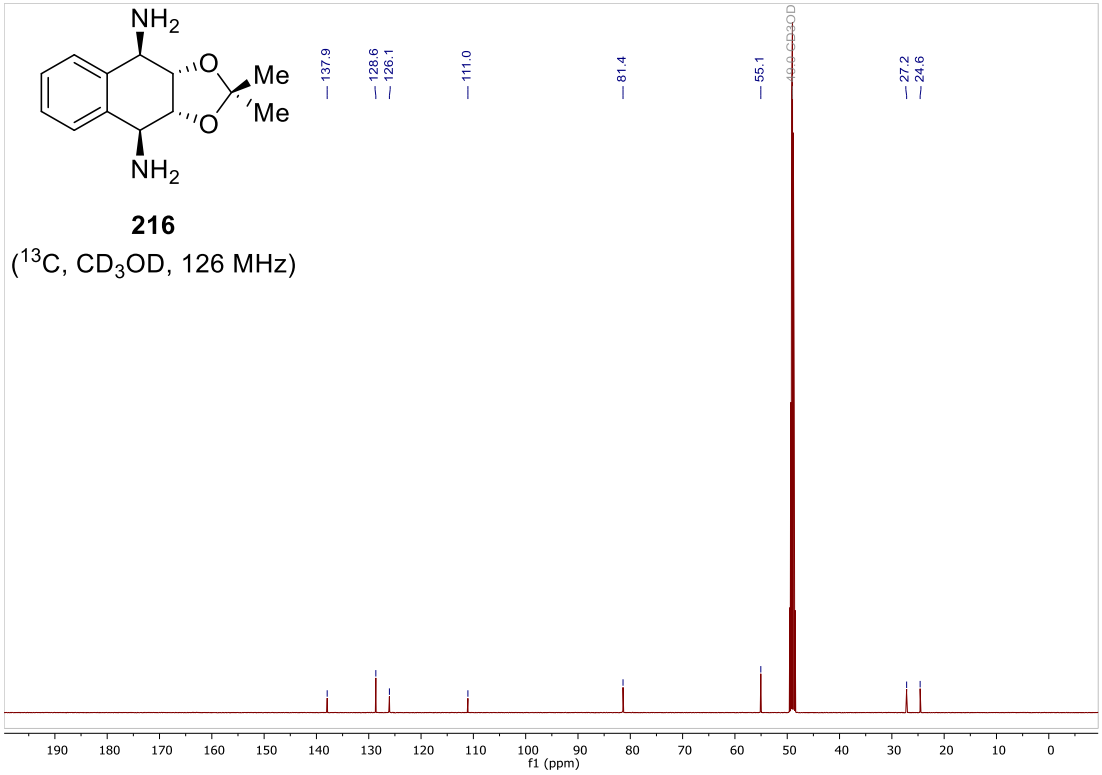

1.6.5.5 - ^{1}H NMR and ^{13}C NMR of pyridine condensed *syn*-1,4-diamine 219

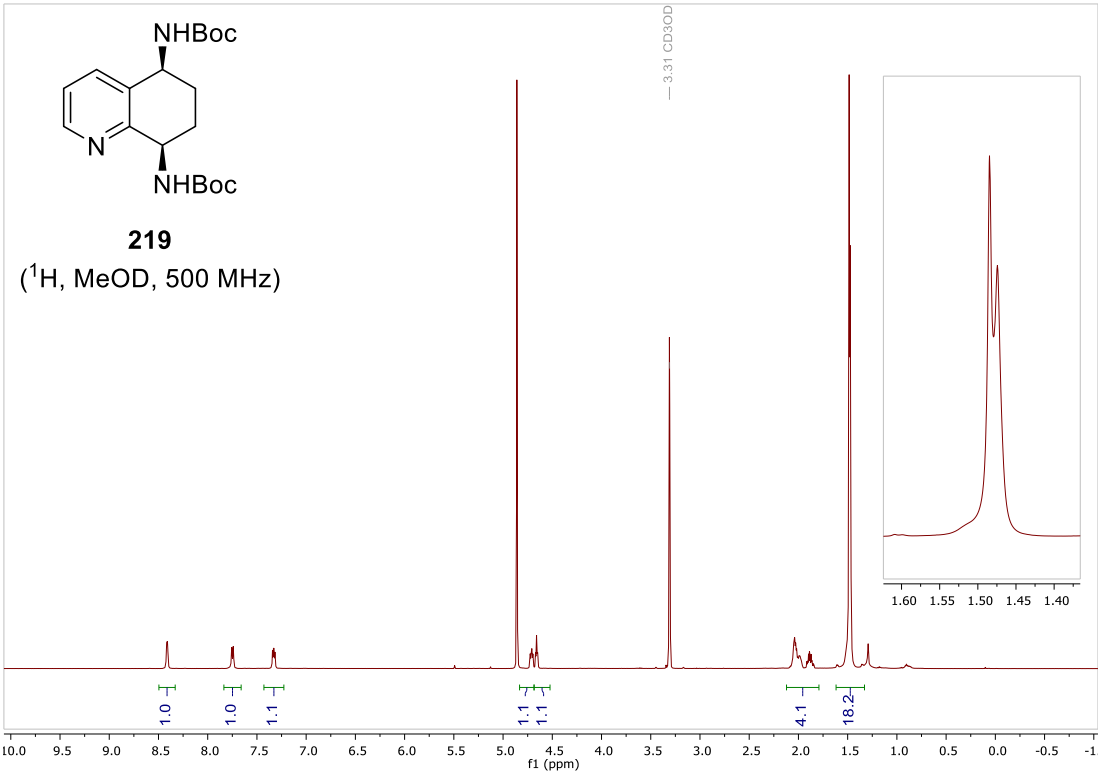

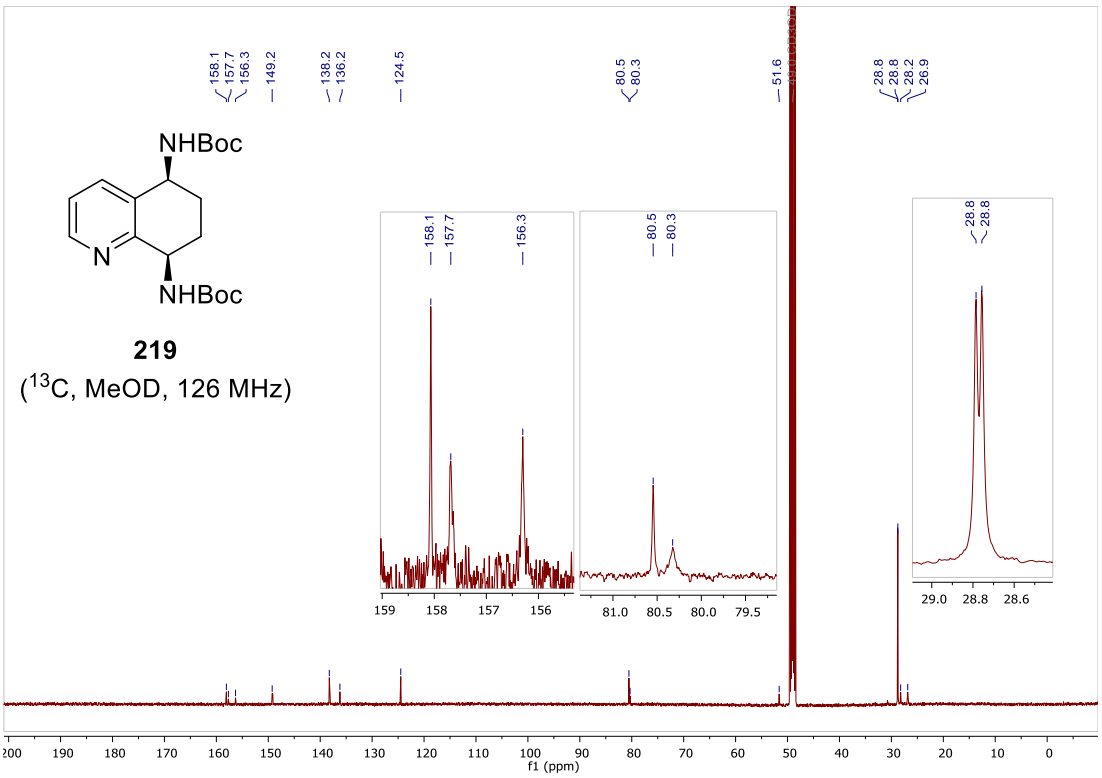

1.6.5.6 - HSQC of pyridine condensed *syn*-1,4-diamine 219

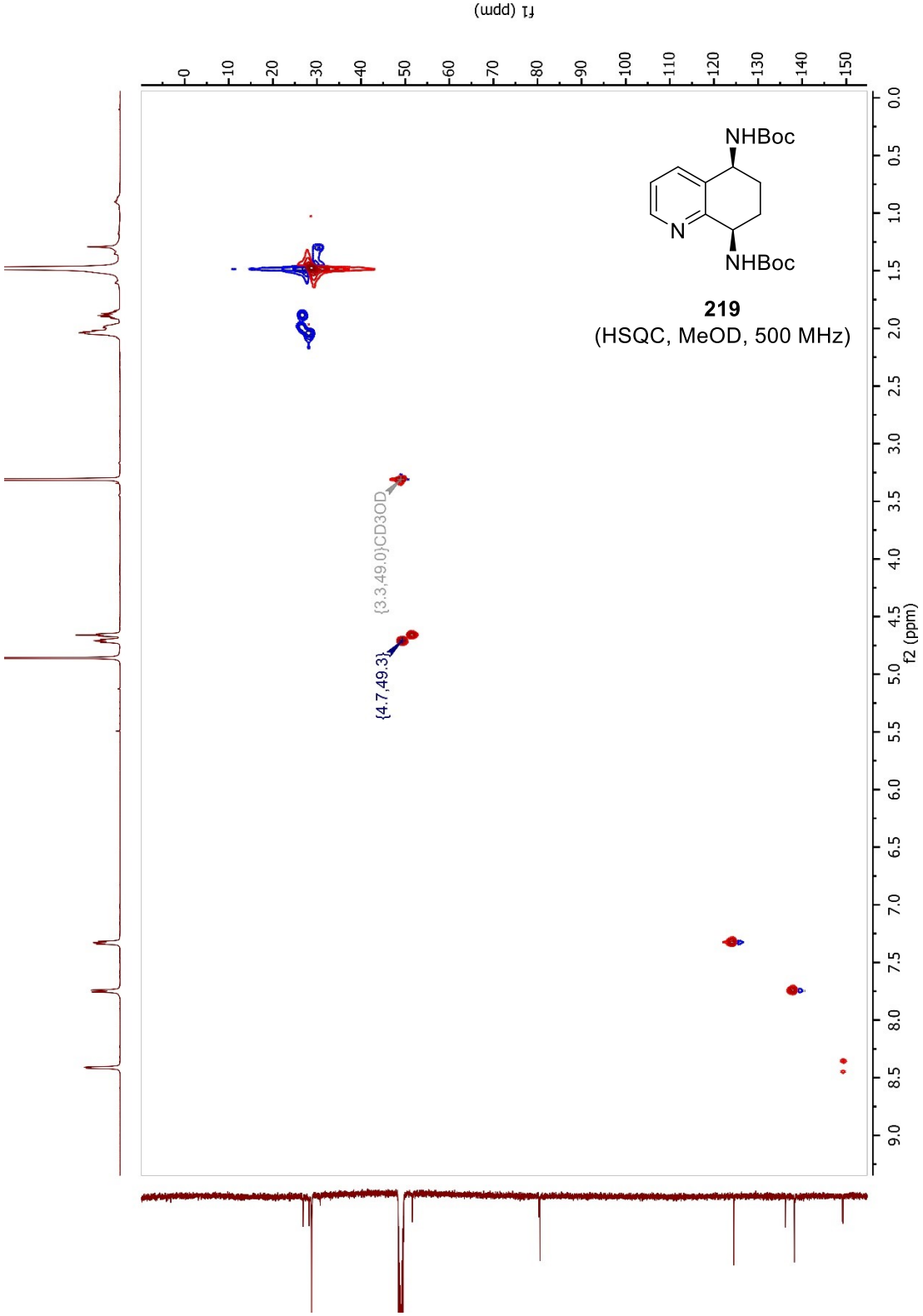

1.6.5.7 - ^{1}H NMR and ^{13}C NMR of pyridine condensed *syn*-1,4-diamine 220

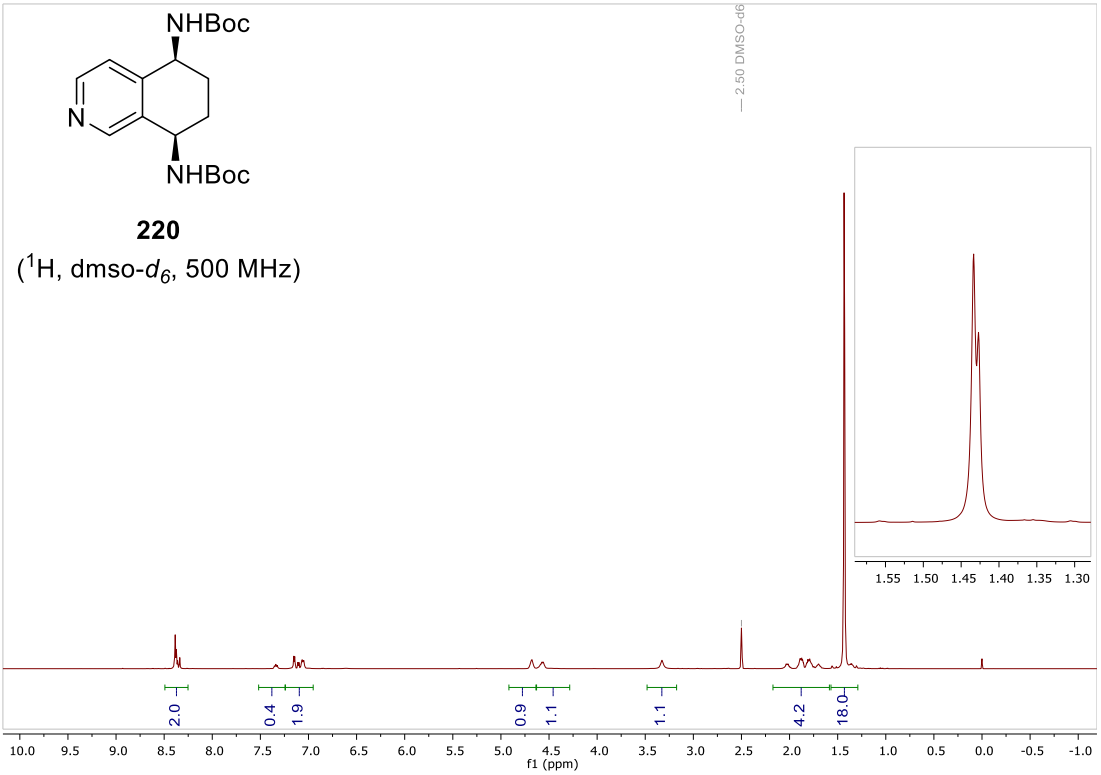

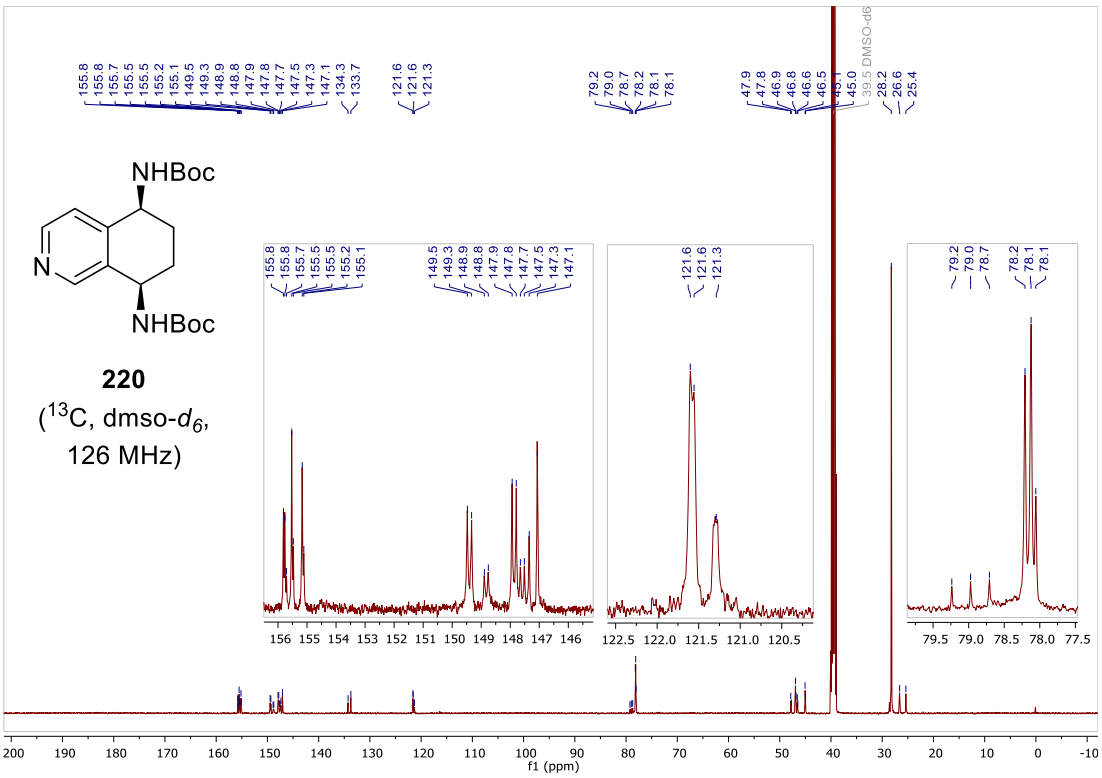

1.6.5.8 - ^{1}H VT-NMR pyridine condensed *syn*-1,4-diamine 220

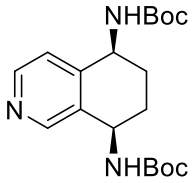

220
(^{1}H VT-NMR, dmso-d_6, 500 MHz)

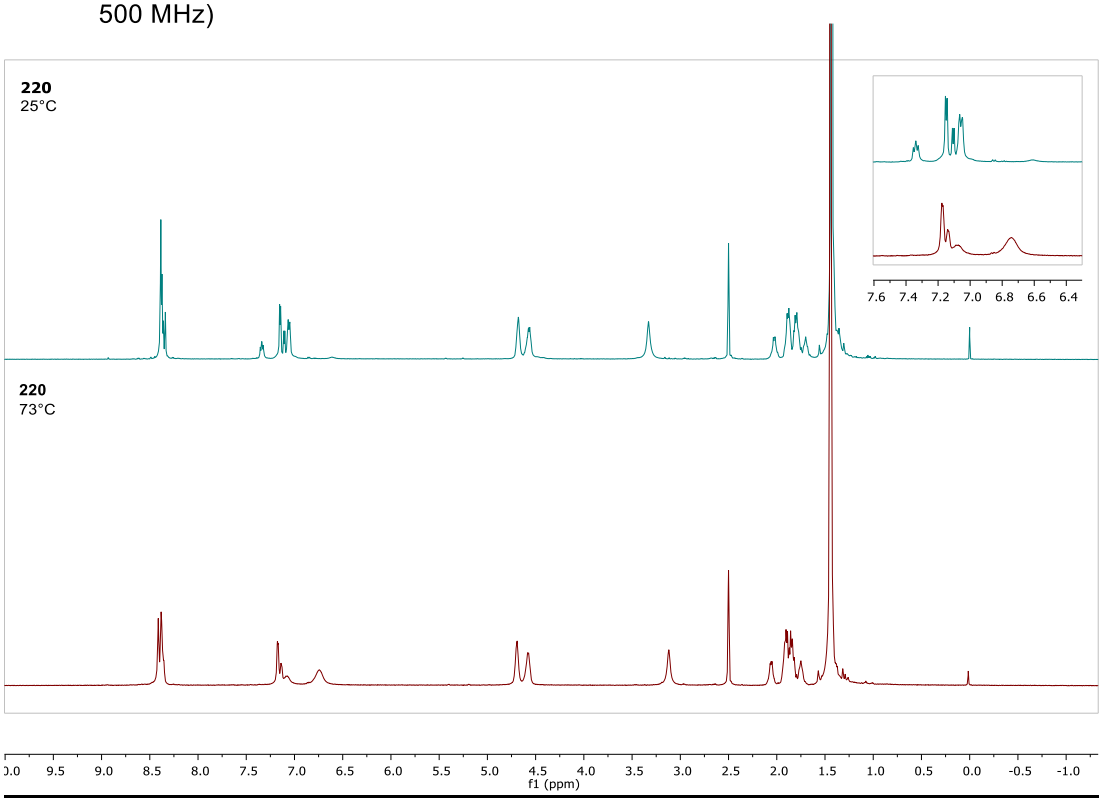

1.6.5.9 - ^{1}H NMR and ^{13}C NMR nitroso cycloadduct 231

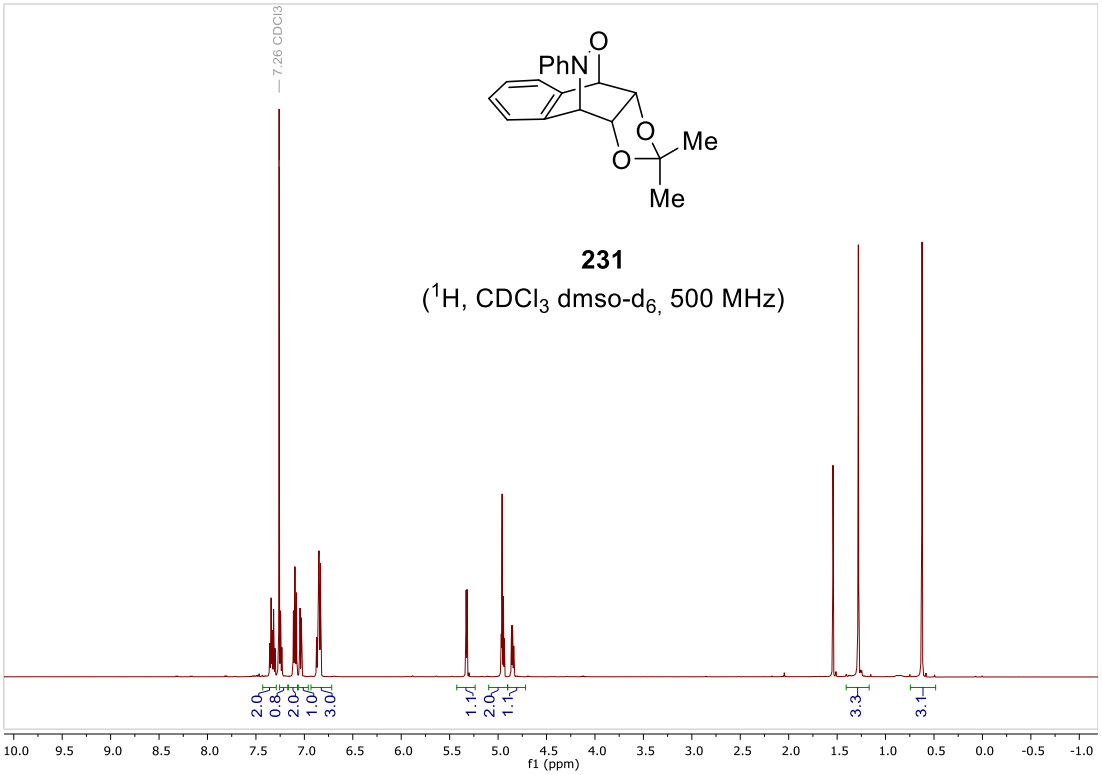

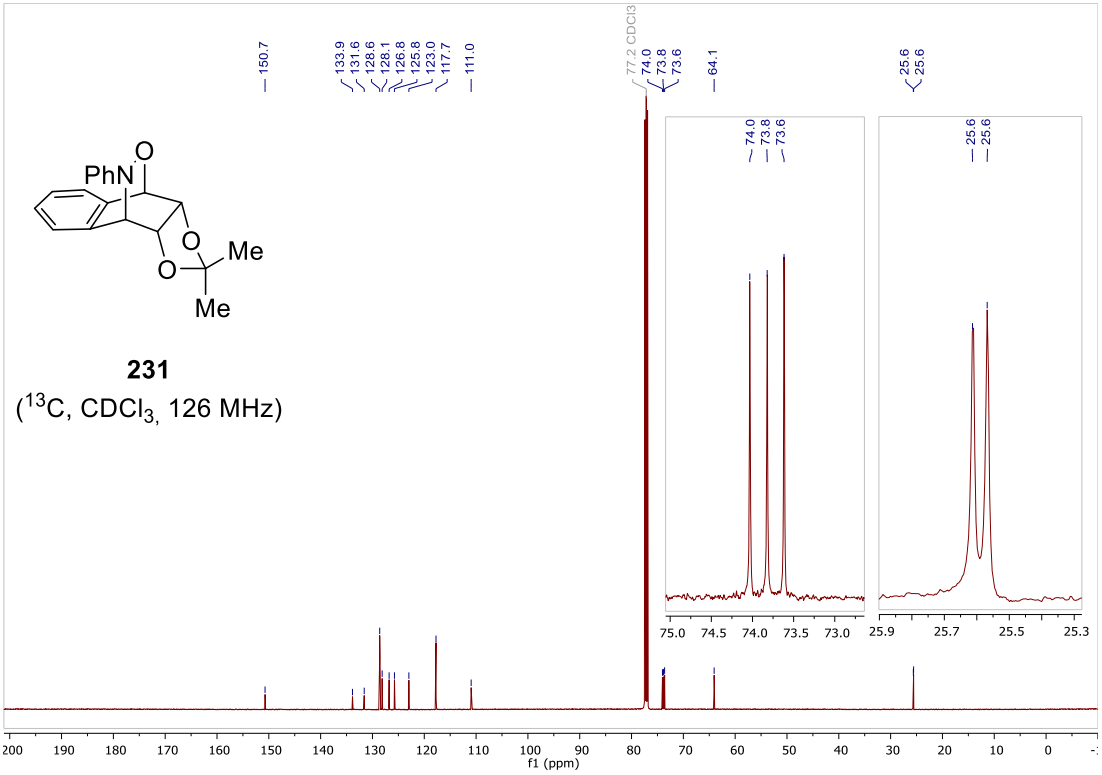

1.6.5.10 - ^{1}H NMR and ^{13}C NMR pyrazine condensed nitroso cycloadduct 233

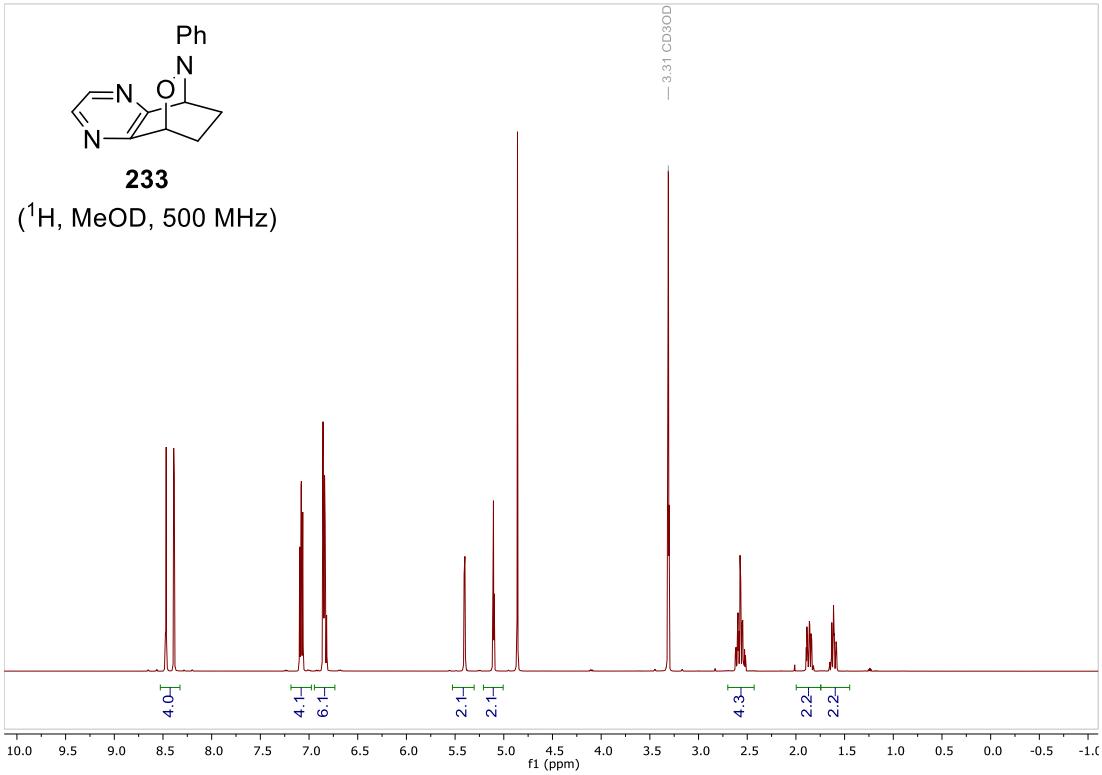

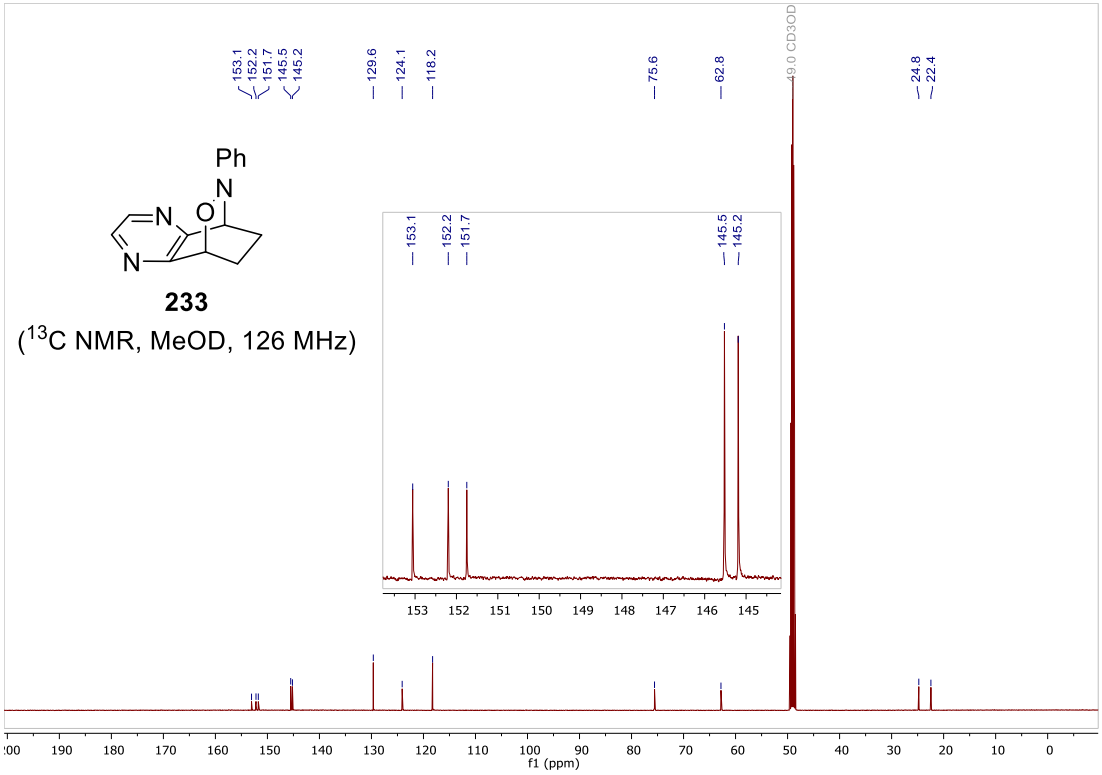

1.6.5.11 - ^{1}H NMR and ^{13}C NMR of the mixture of 226 and 227 (1.0:1.6)

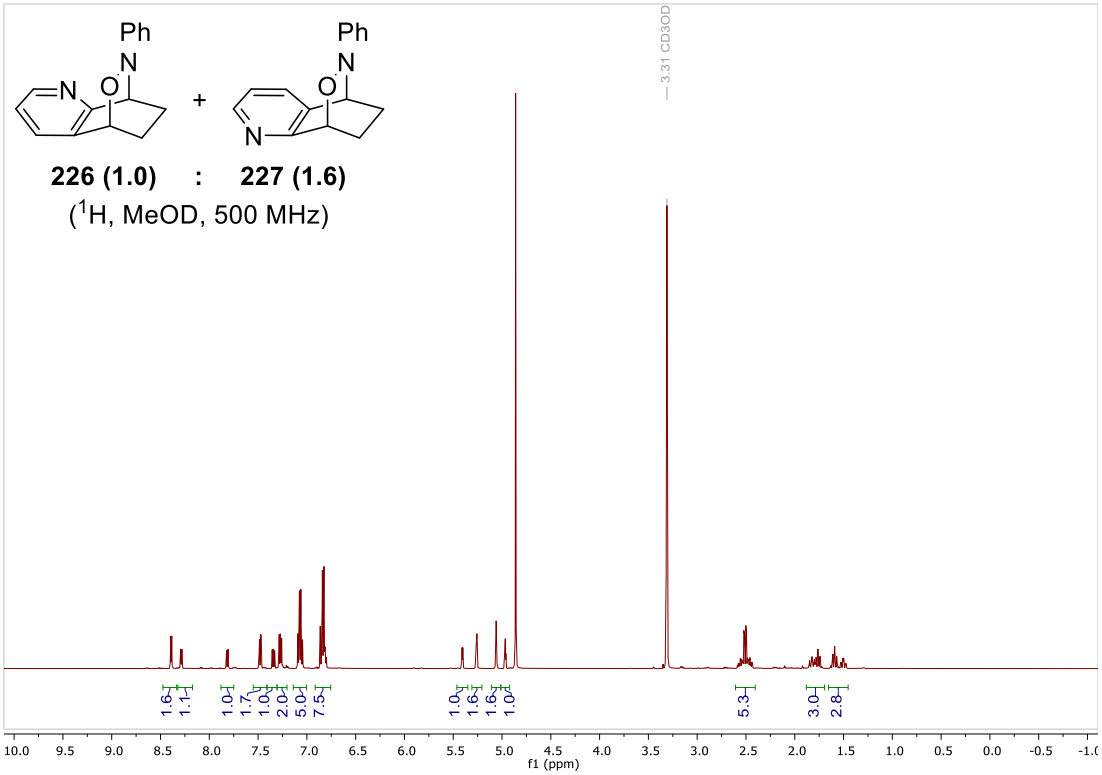

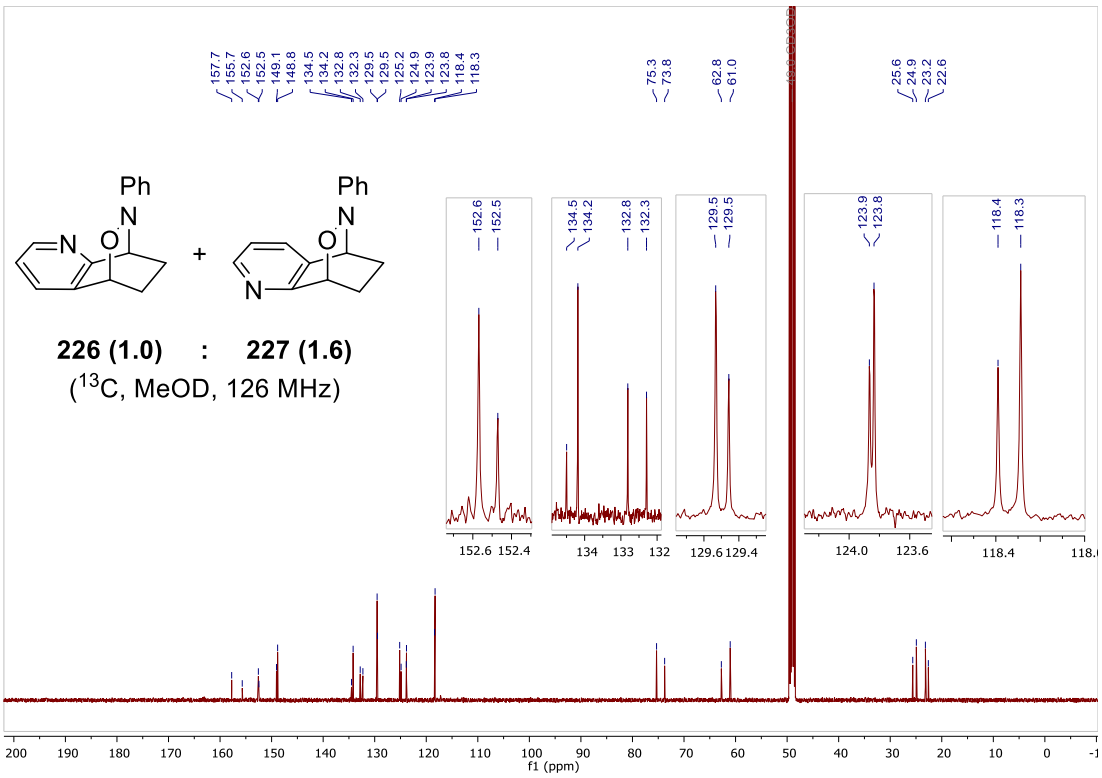

1.6.5.12 - HMBC of the mixture of 226 and 227 (1.0:1.6)

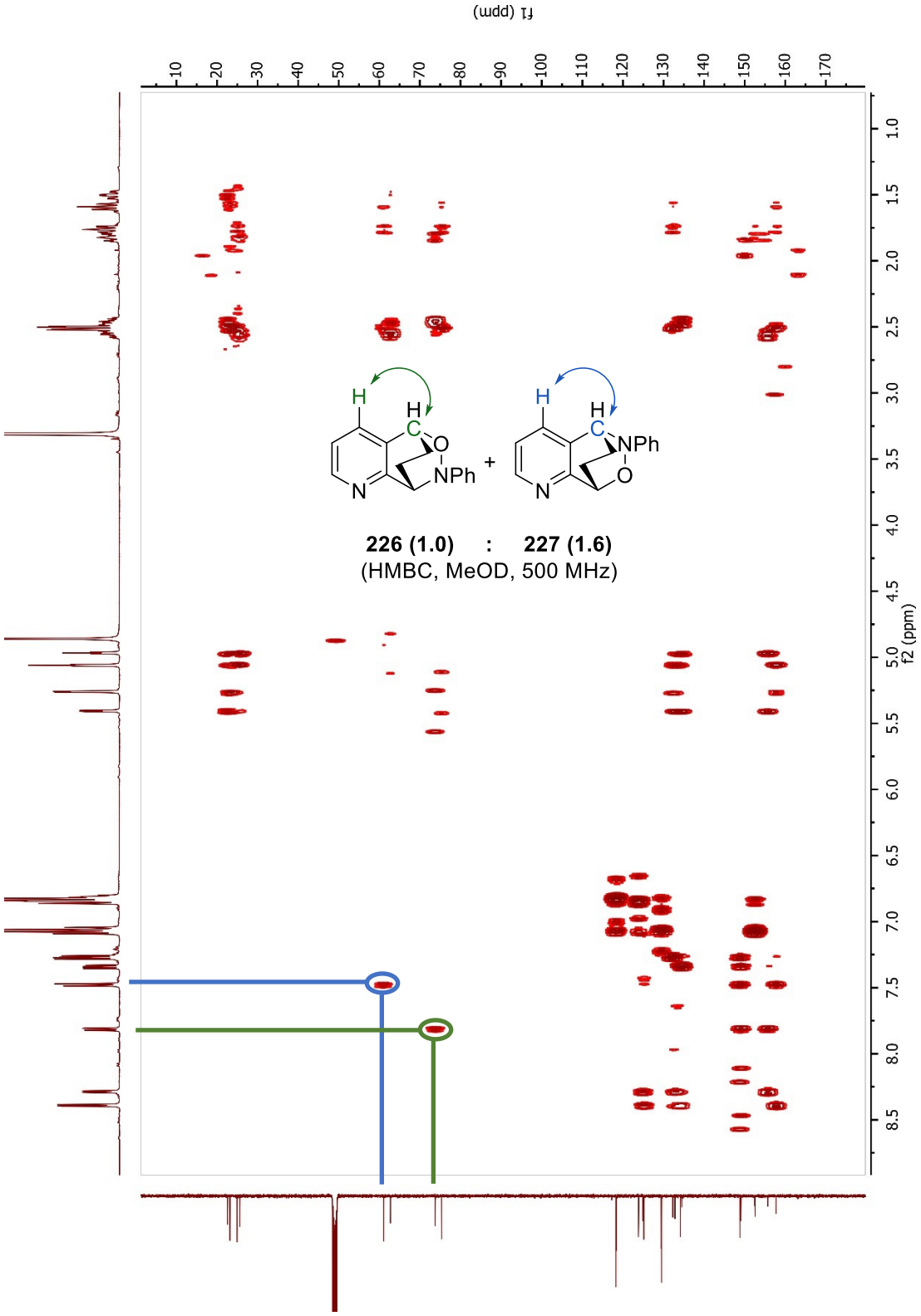

1.6.5.13 - ^{1}H NMR and ^{13}C NMR of the mixture of 226 and 227 (1.0:1.3)

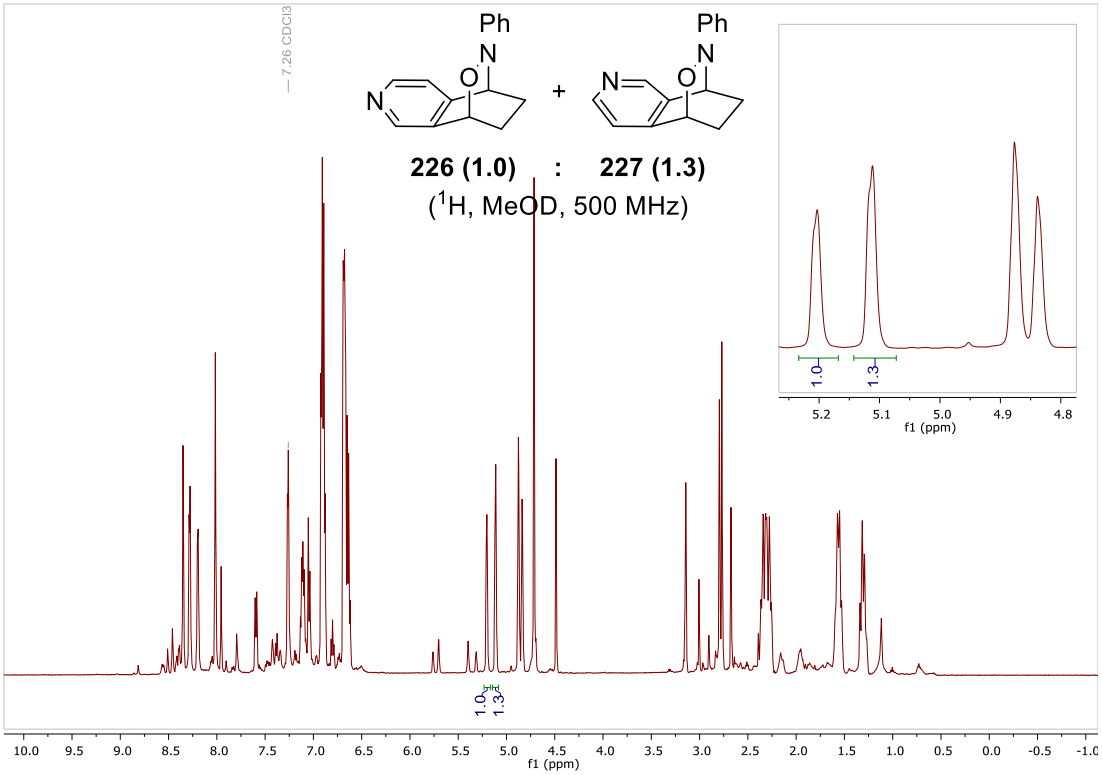

1.6.5.14 - ^{1}H NMR and ^{13}C NMR of the mixture of 226 and 227 (1.0:2.1)

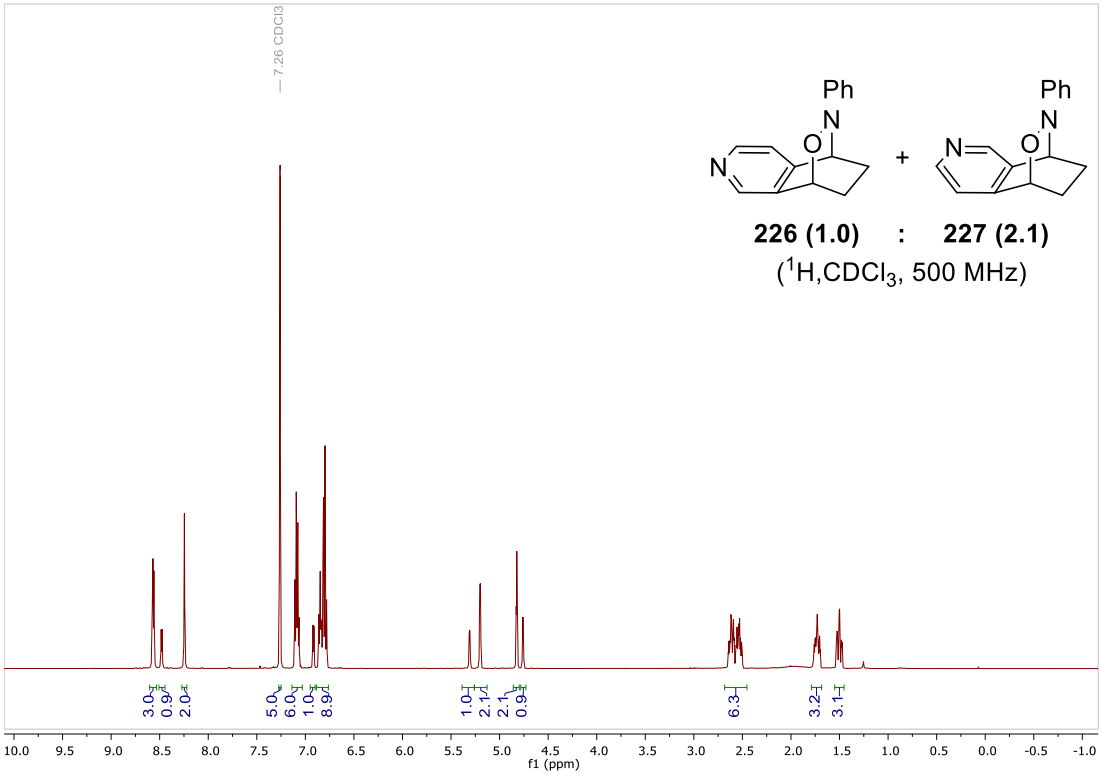

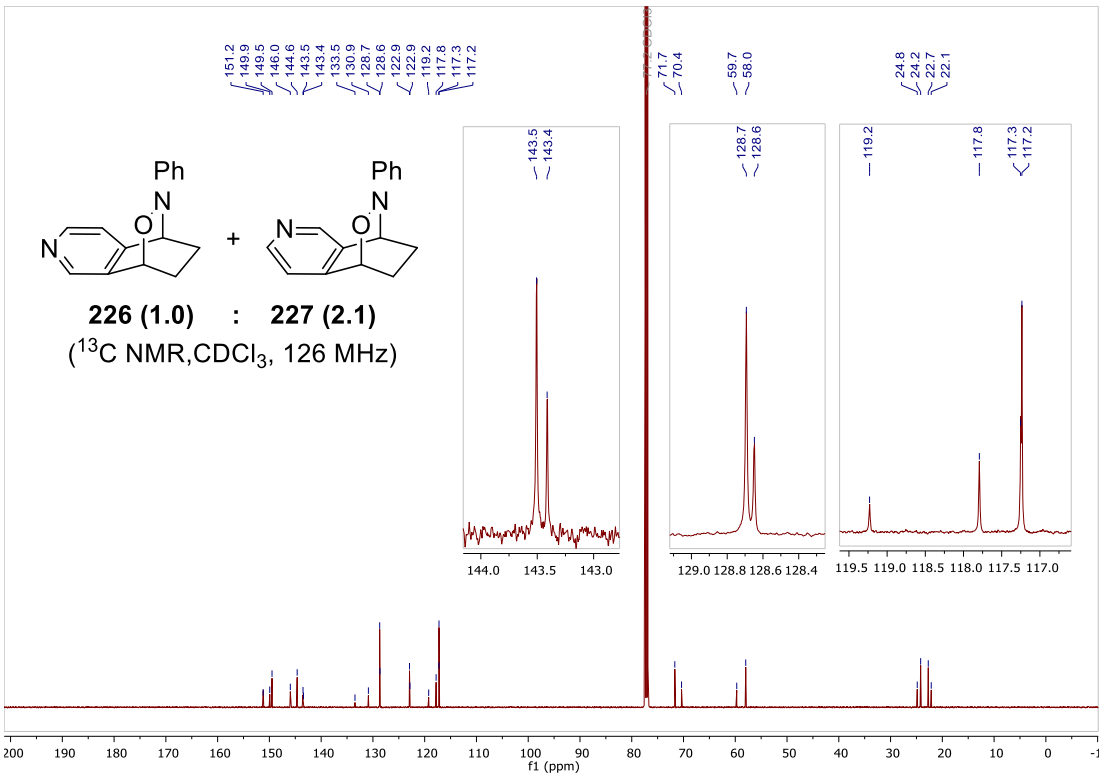

1.6.5.15 - HSQC of the mixture of 227 and 226 (1.0:2.1)

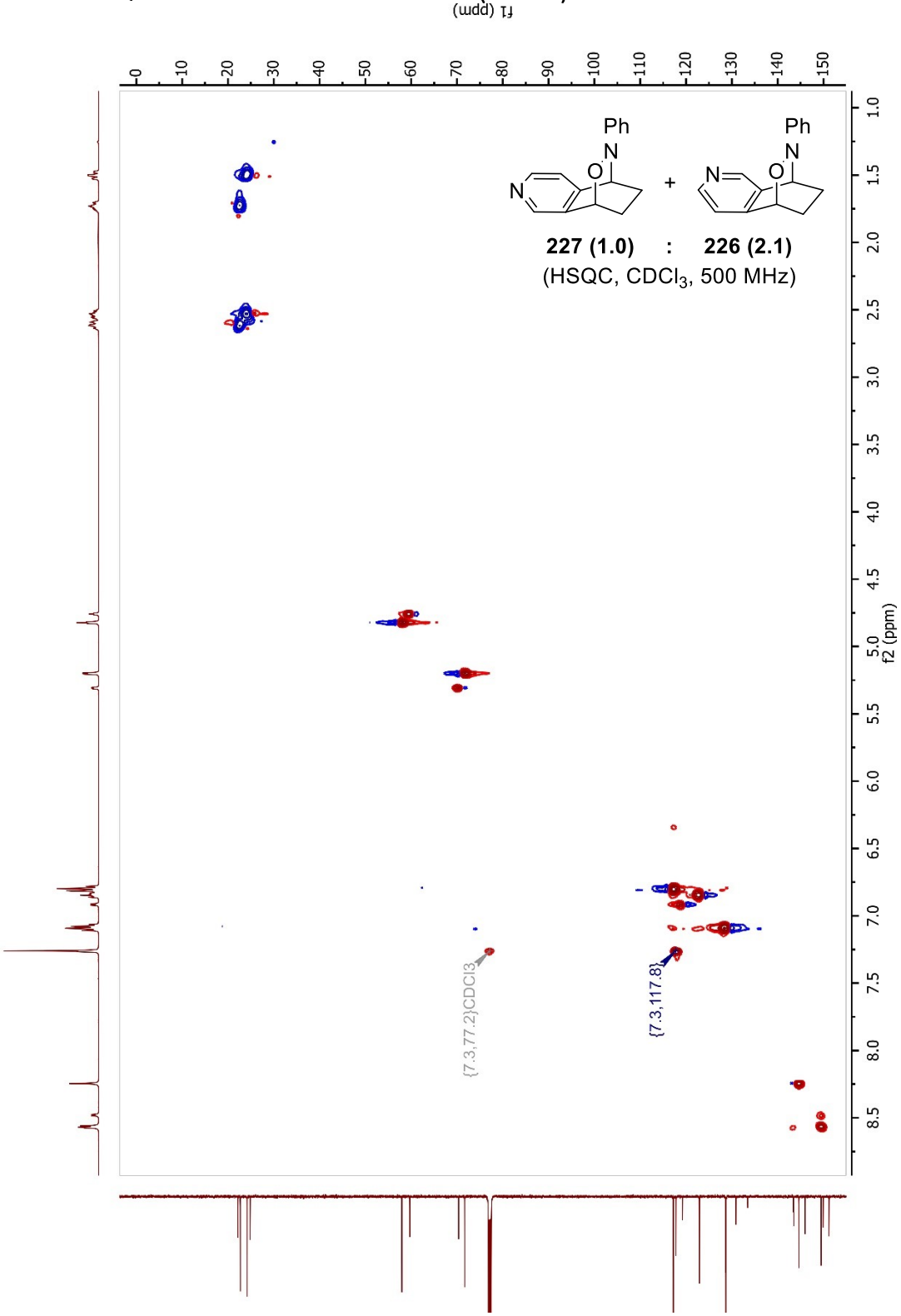

1.6.5.16 - HMBC of the mixture of 227 and 226 (1.0:2.1)

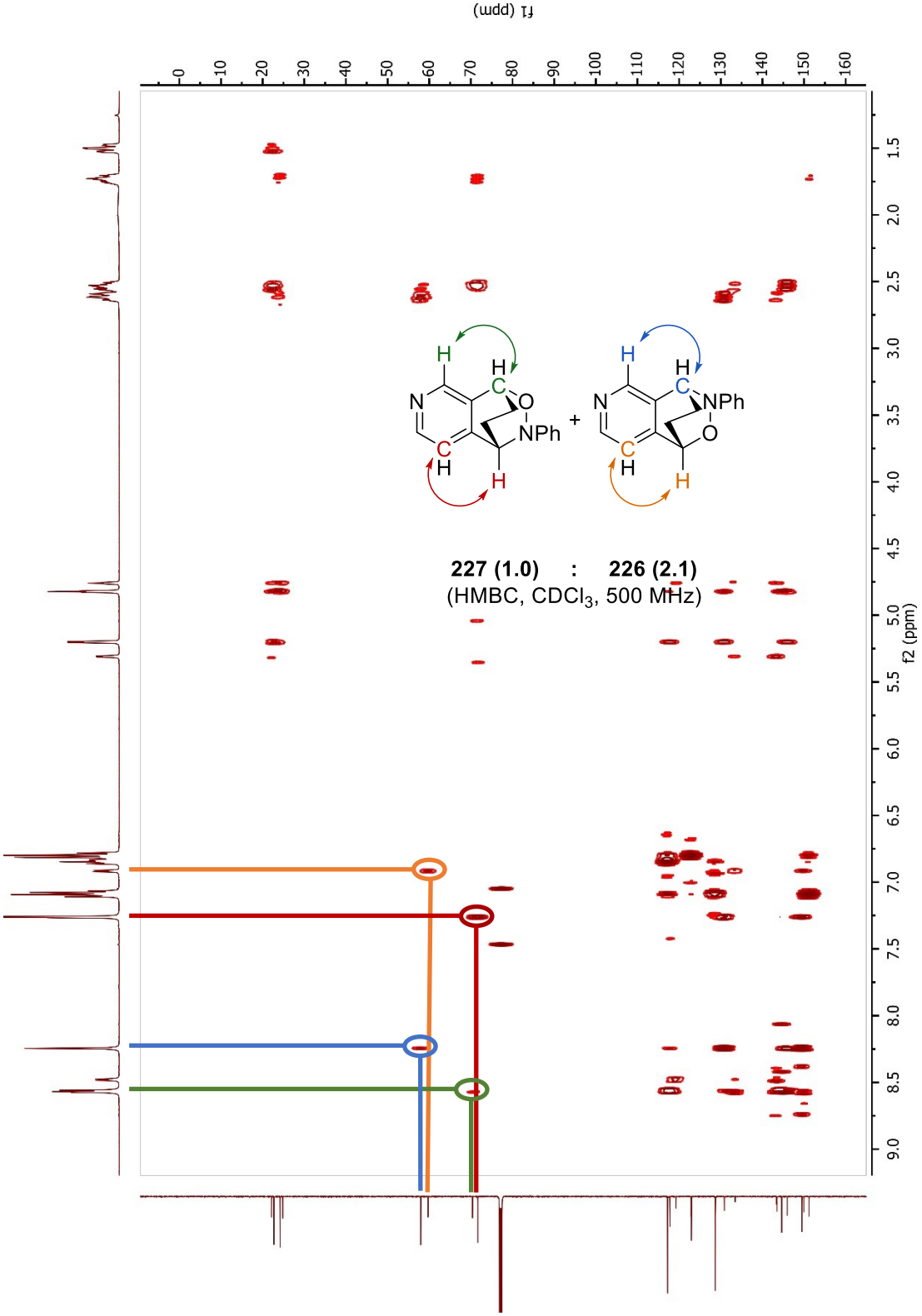

1.6.5.17 - ^{1}H NMR and ^{13}C NMR of the pyridine condensed nitroso cycloadduct 227

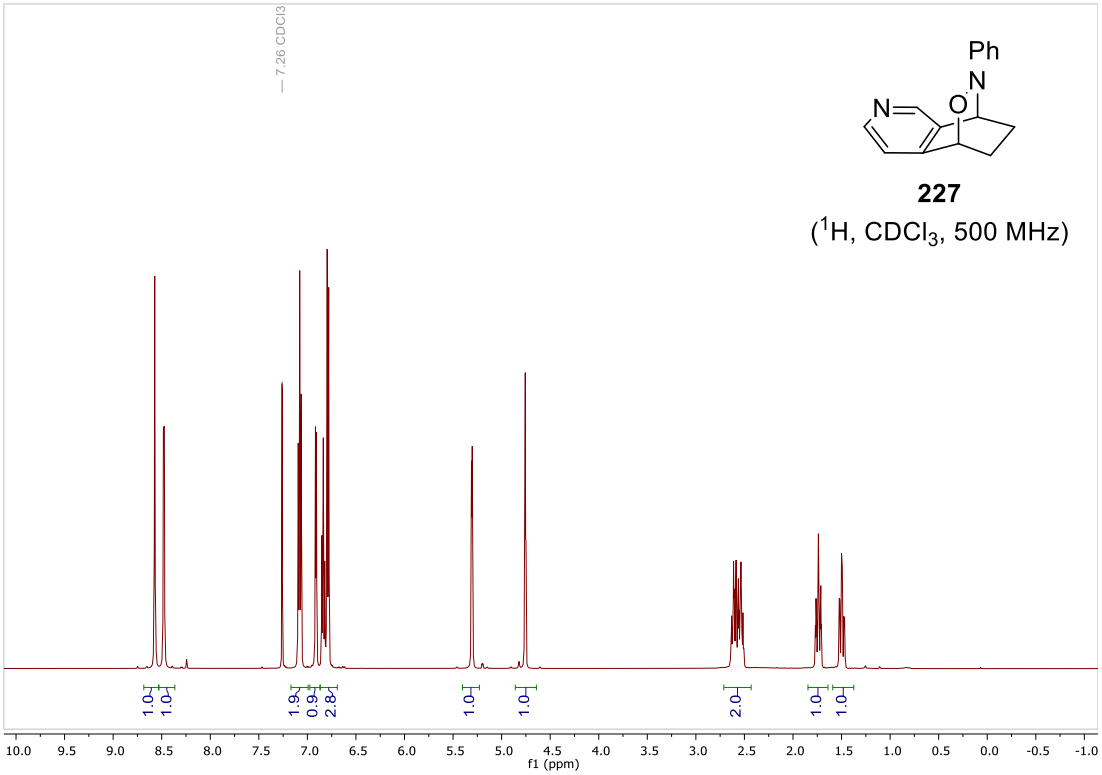

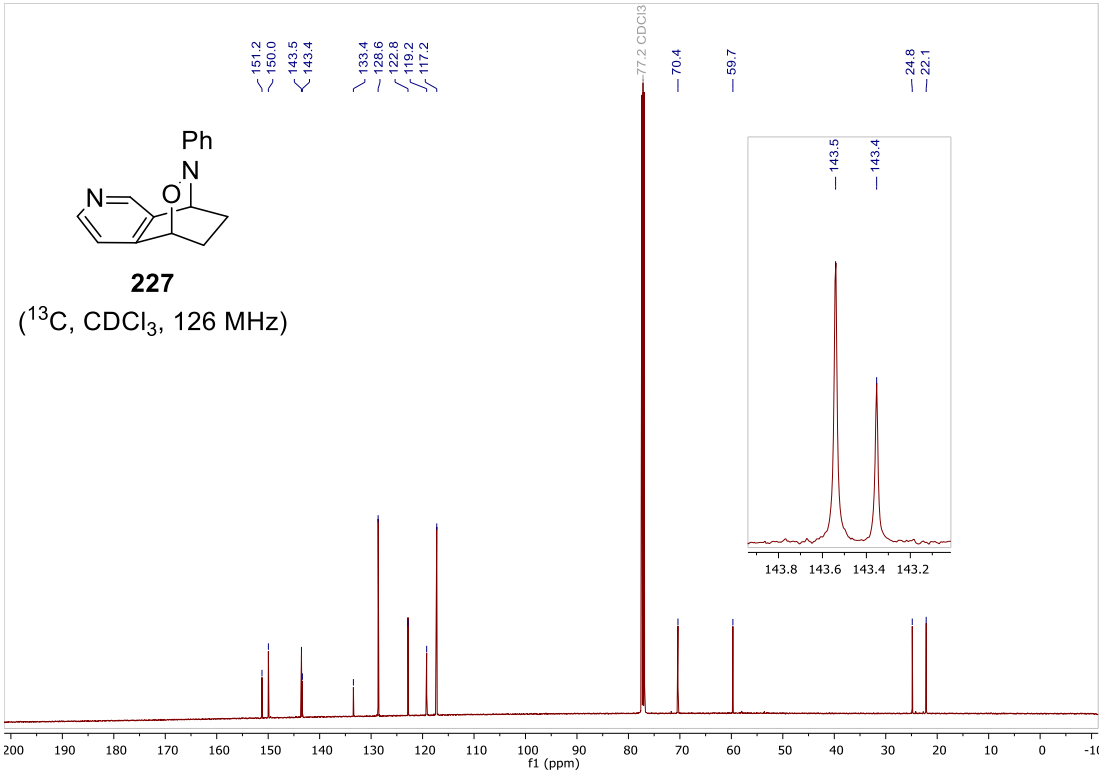

1.6.5.18 - HMBC of the pyridine condensed nitroso cycloadduct 227

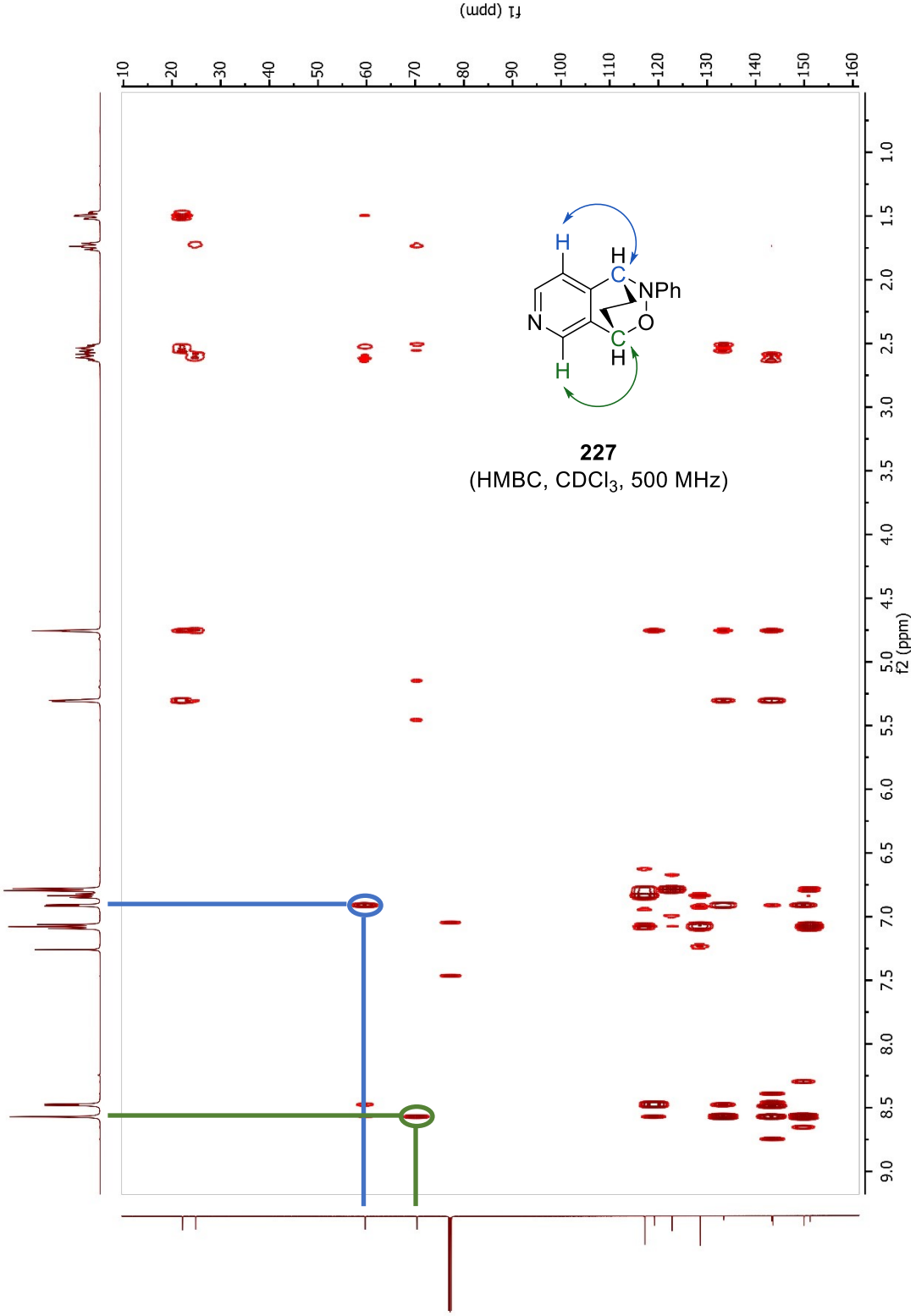

1.6.5.19 - ^{1}H NMR and ^{13}C NMR of the benzene condensed *syn*-1,4-aminol 230

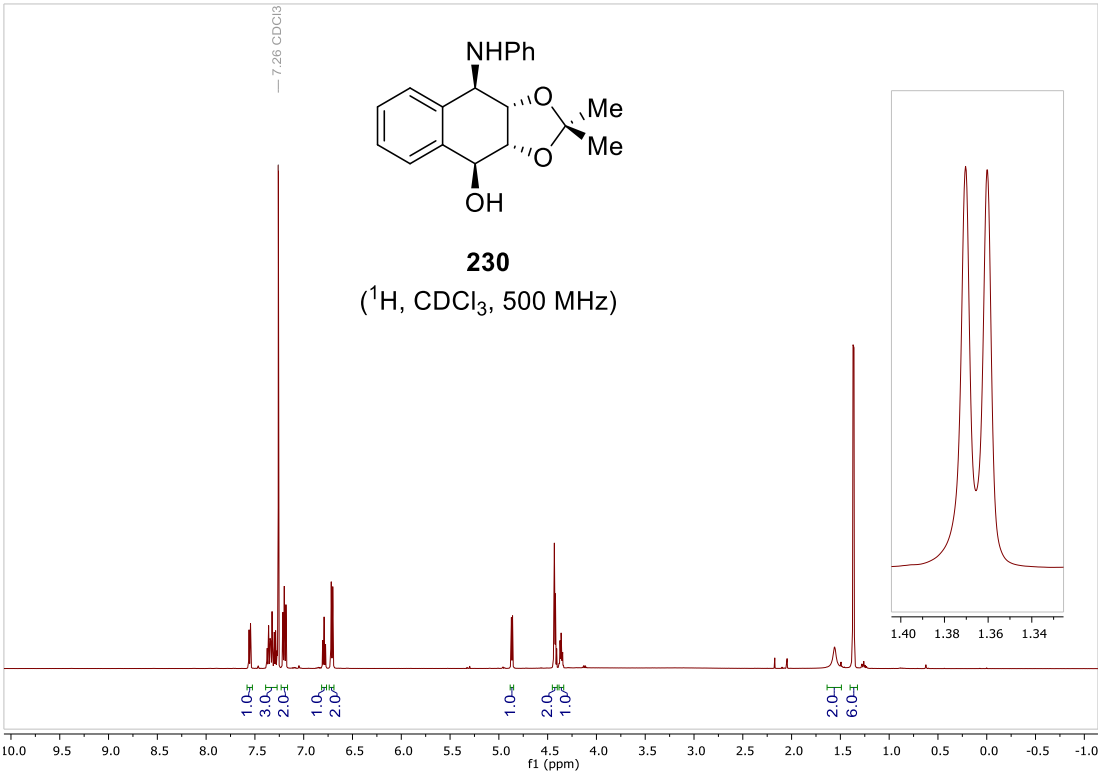

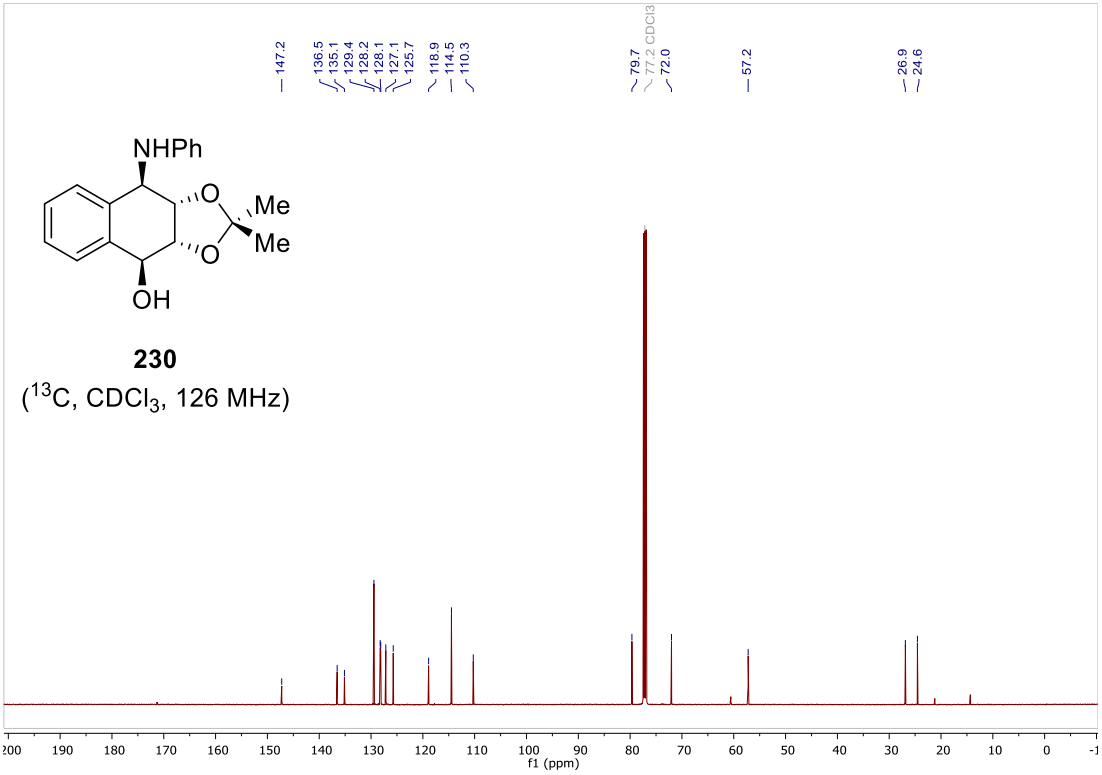

1.6.5.20 - ^{1}H NMR and ^{13}C NMR of the pyrazine condensed *syn*-1,4-aminol 232

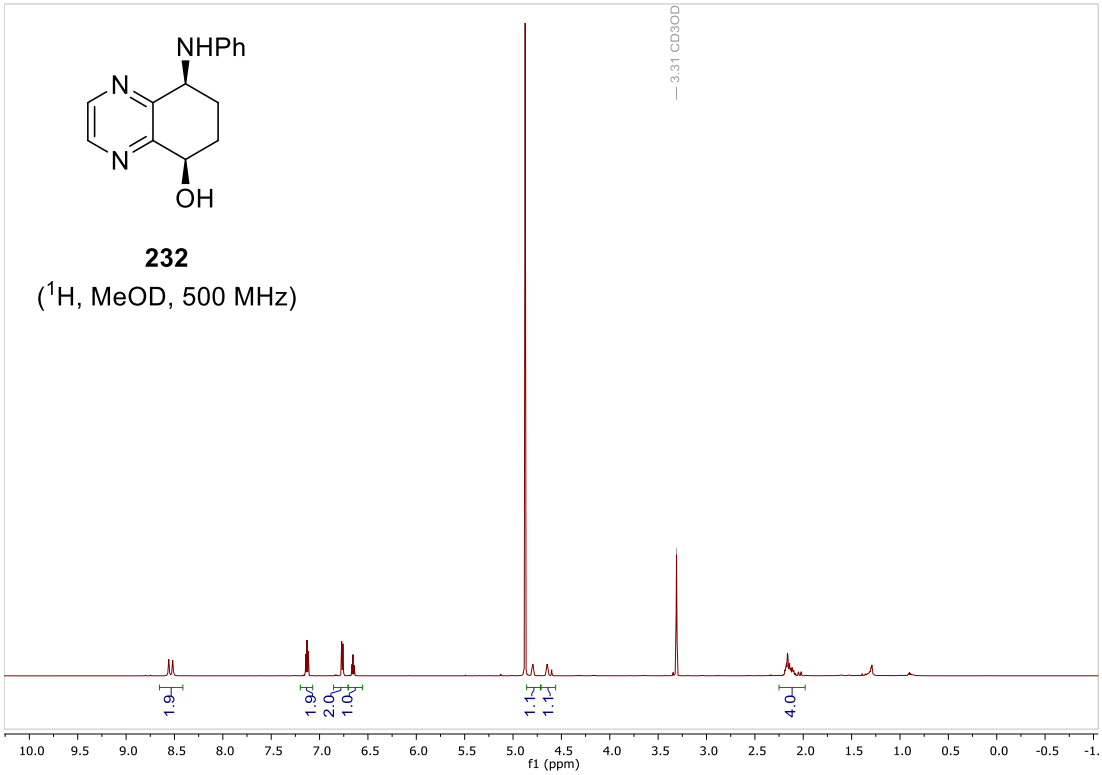

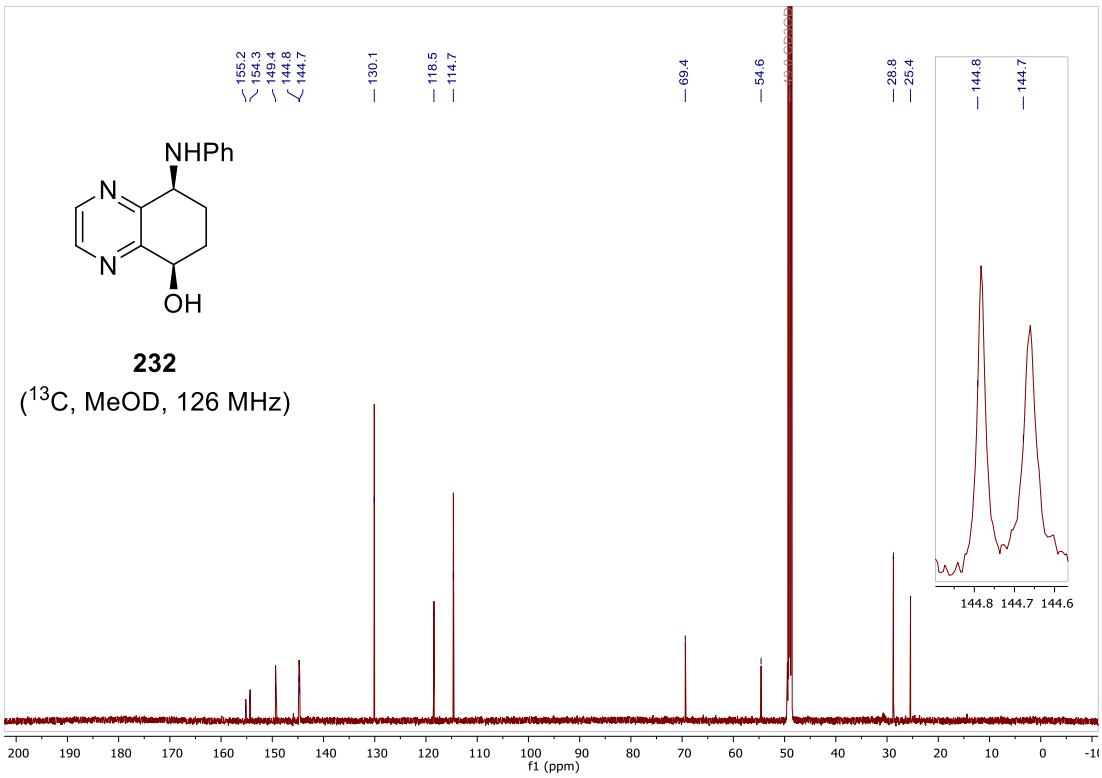

1.6.5.21 - ^{1}H NMR and ^{13}C NMR of the pyridine condensed syn-1,4-aminol 224

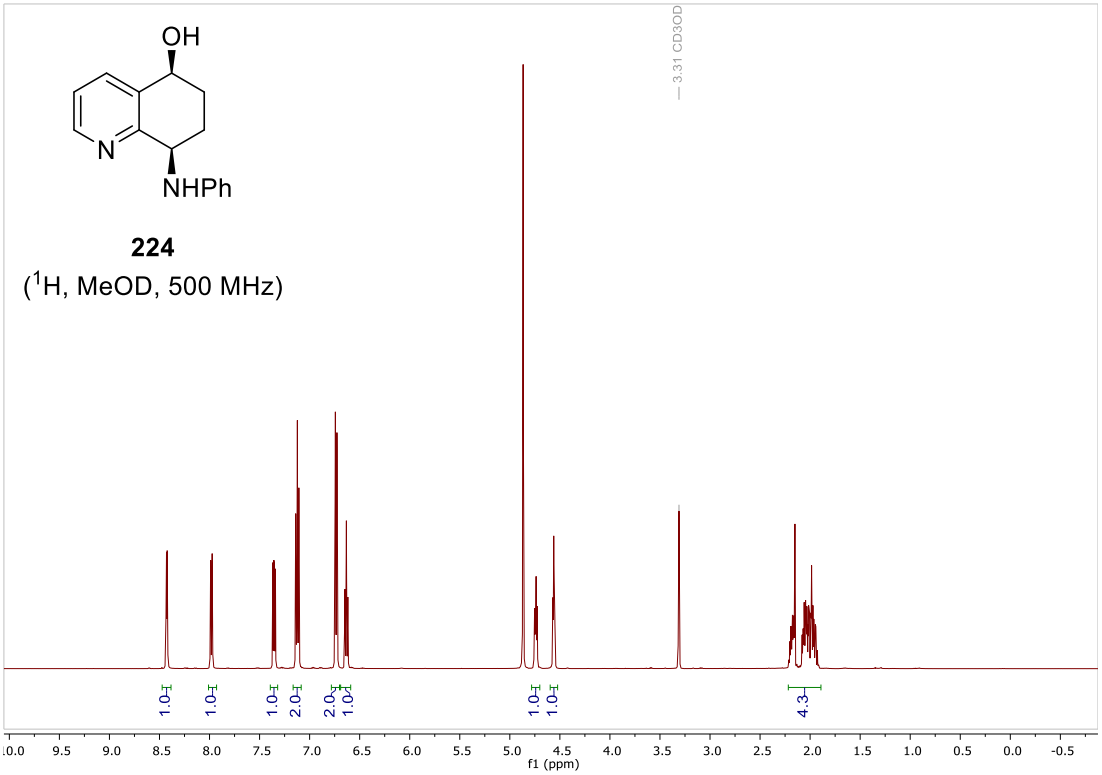

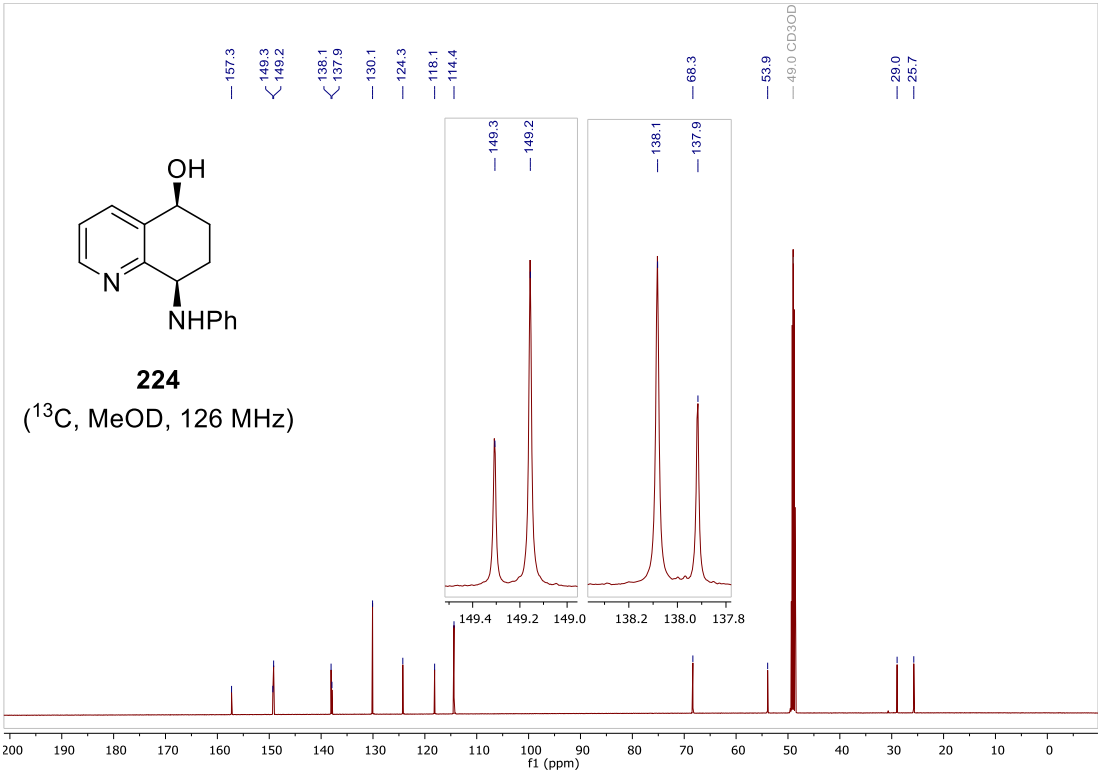

1.6.5.22 - HMBC of the pyridine condensed *syn*-1,4-aminol 224

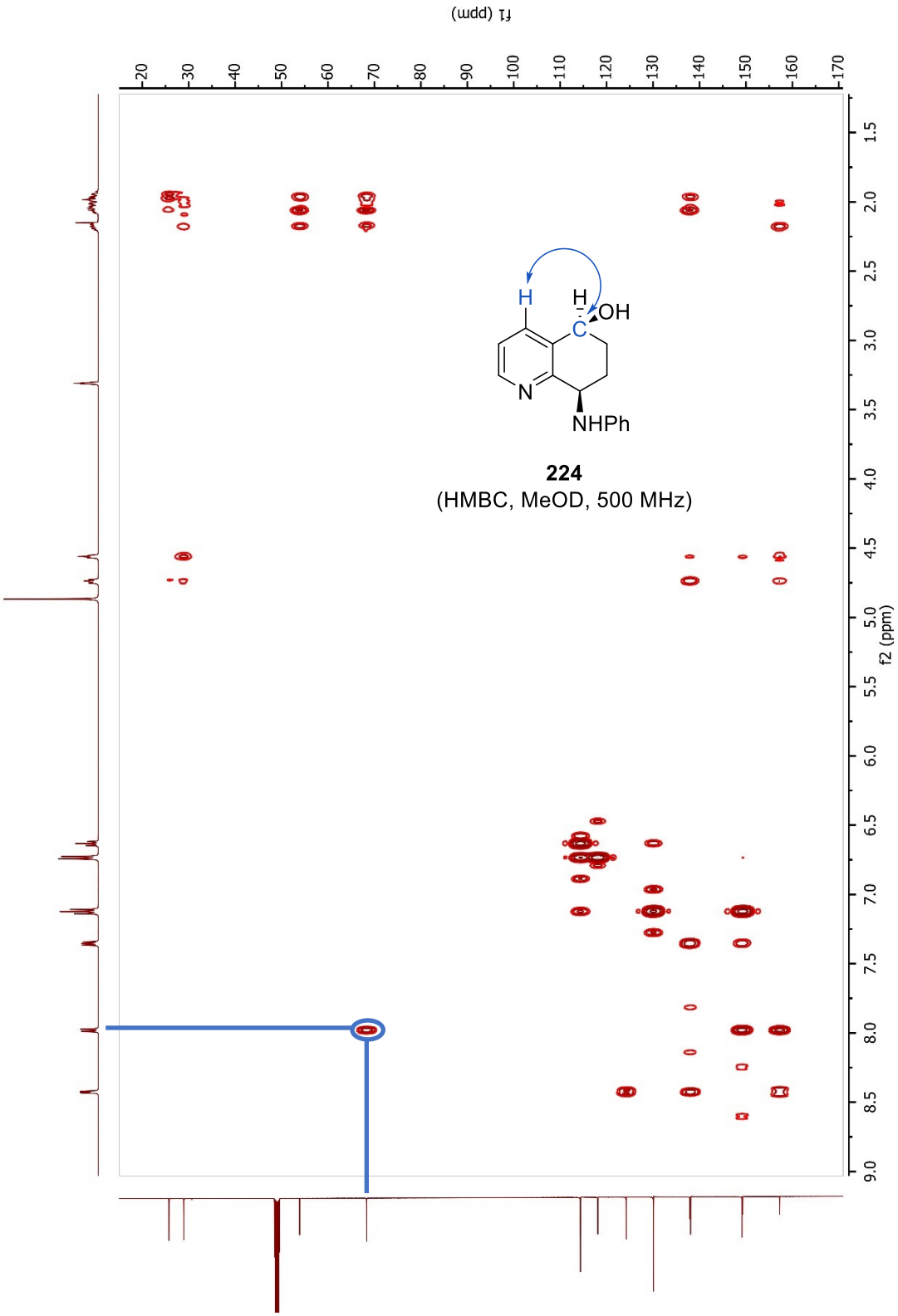

1.6.5.23 - ^{1}H NMR and ^{13}C NMR of the pyridine condensed *syn*-1,4-aminol 225

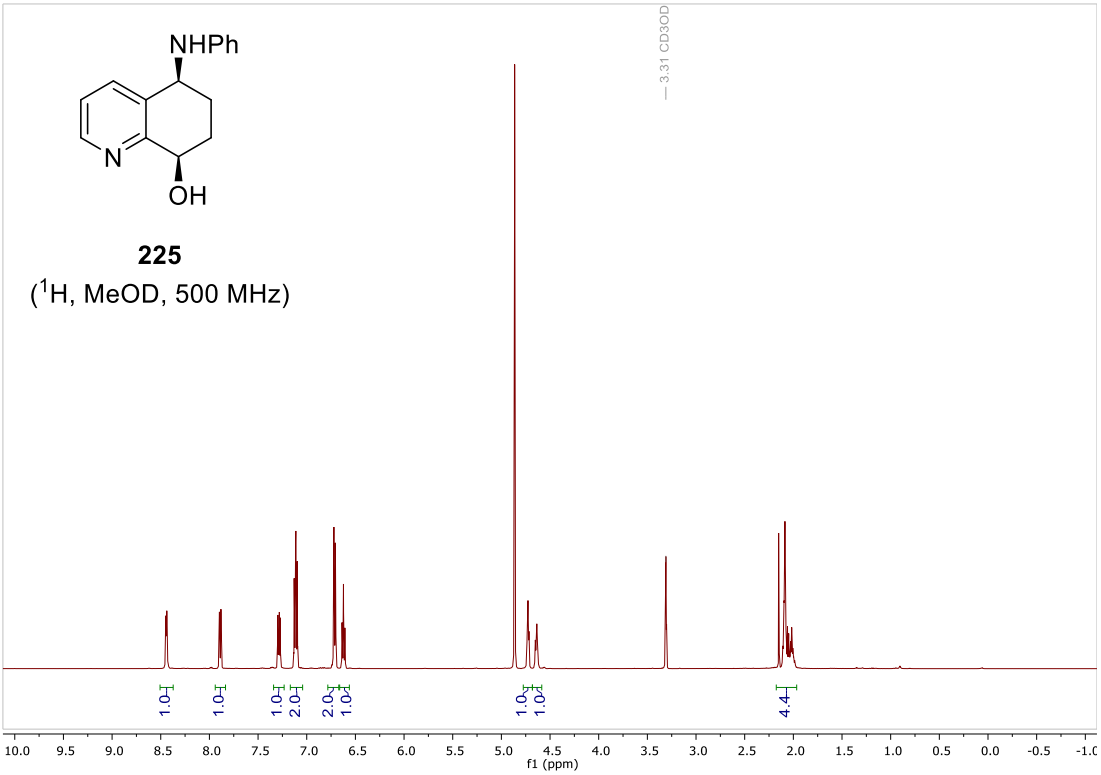

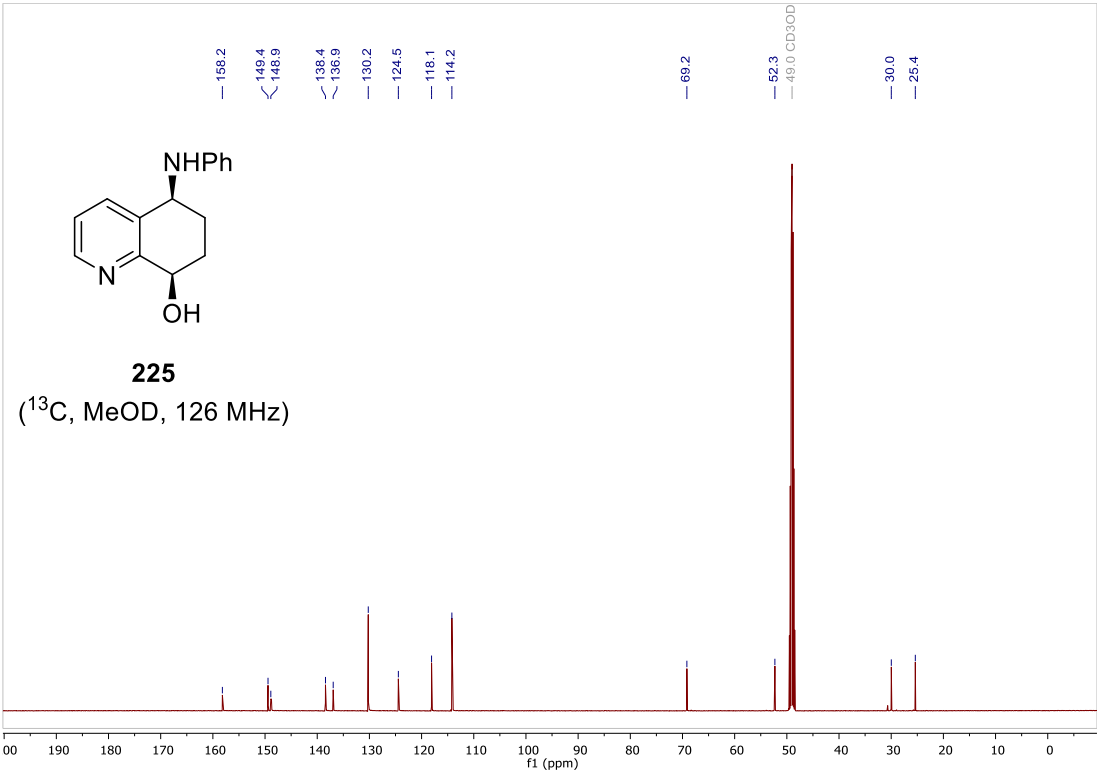

1.6.5.24 - HMBC of the pyridine condensed *syn*-1,4-aminol 225

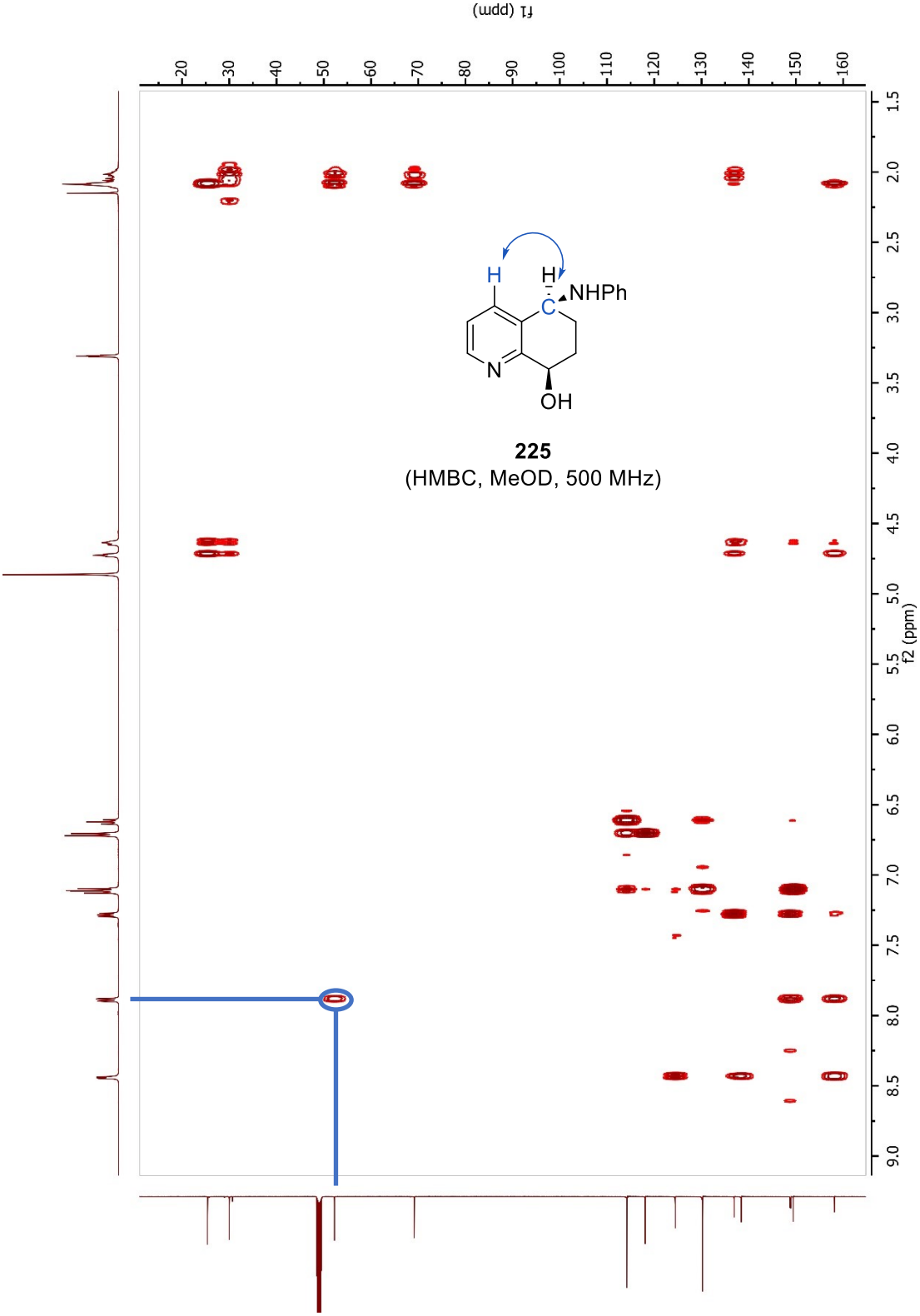

1.6.5.25 - ^{1}H NMR and ^{13}C NMR of the pyridine condensed *syn*-1,4-aminol 229

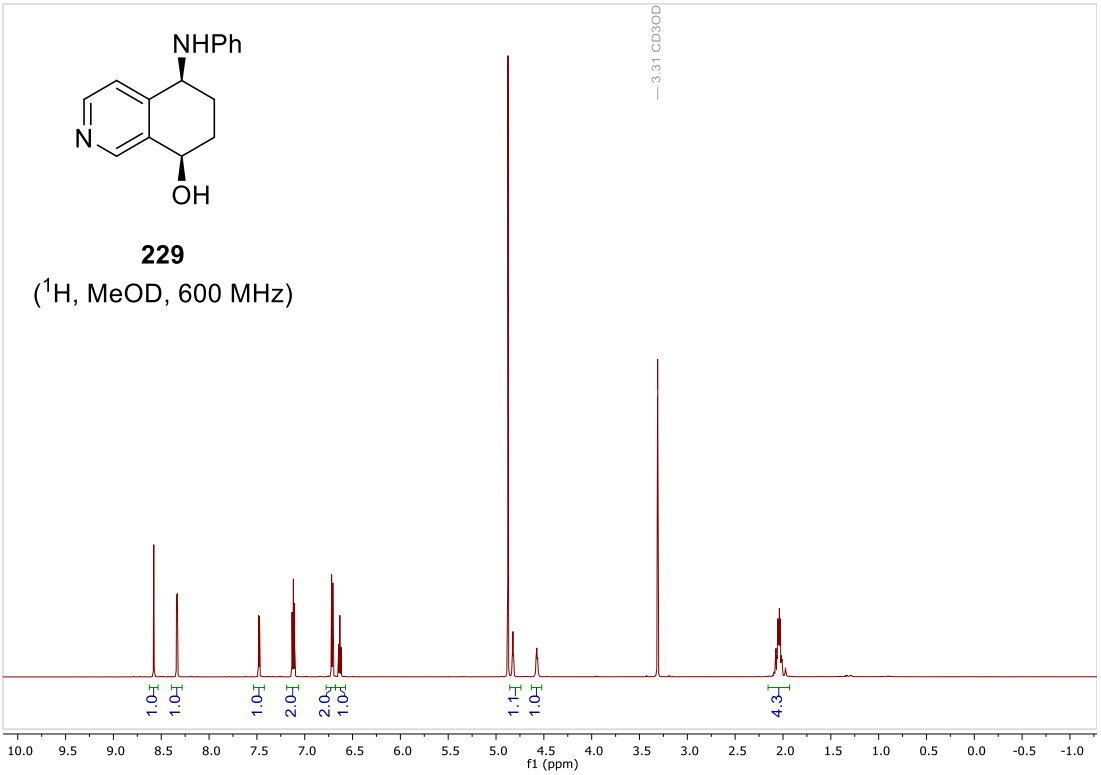

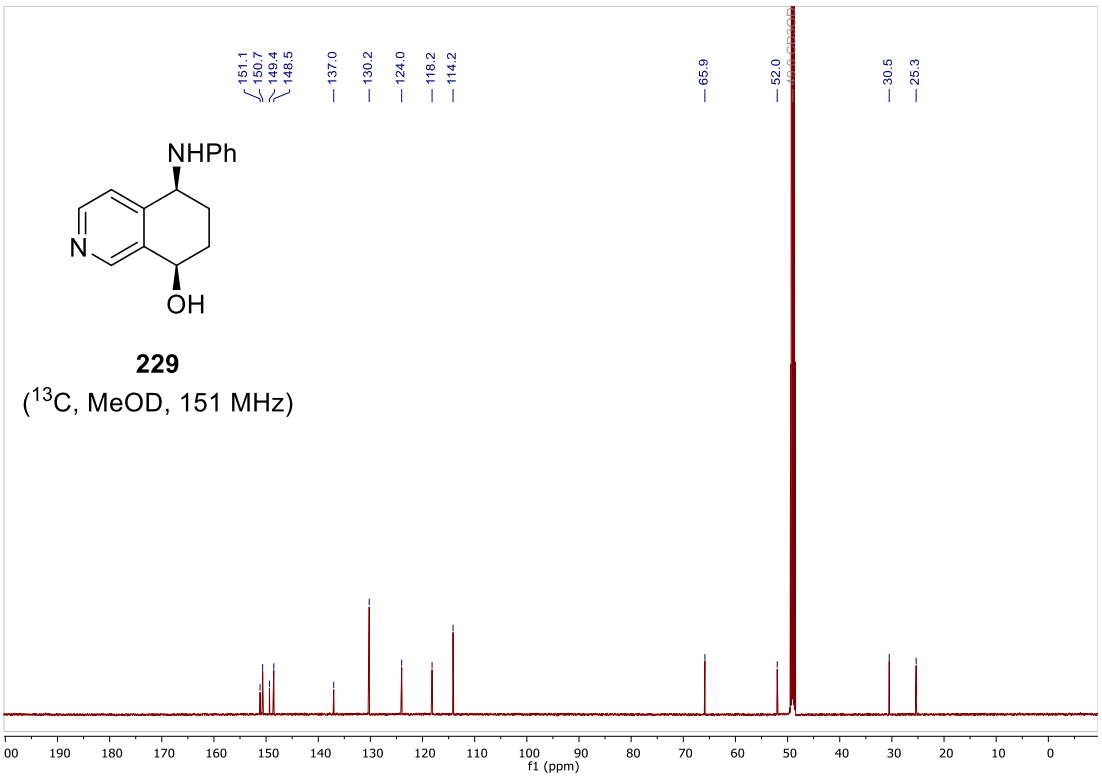

1.6.5.26 - HMBC of the pyridine condensed *syn*-1,4-aminol 229

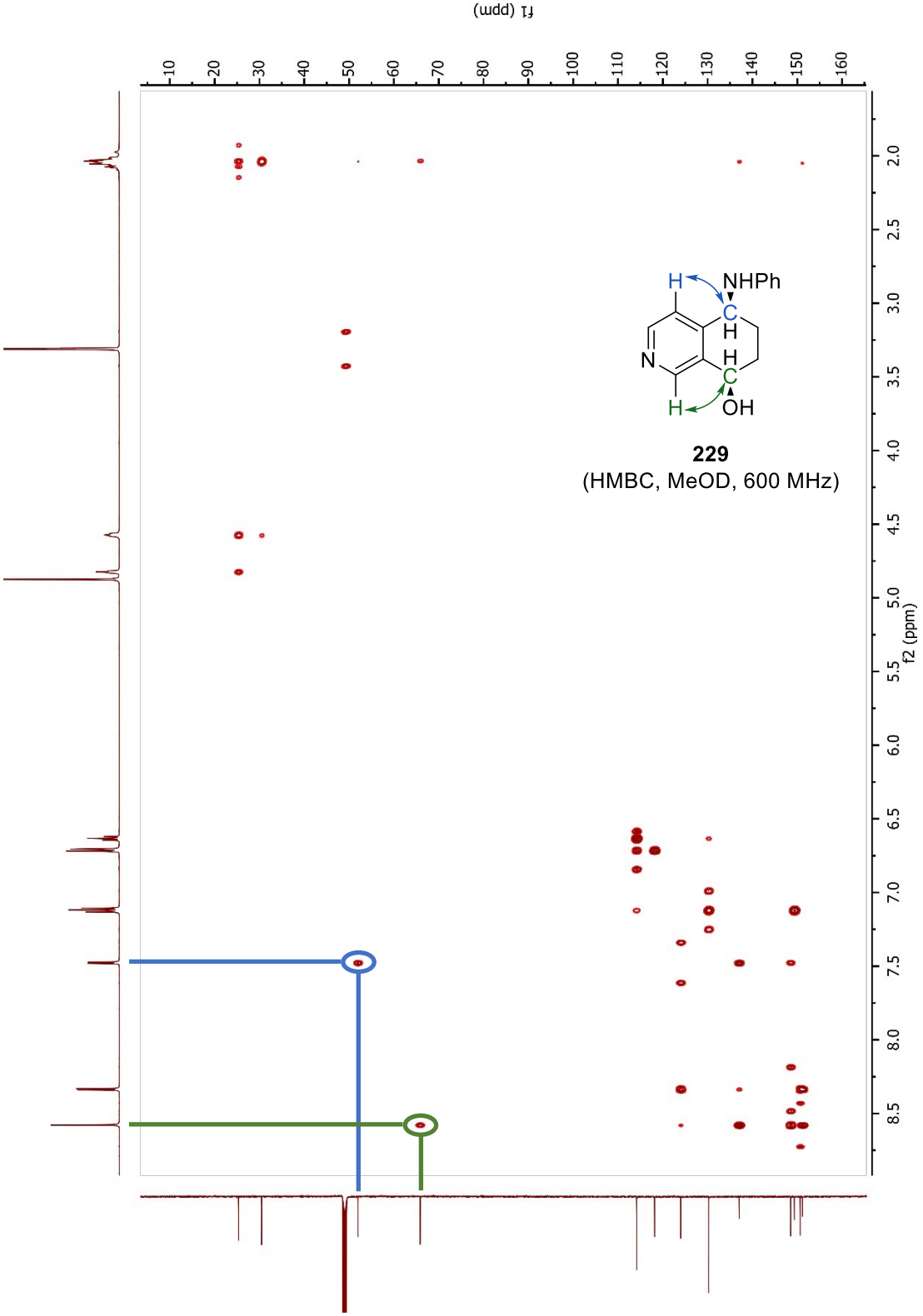

1.6.5.27 - ^{1}H NMR and ^{13}C NMR of the pyridine condensed *syn*-1,4-aminol 228

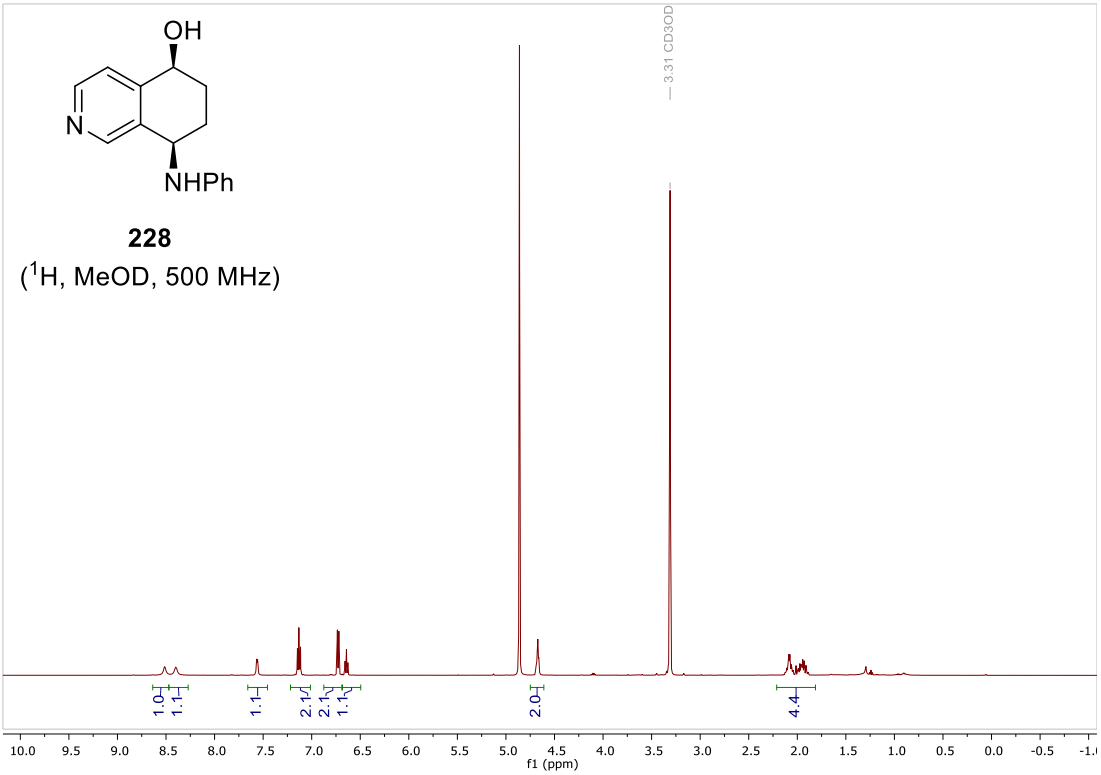

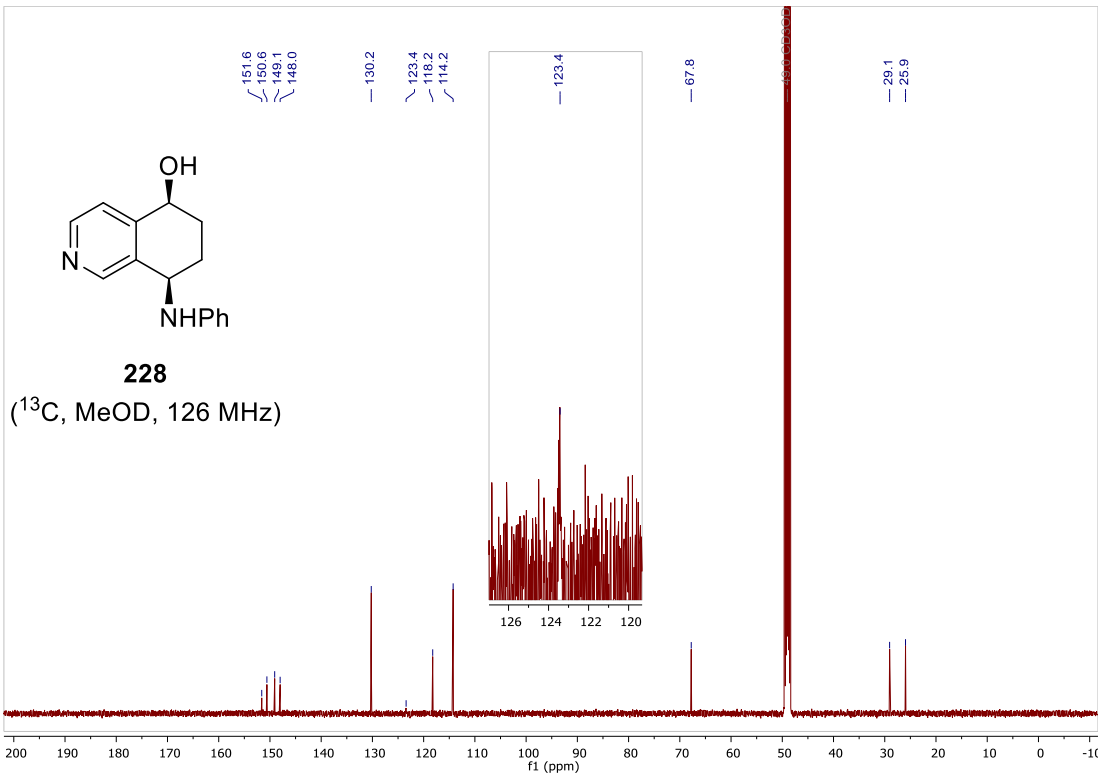

1.6.5.28 - HSQC of the pyridine condensed *syn*-1,4-aminol 228

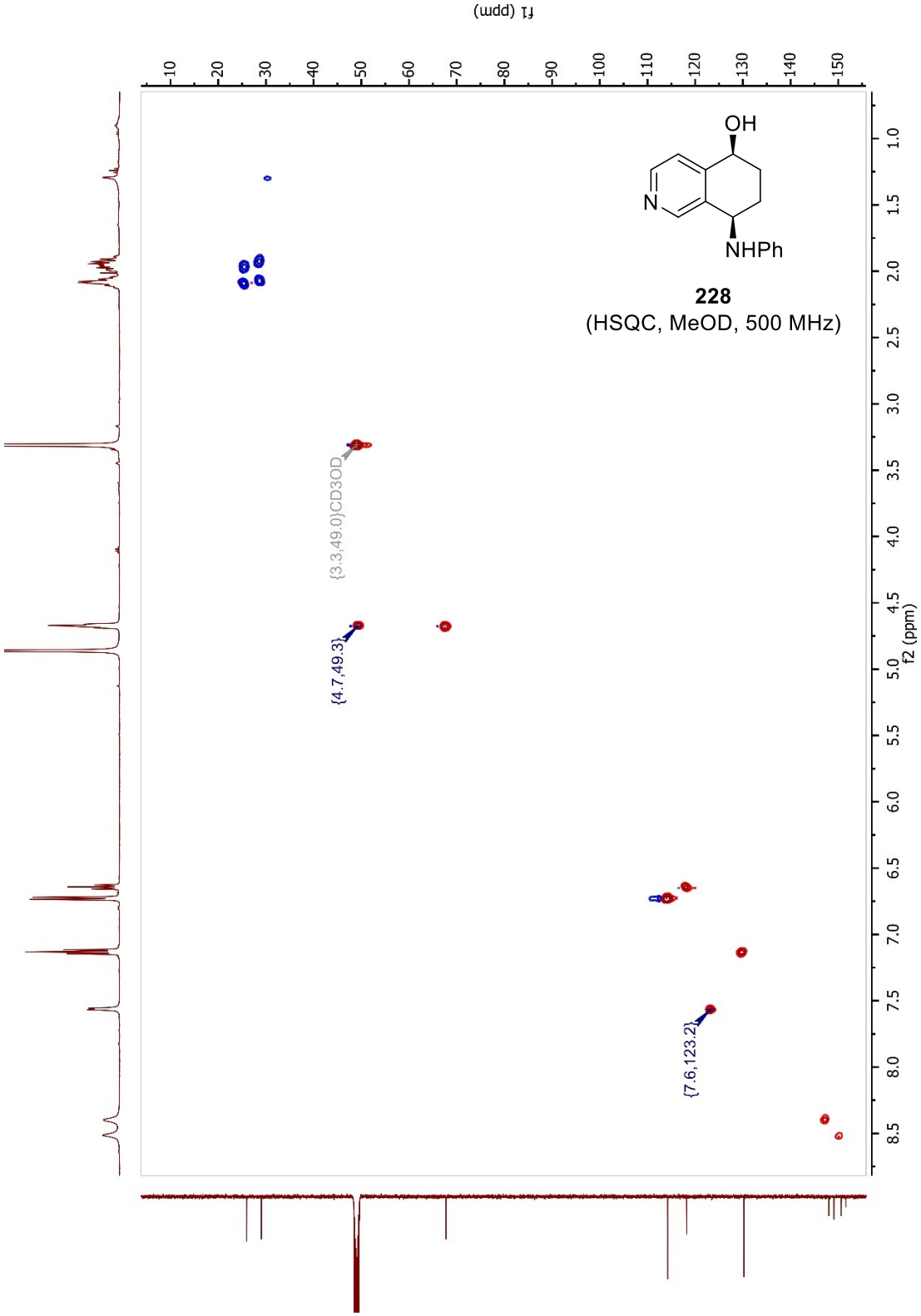

2.0.0.0 - Chapter 2: Synthesis of (hetero)arenes-bicyclo[2.1.1]hexanes sp^2-sp^3 hybrids

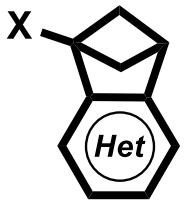

2.1.0.0 - Introduction

2.1.1.0 - Bioisosteres

In recent years, the rise of the "escape from the flatland"[1,2] concept has garnered attention of the medicinal chemistry community to the synthesis of sp^3-rich three-dimensional building blocks.[3,4] The substitution of the structural motif of drug candidates with strained bicyclic scaffolds and bioisosteres has been demonstrated to be a valuable option to improve their physiochemical properties while preserving the pharmacological properties.[5,6] The use of bioisosteres is common in the later stages of drug development to overcome problems related to potential drug candidates.[7] Moreover, bioisosteres have been employed in the investigation of structure-activity relationships and serve as a valuable tool for producing patent-free bioactive compounds.[4,7] The benzene ring is one of the most diffuse structural motifs in biologically active molecules, it can be found in 45%[8–10] of all small-molecule drugs, and it's prevalent in the composition of the 200 most sold drugs in 2020.[11] Nonetheless, benzene rings are among the main contributors of compound attrition in drug discovery.[3] For these reasons, the development of structural motifs that can mimic substituted benzenes is a field of great interest in modern medicinal chemistry. In particular, caged hydrocarbons have emerged as valuable bioisosteres, since they feature rigid 3D structures that project the substituents into precise positions, with similar orientations and distances to the groups they mimic.[7,12]

2.1.1.1 - Bicyclo[1.1.1]pentane

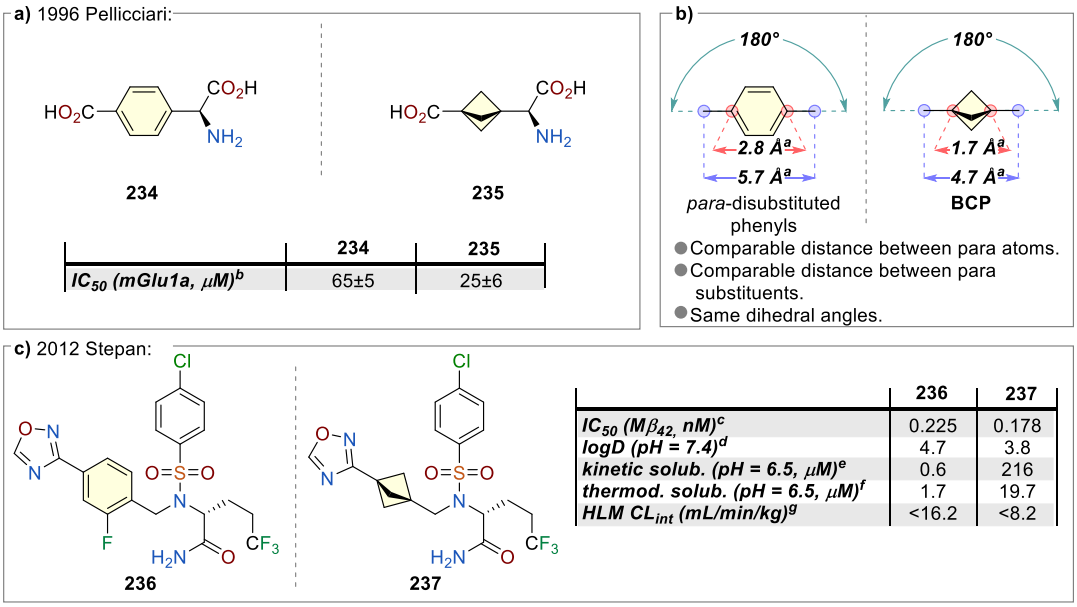

	234	235
IC_{50} (mGlu1a, μM)[b]	65±5	25±6

	236	237
IC_{50} (Mβ42, nM)[c]	0.225	0.178
logD (pH = 7.4)[d]	4.7	3.8
kinetic solub. (pH = 6.5, μM)[e]	0.6	216
thermod. solub. (pH = 6.5, μM)[f]	1.7	19.7
HLM CL_{int} (mL/min/kg)[g]	<16.2	<8.2

Scheme 34. Selected examples of BCP as bioisosteres of phenyls: **a)** Pellicciari *et al.* 1996.[13] **b)** structural comparison between BCPs and *para*-substituted phenyls. **c)** Stepan *et al.* 2012.[14]. [a]Calculated data Senge *et al.*[7].[b]Half-maximal concentration for the inhibition of functional responses in BHK cells(μM). [c] Half maximal inhibitory concentration against γ-secretase (nM). [d] logD = intrinsic distribution coefficient between *n*-octanol and aqueous in phosphate buffer (pH 7.4). [e] Kinetic aqueous solubility (μM) in buffer (pH 6.5). [f] Thermodynamic aqueous solubility (μM) in buffer (pH 6.5). [g] Human Liver Microsome Stability (mL/min/Kg).

Due to their structural similarity, bicycle[1.1.1]pentane (BCP) is the most diffused *para*-substituted bezene ring bioisosteres (**Scheme 34b**). A milestone in this field is the work of Pelliciari *et al.*[13], where in 1996 they replaced the benzene ring in the antagonist of the glutamate receptor of group 1 **234** with a BCP (**Scheme 34a**). The authors measured the activity of the analog **235** and found that it was three times more active than its aromatic counterpart **234**. Another interesting example is furnished by a study conducted by Stepan and coworkers in 2012 (**Scheme 34c**).[14] In this work, the fluorophenyl moiety of the γ-secretase inhibitor **236** was replaced with a BCP ring. The authors observed a general improvement of the physio-chemical properties, with a lower lipophilicity, a higher thermodynamic water solubility, and a

better metabolic stability. Moreover, the analog **237** was found to be more active than **236** and patent-free. This work has shown the utility of bioisosteres to bypass patents in benzene-containing bioactive molecules. Since then, the use of BCPs has become routine in pharmaceutical chemistry, being present in more than 100 patents.[4]

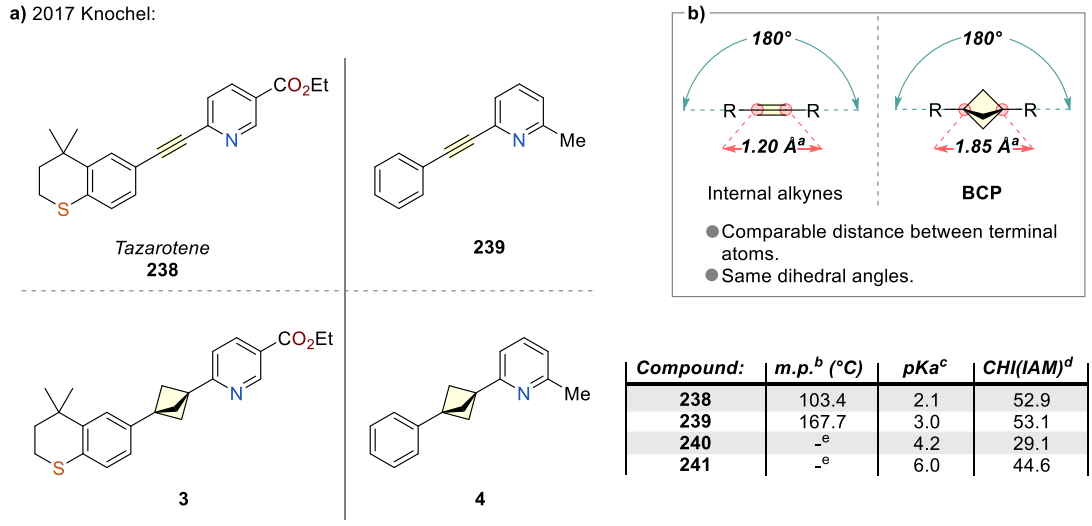

Compound:	m.p.[b] (°C)	pKa[c]	CHI(IAM)[d]
238	103.4	2.1	52.9
239	167.7	3.0	53.1
240	-[e]	4.2	29.1
241	-[e]	6.0	44.6

Scheme 35. a) Selected example of BCP as bioisoster of the phenyl ring in Tazarotene. Knochel *et al.* 2017.[15] **b)** structural comparison between BCP and internal alkynes. [a]Calculated data Senge *et al.*[7].[b]Melting point (°C). [b]pKa of the conjugated acid. [c]Chromatographic hydrophobicity index on immobilize artificial membranes. [e]Liquid at room temperature.

The BCPs have also been used to replace alkyne rings, due to their similar length (**Scheme 35**). Knochel *et al.*[15] synthesized analogs of the drug Tazarotene **238**, used in the treatment of psoriasis, and the glutamate receptor R5 antagonist **239**.(**Scheme 35a**). The physiochemical properties of these analogs were found to be close to those of **238** and **239**. However, a significant change in the pKa of the conjugated acid was observed because of the loss of conjugation.

a) 2015 Carreira:

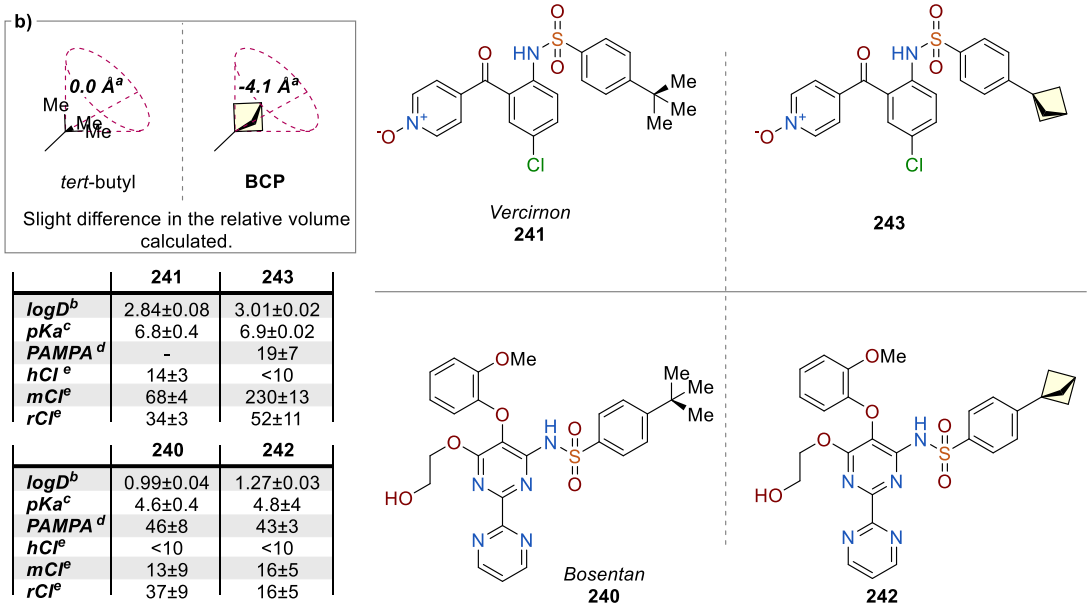

	241	243
logD[b]	2.84±0.08	3.01±0.02
pKa[c]	6.8±0.4	6.9±0.02
PAMPA[d]	-	19±7
hCl[e]	14±3	<10
mCl[e]	68±4	230±13
rCl[e]	34±3	52±11

	240	242
logD[b]	0.99±0.04	1.27±0.03
pKa[c]	4.6±0.4	4.8±4
PAMPA[d]	46±8	43±3
hCl[e]	<10	<10
mCl[e]	13±9	16±5
rCl[e]	37±9	16±5

Scheme 36. a) Selected example of BCP as bioisoster of *tert*-buthyl in Vercirnon and Bosentan, Carreira *et al.*,[16] 2015. **b)** Structural comparison between BCP and *tert*-butyl. [a]Calculated dara Carreira *et. all.*[16]. [b]logD = intrinsic distribution coefficient between *n*-octanol and aqueous buffer (pH 7.4). [c]Acidities determined spectrophotometrically at 23±1°C. [d]Membrane permeability (nms^{-1}) as derived from the parallelartificial membrane permeability assay (PAMPA). [e]Metabolic stability; values describe intrinsic clearance (Cl, [$mMmin^{-1}mg^{-1}$]) in human (h), mouse (m), and rat (r) microsomes.

Alternatively to internal likers, the BCPs have been used to substitute terminal *tert*-butyl groups in *virtue* of their similar volume (**Scheme 36b**). In 2015, Carreira *et al.*[16] applied BCP as *tert*-butyl analogs of patent drugs Bosentan **240** and Vercirnon **241**, obtaining the compounds **242** and **243**. This substitution led to improved physio-chemical properties The biological activity was retained for **243** and increased in the case of the Bosentan-analog **242**.

2.1.1.2 - Bicyclo[2.2.2]octane

The bicyclo[2.2.2]octane rings (BCOs) are structurally similar to *para*-disubstituted phenyl likers, making them ideal analogs (**Scheme 37b**). In 2014, Zhong, Li, and coworkers[17] substituted one of the phenyl rings in the FDA-approved drug Daclatasvir **244**, used for Hepatitis C virus treatment (**Scheme 37a**). The water solubility of the analog **245** was higher than the parent drug, although it was found to be 20-fold less active than Daclatasvir **244** in the gt-1a replicon. The authors attribute the reduced biological activity to specific interactions between the diphenyl spacer and the NS5A protein. Despite that, this work identifies the BCOs as valuable bioisosteres.

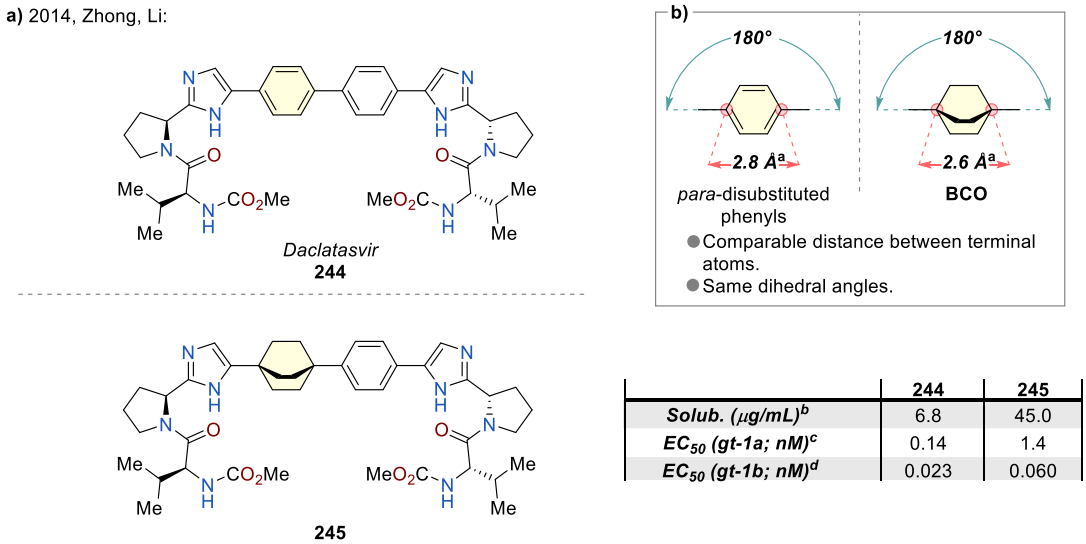

	244	245
Solub. (μg/mL)[b]	6.8	45.0
EC_{50} (gt-1a; nM)[c]	0.14	1.4
EC_{50} (gt-1b; nM)[d]	0.023	0.060

Scheme 37. a) Selected example of BCO as bioisoster of phenyl ring in Daclastasvir. Zhong, Li et al. 2014.[17] **b)** Structural comparison between BCOs and para-substituted phenyl rings. [a]Calculated data Senge et al.[7]. [b]Aqueus solubility (μg/mL) in phosphate buffer (pH 7.4). [c]Half maximal effective concentration (nM) against Hepatitic C virus (gt-1a). [d]Half maximal effective concentration (nM) against Hepatitic C virus (gt-1b).

2.1.1.3 - Cubanes

In 1992, the potential of cubanes (CBs) as benzene bioisosteres was postulated by Eaton *in virtue* of their similar size and shape (**Scheme 38b**).[18] The first experimental evidence emerged in 2016 when Williams, Tsanaktsidis, Savages, and coworkers published a work in which they synthesized and evaluated the biological activity of CB-analogs of drugs and agrochemicals (**Scheme 38a**).[19] The analog **246** of the deacetylase inhibitor SAHA **247**, used for the treatment of cutaneous T-cell lymphoma, was found to have an inhibitor activity close to the parent drug.

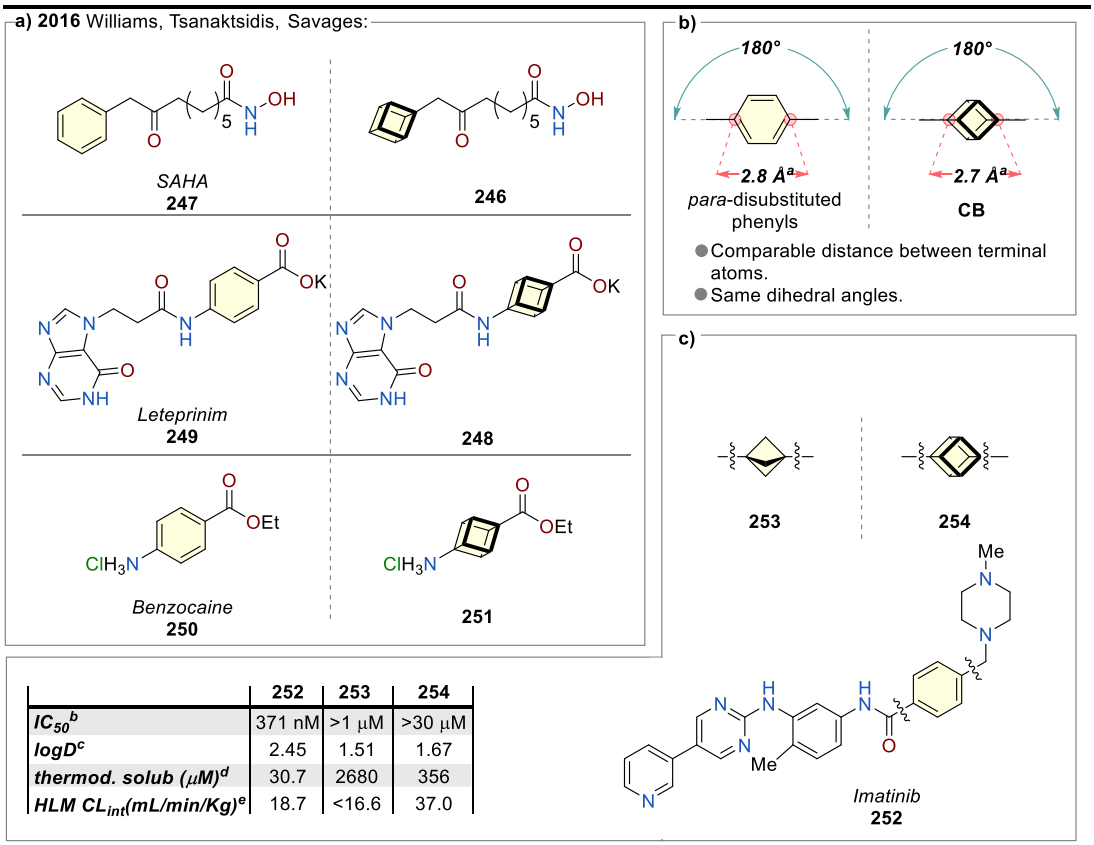

	252	253	254
IC_{50}[b]	371 nM	>1 μM	>30 μM
logD[c]	2.45	1.51	1.67
thermod. solub (μM)[d]	30.7	2680	356
HLM CL_{int}(mL/min/Kg)[e]	18.7	<16.6	37.0

Scheme 38. a) Selected example of CB as bioisoster of phenyl rings. Williams, Tsanaktsidis, Savages *et al*. 2016.[19] **b)** Structural comparison between CBs and para *para*-substituted phenyl rings. **c)** Comparison between Imatinib and its BCP and CB analogs. Stephan *et al.* 2016.[20] [a]Calculated data Senge *et al.*[7]. [b]Half maximal inhibitory concentration against ABL1 kinase. [c]logD = intrinsic distribution coefficient between *n*-octanol and aqueous in

The analog of the neotropics drug Leteprinim **248** exhibited a higher activity than the benzene-containing counterpart **249**. Interestingly, the phenyl ring was also replaced with a CB in the well-known local anesthetic Benzocaine **250**, obtaining the analog **251,** that showed an analog anesthetic efficacy.

Imatinib **252** is a tyrosine kinase inhibitor, used in the treatment of several leukemias. It features four aromatic rings in its structure. In 2016, Stephan and coworkers replaced one of the phenylic rings with a BCP and a CB, obtaining the analogs **253** and **254** (**Scheme 38c**).[20] Both analogs showed higher water solubility, lower lipophilicity, and appropriate metabolic stability. However, their inhibitory activity against the target ABL1 kinase was much lower than the parent drug, with a detrimental effect on its therapeutic activity.

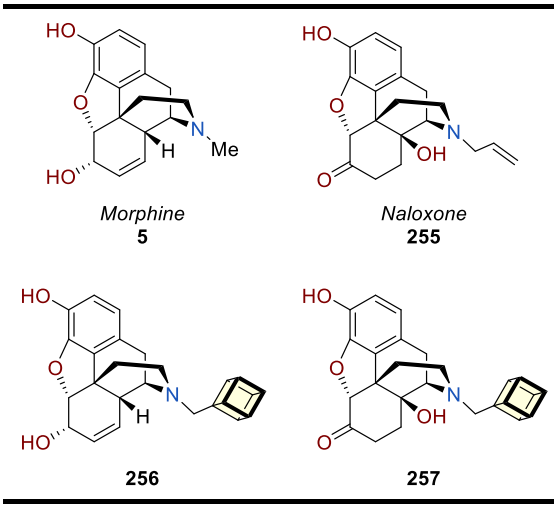

Scheme 39. Substitution of methyl with CB in morpholine scaffolds.

An interesting application of CBs is as methyl bioisosteres, *in virtue* of their electronic similarity. The activity of the morphinoids is known to be influenced by the nature of the nitrogen substituents. Two CB analogs of Morphine **5** and Naloxone **255** were synthesized (**Scheme 39**).[21] CB **256** was found to be more potent than its parent

drug Morphine **5**, while CB **257** exhibited lower activity than the allylic analog Naloxone **255**.

2.1.2.0 - Beyond linear likers: bioisosteres of *ortho*- and *meta*-disubstituted phenyls

During the past decades, the use of strained bicycles to replace *mono*- and *para*-substituted phenyl rings has become routine in medicinal chemistry.[4] Despite that *ortho*- and *meta*-disubstituted phenyls are common in drugs and agrochemicals, being present in more than 170-FDA approved drugs,[4] the synthesis of their saturated analogs remains relatively underdeveloped. Only in the last three years, many efforts have tried to fill this gap in synthetic technology, resulting in an expansion of the accessible structures. In this section, the most recent developments in the synthesis and application of non-linear saturated phenyl analogs will be discussed.

2.1.2.1 - Bioisosteres of *ortho*-substituted benzenes

Several saturated bicyclic structures have been proposed to mimic *ortho*-substituted benzenes. These include 1,2-disubstituted cubanes (CBs), bicyclo[1.1.1]pentanes (BCPs), bicyclo[2.1.1]hexanes (BCPs), and oxabicyclo[2.1.1]hexanes (oBCHs), all of which share a similar distance between the substituents compared to their aromatic counterparts (**Scheme 40**). Recent developments in the synthesis of BCHs and oBCHs are a matter of this thesis and will be treated in detail in **Section 2.1.3.0**, This section will focus on CBs and BCPs. Recently, MacMillan and coworkers have reported the synthesis of CB-1,2-diester **258**, starting from the commercially available CB-1,4-diester **259** (**Scheme 40**).[22] They used a sequence of C-H functionalization/esterification to introduce the *tert*-butyl

ester at position two of the CB **260**. Subsequently, the sterically more exposed ester at position four was hydrolyzed, yielding the acid **261**, decarboxylated in two steps to the final product **262** with an overall yield at 21%. Furthermore, the same group has recently published a novel approach to 2-substituted BCPs, employing a HAT-mediated bromination to introduce a bromide at the position two of diacid **263**.[23] The subsequent esterification furnishes BCP **264,** that was used in a series of silyl-radical-mediated arylations and aminations to introduce aryls and (hetero)aryls into the scaffolds. This method was employed for the synthesis of BCP-analogs of Telmisartan **265** and of the dopamine D3-receptor **266** (**Scheme 40c**, bottom). The analogs exhibited improved physiochemical properties while retaining almost completely the biological activities of the aryl-containing analogs. In 2022, Qin and coworkers expanded the synthetic tools to access multisubstituted BCPs by reporting an intramolecular coupling of cyclobutene-tethered sulfonylhydrazones and boronic esters (**Scheme 40d**).[24] The base-mediated intramolecular coupling employs readily accessible cyclobutanes **267** as starting materials. The ketones **268** are converted into hydrazones **269**, which, once exposed to basic conditions, generate a high-energy bicyclic [2.1.1] zwitterionic intermediate **270,** prone to the subsequent 1,2-metallate rearrangement, delivering multisibstituted BCPs. This method has proven to be operationally simple and general, showing a scope of more than twenty BCPs and allowing the synthesis of [2.1.1], [2.2.1], [3.1.1], and [3.2.1] systems.

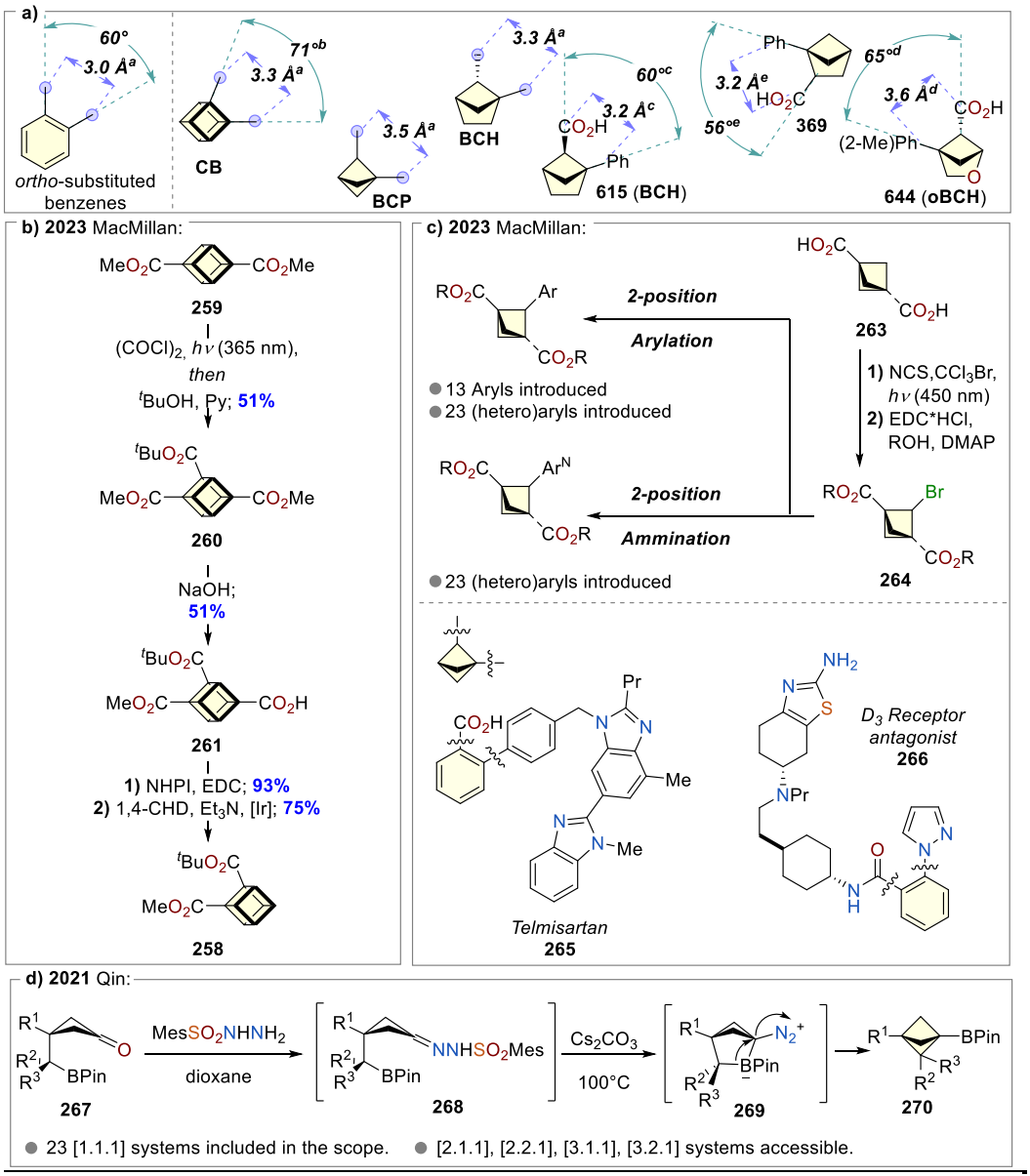

Scheme 40. a) Structural comparison between ortho-substituted phenyls and CBs, BCPs, BCHs, and oBCPs. **b)** Synthesis of the 1,2-disubstituted CB **258** from the 1,4-disubstituted CB **259**. MacMillan et al. 2023.[22] **c)** Introduction of substituents on carbon two of BCPs MacMillan et al. 2023.[23] **d)** Synthesis of 1,2,3-trisubstituted BCPs. Qui et al. 2021[24]. [a]Calculated Myhailiuk et al.[4].[b]Calculated MacMillan et al.[21] [c]Crystallographic data Myhailiuk et al.[48] [d]Crystallographic data Myhailiuk et al.[32] [e]Crystallographic data Myhailiuk et al.[41]

In 2021, Bran *et al.*[25] reported a versatile platform for the synthesis of 1,2-disubstituted BCPs (**Scheme 41**). In this impressive work, several key building blocks for the development of BCPs were obtained starting from the MOM alcohol [1.1.1]propellane **271**, accessed by a sequence previously developed by Schülter *et al.*[26] The synthetic campaign began by optimizing the route to **271**. Accordingly, the ketone **272** was converted in the acrylate **273** employing a Wittig reaction. The ester was converted into the MOM-protected alcohol **274** in a two-step sequence. Exposure of **274** to basic conditions in bromoform yielded the cyclopropane **275**, which was converted into **271** using methyl lithium with a 36% yield over five steps. Once a reliable throughput of **271** was established, the authors worked on the synthesis of the building blocks. The radical difunctionalization with chloroiodomethane furnished **276,** which was used to obtain the synthetically versatile building block **277** using deiodination and acetal-chloride exchange. The hydrolysis of acetate **277** furnished the alcohol **278**, oxidized to acid **279**. A Curtius rearrangement was used to directly convert acid **279** into the Cbz-protected amine **280**. Numerous substituents were introduced at position two starting from **281,** which was obtained through radical difunctionalization. The MOM alcohol was deprotected and oxidized to yield acid **282**. The carboxylic acid was converted into the redox-active amide **283** and handled to deliver the boronic ester **284**. The

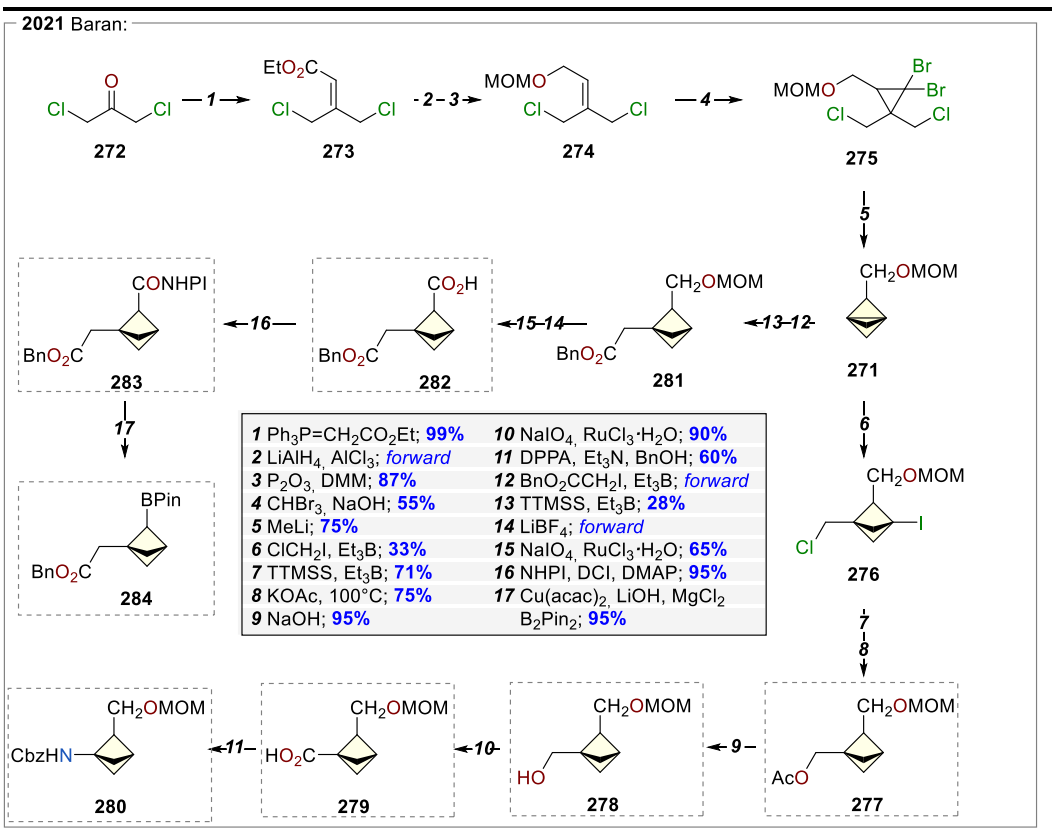

Scheme 41. Synthesis of several 1,2-disubstituted BCPs building blocks. Baran *et al.* 2021.[25]

platform was used to obtain bioisosteres of several drugs, showing the applicability of 1,2-disubstituted BCPs as *ortho*-benzene bioisosteres.

2.1.2.2 - Bioisosteres of *meta*-substituted benzenes

Saturated motifs like cuneanes (CNs), cubanes (CBs), bicyclo[3.1.1]heptanes (BCE), bicyclo[2.1.1]hexanes (BCHs), and oxabicyclo[2.1.1]hexanes (oBCHs) are structurally close to *meta*-disubstituted benzenes (**Scheme 42a**). For this reason, they have been recently investigated as potential bioisosteres. As for the *ortho*-disubstitute benzenes (**Section 2.1.2.1**), the BCHs and oBCHs motifs will be discussed separately in **Section 2.1.3.0**, while this section is dedicated to CNs, CBs, and BCEs.

This year, the group of Wai Lam has described an Ag(I) catalyzed rearrangement of electron-withdrawing substituted CBs **285** to 1,3-disubstituted CNs **286** (**Scheme 42b**).[27] The mechanism began with the oxidative addition of Ag(I) to the more electron-rich C1-C2 bond of **285**, giving the Ag(III)-intermediate **287**. Heterolysis of the C-Ag bond gave the carbocation **288** that delivered the CNs **286** after a σ-bond rearrangement. The scope of the rearrangement was studied, encompassing eleven 1,3-disubstituted CNs with several coupling useful groups, including boronic esters, amides, alcohols, and protected amines. Moreover, by using dielectron-withdrawing substituted CBs, the rearrangement of the oxidative addition/heterolytic event happens in the C2-C3 bond of the CBs, giving access to 2,6-disubstituted CBs. A CN-analog of the anticancer drug Sonidegib **289**, was synthesized using this platform, and its physiochemical and metabolic properties were evaluated. Interestingly, bioisostere **290** shows comparable lipophilicity and higher methanolic stability (intrinsic clearance in mice and humans) than the parent drug **289**. However, its aqueous solubility has resulted to be too low to be measured.

A convenient route toward the useful 1,3-disubstituted CN building block **291** has been described by MacMillan's group (**Scheme 42c**).[22] The diene **292** was used to generate the butadiene *in situ*, which was trapped in a Diels Alder with 2,5-dibromoquinone (2,5-DBQ), leading to **293**. Irradiation of **293** with blue light triggers an intramolecular [2+2], resulting in the formation of the dibromide **294**. Finally, a sequence of Favorskii ring contraction and methylation delivers the diester **291**. To

demonstrate the benefits of the bioisostere, the CB-analog of Lunacaftol **295** was prepared. The physicochemical properties of **296** generally improved by the substitution. Lipophilicity was preserved, and aqueous solubility was improved particularly at low pH, facilitating better absorption throughout the gastrointestinal tract. Analog **296** also shares higher biological activity (lower RC_{50}CFTR), and greater metabolic stability (lower HLM Cl_{int}).

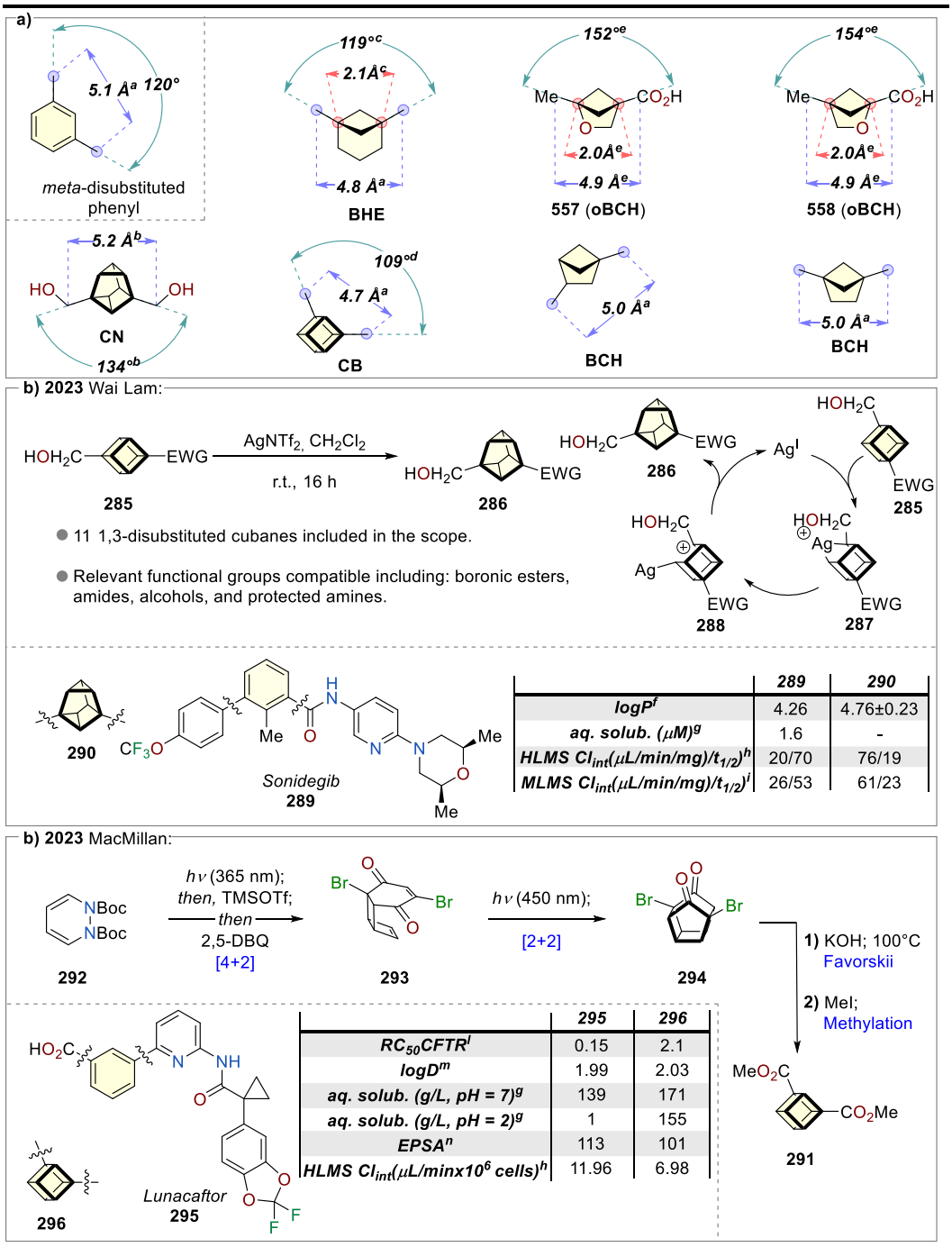

	289	290
logP[f]	4.26	4.76±0.23
aq. solub. (μM)[g]	1.6	-
HLMS Cl_{int}(μL/min/mg)/$t_{1/2}$)[h]	20/70	76/19
MLMS Cl_{int}(μL/min/mg)/$t_{1/2}$)[i]	26/53	61/23

	295	296
RC_{50}CFTR[l]	0.15	2.1
logD[m]	1.99	2.03
aq. solub. (g/L, pH = 7)[g]	139	171
aq. solub. (g/L, pH = 2)[g]	1	155
EPSA[n]	113	101
HLMS Cl_{int}(μL/minx10^6 cells)[h]	11.96	6.98

Scheme 42. a) structural comparison between meta-substituted phenyl rings and CN, CB, BHE, BCH and oBCH. **b)** Synthesis of 1,3-disubstituted CNs from CBs. Wai Lem *et al.* 2023. **c)** Synthesis of 1,3-disubstituted CBs. MacMillan *et al.* 2023. [a] Calculated Myhailiuk *et al.*[4]. [b] Calculated Wai Lam *et al.*[27]. [c] Calculated Uchiyama *et al.*[29]. [d] Calculated MacMillan *et al.*[22] [e] Crystallographic data Myhailiuk *et al.*[31] [f] logP = partition coefficient between *n*-octanol and water. [g] Acqueus solubility. [h] Human Liver Microsome Stability ((μL/min/mg)/$t_{1/2}$). [i] Mouse Liver Microsome Stability). [l] RC_{50}, half-maximal rescue concentration (μM). [m]logD = intrinsic distribution coefficient between *n*-octanol and aqueous in phosphate buffer (pH 7.4). [n]Experimental polar surface area; [d]Acqueus solubility (mg/mL) at pH = 7. [e]Human Liver Microsome Stability.

A series of works have investigated BCEs structures (**Scheme 43**). In 2021, Stephenson *et al.*[28] developed a method in which the BCPs **297** are excited to **298**, undergo a ring opening to produce the diradical **299**, which then intercepts olefines, yielding polisubstituted BCHs **300** (**Scheme 43a**). Thanks to this method, the bioisosteres of Boscalin **301** and the anti-cancer lead compound **302** were successfully synthesized.

In 2022, Uchiyama and coworkers reported a synthetically useful route to the [3.1.1]propellane **305** (**Scheme 43b**) from the commercially available **306**.[29] They explored the addition of the **305** with various reagents, obtaining thioethers **307** and **308**, stannane **309**, iodine **310**, and diester **311**. Nineteen alkyl/aryl iodines were added to **305,** yielding several iodo BCHs **312**. Late-stage functionalizations on the iodines **312** were used to introduce phenyl, boronic esters, carboxylic acids, and alcohols.

Finally, at the beginning of this year, Li *et al.*[30] developed a modular approach to access trisubstituted BCHs **313** from [0.1.1]propellanes **314** and cyclopropyls **315** (**Scheme 43c**). The process is catalyzed by the pyridine-boryl radical **316,** that generates the ketyl **317** radical from the keto-cyclopropane **315**. A ring-opening sets the allylic radical **318,** that adds to the [0.1.1]propellanes forming the intermediate **319**. Radical cyclization and catalyst regeneration deliver the bicyclic products. This

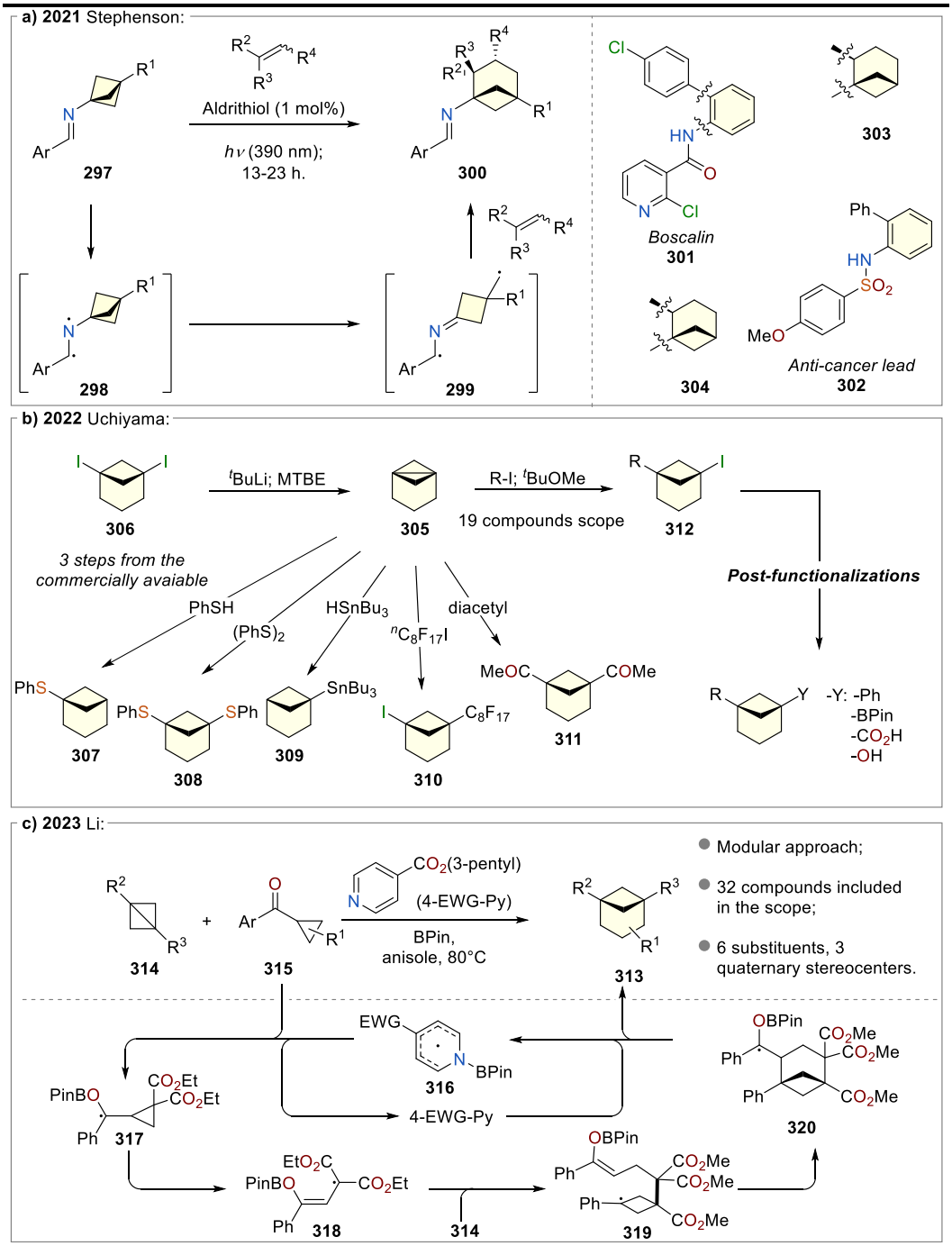

Scheme 43. a) Synthesis of polisubstituted BCOs from BCPs and their application in the BCO-Boscalin analog **303**. **b)** Diversification of the diiodo BCO **306** in useful 1,4-disubstituted BCO building blocks. Uchiyama *et al.* 2022.[29] **c)** Synthesis of tri-substituted BCOs **313** using pyridine-boryl radical catalysis. Li *et al.* 2023.[30]

approach has proven to be synthetically powerful, exhibiting a wide scope, and allowing the introduction of six substituents and three quaternary stereocenters.

2.1.3.0 - Synthesis of bicyclo[2.1.1]hexanes and 2-oxabicyclo[2.1.1]hexanes

The synthesis of *meta*- and *ortho*-benzene bioisosteres is a cutting-edge field in modern organic chemistry. bicyclo[2.1.1]hexanes (BCHs) structures share several structural parameters with disubstituted benzenes, making them ideal candidates for bioisosteres. In recent years, several synthetic campaigns have targeted these intriguing structures, bringing significant progress in their synthesis and manipulation. The number of positions amenable to diversification has grown significantly, employing methodologies that are becoming milder and more practical. These studies are laying the groundwork for the future development of saturated building blocks and drug analogs that could have a great impact on medicinal chemistry.

In this section, the state of the art in this field will be reviewed and organized for exit vectors introduced. Along with bicyclo[2.1.1]hexanes (BCHs), the less recently introduced 2-oxabicyclo[2.1.1]hexanes (oBCHs) will be treated, representing structural analogs of BCHs with improved physio-chemical properties.[31,32]

2.1.3.1 - 1,2 exit vectors

The intramolecular [2+2] photocycloadditions of 1,5-diolefins are the most exploited reaction in the construction of BCHs.[33–35] One of the first examples was furnished in 1990 by Carpenter *et al.*[36] (**Scheme 44a**), where the terminal alkynes **321** were reduced to vinyl stannanes **322**, which then cyclized to form bicycles **323** after the alcohol oxidation to ketone. While these synthetic pathways furnish direct access to 2-ketones amenable for further transformations, it relied of mercury lamps, requiring special equipment, and making this reaction technically challenging. Moreover, the use of toxic stannanes poses a severe limitation to the scalability of the entire process.

In 2022, our collaborators at SpiroChem contributed to the development of a scalable synthetic route for 2-keto-BCHs (**Scheme 44b**).[37] Benzyl acetaldehyde **324** was chosen as the starting material, since its olefination with Eschenmoser's salt furnished the acrylate **325** in a quantitative yield. Allylation of the aldehyde gave the alcohol **326,** which was then exposed to Dess Martin periodinane yielding the ketone **327**. The [2+2] photocycloaddition was performed by means of the catalyst $Ir[(dF(CF_3)ppy)_2(dtbbpy)]PF_6$, known as triplet sensitizer and previously used in intramolecular [2+2].[38] The reaction was run in acetonitrile, using simple blue LEDs as the light source, resulting in a yielding and scalable route to ketone **328**. The scope of the process was extended to *para*-substituted benzyl acetaldehydes introducing

bromo, fluoro, and methyl in the *para* position of the phenyl ring (**329**, **330**, and **331**. **Scheme 44b**).

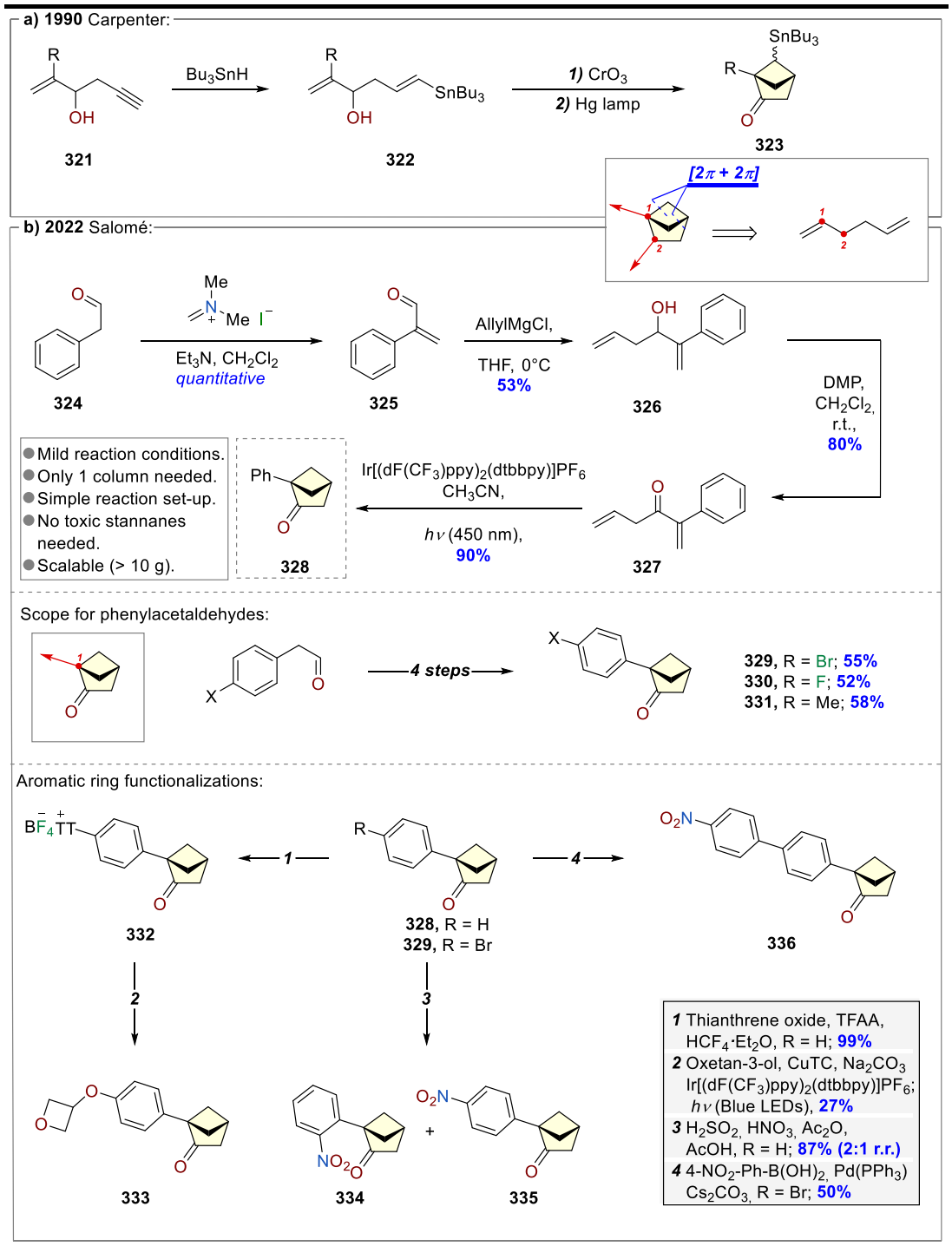

Scheme 44. Synthesis of 1,2-disubstituted BCHs **a)** Carpenter, *et al.* 1990.[36] **b)** Salomè, *et. al* 2022.[37]

A set of functionalizations on the phenyl ring was used after the cyclization. The phenyl ring of **328** was thianthrenated allowing the introduction of an oxetan ring in compound **333**. The nitration of the phenyl ring in **328** furnishes the nitro compounds **334** and **335** as a 2:1 regiomeric mixture. Furthermore, a Suzuki coupling on the aryl bromide **329** was used to introduce the *para*-nitro phenyl ring in bicycle **336**. The ketone at position two has resulted in a useful point of diversification, being amenable to various transformations (**Scheme 45a**). Quenching the enolate with ethyl formiate furnished aldehyde **337** with a 17% yield. The carbonyl has resulted to be amenable for nucleophilic attacks, leading to the formation of hydrazone **338** when exposed to tosylhydrazine. Other nucleophiles such as TMSCN and MeMgBr, reacted with ketone **328** yielding cyanohydrine **339** and tertiary alcohol **340**. Both the Wittig and the Horner-Wadsworth-Emmons-Wittig reactions were used to yield respectively the methyl-vinyl ether **341** and the ethyl acrylate **342**. The exposure of ether **341** to acid conditions furnishes the homologated aldehyde **343,** which is further oxidized under Pinnick's conditions to carboxylic acid **344** in a quantitative yield. A Pd/C hydrogenation was used to reduce the double bond in acrylate **342**, introducing a saturated chain in **345**. Finally, BCH was used as a platform for ring expansion, obtaining the cyclic ester **346** from a Bayer-Villiger with *m*CPBA and cyclic amide **347** *via* Schmidt reaction. To demonstrate the possibility of introducing aliphatic substituents at position one, a synthetic route for the TBS-protected alcohol **348** was developed (**Scheme 45b**). The synthetic pathway began with methyl acrylate

349, which was converted into the Weinreb amide **350** *via* a three-step sequence involving saponification, TBS protection, and amidation. The allylation of the Weinreb amide **350** yielded the 1,5-diketone **351**, amenable for intramolecular [2+2]. In this case, the absence of the aromatic counterpart increases the energy of the triplet excited state (E_T), resulting in low conversion under the previously used conditions (**Scheme 45**, [Ir] E_T = 260 KJ/mol). *In virtue* of its higher triplet energy (E_T = 270 KJ/mol),[38] the known photosensitizer 2-isopropyl thioxanthone (ITX)[40] was employed in combination with black light (λ = 365 nm), obtaining the desired BCH with a 72% yield. Subsequently, BCH **348** was applied for the construction of a difunctionalized building block (**Scheme 45c**). A two-step sequence involving hydroxylamine condensation and sodium borohydride reduction in the presence of Ni(II) and Boc_2O furnished the Boc amine **352**. The TBS alcohol in **352** was deprotected with TBAF and oxidized into the acid **353**. A Curtius rearrangement yielded the bis-protected amine **354**. The orthogonality of the protections was proved by the selective deprotection of the Boc amine at position 2 using TFA obtaining **355**.

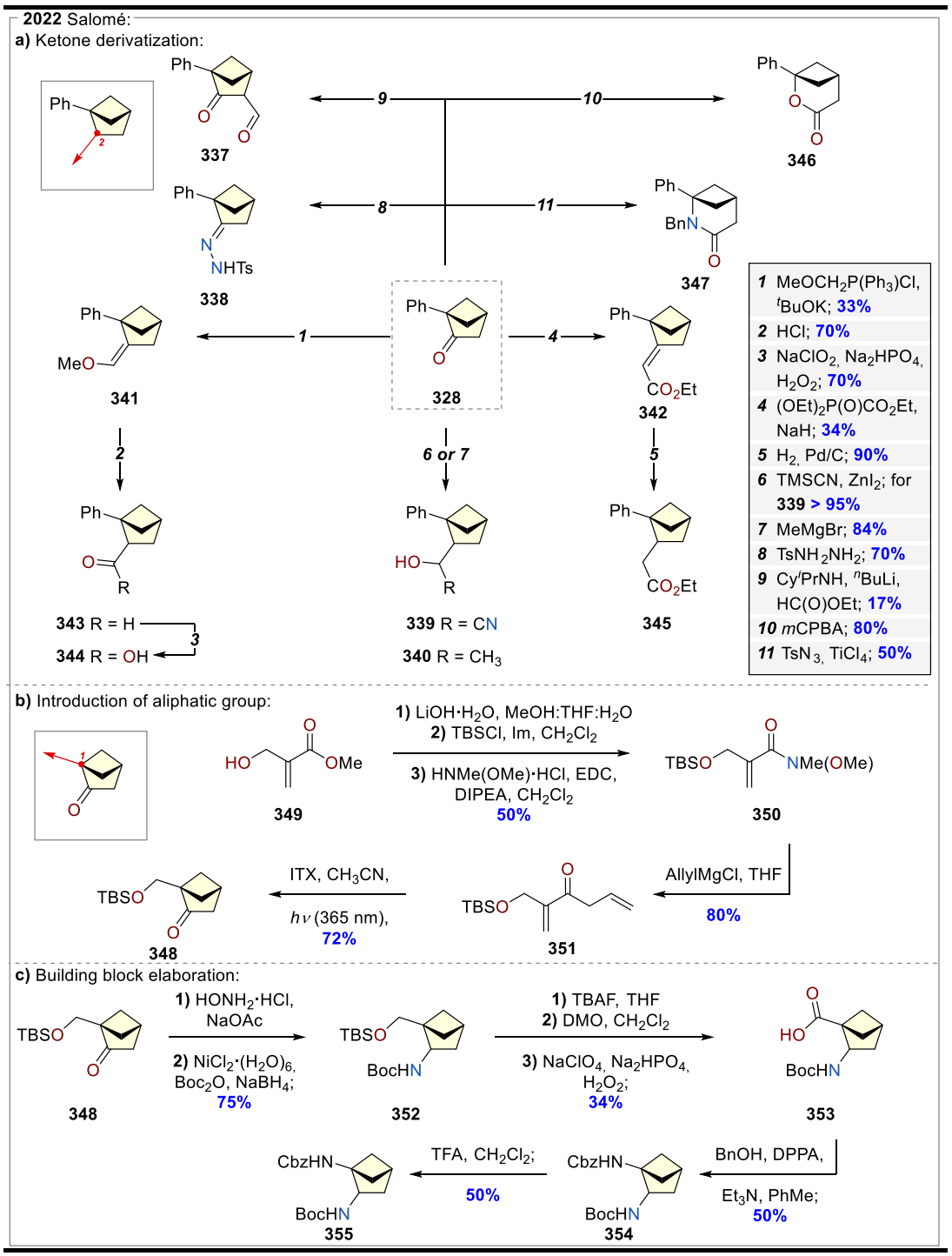

Scheme 45. Synthesis of 1,2-disubstituted BCHs, Salomè *et. al.* 2022.[37] **a)** Derivatizations of the ketone **328**. **b)** Synthesis of the TBS-alcohol **348**. **c)** Synthesis of 1,2-disubstituted building blocks.

In a preprint work recently published by Mychailiuk *et al.*[41], an intramolecular [2+2] was used to construct 1,2-disubstituted BCHs esters **356** from 1,5-diolefins **357** (**Scheme 46a**). Saponification of esters **356** was carried out to obtain easily crystallizable acids **358**. Differently substituted arenes (**359**-**364**), pyridines (**365** and **366**), and five-membered (hetero)arenes (**367** and **368**) were introduced at position one (**Scheme 46b**). The crystal structure of acid **369** was compared with the structure of *ortho*-methyl benzoic acid **370,** reveling similar angles and distances between the substituents (**Scheme 46c**). The possibility of including different substituents at position one was explored, and oxidative cleavage of the phenyl in **369** was used to introduce an acid at position one, obtaining the useful difunctionalized building block **371** (**Scheme 46d**). Finally, several analogs of biologically active compounds were obtained, including analogs of Boscalin **301**, Fluxapyroxad **372**, and Lomitapide **373,** often used for bioisosteres comparisons. The BCH-analogs (**374**, **375**, and **376**) showed higher inhibition activity of the growth of fungi strain *Aspergillus niger*.

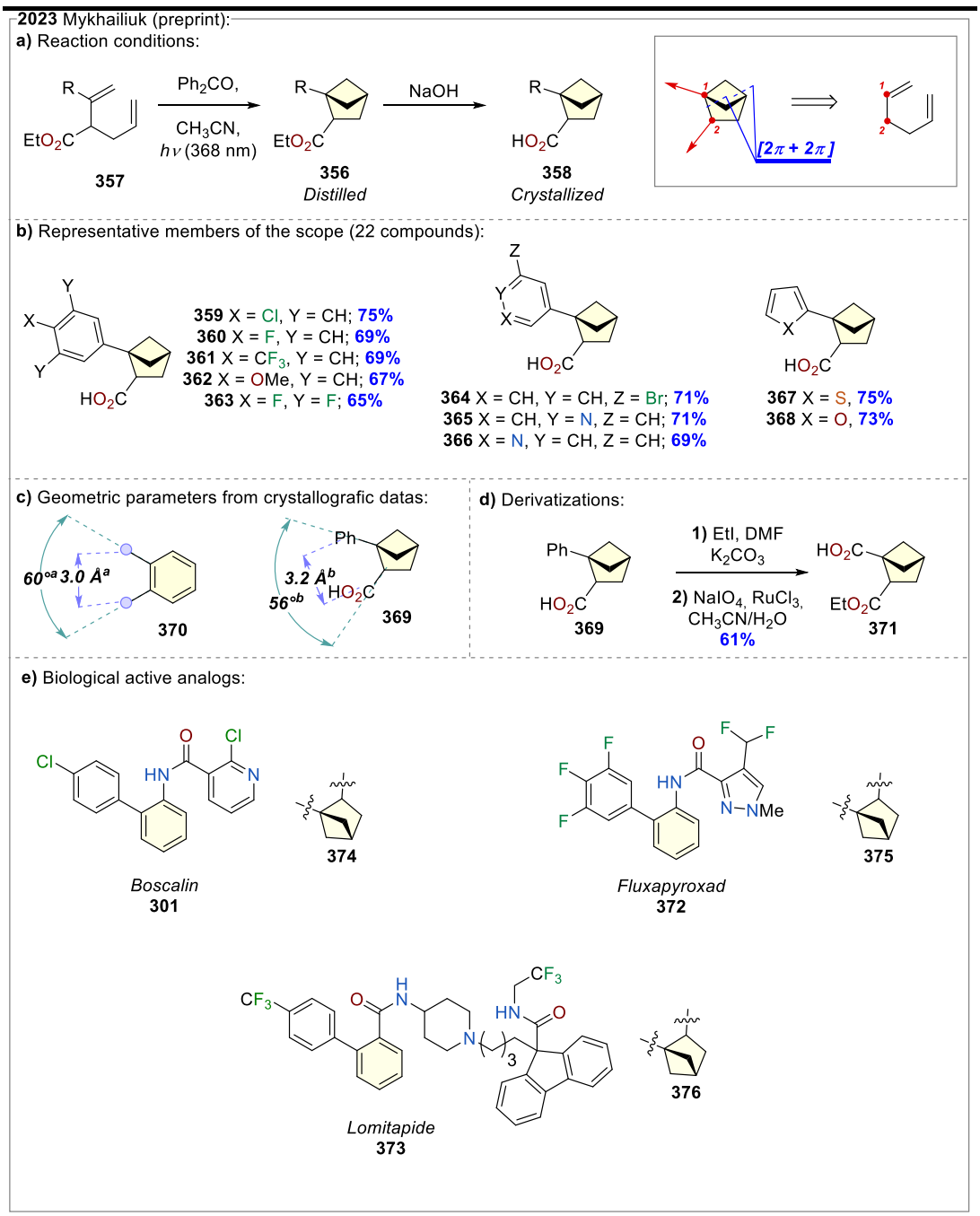

Scheme 46. Synthesis of 1,2-disubstituted BCHs, Mykhailiuk *et. al.* 2023[41] (preprint). **a)** Reaction conditions. **b)** Representative members of the scope. **c)** Structural parameters comparison **d)** Derivatizations of **369**. **e)** Biological active analogs of Boscalin 301, Fluxapyroxad **372**, and Lomitapide **373**. [a]Calculated data, Mykhailiuk *et al.*[4] [b]Crystallographic data, Mykhailiuk *et al.*[41]

An alternative approach to 1,2-disubstituted BCHs **376**, developed by Brown in 2022, involves [2π + 2σ] cycloaddition between alkenes **377** and bicyclo[1.1.0]butanes (BCBs) **378** (**Scheme 47a**).[42] This method exploits an innovative mode of activation of BCBs, involving the triplet sensitizer 2,2'-dimethyl thioxantone (2,2'-TX). The substrate scope (**Scheme 47b**) is wide (32 BCHs) and includes differently substituted phenyl rings (**379**, **380**, and **381**), several (hetero)arenes (**382** – **386**), and various useful functional groups at position two, such as the acetylated alcohol **387**, the silane **388**, and the boronic ester **389**. Due to their low triplet energy, the substrate scope is limited to naphthyl BCBs (E_T = 226 Kj/mol for **378**). Despite this limitation, differently substituted naphthyl-BCBs were used, yielding the 3-methyl, 4-methyl, and 5-methyl BCHs **390**, **391**, and **392**. A quaternary carbon was introduced into BCH **393** with a 37% yield. The proposed mechanism begins with energy transfer from the exited 2,2'-TX and the BCB **378**, generating its triplet state $T_1(\pi\text{-}\pi^*)$ or **378** (**Scheme 47c**). The bond cleavage of **378** is induced by strain release, yielding the triplet diradical **394**, which captures styrene **395** forming **396**. Finally, an intersystem crossing (ISC) leads to the singlet diradical amenable for radical coupling, forming the product **379**. This strategy allows the construction of 1,2-disubstituted BCHs in a modular way, disconnecting the bonds between carbon 1/2 and 3/4, and represents

the first example of energy transfer in a strain-release-driven transformation.

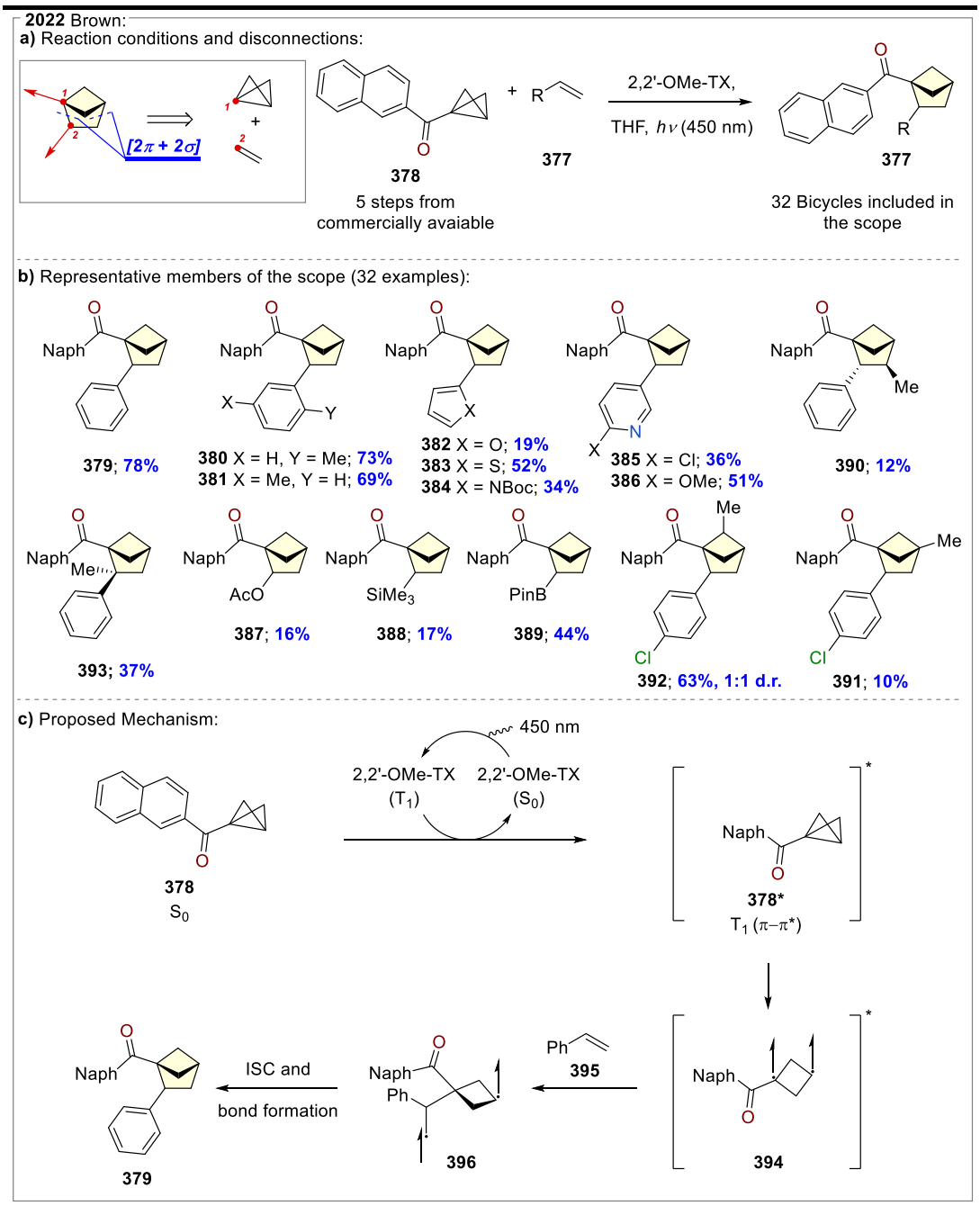

Scheme 47. Synthesis of 1,2-disubstituted BCHs, Brown *et. al.* 2022.[42] **a)** Reaction conditions. **b)** Reaction scope. **c)** Proposed mechanism.

2.1.3.2 - 1,2,3 exit vectors

A unique strategy to (hetero)cycles-condensed BCHs **397** was published by Glorius in 2022.[43] Similarly to Brown's work,[42] the bicyclic scaffold is built in a [2π + 2σ] cycloaddition between BCBs **398** and alkenes **399**. However, in this case, the thioxanthone (TX) photosensitizer interacts with the single state of the olefin. For this reason, the reaction is limited to coumarins, flavones and indoles (**Scheme 48a**). The substrate scope is very rich, allowing the introduction of various useful functional groups at position one, such as the amide **400**, the Weinreb amide **401**, the ester **402**, the pinacol boronate **403**, and the ketone **404,** adopting different BCBs (**Scheme 48b**). The coumarin scope was investigated, allowing the introduction of several substituents in various positions of the coumarin aromatic ring (**405** - **411**). The reaction with 3-substituted coumarins enables the introduction of functional groups at position two: this is the case of the acetylated alcohol **412**, the ketone **413**, and the ethyl ester **414**. From 2-cyano coumarin, BCH **415** was obtained, characterized by the presence of a nitrile group on carbon three. The reaction was applied to flavones and indoles, yielding the Weinreb amides **416** and **417** from the former, and the BCH-indoline condensed compound **418** from the latter. Computational studies were used to propose a mechanism that begins with the energy transfer from the photosensitizer and the coumarin **419**, giving the triplet diradical **420** (**Scheme 49a**). The triplet state of coumarin **420** approaches the BCB **421** from the exciples **422**, where the C-C bond is formed.

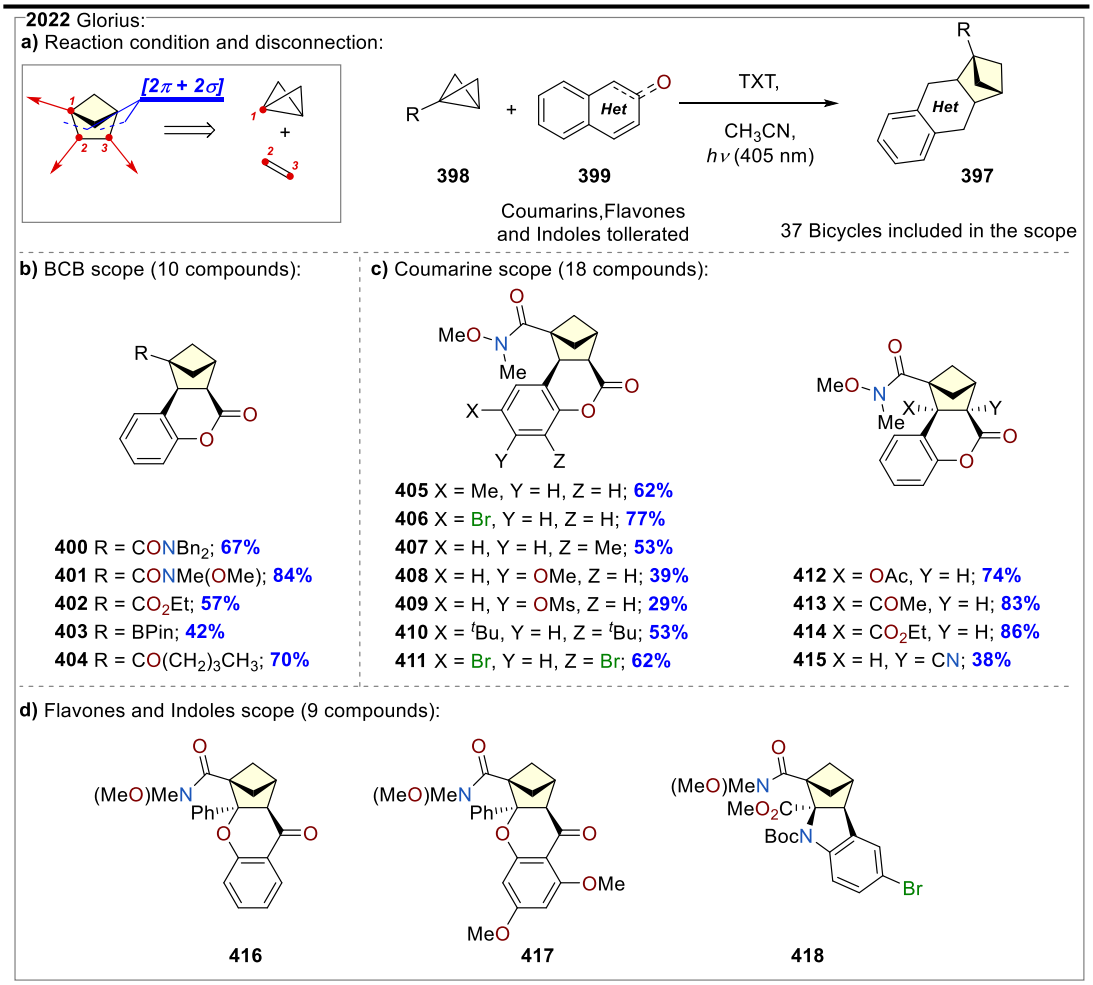

Scheme 48. Synthesis of 1,2,3-trisubstituted BCHs, Glorius *et. al.* 2022.[43] **a)** Reaction conditions. **b)** BCP scope. **c)** Coumarin scope. **d)** Flavones and Indoles scope.

The two possible transition states (**423** and **424**) were calculated to rationalize the regioselectivity. The approach of the α-carbonyl position of coumarin with position three of the BCB (transition state **424**) was found to be thermodynamically favorable ($\Delta\Delta G^{\ddagger}$ = 2.8 Kcal/mol), in agreement with the observed regioselectivity. Finally, an intersystem crossing result in the 1,5-diradical **426,** that forms the second C-C bond in a *cis*-selective radical coupling and radical delivering the product **427**. This last passage represents the diastereoselective determining step. The utility of these heterocycle-BCH condensed adducts was demonstrated through a series of derivatizations (**Scheme 49b**). The boronic ester **428** was oxidized to the corresponding alcohol **429** and used in C(sp^2)-C(sp^2) and C(sp^2)-C(sp^3) couplings, yielding the furane **430** and the ester **431**. The amidation of the ester **432** with piperidine furnished the amide **433**, while its treatment with methyl iodine and lithium aluminum hydride furnished respectively the transposed Weinreb amide **434** and the cyclic hemiacetal **435**.

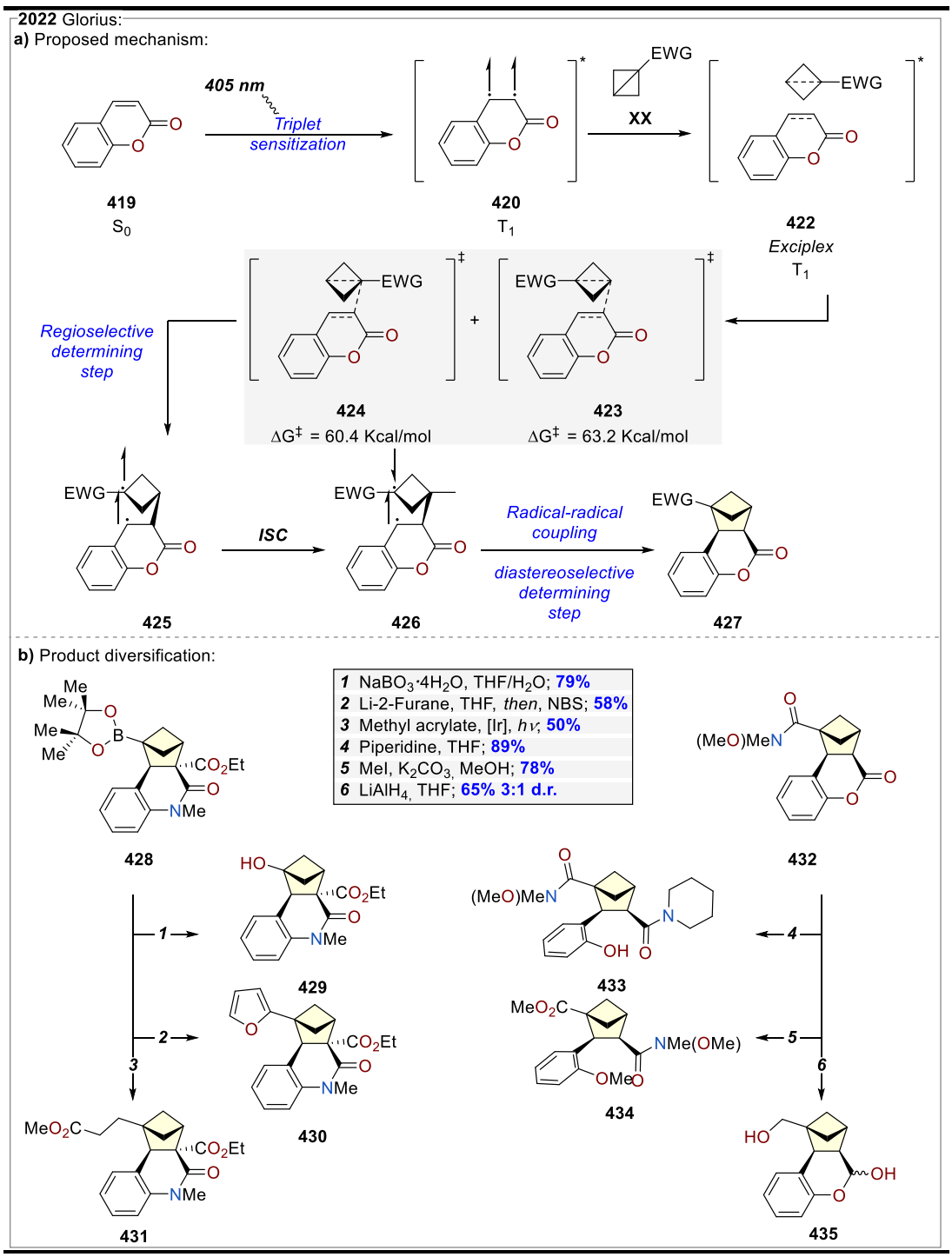

Scheme 49. Synthesis of 1,2,3-trisubstituted BCHs, Glorius *et. al.* 2022.[43] **a)** Proposed mechanism. **b)** Product derivatizations.

2.1.3.3 - 1,2,4 exit vectors

Three very recent works have been published that allow the simultaneous introduction of substituents in positions one, two, and four. In 2023, Procter developed a samarium catalyzed intermolecular insertion of alkenes **436** into BCBs **437** (**Scheme 50a**).[44] Unlike the works of Brown and Glorious, the mechanism doesn't require the use of phosensitizable substrates, making the substrate scope more general. The substituents in positions one and four are controlled by the BCBs **437** (**Scheme 50b**). In position four, alkylic chains (**439** and **440**) and benzylic ether (**441**) were introduced. Various aliphatic ketones were introduced in position one, including alkylic chains of different lengths (**442** - **445**), the diphenyl group in compound **446,** and carbocycles of different dimensions (**447** – **451**). Interestingly, the cyclopropane in ketone **451** remains unaltered under the radical reaction conditions, proving the selectivity of this protocol. Different electron-poor olefins were reacted, introducing groups in position one of the BCHs (**Scheme 50c**). The process is compatible with a broad range of functionalities, including esters (**452** - **454**), trifluoromethyl (**455**), silicate (**456**), ether (**457**), and primary chloride (**458**). Together with acrylates, the reaction has also proven to be suitable for vinyl sulfones (**459** and **460**), vinyl sulfonate ester (**461**), vinyl sulfonyl fluoride (**462**) and vinyl sulfonamide (**463**). The proposed mechanism (**Scheme 50d**) involves single electron transfer (SET) between samarium iodine and ketone **437**, forming the ketyl radical **464**.

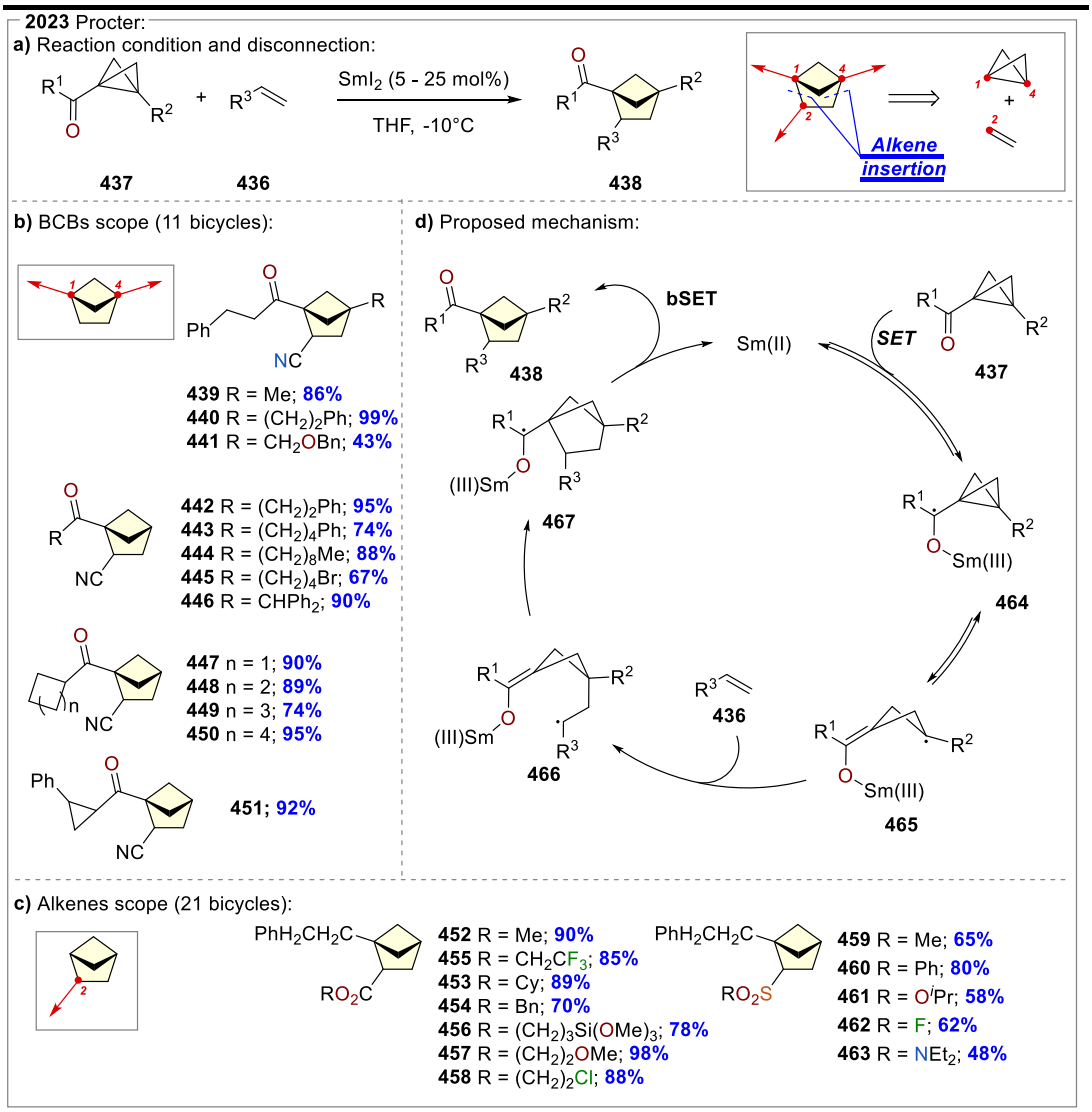

Scheme 50. Synthesis of 1,2,4-trisubstituted BCHs, Procter *et. al.* 2023.[44] **a)** Reaction conditions. **b)** BCBs scope. **c)** Alkenes scope. **d)** Proposed mechanism.

The reaction then proceeds *via* the ring opening of the BCB, yielding the radical **465**, which reacts with the electron-poor olefine **436,** delivering the radical **466**. A radical rebound with the samarium enolate generates the bicyclic scaffold in the ketyl radical **467**. The product **438** is delivered by a back single electron transfer (bSET) that restores the samarium catalyst. Several manipulations were performed on ketone **442** (**Scheme 51a**). The carbonyl group was selectively reduced with sodium borohydride to access alcohol **468**, the nitrile group was reduced to primary alcohol **469** using a method orthogonal to the ketone. The nitrile was hydrolyzed, yielding both amide **470** and acid **471**. Finally, a Bayer-Villiger oxidation was used to obtain ester **472**. The utility of these building blocks in the construction of bioisosteres was proved by the synthesis of the saturated analog of the broad-spectrum antimicrobial Phthalylsulfathiazole **473** (**Scheme 51b**). The comparison of the computed lowest energy conformations of **473** and its BCH analog **474** reveals that the BCH effectively mimics the *ortho*-disubstituted phenyl ring. In particular, the distances between the substituents were found to be identical (**Scheme 51b**). This method features a wide functional group tolerance and excellent atom economy, but it is limited to monosubstituted electron-poor olefins.

In 2022, Li reported a unique method for the remote activation of pyridine-cyclopropanes and pyridine-BCBs **475**, using the bornyl radical as a catalyst.[45]

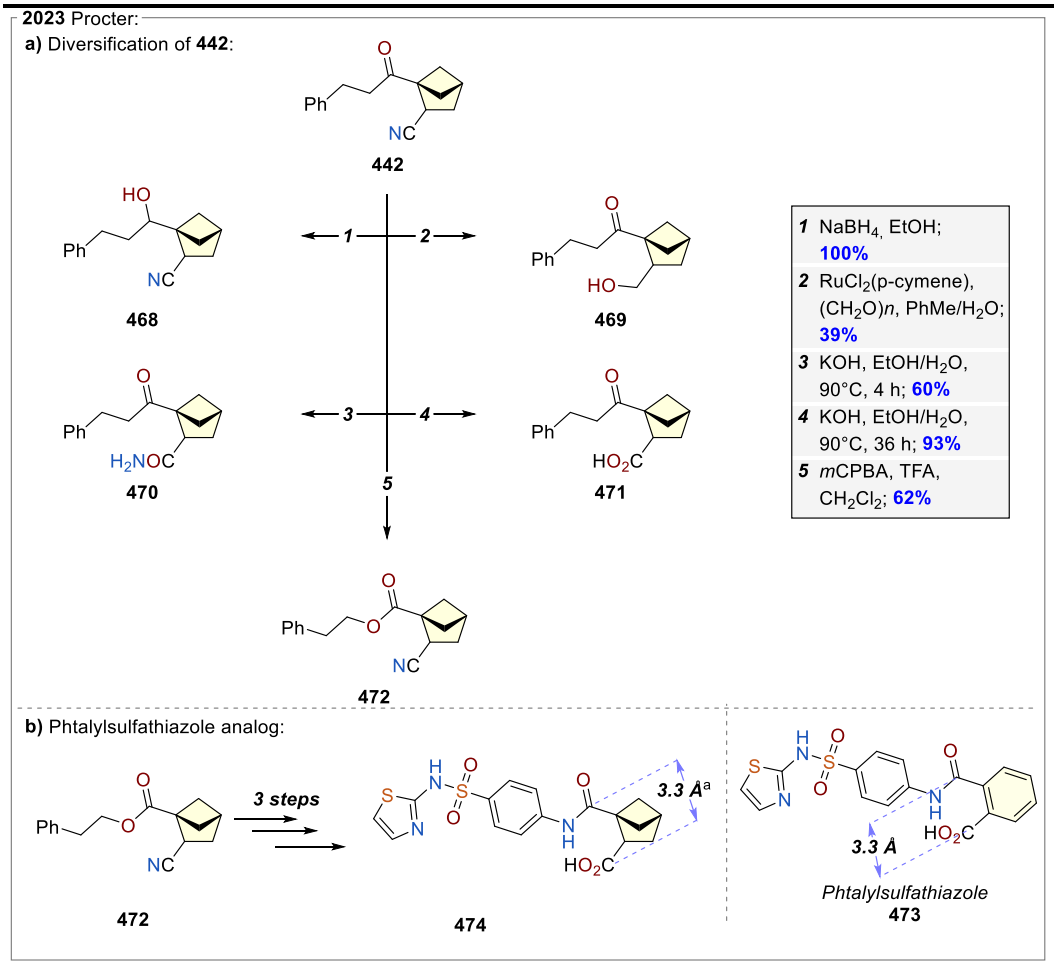

Scheme 51. Synthesis of 1,2,4-trisubstituted BCHs, Procter *et al.* 2023.[44] **a)** Diversification of **442**. **b)** The BCH analog of Phtalylsulfthiazole **473**. [a]Calculated.

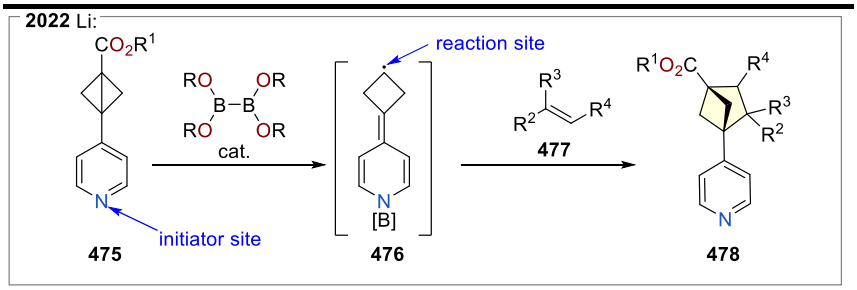

Scheme 52. Dearomative/rearomative radical transmission through-pyridine concept.

In this approach, the bornyl radical reacts with the nitrogen of the pyridinic ring, representing the initiation site of the reaction (**Scheme 52**). The C-C bond of the BCB moiety is then cleaved, generating the radical **476,** that reacts with the olefine **477** in a [3+2] cycloaddition, producing the BCH scaffold **478**. Even though it is limited to pyridine BCHs, the process has proven to tolerate a wide range of functional groups, introducing esters (**479** - **481**), nitrile (**482**), and amide (**483**) at position four (**Scheme 53b**). Position two is amenable for functionalization (**484** - **487**). Reaction with 1,2-dihydronaphthalene and coumarin led to the cyclic structures **488** and **489,** respectively. The 1,2,3,4-thetrafunctionalized BCH **490** was obtained by reacting ethyl cinnamate with pyridine-BCH. Interestingly, this reaction is particularly suitable for achieving spirocyclic, as shown in structures **491**, **492**, and the spirolactone **493**.

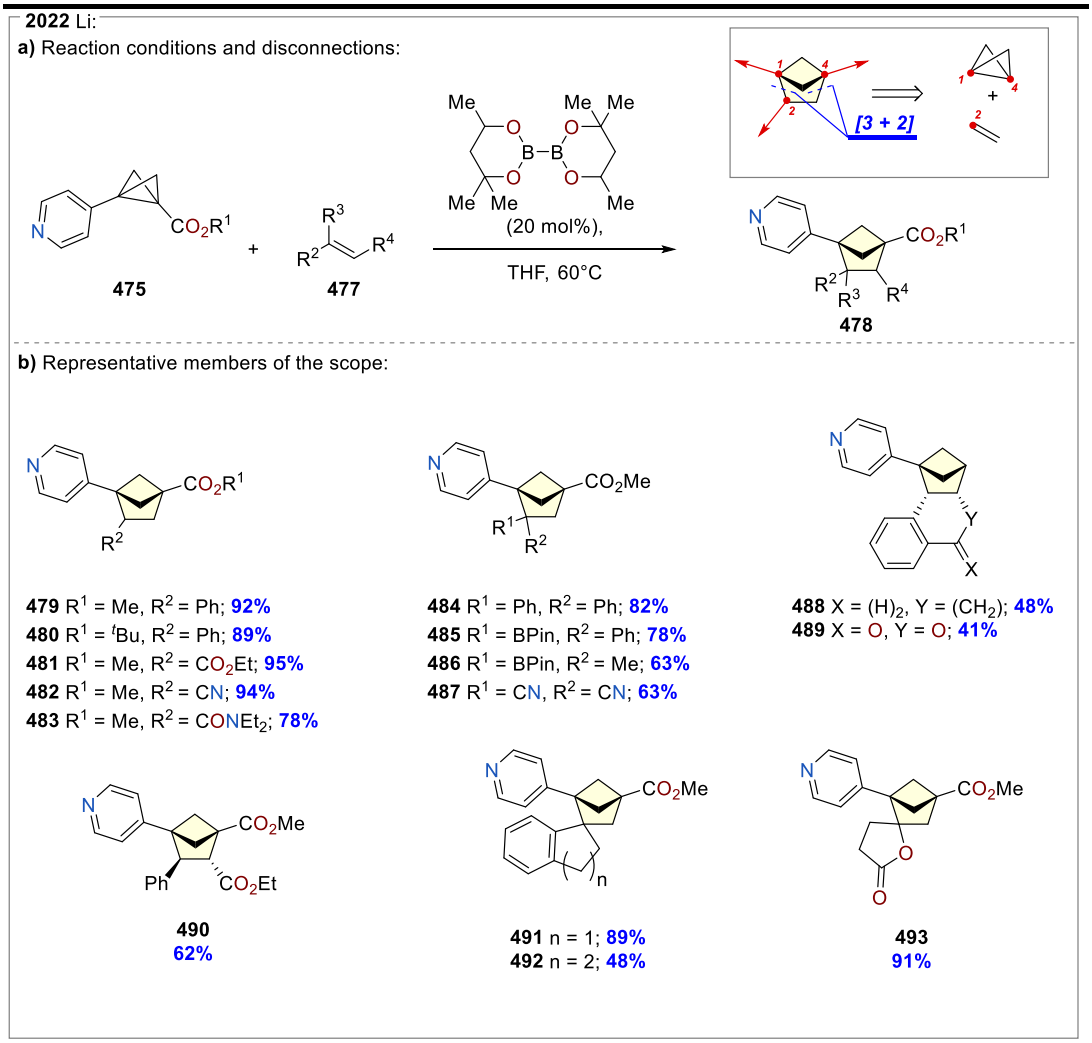

Scheme 53. Synthesis of 1,2,4-trisubstituted BCHs, Li *et. al.* 2022.[45] **a)** Reaction conditions. **b)** Reaction scope.

In 2023, Wang reported a pyridine-boryl radical catalyzed cycloaddition between naphthyl ketone-BCBs **494** and olefines **495** (**Scheme 54**).[46] Unlike the method reported by Li,[45] the reaction conditions are milder (**Scheme 54a**), avoiding elevated temperatures, and the catalytic species is the pyridine-boryl radical **497**. The proposed mechanism begins with the formation of the ketyl radical **498** from the reaction of the naphthyl ketone-BCB **499** and **497**. Pyridine dissociation occurs, delivering the second ketyl radical **500,** that undergoes a strain release C-C bond fragmentation, leading to the planar butyl radical **501**. This radical is trapped by the electron-poor olefine **502,** yielding the radical **503**, which couples with the boron enolate intramolecularly, forming the latest ketyl radical **504**. Finally, the pyridine coordinates to the boron center, triggering the restoration of the catalyst and the delivery of the product **506**. The reaction scope is wide and includes forty-two compounds (**Scheme 54c**). Several acrylates and vinyl sulfones were used as olefines, yielding the esters (**507** – **509**), amide (**510**), and the sulfones (**511** and **512**). Phenyl and methyl were introduced at position four (**513** - **519**), while ester (**513** - **518**), phenyl (**514** - **519**), and thiophene (**515**) were introduced at the position two. The scope of the BCB ketones is not only limited to **499**; phenyl ketones (**520 - 522**), *ortho*-, *meta*-, and *para*- substituted phenyl ketones (**523**, **524**), and the pyridine **525** were also introduced.

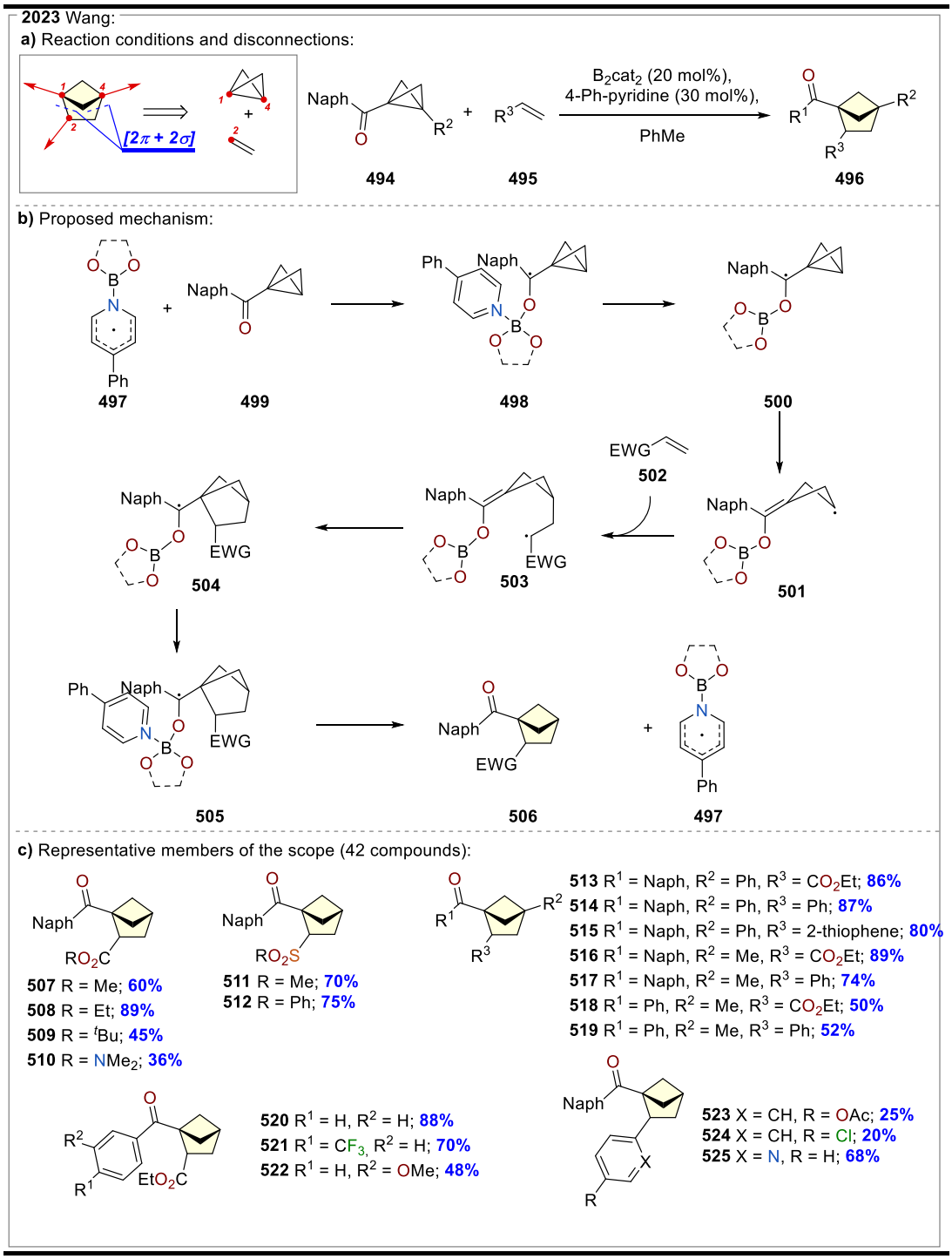

Scheme 54. Synthesis of 1,2,4-trisubstituted BCHs, Wang *et. al.* 2022.[46] **a)** Reaction conditions. **b)** Proposed mechanism. **c)** Representative members of the scope.

2.1.3.4 - 1,4 exit vectors

The first example of the construction of a 1,4-disubstituted BCH was reported in 1973 by Bloomfield *et al*. (**Scheme 55**).[47] In this pioneering work, the authors reported the intramolecular [2+2] cycloaddition of the adipate derivative **526** to yield the 1,4-diester **527**.

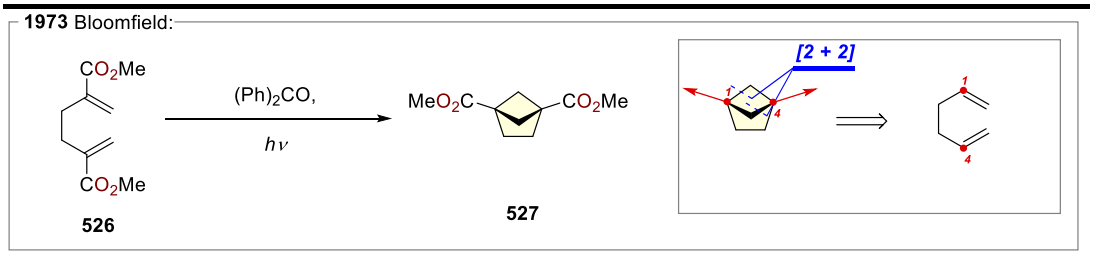

Scheme 55. Synthesis of the 1,4-disubstituted BCH **527** from the diene **526**, Bloomfield *et. al.* 1973.[47]

More recently, in 2020, Mykhauliuk and coworkers published the synthesis of 2-oxabicyclo[2.1.1]hexanes (oBCH) in which positions one and two have been vectorized (**Scheme 56**).[31] These structures are emerging as analogs of BCHs and BCPs with improved physiochemical properties. The reaction relies on the generation of an iodonium ion on the olefine **528**, which is intramolecularly opened in an S_N2 by the alcohol moiety, yielding the bicyclic structures. The 1-substituted oBCH **529** was obtained in good yield using molecular iodine The authors then introduced methyl (**530**) and phenyl (**531**) in position four. The transformation was performed with functionalized cyclobutanes, giving the ester **532** and the nitrile **533**. The Cbz-protected amide with the primary iodine was found to be unstable, the iodine was converted *in situ* in the bench-stable acetylated alcohol **534**.

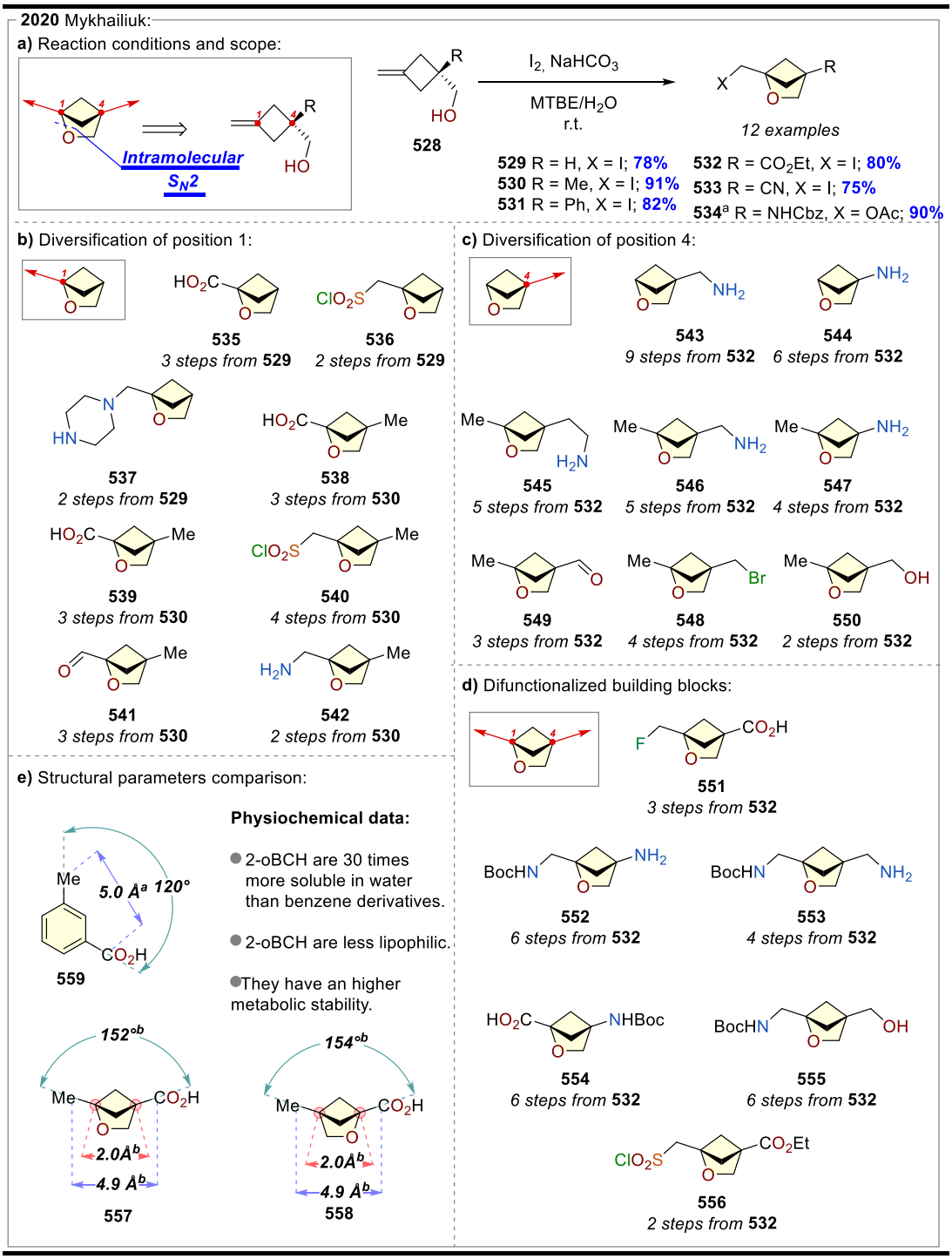

Scheme 56. Synthesis of 1,4-Disubstituted oBCHs, Mykhailiuk *et. al.* 2020.[31] **a)** Reaction conditions and scope. **b)** Diversification of position 1. **c)** Diversification of position 2. **d)** Difucntionalized building blocks. **d)** Structural comparison between **559** and the oBCHs **557** and **558** (Crystallographic data). [a]Calculated data, Myhailiuk *et al.*[4]. [b] Crystallographic data, Myhailiuk *et al.*[31].

A series of transformations were used to expand the vectors one and four (**Scheme 56b** and **55c**). Firstly, the chemistry of the primary iodine was exploited to obtain a series of monofunctionalized (**535** – **537**) and 4-methylated monofunctionalized (**538** – **542**) oBCHs. The carboxylic acids **535** and **539**, the sulfonamides **536** and **540**, the amines **537** and **542**, and the aldehyde **539** were all obtained in a few steps from the corresponding iodides (**Scheme 56b**). Several coupling-relevant functionalities were also introduced at position four (**Scheme 56c**), including amines of different lengths (**543** – **547**), primary bromide (**548**), aldehyde (**549**), and primary alcohol (**550**). Finally, a series of useful difunctionalized building blocks (**Scheme 56d**) were synthesized, yielding the fluorinated acid **551**, the mono-protected diamines **552** and **553**, the amino acid **554**, the aminol **555**, and the sulfonyl chloride/ester **556**. To prove the value of oBCHs as bioisosteres of *meta*-substituted benzenes, the crystal structures of the carboxylic acids **557** and **558** were compared with the crystallographic data of the *meta*-methylbenzoic acid **559** (**Scheme 56e**). The angles and the distances between the substituents were found to be similar. Moreover, the physiochemical properties of several derivatives were measured, revealing that the oBCHs feature higher water solubilities, lower lipophilicities, and higher metabolic stabilities compared to the benzene derivatives.

2.1.3.5 - 1,3,4,5 exit vectors

A [2π+2σ] approach to the oBCHs **560** was reported by Glorius and coworkers in 2022 (**Scheme 57**).[32] This method allows the simultaneous introduction of

substituents in positions one, three, four, and five tracing back the bicyclic structures to BCBs **561** and benzoformiate esters **562**. The reaction mechanism is similar to the one used for the construction of BCHs reported by the same group (**Section 2.1.3.2**, **Scheme 48**).[43] A triplet sensitizer, in this case, the iridium catalyst $[Ir(dF(CF_3)ppy)_2(dtbbpy)]PF_6$, is used to generate the triplet diradical **563** from the formate ester **564**. The reaction between the diradical **563** and the BCB **564** yields the intermediate **565,** which, after a series of ISC and radical couplings, produces the bicycle **566**. Differently from before, a hydrogen atom transfer (HAT) undergoes between the bicycle **566** and the diradical **563**, triggering the aryl transfer that generates stabilized radical **567,** passing through the transition state **568**. The HAT is in equilibrium; therefore, the regioselectivity of the reaction is controlled by the higher stability of ketyl radical **569** over the secondary radical **568,** that could undergo a back hydrogen transfer. The product **570** is delivered by the donation of a hydrogen atom to radical **569**. Due to steric hindrance, the hydrogen donor can only approach the radical **569** from the opposite face of the phenyl, leading to *cis*-diastereoisomers. The benzoformiate esters control the substituents in positions three and five. Several esters were found to be compatible with the reaction conditions (**571** - -**575**, **Scheme 58a**). The possibility to introduce substituents in the *para*-position of the phenyl ring. in position five was explored, achieving the chloride **576**, the *para*-tolyl **577**, the trifluoro methyl **578**, the methyl ester **579**, the *para*-methoxy benzene **580**, and the *para*-trifluoromethoxy benzene **581**. The *meta*-position was decorated with fluoride

(**582**), methyl (**583**), and trifluoromethyl (**584**), while only one example of *ortho*-fluorobenzene was presented **585**.

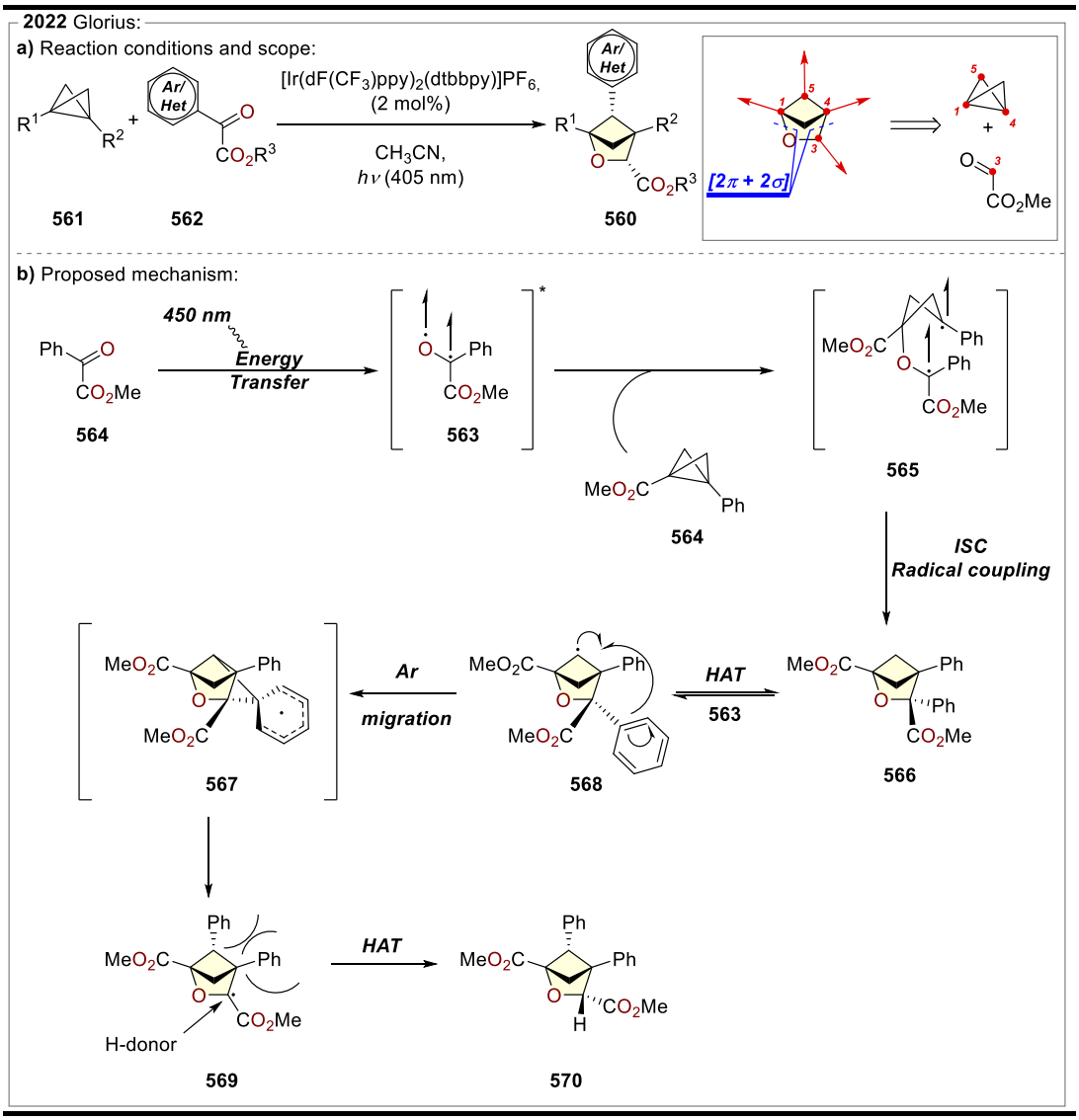

Scheme 57. Synthesis of 1,3,4,5-Polysubstituted oBCHs, Glorius *et. al.* 2022.[32] **a)** Reaction conditions. **b)** Proposed mechanism.

Screening the scope of the BCBs (**Scheme 58b**), different esters were introduced at position one (**586** and **587**), while position four was found to tolerate *para*- (**588** - **590**) and *meta*-substituted benzenes (**591** and **592**). Finally, the bicycle **571** was derivatized (**Scheme 58c**), and its reduction with lithium aluminum hydride led to the diol **593** with an 88% yield. The saponification of both the esters was achieved using sixteen equivalents of lithium hydroxide (**594**), while by decreasing the equivalents of the base to four, the selective hydrolysis of the ester at position one was observed (**595**).

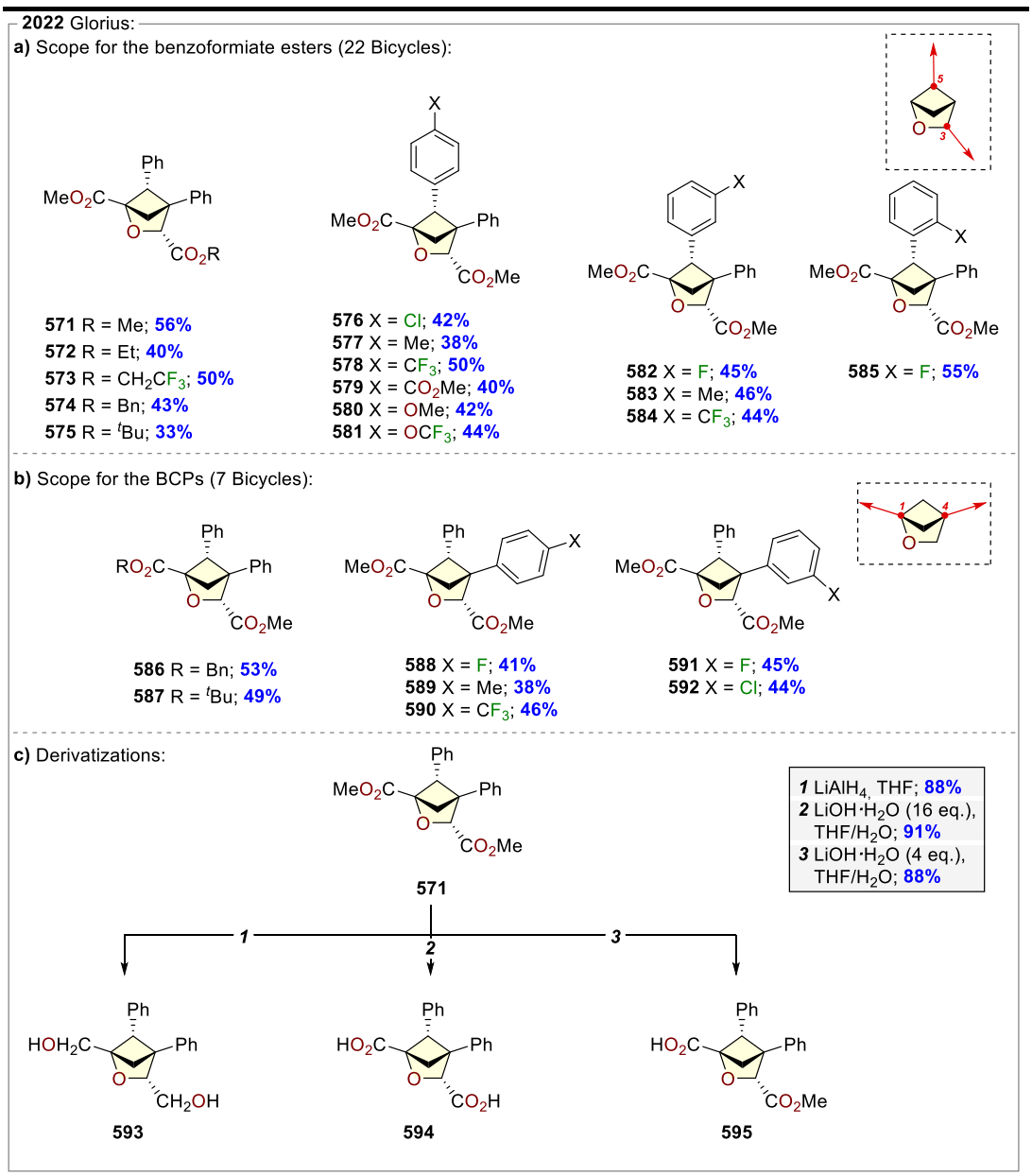

Scheme 58. Glorius *et. al.* 2022.[32] **a)** Scope for benzoformiate esters. **b)** Scope for BCPs. **c)** Dericatizations of **571**.

2.1.3.6 - 1,5 and 4,6 exit vectors

Two recent works from the group of Mykhailiuk have introduced exit vectors in positions one and five of BCHs and in positions four and six of oBCHs, obtaining linkers that mimic *meta*-benzene. The first dates back to 2020 when an intramolecular [2+2] was used to build the disubstituted BCHs (**Scheme 59a**).[48] Benzophenone was used as photosensitized, employing black light and acetonitrile as a solvent. The α,β-unsaturated esters **596** were prepared through Horner-Wadsworth-Emmons Wittig reactions, leading to low diastereoselectivities Since the separation of the diastereoisomers of esters **597** has resulted to be problematic, esters **597** were hydrolyzed in a second step, obtaining the free acids **598**, that were crystallized as single stereoisomers. The reaction scope (**Scheme 59b**). includes several *para*-substituted phenyls (**599** - **602**), the trifluorinated phenyl ring **603**, the *meta*-bromobenzene **604**, and the pyridines **605** and **606**. Five membered rings heteroaromatics were introduced, obtaining the oxazole **607**, the thiophene **608**, the thiazole **609**, and the furane **610**. In addition to the carboxylic acids, the nitrile was also introduced in position five in the BCH **611** and the pyridine **612** both isolated as single stereoisomers. Compounds **610** and **612** were derivatized to achieve difunctionalized building blocks that can serve as analogs of *meta*-disubstituted benzenes (**Scheme 59c**). A two-step sequence was used to methylate the acid **610** and cleave the furan, obtaining the ester/carboxylic acid **613**. Hydrogenation of the pyridine **612** gives access to the saturated amino acid **614**.

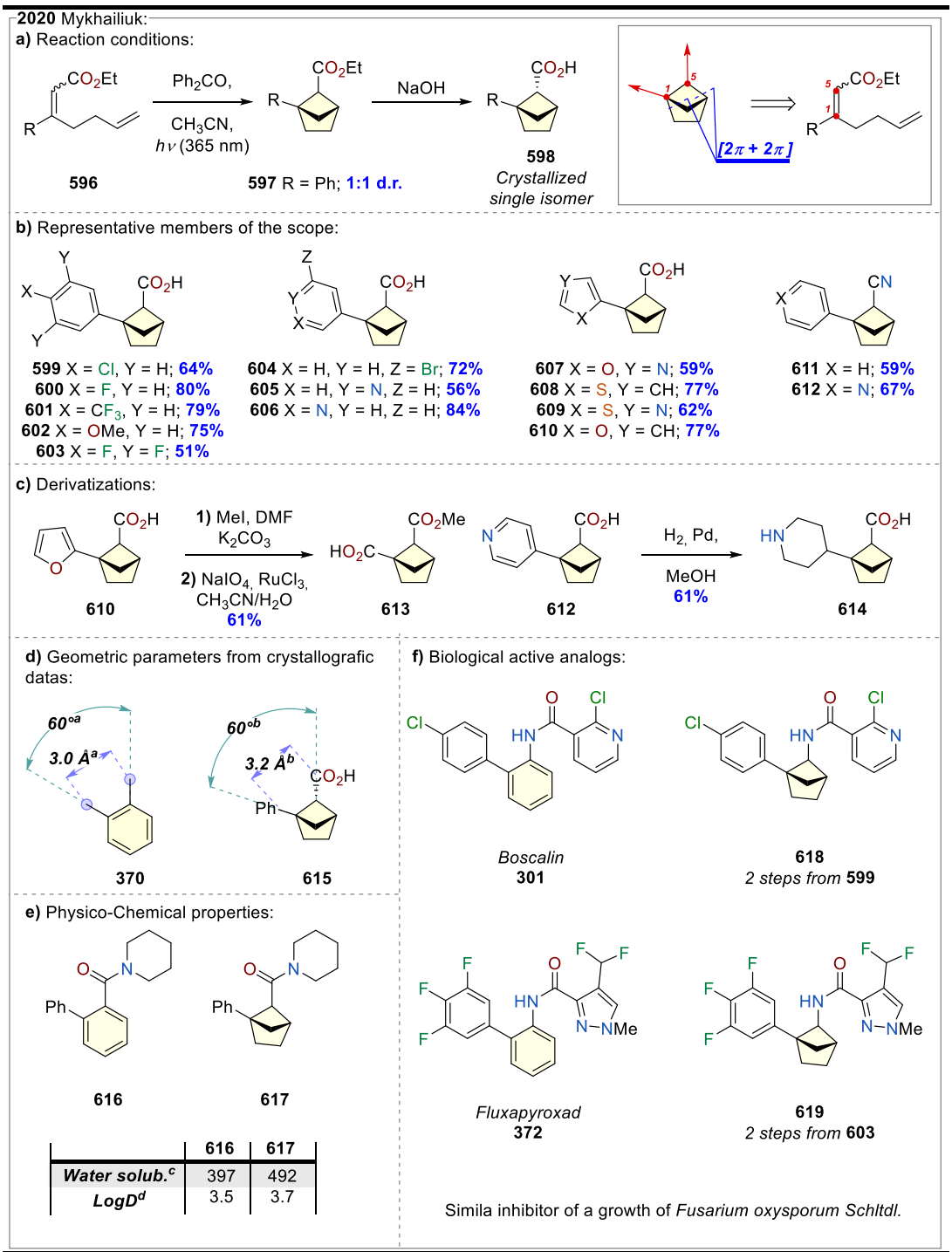

Scheme 59. Synthesis of 1,5-disubstituted BCHs, Mykhailiuk *et. al.* 2020.[48] **a)** Reaction conditions. **b)** Representative members of the scope. **c)** Derivatizations of **610** and **612**. **d)** Structural parameters comparison (Crystallographic data). **e)** Evaluation of physiochemical properties. **f)** Biological active analogs of Boscalin **301** and Fluxapyroxad **372**. [a]Calculated Myhailiuk *et al.*[4] .[b]Crysrallographic data. [c]Water solubility

The geometric parameter (angles and distances between the substituents) obtained from the crystal structure of **615** resulted close to those of *meta*-disubstituted benzenes **370** (**Scheme 59d**), proving their structural analogy. The physicochemical properties of **616** and its BCH bioisoster **617** were measured (**Scheme 59e**), finding that **617** has higher water solubility and comparable lipophilicity (logD) to its aromatic counterpart **616**. Finally, analogs of the fungicides Boscalin **301** and Fluxopyroxade **372** were synthesized, respectively in two steps from **599** and two steps from **603** (**618** and **619**). Their biological activity against *Fusarium oxysporum Schltdl.* was found to be comparable to one of the commercial fungicides. Together, these results show that the 1,5-disubstituted BCHs **596** are valuable bioisosteres of *ortho*-benzenes, leading to analogs with similar structural features, improved physiochemical properties, and similar biological activity.

In a more recent work, intramolecular [2+2] cycloaddition was expanded to vinyl allyl ethers **620** (**Scheme 60a**) yielding 4,5-disubstituted oBCHs **621**.[32] As in the previous work, saponification of the oBCHs esters **621** was necessary to isolate the acids **622** as single crystallizable stereoisomers. Several substituents were introduced in the *para* and *meta* positions of the benzenic ring on carbon four (**623** – **631**, **Scheme 60b**). The process is also useful for introduing substituents in the *ortho* position, giving *ortho*-methoxy benzene **632** and *ortho*-trifluoromethyl **633**. The scope was also expanded to substituted pyridines (**634** - **637**). The BCH (**618**, **619**, **640**, and **641**) and oBCH (**638**, **639**, **642**, and **643**) analogs of Boscalin **301**,

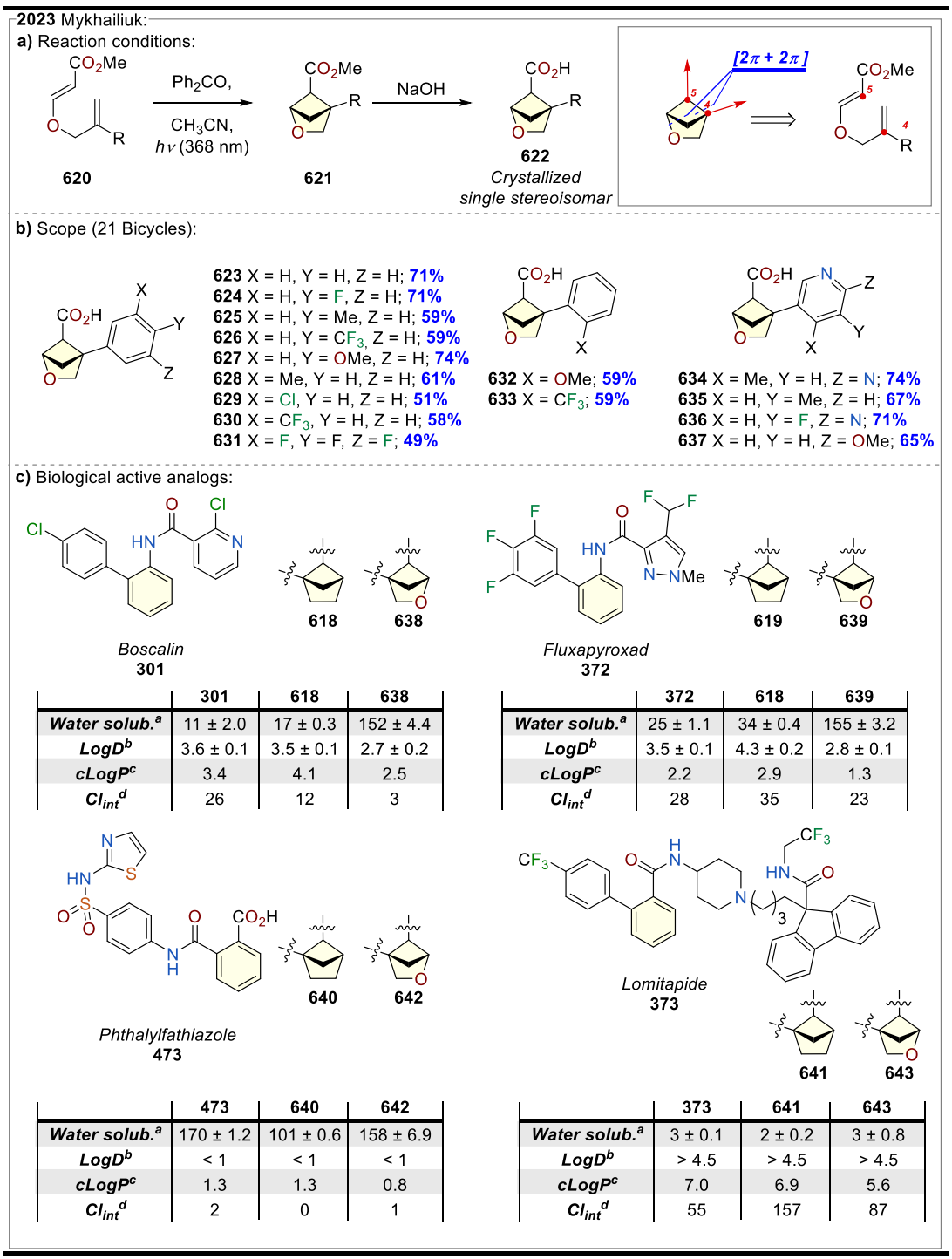

	301	618	638
Water solub.[a]	11 ± 2.0	17 ± 0.3	152 ± 4.4
LogD[b]	3.6 ± 0.1	3.5 ± 0.1	2.7 ± 0.2
cLogP[c]	3.4	4.1	2.5
Cl_{int}[d]	26	12	3

	372	618	639
Water solub.[a]	25 ± 1.1	34 ± 0.4	155 ± 3.2
LogD[b]	3.5 ± 0.1	4.3 ± 0.2	2.8 ± 0.1
cLogP[c]	2.2	2.9	1.3
Cl_{int}[d]	28	35	23

	473	640	642
Water solub.[a]	170 ± 1.2	101 ± 0.6	158 ± 6.9
LogD[b]	< 1	< 1	< 1
cLogP[c]	1.3	1.3	0.8
Cl_{int}[d]	2	0	1

	373	641	643
Water solub.[a]	3 ± 0.1	2 ± 0.2	3 ± 0.8
LogD[b]	> 4.5	> 4.5	> 4.5
cLogP[c]	7.0	6.9	5.6
Cl_{int}[d]	55	157	87

Scheme 60. Synthesis of 4,5-disubstituted oBCHs, Mykhailiuk *et. al.* 2023.[32] **a)** Reaction conditions. **b)** Representative members of the scope. **c)** Biological active analogs of Boscalin **301**, Fluxapyroxad **372**, Phthalylfathiazole **473**, and Lomitapide **373**. [a]Experimental kinetic solubility in phosphate buffer (pH = 7.4, μM). [b]logD = intrinsic distribution coefficient between *n*-octanol and aqueous in phosphate buffer (pH 7.4). [c]clogP = calculated partition coefficient between *n*-octanol and water. [d]Human Liver Microsome Stability ($\mu Lmin^{-1}mg^{-1}$).

Fluxapyroxad **372**, Phthalylsulfathiaxole **473**, and Lomitapide **373** were synthesized, and their physiochemical properties were evaluated (**Scheme 59c**). The presence of oBCH as a linker drastically increases the water solubility of the Boscalin **301** analog **638** and the Fluxapyroxad **372** analog **639**. The solubility of **643** is indeed close to that of Lomitapide **373,** while in the case of **642,** the solubility was even lower than that of the original drug **473**. Two parameters were used to evaluate lipophilicity: calculated logP (clogP, where P is the partition coefficient) and experimental logD (where D is the distribution coefficient). In summary, the replacement of benzene rings with BCHs or oBCHs decreases lipophilicity. The influence of the linkers on metabolic stability (Cl_{int}) is complex. For Boscalin **301,** the substitution of the benzene ring with BCH increases stability (**618**), and the substitution with oBCH in **638** increases it even more. In the case of Fluxapyroxad **372,** the presence of oBCH increases stability (**639**), and the presence of BCH decreases it (**619**). The metabolic stability of Lomitapide **373** is increased more by the introduction of BCH than by the introduction of oBCH (**641** vs **643**), while the substitution with saturated bioisosteres has a slight influence on the stability of Phthalylsulfathiaxole **473**. The biological activity of Boscalin **301** and Fluxapyroxad **372** was compared with those of the analogs, finding that the different linkers slightly affect bioactivity.

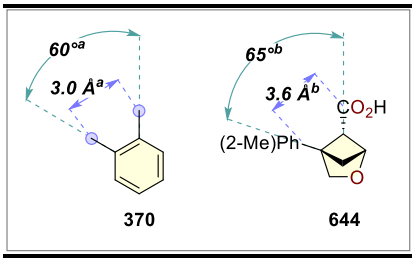

Scheme 61. Structural parameters comparison. [a]Calculated data, Mykhailiuk *et al.*[4]. [c]Crystallographic data, Mykhailiuk *et al.*[32].

The structural analogy between oBCHs and *meta*-substituted benzenes can be visualized through the angle and distances between substituents in **644**, obtained from its crystal structure (**Scheme 61**, comparison between **370** and **644**).

2.2.0.0 - Aim of the project

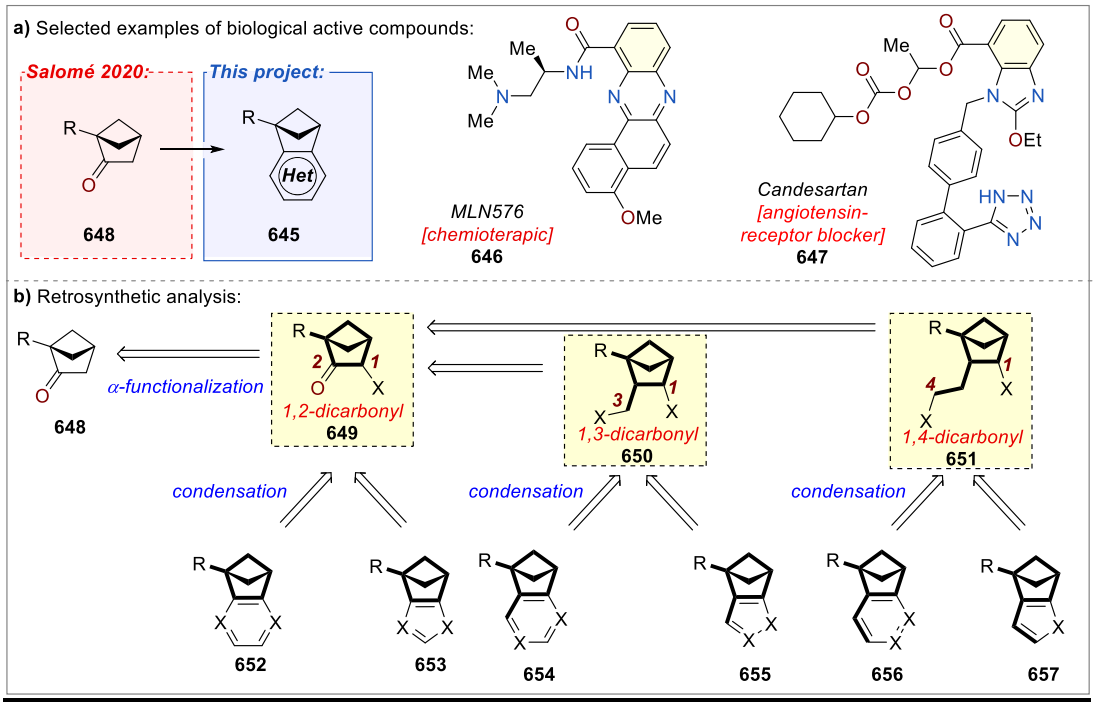

Scheme 62. Aim of the project. **a)** Selected examples of biological active compounds containing benzene-(hetero)aryl condensed motifs. **b)** Retrosynthetic analysis for sp^2-sp^3 (hetero)aryls-BCHs building blocks.

In recent year, the interest in sp^2-sp^3 hybrid building blocks has been rising,[49–51] given the importance of bicyclo[2.1.1]hexanes (BCHs) as bioisosteres of *ortho*-disubstituted benzenes (**Section 2.1.2.1**). We believe that the construction of BCH-(hetero)aromatic condensed building blocks **645** can be beneficial in the improvement of bioactive small molecules miming *ortho*-substituted benzenes condensed with (hetero)aromatics. This type of structural motif is shared by several drugs, such as the chemotherapeutic ML576 **646,** under investigation for the treatment of solid tumors,[52] and Candesartan **647,** an FDA-approved angiotensin-receptor blocker used for managing hypertension (**Scheme 62a**).[53] As we have discussed in **Section 2.1.3.1**, our collaborators at SpiroChem have recently published a scalable and mild route toward 1-substituted-2-ketones **648** (**Scheme 62a**).[37] My project

aims to exploit ketone **648** to build (hetero)aromatics-BCH condensed scaffolds **645**, obtaining unprecedented building blocks. Through retrosynthetic analysis, we envision that 1,4- 1,3- and 1,2- diketone analogs (**649**, **650**, and **651**) can act as late-stage intermediates for the synthesis of a wide range of (hetero)aromatics (**652** – **657**, **Scheme 62b**). The 1,2-dicarbonyl analogs **649** can be obtained through the α-functionalization of ketones **648**, while **650** and **651** are accessible from **649** by exploiting the ketone chemistry.

2.3.0.0 - Results and Discussion

2.3.1.0 - α-functionalization of the ketone 328 and 1,2-dicarbonyl condensation

We began the synthetic campaign by screening conditions for the α-functionalization of 1-phenyl-2-ketone BCH **328** (**Scheme 63**) This ketone was chosen for screening due to its easy accessibility from phenylacetaldehyde **324** (**Section 2.1.3.1**, **Scheme 44b**).[37] We hypothesized that the α-bromo ketone could be a valuable intermediate, being the starting material of several (hetero)aromatics synthesis. Accordingly, the ketone **328** was exposed to bromination in acid conditions (**Scheme 63**, **Table 1**, entry 1), leading to the recovery of the starting material. The same result was obtained for the α–nitrosylation using isoamyl nitrite (*sia*-ONO) and chloridoid acid (**Scheme 63**, **Table 1**, entry 2). We decided to try quenching the enolate with a series of electrophiles, taking advantage of the work of Salomé *et al.*[37] on the α-carbonylation of **328** (**Section 2.1.3.1**, **Scheme 45a**). The non-trivial base Cy^{i}PrNLi was used for the deprotonation. Bromination attempts with N-bromo succinimide (NBS) and

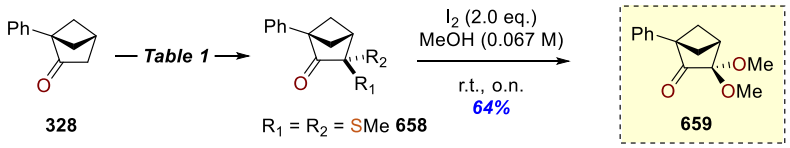

Table 1: Optimization of the 1,2-dicarbonyl analog

Entry	*Conditions:*	R_1	R_2	*Yield (%)*
1	Br_2, AcOH, r.t.	H	Br	***0***
2	*sia*-ONO, $HCl^{2M, aq.}$, MeOH, 60°C	H	NO	***0***
3	Cy^{i}PrNLi, THF, -78°C *then* NBS	H	Br	***0***
4	Cy^{i}PrNLi, THF, -78°C *then* Br_2	H	Br	*degradation*
5	Cy^{i}PrNLi, THF, -78°C *then sia*-ONO	H	NO	***0***
6	Cy^{i}PrNLi, THF, -78°C *then* TsSMe	SMe	SMe	***14***
7	Cy^{i}PrNLi (2.3 eq.)i, HMPA (1.0 eq.), THF (0.1 M), -78°C *then* TsSMe (6.0 eq.)	SMe	SMe	***63***

Scheme 63. α-functionalization of the ketone **328**. **Table 1:** condition used.

bromide were unsuccessful, leading to the complete recovery of **328** for NBS (**Scheme 63**, **Table 1**, entry 3) and the sole degradation of the starting material using bromide (**Scheme 63**, **Table 1**, entry 4). No conversion was also observed when quenching the enolate with isoamyl nitrite (**Scheme 63**, **Table 1**, entry 5), while promising results were obtained using S-methyl 4-methylbenzene sulfonothioate (TsSMe) as electrophile (**Scheme 63**, **Table 1**, entry 6), isolating the thioacetal **658** with a 14% yield. We found that the use of hexamethylphosphoramide (HMPA) as an additive increased the yield to 64%. The thioacetalization proved to be scalable up to the gram scale, effectively providing a useful amount of **658**. The thioacetal group was exchanged for the more practical dimethoxy acetal group by exposing **658** to iodine in methanol at reflux, yielding the 1,2-dicarbonyl analog **659** in 64% of yield.

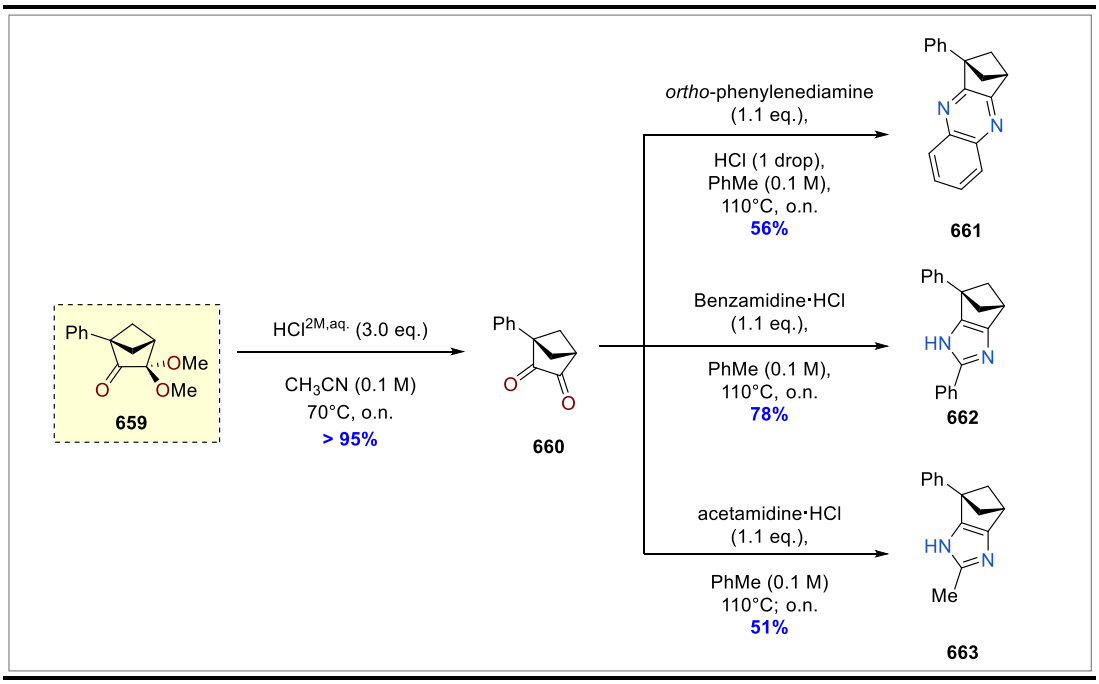

Scheme 64. Synthesis of quinoxaline **661** and imidazoles **662** and **663** from the acetal **659**.

Once a reliable route toward the 1,2-dicarbonyl analog **659** was established, we proceeded to explore its condensation with diamines and amidines (**Scheme 64**). The acetal **659** was hydrolyzed in acid conditions, yielding the diketone **660**. Direct condensation in toluene of **660** with *ortho*-phenylenediamine, benzamidine, and acetamidine furnished respectively the quinoxaline **661**, and the imidazoles **662** and **663**, all isolated in good yields.

2.3.2.0 - Toward 1,3-dicarbonyls

Several olefinations of ketone **659** have been adopted to introduce an electrophilic acceptor in position 3 (**Scheme 65**, **Table 1**), including Wittig homologation (**Scheme 65**, **Table 1**, entry 1), Ramirez (**Scheme 65**, **Table 1**, entry 2), and Petersen olefination (**Scheme 65**, **Table 1**, entry 3), although with disappointing results. Only in the case of the Petersen olefination we were able to isolate the α-hydroxysilane intermediate, but all the attempts to trigger the elimination were unsuccessful. The Tebbe's reagent ultimately furnished the olefin **664** with a 35% yield (**Scheme 65**, Table 1, entry 4), and the dimethoxy acetal was successfully deprotected, delivering α,β-unsaturated ketone **665** (**Scheme 66**). Attempts at derivatization of the α,β-unsaturated ketone **665** are still ongoing; direct cyclization with hydrazine did not result in any conversion. We believe that the introduction of an electrophilic acceptor in position 3 (**667**) would facilitate the condensation into (hetero)cycle. For this purpose, the hydroboration/oxidation of the ketone **664** has been attempted, unfortunately with no result. An alternative strategy we plan to evaluate relies on the introduction of oxygen as a surrogate, such as an oxime (**668**), through an oxa-Michael. A two-step sequence of oxidation/condensation could then provide the desired (hetero)cycle.

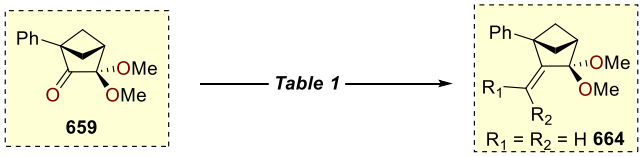

Table 1: Optimization of the 1,3-dicarbonyl analog

Entry	*Conditions:*	R_1	R_2	*Yield (%)*
1	Ph_3PCH_2OMeCl, ^tBuOK, THF from -78°C to r.t	H	OMe	*0*
2	CBr_4, PPh_3, PhMe, 80°C	Br	Br	*0*
3	$TMSCH_2Li$, THF, -78°C, *then* KH, THF*	SMe	SMe	*0*
4	Tebbe's reagent, THF, 0°C to r.t.	SMe	SMe	*35*

**α-hydroxysilane isolated (Y = 63%)*

Scheme 65. Attempts in obtain 1,3-dikarbonyls surrogates. **Table 1**: conditions used.

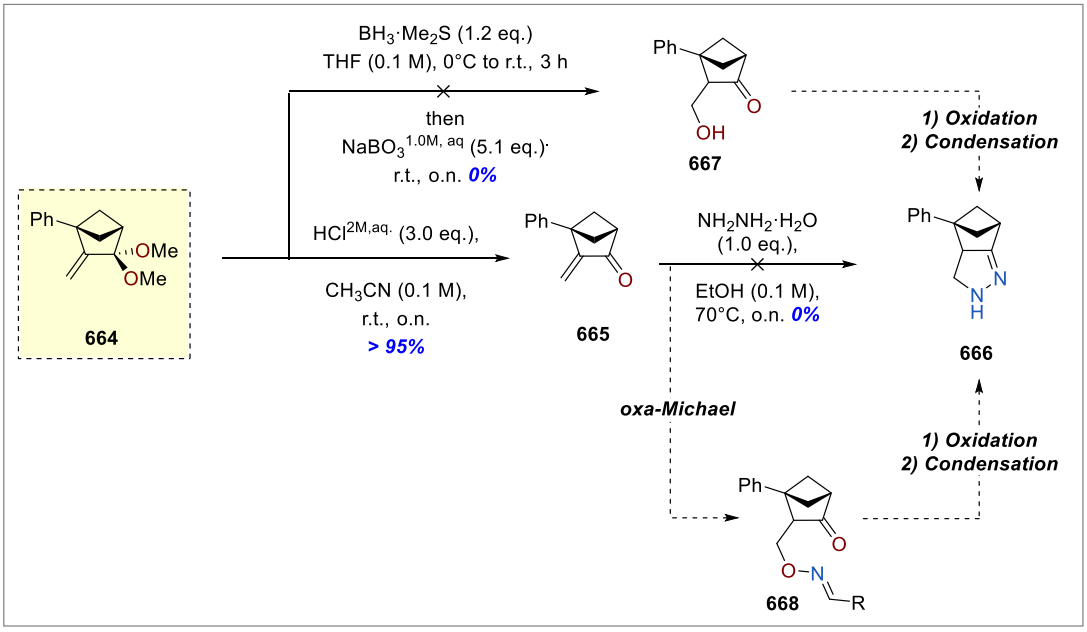

Scheme 66. Deprotection of the acetal **664** to **665** and attempts to obtain the pyrazole condensed adduct **666**.

2.3.3.0 - Condensation of 1,4-dicarbonyl intermediate

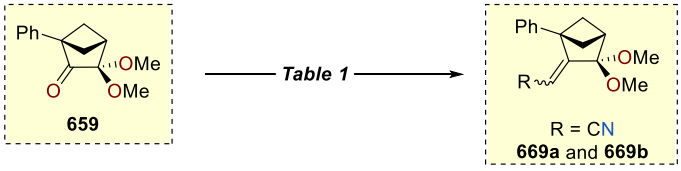

Table 1: Optimization of the 1,4-dicarbonyl analog

Entry	*Conditions:*	*R*	*Yield (%)*
1	Ph_3PCHCO_2Et, CH_2Cl_2, r.t. to 40°C	CO_2Et	*0*
2	$(EtO)_2POCH_2CO_2Et$, NaH, THF, 0°C to r.t.	CO_2Et	*0*
3	$(EtO)_2POCH_2COMe$, NaH, THF, 0°C to r.t.	COMe	*0*
4	$(EtO)_2POCH_2CN$, NaH, THF, 0°C to r.t.	CN	*75 (3.5:1 d.r.)*
5	$(EtO)_2POCH_2CO_2Et$, NaH, THF, 0°C to 66°C	CO_2Et	*0*

Scheme 67. Attempts in obtain 1,4-dikarbonyls surrogates. **Table 1**: conditions used.

To obtain 1,4-dicarbonyl analogs (**Scheme 67**), the Wittig olefination failed, and the Horner-Wadsworth-Wittig was tried in different conditions, resulting in the introduction of the sterically less demanding methylene-cyano group in the intermediate **669** (**Scheme 67**, **Table 1**, entry 4). Both regioisomers were isolated with an 88% yield and a 2.4:1 diastereomeric ratio (**669a** and **669b**). The major diastereoisomer **669a** was subjected to a sequence of reactions including basic nitrile

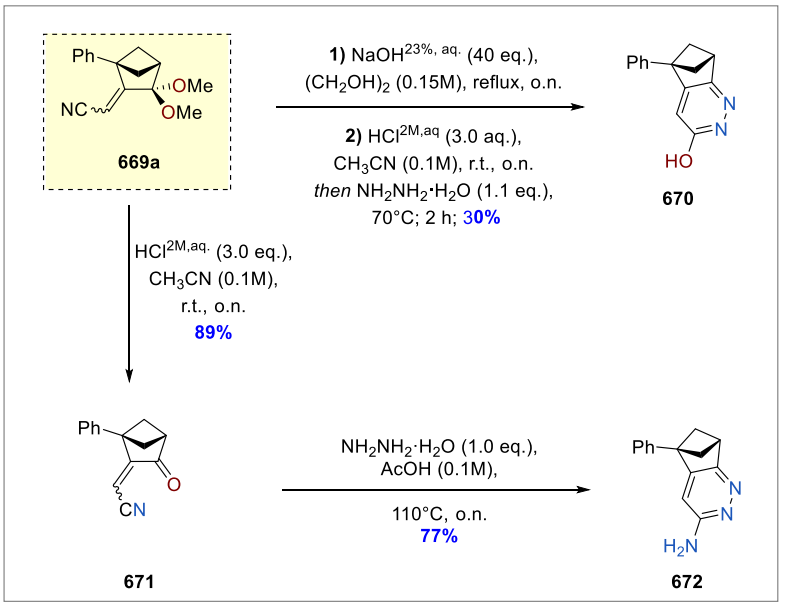

Scheme 68. Synthesis of the pyridazine adducts **670** and **672**.

hydrolysis, acetal deprotection, and hydrazine condensation, delivering the hydroxy pyridazine **670** (**Scheme 68**). Deprotection of acetal **669a** resulted in the ketone **671**, which was successfully condensed with hydrazine to produce the amino pyridazine **672** in a 77% yield.

After the six-membered ring (hetero)cycles, we move to the introduction of five-membered rings (**Scheme 69**). The regioisomer **669a** was exposed to lithium alluminiumhydride and $NiCl_2/NaBH_4$ in the attempt to obtain the Boc-amine **673** and the allylic amine **674**, both amenable for the condensation to pyrrole **675**. The allylic Boc-amine **673** was successfully yielded by the first protocol, while the second did not result in any conversion. Currently, we are investigating the cyclization of **673** cyclization in acid conditions in our laboratory. We think that obtaining the Paal-Knorr intermediate **676** would be greatly advantageous, as it would give direct access to pyrrole **675**, furan **677**, and thiophene **678**. To achieve this, we hydrogenated **669a,** resulting in the aliphatic nitrile **679**. Unfortunately, the reduction with DBALH led to the complete recovery of **669a** and, similarly, other reductive protocols to reduce the nitrile to amine were unsuccessful.

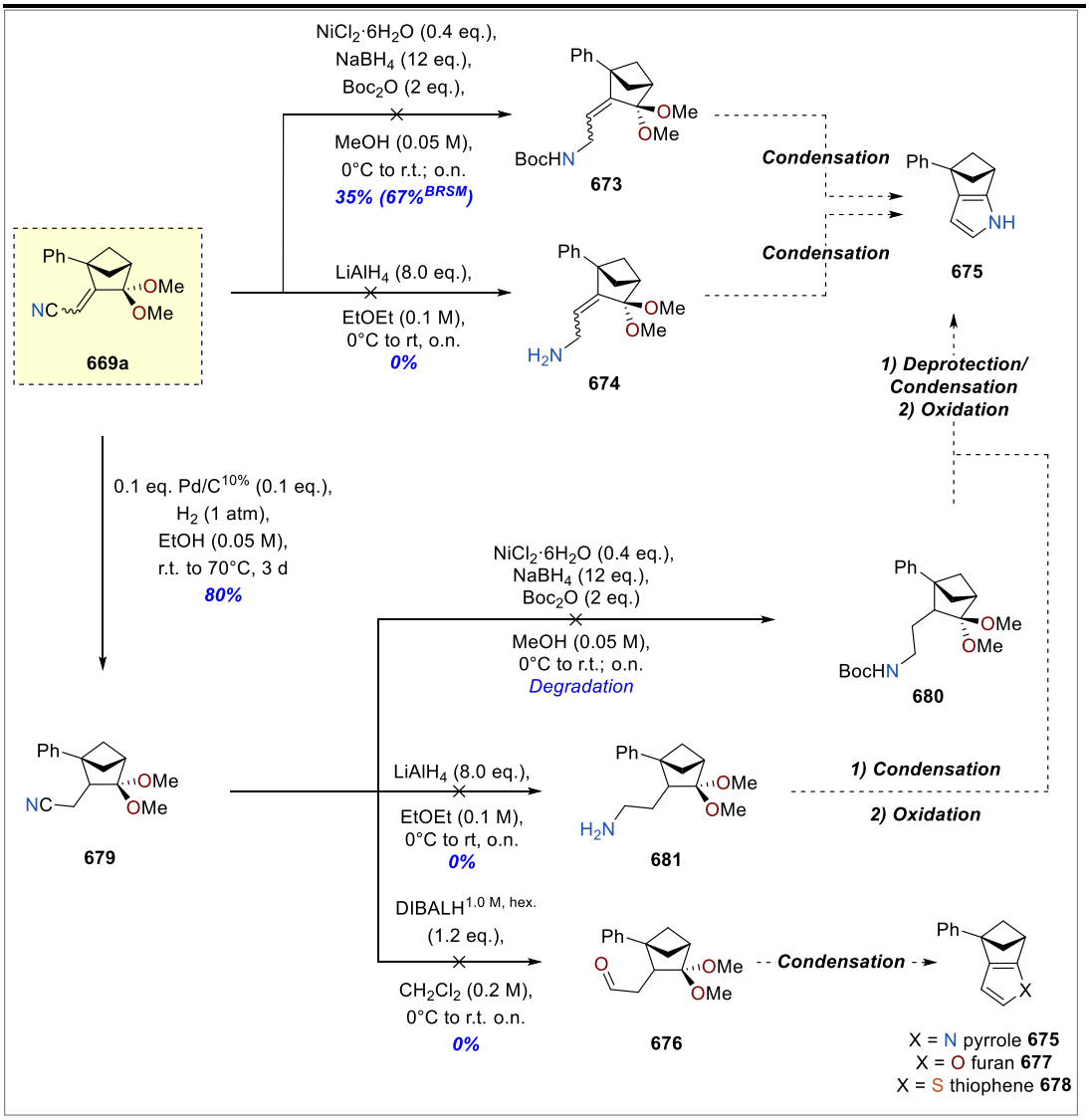

Scheme 69. Possible strategy to obtain pyrrole **675**, furan **677**, and thiophene **678** from **667**.

2.3.4.0 – Outlooks toward the diversification of the position 1

We believe that the introduction of an ester group at position one of our building blocks would be ideal for the diversification of that position through coupling reactions. With this idea in mind, we planned to develop a library of esters (**682**-**686**) (**Scheme 70a**) from the known TBS-alcohol **328**[37] exploiting the previously developed chemistry, protecting group manipulations, and oxidations.

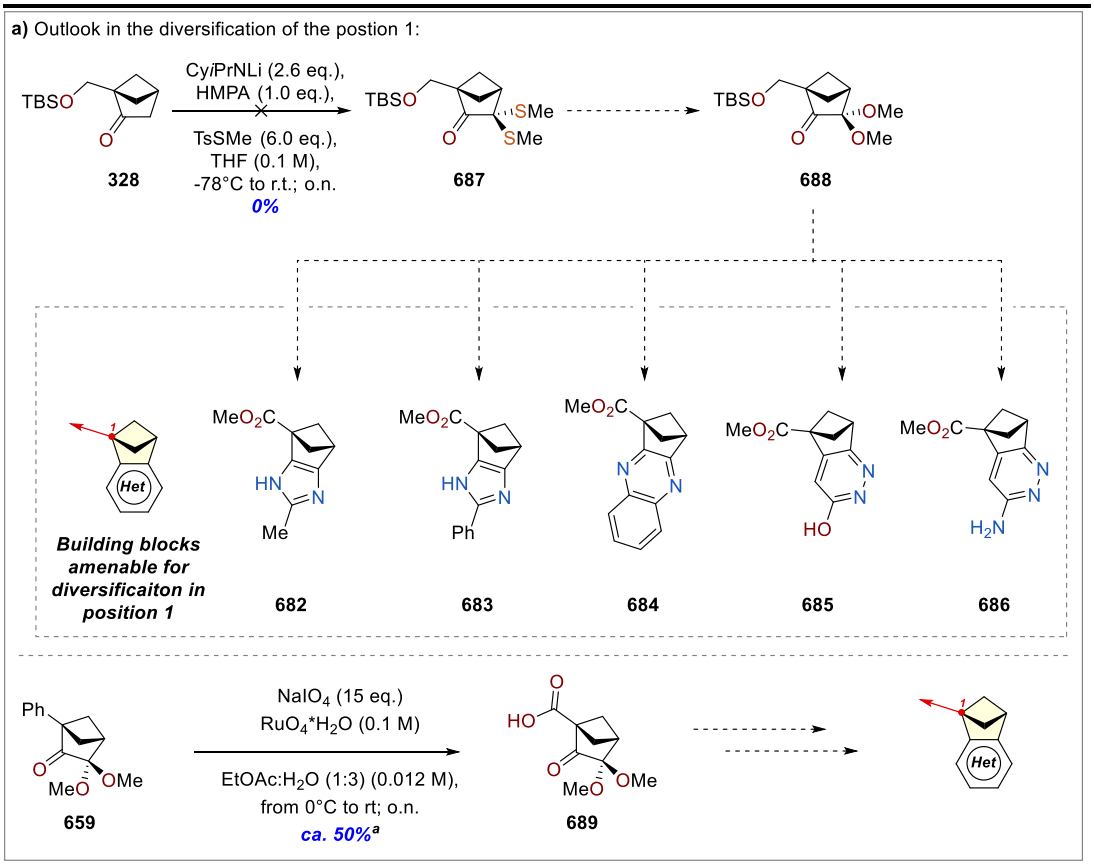

Scheme 70. Future prospectives on the development of building block amenable for the diversification of the position 1 **a)** Strategy proposed from the TBS-alcohol **328. b)** Oxidative cleavage of **659** to obtain the synthetically useful intermediate **688**. [a]Yield evaluated on the crude.

Unfortunately, our multiple attempts to obtain the thioacetal **687** precursor of acetal **688** failed. To overcome this problem, we tried the oxidative cleavage of the phenyl ring in **659**, obtaining acid **689** with encouraging results (**Scheme 70b**).

These results are preliminary; however, they encourage us to pursue this strategy, which would expand the number of accessible building blocks.

2.4.0.0 – Conclusions and outlooks

In conclusion, the synthetic campaign has proved to be successful, allowing the synthesis of several classes of (hetero)arenes-BCH sp^2-sp^3 hybrids. A new method for the α-functionalization of ketone **328** has been developed, giving access to acetal **659**. This intermediate is amenable to the synthesis of quinoxaline (**661**) and imidazoles (**662** and **663**). Furthermore, the construction of 1,4-dicarbonils from acetal **659** led to pyridazines **670** and **672**. The intermediates accessed in this survey hold significant synthetic value and could give access to other classes of (hetero)cycles, including pyrazoles, pyrroles, furans, and thiophenes. The construction of Paal-Knorr intermediate surrogates and the exploration of the chemistry of the acrylate **665** will be the subject of further investigations by our group. Moreover, encouraging results were obtained in the synthesis of acid **689,** which could serve as a precursor for a library of (hetero)arenes-BCH sp^2-sp^3 hybrids that can be diversified at position 1.

2.5.0.0 - References

(1) Lovering, F.; Bikker, J.; Humblet, C. Escape from Flatland: Increasing Saturation as an Approach to Improving Clinical Success. *J. Med. Chem.* **2009**, *52* (21), 6752–6756. https://doi.org/10.1021/jm901241e.

(2) Lovering, F. Escape from Flatland 2: Complexity and Promiscuity. *MedChemComm* **2013**, *4* (3), 515–519. https://doi.org/10.1039/C2MD20347B.

(3) Ritchie, T. J.; Macdonald, S. J. F. The Impact of Aromatic Ring Count on Compound Developability – Are Too Many Aromatic Rings a Liability in Drug Design? *Drug Discov. Today* **2009**, *14* (21), 1011–1020. https://doi.org/10.1016/j.drudis.2009.07.014.

(4) K. Mykhailiuk, P. Saturated Bioisosteres of Benzene: Where to Go Next? *Org. Biomol. Chem.* **2019**, *17* (11), 2839–2849. https://doi.org/10.1039/C8OB02812E.

(5) Auberson, Y. P.; Brocklehurst, C.; Furegati, M.; Fessard, T. C.; Koch, G.; Decker, A.; La Vecchia, L.; Briard, E. Improving Nonspecific Binding and Solubility: Bicycloalkyl Groups and Cubanes as Para-Phenyl Bioisosteres. *ChemMedChem* **2017**, *12* (8), 590–598. https://doi.org/10.1002/cmdc.201700082.

(6) Levin, M. D.; Kaszynski, P.; Michl, J. Bicyclo[1.1.1]Pentanes, [n]Staffanes, [1.1.1]Propellanes, and Tricyclo[2.1.0.02,5]Pentanes. *Chem. Rev.* **2000**, *100* (1), 169–234. https://doi.org/10.1021/cr990094z.

(7) Locke, G. M.; Bernhard, S. S. R.; Senge, M. O. Nonconjugated Hydrocarbons as Rigid-Linear Motifs: Isosteres for Material Sciences and Bioorganic and Medicinal Chemistry. *Chem. – Eur. J.* **2019**, *25* (18), 4590–4647. https://doi.org/10.1002/chem.201804225.

(8) Taylor, R. D.; MacCoss, M.; Lawson, A. D. G. Rings in Drugs. *J. Med. Chem.* **2014**, *57* (14), 5845–5859. https://doi.org/10.1021/jm4017625.

(9) Das, P.; Delost, M. D.; Qureshi, M. H.; Smith, D. T.; Njardarson, J. T. A Survey of the Structures of US FDA Approved Combination Drugs. *J. Med. Chem.* **2019**, *62* (9), 4265–4311. https://doi.org/10.1021/acs.jmedchem.8b01610.

(10) Nilova, A.; Campeau, L.-C.; Sherer, E. C.; Stuart, D. R. Analysis of Benzenoid Substitution Patterns in Small Molecule Active Pharmaceutical Ingredients. *J. Med. Chem.* **2020**, *63* (22), 13389–13396. https://doi.org/10.1021/acs.jmedchem.0c00915.

(11) McGrath, N. A.; Brichacek, M.; Njardarson, J. T. A Graphical Journey of Innovative Organic Architectures That Have Improved Our Lives. *J. Chem. Educ.* **2010**, *87* (12), 1348–1349. https://doi.org/10.1021/ed1003806.

(12) Stockdale, T. P.; Williams, C. M. Pharmaceuticals That Contain Polycyclic Hydrocarbon Scaffolds. *Chem. Soc. Rev.* **2015**, *44* (21), 7737–7763. https://doi.org/10.1039/C4CS00477A.

(13) Pellicciari, R.; Raimondo, M.; Marinozzi, M.; Natalini, B.; Costantino, G.; Thomsen, C. (S)-(+)-2-(3′-Carboxybicyclo[1.1.1]Pentyl)- Glycine, a Structurally New Group I Metabotropic Glutamate Receptor Antagonist. *J. Med. Chem.* **1996**, *39* (15), 2874–2876. https://doi.org/10.1021/jm960254o.
(14) Stepan, A. F.; Subramanyam, C.; Efremov, I. V.; Dutra, J. K.; O'Sullivan, T. J.; DiRico, K. J.; McDonald, W. S.; Won, A.; Dorff, P. H.; Nolan, C. E.; Becker, S. L.; Pustilnik, L. R.; Riddell, D. R.; Kauffman, G. W.; Kormos, B. L.; Zhang, L.; Lu, Y.; Capetta, S. H.; Green, M. E.; Karki, K.; Sibley, E.; Atchison, K. P.; Hallgren, A. J.; Oborski, C. E.; Robshaw, A. E.; Sneed, B.; O'Donnell, C. J. Application of the Bicyclo[1.1.1]Pentane Motif as a Nonclassical Phenyl Ring Bioisostere in the Design of a Potent and Orally Active γ-Secretase Inhibitor. *J. Med. Chem.* **2012**, *55* (7), 3414–3424. https://doi.org/10.1021/jm300094u.
(15) Makarov, I. S.; Brocklehurst, C. E.; Karaghiosoff, K.; Koch, G.; Knochel, P. Synthesis of Bicyclo[1.1.1]Pentane Bioisosteres of Internal Alkynes and Para-Disubstituted Benzenes from [1.1.1]Propellane. *Angew. Chem. Int. Ed.* **2017**, *56* (41), 12774–12777. https://doi.org/10.1002/anie.201706799.
(16) Westphal, M. V.; Wolfstädter, B. T.; Plancher, J.-M.; Gatfield, J.; Carreira, E. M. Evaluation of Tert-Butyl Isosteres: Case Studies of Physicochemical and Pharmacokinetic Properties, Efficacies, and Activities. *ChemMedChem* **2015**, *10* (3), 461–469. https://doi.org/10.1002/cmdc.201402502.
(17) Zhong, M.; Peng, E.; Huang, N.; Huang, Q.; Huq, A.; Lau, M.; Colonno, R.; Li, L. Discovery of Functionalized Bisimidazoles Bearing Cyclic Aliphatic-Phenyl Motifs as HCV NS5A Inhibitors. *Bioorg. Med. Chem. Lett.* **2014**, *24* (24), 5731–5737. https://doi.org/10.1016/j.bmcl.2014.10.057.
(18) Eaton, P. E. Cubanes: Starting Materials for the Chemistry of the 1990s and the New Century. *Angew. Chem. Int. Ed. Engl.* **1992**, *31* (11), 1421–1436. https://doi.org/10.1002/anie.199214211.
(19) Chalmers, B. A.; Xing, H.; Houston, S.; Clark, C.; Ghassabian, S.; Kuo, A.; Cao, B.; Reitsma, A.; Murray, C.-E. P.; Stok, J. E.; Boyle, G. M.; Pierce, C. J.; Littler, S. W.; Winkler, D. A.; Bernhardt, P. V.; Pasay, C.; De Voss, J. J.; McCarthy, J.; Parsons, P. G.; Walter, G. H.; Smith, M. T.; Cooper, H. M.; Nilsson, S. K.; Tsanaktsidis, J.; Savage, G. P.; Williams, C. M. Validating Eaton's Hypothesis: Cubane as a Benzene Bioisostere. *Angew. Chem. Int. Ed.* **2016**, *55* (11), 3580–3585. https://doi.org/10.1002/anie.201510675.
(20) Nicolaou, K. C.; Vourloumis, D.; Totokotsopoulos, S.; Papakyriakou, A.; Karsunky, H.; Fernando, H.; Gavrilyuk, J.; Webb, D.; Stepan, A. F. Synthesis and Biopharmaceutical Evaluation of Imatinib Analogues Featuring Unusual Structural Motifs. *ChemMedChem* **2016**, *11* (1), 31–37. https://doi.org/10.1002/cmdc.201500510.

(21) Cheng, C.-Y.; Hsin, L.-W.; Lin, Y.-P.; Tao, P.-L.; Jong, T.-T. N-Cubylmethyl Substituted Morphinoids as Novel Narcotic Antagonists. *Bioorg. Med. Chem.* **1996**, *4* (1), 73–80. https://doi.org/10.1016/0968-0896(95)00165-4.
(22) Wiesenfeldt, M. P.; Rossi-Ashton, J. A.; Perry, I. B.; Diesel, J.; Garry, O. L.; Bartels, F.; Coote, S. C.; Ma, X.; Yeung, C. S.; Bennett, D. J.; MacMillan, D. W. C. General Access to Cubanes as Benzene Bioisosteres. *Nature* **2023**, *618* (7965), 513–518. https://doi.org/10.1038/s41586-023-06021-8.
(23) Garry, O. L.; Heilmann, M.; Chen, J.; Liang, Y.; Zhang, X.; Ma, X.; Yeung, C. S.; Bennett, D. J.; MacMillan, D. W. C. Rapid Access to 2-Substituted Bicyclo[1.1.1]Pentanes. *J. Am. Chem. Soc.* **2023**, *145* (5), 3092–3100. https://doi.org/10.1021/jacs.2c12163.
(24) Yang, Y.; Tsien, J.; Hughes, J. M. E.; Peters, B. K.; Merchant, R. R.; Qin, T. An Intramolecular Coupling Approach to Alkyl Bioisosteres for the Synthesis of Multisubstituted Bicycloalkyl Boronates. *Nat. Chem.* **2021**, *13* (10), 950–955. https://doi.org/10.1038/s41557-021-00786-z.
(25) Zhao, J.-X.; Chang, Y.-X.; He, C.; Burke, B. J.; Collins, M. R.; Del Bel, M.; Elleraas, J.; Gallego, G. M.; Montgomery, T. P.; Mousseau, J. J.; Nair, S. K.; Perry, M. A.; Spangler, J. E.; Vantourout, J. C.; Baran, P. S. 1,2-Difunctionalized Bicyclo[1.1.1]Pentanes: Long–Sought-after Mimetics for Ortho/Meta-Substituted Arenes. *Proc. Natl. Acad. Sci.* **2021**, *118* (28), e2108881118. https://doi.org/10.1073/pnas.2108881118.
(26) Klopsch, R.; Schlüter, A.-D. A [1.1.1]Propellane with an Unprotected Hydroxy Group in the Side Chain. *Tetrahedron* **1995**, *51* (38), 10491–10496. https://doi.org/10.1016/0040-4020(95)00628-L.
(27) Smith, E.; Jones, K. D.; O'Brien, L.; Argent, S. P.; Salome, C.; Lefebvre, Q.; Valery, A.; Böcü, M.; Newton, G. N.; Lam, H. W. Silver(I)-Catalyzed Synthesis of Cuneanes from Cubanes and Their Investigation as Isosteres. *J. Am. Chem. Soc.* **2023**, *145* (30), 16365–16373. https://doi.org/10.1021/jacs.3c03207.
(28) Harmata, A. S.; Spiller, T. E.; Sowden, M. J.; Stephenson, C. R. J. Photochemical Formal (4 + 2)-Cycloaddition of Imine-Substituted Bicyclo[1.1.1]Pentanes and Alkenes. *J. Am. Chem. Soc.* **2021**, *143* (50), 21223–21228. https://doi.org/10.1021/jacs.1c10541.
(29) Iida, T.; Kanazawa, J.; Matsunaga, T.; Miyamoto, K.; Hirano, K.; Uchiyama, M. Practical and Facile Access to Bicyclo[3.1.1]Heptanes: Potent Bioisosteres of Meta-Substituted Benzenes. *J. Am. Chem. Soc.* **2022**, *144* (48), 21848–21852. https://doi.org/10.1021/jacs.2c09733.
(30) Yu, T.; Yang, J.; Wang, Z.; Ding, Z.; Xu, M.; Wen, J.; Xu, L.; Li, P. Selective [2σ + 2σ] Cycloaddition Enabled by Boronyl Radical Catalysis: Synthesis of Highly Substituted Bicyclo[3.1.1]Heptanes. *J. Am. Chem. Soc.* **2023**, *145* (7), 4304–4310. https://doi.org/10.1021/jacs.2c13740.

(31) Levterov, V. V.; Panasyuk, Y.; Pivnytska, V. O.; Mykhailiuk, P. K. Water-Soluble Non-Classical Benzene Mimetics. *Angew. Chem. Int. Ed.* **2020**, *59* (18), 7161–7167. https://doi.org/10.1002/anie.202000548.
(32) Liang, Y.; Kleinmans, R.; Daniliuc, C. G.; Glorius, F. Synthesis of Polysubstituted 2-Oxabicyclo[2.1.1]Hexanes via Visible-Light-Induced Energy Transfer. *J. Am. Chem. Soc.* **2022**, *144* (44), 20207–20213. https://doi.org/10.1021/jacs.2c09248.
(33) Saya, J. M.; Vos, K.; Kleinnijenhuis, R. A.; van Maarseveen, J. H.; Ingemann, S.; Hiemstra, H. Total Synthesis of Aquatolide. *Org. Lett.* **2015**, *17* (15), 3892–3894. https://doi.org/10.1021/acs.orglett.5b01888.
(34) Kleinnijenhuis, R. A.; Timmer, B. J. J.; Lutteke, G.; Smits, J. M. M.; de Gelder, R.; van Maarseveen, J. H.; Hiemstra, H. Formal Synthesis of Solanoeclepin A: Enantioselective Allene Diboration and Intramolecular [2+2] Photocycloaddition for the Construction of the Tricyclic Core. *Chem. – Eur. J.* **2016**, *22* (4), 1266–1269. https://doi.org/10.1002/chem.201504894.
(35) Takao, K.; Kai, H.; Yamada, A.; Fukushima, Y.; Komatsu, D.; Ogura, A.; Yoshida, K. Total Syntheses of (+)-Aquatolide and Related Humulanolides. *Angew. Chem. Int. Ed.* **2019**, *58* (29), 9851–9855. https://doi.org/10.1002/anie.201904404.
(36) Newman-Evans, R. H.; Simon, R. J.; Carpenter, B. K. The Influence of Intramolecular Dynamics on Branching Ratios in Thermal Rearrangements. *J. Org. Chem.* **1990**, *55* (2), 695–711. https://doi.org/10.1021/jo00289a053.
(37) Herter, L.; Koutsopetras, I.; Turelli, L.; Fessard, T.; Salomé, C. Preparation of New Bicyclo[2.1.1]Hexane Compact Modules: An Opening towards Novel Sp3-Rich Chemical Space. *Org. Biomol. Chem.* **2022**, *20* (46), 9108–9111. https://doi.org/10.1039/D2OB01669A.
(38) Zhao, J.; Brosmer, J. L.; Tang, Q.; Yang, Z.; Houk, K. N.; Diaconescu, P. L.; Kwon, O. Intramolecular Crossed [2+2] Photocycloaddition through Visible Light-Induced Energy Transfer. *J. Am. Chem. Soc.* **2017**, *139* (29), 9807–9810. https://doi.org/10.1021/jacs.7b05277.
(39) Elliott, L. D.; Kayal, S.; George, M. W.; Booker-Milburn, K. Rational Design of Triplet Sensitizers for the Transfer of Excited State Photochemistry from UV to Visible. *J. Am. Chem. Soc.* **2020**, *142* (35), 14947–14956. https://doi.org/10.1021/jacs.0c05069.
(40) Strieth-Kalthoff, F.; J. James, M.; Teders, M.; Pitzer, L.; Glorius, F. Energy Transfer Catalysis Mediated by Visible Light: Principles, Applications, Directions. *Chem. Soc. Rev.* **2018**, *47* (19), 7190–7202. https://doi.org/10.1039/C8CS00054A.
(41) Denisenko, A.; Garbuz, P.; Makovetska, Y.; Shablykin, O.; Lesyk, D.; Al-Maali, G.; Korzh, R.; Sadkova, I.; Mykhailiuk, P. 1,2-Disubstituted Bicyclo[2.1.1]Hexanes as Bioisosteres of the Ortho-Substituted Benzene. ChemRxiv August 22, 2023. https://doi.org/10.26434/chemrxiv-2023-78z7p.

(42) Guo, R.; Chang, Y.-C.; Herter, L.; Salome, C.; Braley, S. E.; Fessard, T. C.; Brown, M. K. Strain-Release [2π + 2σ] Cycloadditions for the Synthesis of Bicyclo[2.1.1]Hexanes Initiated by Energy Transfer. *J. Am. Chem. Soc.* **2022**, *144* (18), 7988–7994. https://doi.org/10.1021/jacs.2c02976.
(43) Kleinmans, R.; Pinkert, T.; Dutta, S.; Paulisch, T. O.; Keum, H.; Daniliuc, C. G.; Glorius, F. Intermolecular [2π+2σ]-Photocycloaddition Enabled by Triplet Energy Transfer. *Nature* **2022**, *605* (7910), 477–482. https://doi.org/10.1038/s41586-022-04636-x.
(44) Agasti, S.; Beltran, F.; Pye, E.; Kaltsoyannis, N.; Crisenza, G. E. M.; Procter, D. J. A Catalytic Alkene Insertion Approach to Bicyclo[2.1.1]Hexane Bioisosteres. *Nat. Chem.* **2023**, *15* (4), 535–541. https://doi.org/10.1038/s41557-023-01135-y.
(45) Xu, M.; Wang, Z.; Sun, Z.; Ouyang, Y.; Ding, Z.; Yu, T.; Xu, L.; Li, P. Diboron(4)-Catalyzed Remote [3+2] Cycloaddition of Cyclopropanes via Dearomative/Rearomative Radical Transmission through Pyridine. *Angew. Chem. Int. Ed.* **2022**, *61* (52), e202214507. https://doi.org/10.1002/anie.202214507.
(46) Liu, Y.; Lin, S.; Li, Y.; Xue, J.-H.; Li, Q.; Wang, H. Pyridine-Boryl Radical-Catalyzed [2π + 2σ] Cycloaddition of Bicyclo[1.1.0]Butanes with Alkenes. *ACS Catal.* **2023**, *13* (7), 5096–5103. https://doi.org/10.1021/acscatal.3c00305.
(47) Bloomfield, J. J.; Owsley, D. C. Intramolecular Photochemical Cyclization of α,α'-Dimethylene Diesters. *Tetrahedron Lett.* **1973**, *14* (21), 1795–1798. https://doi.org/10.1016/S0040-4039(01)96242-2.
(48) Denisenko, A.; Garbuz, P.; Shishkina, S. V.; Voloshchuk, N. M.; Mykhailiuk, P. K. Saturated Bioisosteres of Ortho-Substituted Benzenes. *Angew. Chem. Int. Ed.* **2020**, *59* (46), 20515–20521. https://doi.org/10.1002/anie.202004183.
(49) Tomohiro, D.; Hiroki, Y.; Takahiro, N. α, β-UNSATURATED AMIDE COMPOUND, December 27, 2018. https://patentscope.wipo.int/search/en/detail.jsf?docId=WO2018235926 (accessed 2023-08-12).
(50) Janda, K. D.; Dickerson, T. J. Nicotine Immunoconjugates. WO2009120954A2, October 1, 2009. https://patents.google.com/patent/WO2009120954A2/en/en17 (accessed 2023-08-12).
(51) Graceffa, R.; Kaller, M.; La, D.; Lopez, P.; Patel, V. F.; Zhong, W. Substituted Pyrano [2,3-b] Pyridinamine Compounds as Beta-Secretase Modulators and Methods of Use. US20100120774A1, May 13, 2010. https://patents.google.com/patent/US20100120774/en (accessed 2023-08-12).
(52) Nicolantonio, F. D.; Knight, L. A.; Palma, S. D.; Sharma, S.; Whitehouse, P. A.; Mercer, S. J.; Charlton, P. A.; Norris, D.; Cree, I. A. Ex Vivo Characterization of

XR11576 (MLN576) against Ovarian Cancer and Other Solid Tumors. *Anticancer. Drugs* **2004**, *15* (9), 849.

(53) Husain, A.; Azim, M. S.; Mitra, M.; Bhasin, P. S. A Review on Candesartan: Pharmacological and Pharmaceutical Profile. *J. Appl. Pharm. Sci.* **2011**, *:* (Issue), 12–17.

2.6.0.0 - Experimental section

2.6.1.0 - -Material and methods

2.6.1.1 - General procedures

Unless otherwise noted, all reactions were carried out under an ambient atmosphere. All chemicals and dry solvents were purchased from commercial suppliers and used as received. S-Methyl 4-methylbenzenesulfonothioate (TsSMe)[1] and the ketone **328**[2] were prepared based on the literature procedure. Analytical thin-layer chromatography was performed on Merck silica gel 60 F254 aluminum plates. Visualization was accomplished with UV light and/or potassium permanganate ($KMnO_4$), ninhydrin, or vanillin solutions. Retention factor (R_f) values reported were measured using a 5 × 2 cm TLC plate in a developing chamber containing the solvent system described. Medium pressure liquid chromatography (MPLC) was performed on a Biotage® Isolera™ Four with builtin UV-detector and fraction collector with Agela technologies silica gel columns. ^{1}H and ^{13}C NMR spectra were recorded on Bruker spectrometer at 400 MHz or 300 MHz Nanalysis NMReady-60PRO spectrometer at 60 MHz. Spectra are referenced to residual chloroform (δ = 7.26 ppm, ^{1}H; 77.16 ppm, ^{13}C) or residual methanol (δ = 3.31 ppm, ^{1}H; 49.00 ppm, ^{13}C). Chemical shifts are reported in parts per million (ppm). Multiplicities are indicated by s (singlet), d (doublet), t (triplet), q (quartet), m (multiplet), and br

[1] Allin *et al., J. Org. Chem.* **2017**, *82*, 12209−122231.
[2] Salomé *et al*., *Org. Biomol. Chem*., **2022**, *20*, 9108.

(broad). Coupling constants J are reported in Hertz (Hz). High resolution mass spectrometry (MS) was performed by University of Basel. Electrospray ionization (ESI+) spectra were performed using a time-of-flight (TOF) mass analyzer. Data are reported in the form of m/z (intensity relative to the base peak = 100). Infrared spectra were measured neat on either a Perkin-Elmer spectrum BX FT-IR spectrometer or Agilent Cary 630 FTIR with ATR. Peaks are reported in cm^{-1} with indicated relative intensities: s (strong, 0–33% T); m (medium, 34–66% T), w (weak, 67–100% T), and br (broad). Visible-light spectrum of LED was recorded using an Avantes Sensline Avaspec-ULS TEC Spectrometer. Melting points of solids, compounds that solidified after chromatography, were measured on a Buchi B-540 melting point apparatus and are uncorrected.

2.6.1.2 - Abbreviations

TsSMe = S-Methyl 4-methylbenzenesulfonothioate, THF = tetrahydrofuran, HMPA = hexamethylphosphoramide.

2.6.1.3 - Photochemical Set-Up

High-Intensity Photoreactors were custom designed and built in coordination with the mechanical workshop in the Department of Chemistry and Biosciences at ETH Zürich having blue LEDs, equally spaced in a circle design, powered by a 10.3 A power supply, emitting 350 W of light. The LEDs were water-cooled and further cooled by built-in fans to maintain an ambient temperature.

2.6.2.0 - Procedures

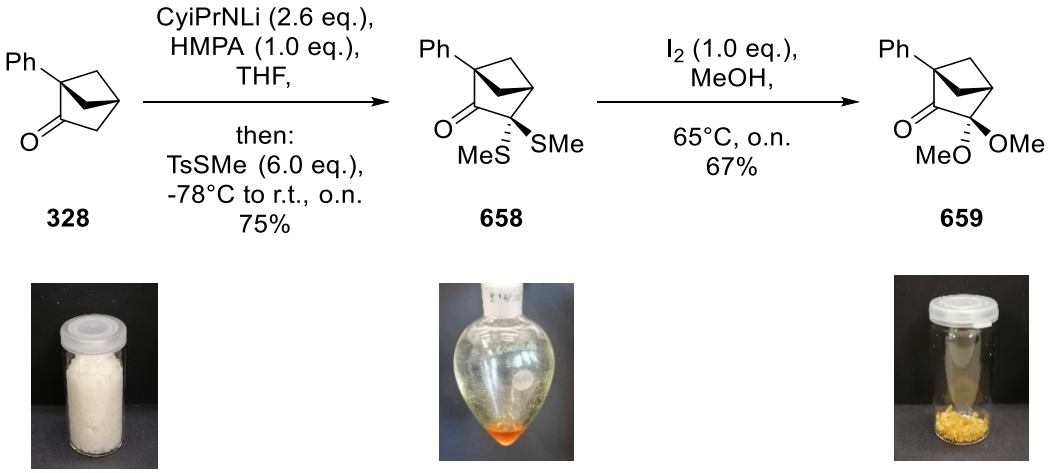

Scheme S1. α-functionalization intermediate **328** to the acetal **659.**

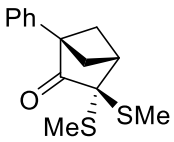

658

2.6.2.1 – Thioacetal 658. In a dry round-bottom flask solution of N-(Propan-2-yl)cyclohexanamine (7.4 mL, 2.60 equiv., 45 mmol) in dry THF (120 mL) was cooled stirring at 0°C under an inert atmosphere. *n*-BuLi (29 mL, 2.70 equiv., 1.6 molar, 0.78 mmol) was added to the mixture dropwise at 0°C over 30 min. The reaction mixture was cooled to -78°C and a solution of ketone **328** (3.0 g, 1.0 equiv., 17 mmol) in THF (25 mL) was added dropwise and further stirred for 1 hour before adding HMPA (3.0 mL, 1 equiv., 17 mmol) at once. The resultant solution was stirred for 3 hours at -78°C. Then, TsSMe (21 g, 6.0 equiv., 102 mmol) in THF (25 mL) was added dropwise under stirring and left to reach room temperature overnight. The reaction mixture was cooled at 0°C and quenched with a saturated aqueous solution of NH_4Cl (200 mL). The organic layer was separated, and the aqueous phase was extracted with EtOAc (3 x 300 mL). The combined organic

phases were dried on anhydrous $MgSO_4$, filtered, and purified by flash chromatography (SiO_2; 95:5 *c*-hexanes:EtOAc) to provide the title compound **658** (2.41 g, 63%) as a brownish-yellow oil.

R_f 0.5 (*c*-hexane:EtOAc = 95:5, UV, $KMnO_4$).

^{1}H NMR (400 MHz, $CDCl_3$) δ 7.40 – 7.27 (m, 3H), 7.20 – 7.13 (m, 2H), 2.86 (t, *J* = 3.6 Hz, 1H), 2.82 (dd, *J* = 4.7, 2.1 Hz, 2H), 2.47 (td, *J* = 4.3, 3.8, 2.0 Hz, 2H), 2.26 (s, 6H).

^{13}C NMR (75 MHz, $CDCl_3$) δ 135.9, 128.5, 127.5, 126.9, 67.1, 66.8, 44.0, 41.1, 12.2.

IR (ATR, neat, cm^{-1}): 2920 (m), 1753 (s), 1436 (m), 802 (s), 698 (s).

HRMS (EI+/QTOF, m/z) calcd. For $C_{14}H_{16}NaOS_2^+$ $[M+Na]^+$ calc.: 287.0535; found: 287.0534.

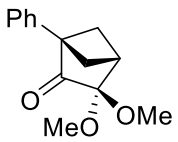

659

2.6.2.2 – Acetal 659. A solution of Thioacetal **658** (2.41 g, 1.0 equiv. 18.2 mmol) and iodine (4.63 g, 2.0 equiv., 18.2 mmol) in methanol (137 mL) was heated at 65°C overnight. The reaction mixture was cooled, diluted with EtOAc (100 mL), and washed with saturated aqueous $Na_2S_2O_3$ (150 mL). The organic phase was separated, extracted with EtOAc (3 x 20 mL), and washed with saturated aqueous $NaHCO_3$ solution and water. The combined organic phases were dried on anhydrous $MgSO_4$, filtered, and purified by flash chromatography (SiO_2; 100:0-90:10 *c*-hexanes:EtOAc) to provide the title compound **659** (1.35 g, 64%) as a yellow solid.

R_f 0.4 (*c*-hexane:EtOAc = 9:1, UV, $KMnO_4$, vanillin (brown)).

^{1}H NMR (300 MHz, $CDCl_3$) δ 7.40 – 7.27 (m, 3H), 7.16 – 7.10 (m, 2H), 2.98 (t, J = 3.7 Hz, 1H), 2.37 (ddd, J = 4.9, 3.7, 2.0 Hz, 2H), 2.28 (dd, J = 4.9, 2.0 Hz, 2H).

^{13}C NMR (75 MHz, $CDCl_3$) δ 205.7, 135.90, 128.5, 127.5, 126.8, 120.13, 102.4, 65.0, 51.0, 38.7, 38.4.

IR (ATR, neat, cm^{-1}): 2945 (m), 1767 (s), 1447 (m), 1142 (s), 696 (s), 849 (s).

HRMS (EI+/QTOF, m/z) calcd. For $C_{14}H_{16}NaO_3$ $[M+Na]^+$ calc.: 255.0992; found: 255.0995.

m.p. 60 – 61°C.

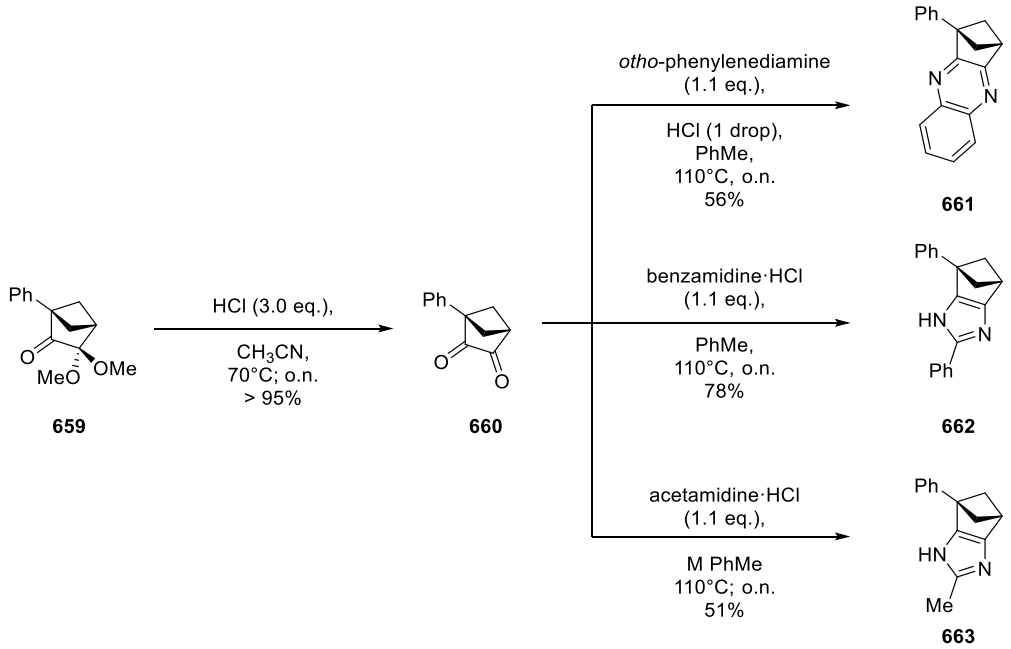

Scheme S2. Derivatization of **660** into the quinoxaline **661** and the imidazoles **662** and **663**.

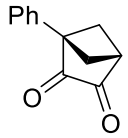

660

2.6.2.3 - Diketone 660. To a solution of the acetal **659** (200 mg, 1.0 equiv., 0.861 mmol) in acetonitrile (8.6 mL) was added a 2M aqueous solution of HCl (1.3 mL, 3.0 equiv., 2.58 mmol). The mixture was heated at 70°C and

stirred overnight. After this period, complete conversion of the acetal **659** was observed from TLC. The mixture was cooled and diluted with EtOAc (10 mL), separating the organic phase which was extracted with EtOAc (3 x 20 mL). The combined organic phases were dried on anhydrous $MgSO_4$, filtered, and the volatiles were removed providing yellow foam containing the title compound **660** (155 mg, > 95%). The NMR of the crude confirms the presence of the title compound that was used without any purification in the further condensations.

R_f 0.3 (*c*-hexane:EtOAc = 7:3, UV, $KMnO_4$, vanillin (brown)).

^{1}H NMR (400 MHz, $CDCl_3$) δ 7.39 – 7.19 (m, 3H), 7.15 – 7.04 (m, 2H), 3.37 (t, J = 3.8 Hz, 1H), 2.90 (ddd, J = 5.3, 3.7, 2.4 Hz, 2H), 2.26 (dd, J = 5.3, 2.4 Hz, 2H).

IR (ATR, neat, cm^{-1}): 2993 (w), 1770 (s), 1144 (m), 1067 (m), 991 (w), 907 (s), 727 (s), 696 (s).

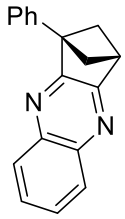

661

2.6.2.4 - Quinoxaline 661. The residue **660** (78 mg, 1.0 equiv., 0.34 mmol) was dissolved in toluene (3.4 mL). *otho*-phenylenediamine (39 μL, 1.1 equiv., 0.37 mmol) was added along with one drop of concentrated HCl (37% in water). The mixture was heated at 110°C overnight. The reaction mixture was cooled, and the volatiles were removed at 70°C. Reverse phase chromatography with Interchim® puriFlash XS520Plus (PF-15C18HP, 4.0 g, 5%-95% CH_3CN in Water) provides the title quinoxaline **661** (49 mg, 56%) as a white amorphous solid.

R_f 0.2 (*c*-hexane:EtOAc = 9:1, UV, $KMnO_4$, vanillin (dark brown)).

^{1}H NMR (400 MHz, $CDCl_3$) δ 7.98 – 7.90 (m, 2H), 7.65 – 7.54 (m, 2H), 7.51 – 7.44 (m, 4H), 7.42 – 7.34 (m, 1H), 3.54 (t, J = 3.0 Hz, 1H), 3.18 (ddd, J = 4.2, 3.0, 1.9 Hz, 2H), 2.95 (dd, J = 4.2, 1.9 Hz, 2H).

^{13}C NMR (101 MHz, $CDCl_3$) δ 168.10, 167.98, 140.44, 139.75, 136.75, 129.13, 128.85, 128.39, 128.20, 127.76, 127.06, 59.75, 59.39, 42.23.

IR (ATR, neat, cm^{-1}): 3029 (w), 1602 (w), 1005 (m), 760 (s), 697 (s).

HRMS (EI+/QTOF, m/z) calcd. For $C_{18}H_{15}N_2$ $[M+H]^+$ calc.: 259.1230; found: 259.1233.

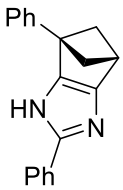

662

2.6.2.5 - Imidazole 662. The residue **660** (49 mg, 1.0 equiv., 0.21 mmol) was dissolved in toluene (2.1 mL). along with benzamidine hydrochloride (45 mg, 1.1 equiv., 0.23 mmol). The mixture was heated at 110°C overnight. After this period, the reaction mixture was cooled and the volatiles were removed at 70°C. Reverse phase chromatography with Interchim® puriFlash XS520Plus (PF-15C18HP, 4.0 g, 5%-95% CH_3CN in Water with 0.1% HCOOH) provide the title product **662** (65 mg, 78%) as a white amorphous solid.

R_f 0.3 (CH_2Cl_2:MeOH = 95:5, UV, $KMnO_4$, vanillin (dark brown)).

^{1}H NMR (300 MHz, MeOD) δ 8.48 (s, 0.6H), 7.92 (dd, *J* = 7.3, 1.7 Hz, 2H), 7.86 – 7.75 (m, 1H), 7.65 (t, *J* = 7.8 Hz, 2H), 7.44 – 7.24 (m, 5H), 2.94 (t, *J* = 3.0 Hz, 1H), 2.51 (dd, *J* = 10.2, 7.6 Hz, 1H), 2.10 (dd, *J* = 7.6, 2.9 Hz, 1H), 1.99 (dd, *J* = 8.7, 3.3 Hz, 1H), 1.67 (dd, *J* = 10.2, 8.7 Hz, 1H).

^{13}C NMR (75 MHz, MeOD) δ 165.4, 139.1, 136.2, 130.8, 130.5, 129.6, 129.2, 128.3, 123.8, 97.8, 97.2, 62.9, 45.9, 38.5, 36.8.

IR (ATR, neat, cm^{-1}): 3062 (s), 1583 (s), 1496 (m), 1168 (s), 697 (s).

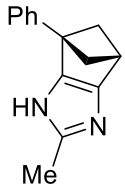

663

2.6.2.6 - Imidazole 663. The residue **660** (22 mg, 1.0 equiv., 0.12 mmol) was dissolved in toluene (1.2 mL). along with acetamidine hydrochloride (12 mg, 1.1 equiv., 0.13 mmol). The mixture was heated at 110°C overnight. After this period, the reaction mixture was cooled and the volatiles were removed at 70°C. Reverse phase chromatography with Interchim® puriFlash XS520Plus (PF-15C18HP, 4.0 g, 5%-95% CH_3CN in Water with 0.1% HCOOH) provide the title **663** product as a white solid (15 mg, 51%).

R_f 0.4 (CH_2Cl_2:MeOH = 95:5, UV, $KMnO_4$, vanillin (dark brown)).

^{1}H NMR (400 MHz, DMSO-d6) δ 7.38 – 7.15 (m, 5H), 2.62 (t, J = 2.9 Hz, 1H), 2.25 (dd, J = 10.0, 7.0 Hz, 1H), 2.13 (s, 3H), 1.89 (dd, J = 7.0, 3.0 Hz, 1H), 1.73 (dd, J = 8.2, 3.3 Hz, 1H), 1.46 (dd, J = 10.0, 8.2 Hz, 1H).

^{13}C NMR (75 MHz, DMSO) δ 165.3, 138.7, 127.8, 127.1, 126.7, 96.5, 96.3, 60.1, 43.6, 37.2, 35.5, 12.7.

IR (ATR, neat, cm^{-1}): 3108 (s), 2963 (s), 1585 (s), 1318 (m), 1165 (m), 699 (s).

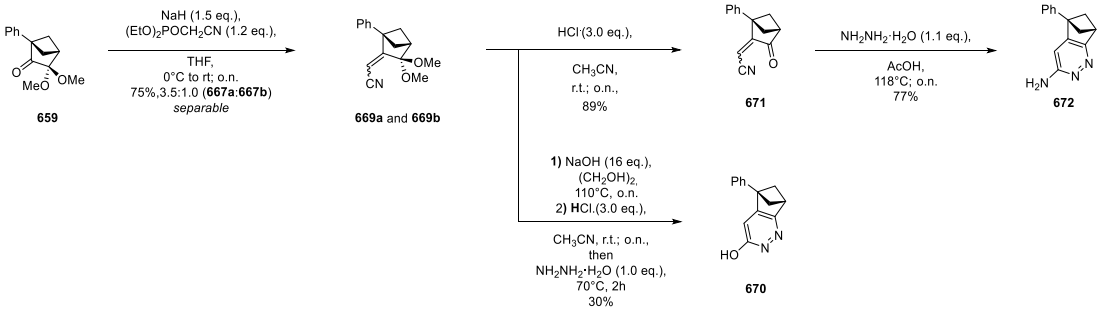

Scheme S3. Conversion of acetal **659** to the pyridazynes **668** and **670**.

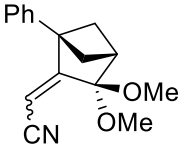

669a and **669b**

2.6.2.7 - Nitriles 667a and 667b. NaH (60 % in mineral oil, 130 mg, 1.50 equiv., 3.22 mmol) was suspended in dry THF (16 mL) and the suspension was cooled to 0 °C. Diethyl cyanomethylphosponate (522

μL, 1.5 equiv., 3.22 mmol) was added and the reaction was stirred for 15 minutes at this temperature. The acetal **659** (500 mg, 1.0 equiv., 2.16 mmol) was added as a solution in THF (6.0 mL) and the reaction mixture was allowed to warm to room temperature overnight. Upon completion of the reaction, EtOAc (10 mL) and water (10 mL) were added. The layers were separated, and the aqueous phase was extracted with EtOAc (3 x 30 mL). The combined organic phases were washed with brine, dried on anhydrous $MgSO_4$, filtered, and purified by flash chromatography (SiO_2; 100:0-90:10 *c*-hexanes:EtOAc) to afford **669a** as an amorphous yellow solid and **669b** as a yellow solid (410 mg, combined yield 88% 3.5:1.0).

669a:

R_f 0.4 (*c*-hexane:EtOAc = 9:1, UV, $KmnO_4$, vanillin (blue)).

^{1}H NMR (400 MHz, $CHCl_3$) δ 7.40 – 7.33 (m, 2H), 7.33 – 7.27 (m, 1H), 7.08 – 7.01 (m, 2H), 4.81 (s, 1H), 2.88 (t, J = 2.9, 1H), 2.20 – 2.08 (m, 4H).

^{13}C NMR (101 MHz, $CDCl_3$) δ 171.5, 137.7, 128.9, 127.7, 126.7, 117.2, 107.6, 89.9, 61.3, 51.5, 41.3, 40.0.

IR (ATR, neat, cm^{-1}): 2945 (m), 2222 (m), 1165 (s), 1134 (s), 1070 (s), 766 (s).

HRMS (EI+/QTOF, m/z) calcd. For $C_{16}H_{17}NNaO_2^+$ $[M+Na]^+$ calc.: 278.1151; found: 278.1151.

m.p. 94 – 96°C.

669b:

R_f 0.5 (*c*-hexane:EtOAc = 8:2, UV, $KMnO_4$, vanillin (brown)).

^{1}H NMR (400 MHz, $CDCl_3$) δ 7.45 – 7.31 (m, 3H), 7.23 – 7.13 (m, 2H), 3.39 (s, 6H), 2.85 (q, *J* = 2.6, 1.9 Hz, 1H), 2.19 (d, *J* = 1.7 Hz, 4H).

^{13}C NMR (101 MHz, $CDCl_3$) δ 169.3, 137.9, 128.6, 128.2, 127.2, 114.0, 107.1, 90.0, 61.0, 50.3, 41.8, 39.6.

IR (ATR, neat, cm^{-1}): 2955 (m), 2223 (w), 1691 (m), 1365 (m), 1137 (s), 1068 (s), 769 (s), 698 (s).

HRMS (EI+/TOF, m/z) calcd. For $C_{16}H_{17}NNaO_2^+$ $[M+Na]^+$ calc.: 278.1151; found: 278.1149.

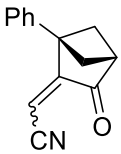

671

2.6.2.8 - Nitrile 671. To a solution of the nitrile **669a** (50 mg, 1.0 equiv., 0.196 mmol) in acetonitrile (2.0 mL) was added an aqueous solution of HCl (2 M, 294 μL, 3.0 equiv., 0.587 mmol). The mixture was stirred at room temperature overnight. After cooling the reaction mixture was diluted with EtOAc (10 mL). The organic phase was separated, and the aqueous phase was extracted with EtOAc (3 x 20 mL). The combined organic phases were dried on anhydrous $MgSO_4$, filtered, and the volatiles were removed. The crude product was purified by flash chromatography (SiO_2, 9:1 *c*-hexane:EtOAc) to provide the title compound **671** (40 mg, 89%).

R_f 0.3 (*c*-hexane:EtOAc = 8:2, UV, $KMnO_4$).

^{1}H NMR (300 MHz, $CDCl_3$) δ 7.52 – 7.31 (m, 4H), 7.18 – 7.05 (m, 2H), 5.00 (s, 1H), 3.23 (td, *J* = 3.0, 0.7 Hz, 1H), 2.67 (ddd, *J* = 4.8, 3.0, 2.1 Hz, 2H), 2.26 (dd, *J* = 4.6, 2.2 Hz, 2H).

^{13}C NMR (75 MHz, $CDCl_3$) δ 198.0, 165.5, 136.1, 129.1, 128.2, 126.0, 114.3, 91.9, 60.0, 49.9, 43.1.

IR (ATR, neat, cm^{-1}): 3031 (m), 2221 (s), 1757 (s), 1655 (s), 1501 (s), 952 (s), 840 (s), 772 (s), 702 (s).

HRMS (EI+/QTOF, m/z) calcd. For $C_{14}H_{11}NNaO_2^+$ $[M+Na]^+$ calc.: 232.0733; found: 232.0734.

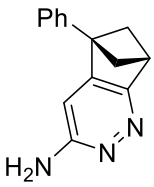

672

2.6.2.9 - Pyridazine 672. To a solution of the ketone **671** (22 mg, 1.0 equiv., 0.103 mmol) in acetic acid (1.03 mL) hydrate hydrazine (5.2 μL, 1.0 equiv., 0.103 mL) was added. The reaction mixture was heated at 118°C overnight. After this period, the reaction mixture was cooled and the volatiles were removed at 70°C. Reverse phase chromatography with Interchim® puriFlash XS520Plus (PF-15C18HP, 4.0 g, 5%-95% CH_3CN in Water) provides the pyridazine **672** (18 mg, 77%) as a white amorphous solid.

R_f 0.4 (CH_2Cl_2:MeOH 98:2, UV, $KMnO_4$, ninhydrin).

^{1}H NMR (400 MHz, MeOD) δ 7.43 (dd, *J* = 8.1, 6.7 Hz, 2H), 7.38 – 7.31 (m, 1H), 7.31 – 7.26 (m, 2H), 6.42 (s, 1H), 3.37 (t, *J* = 2.7 Hz, 1H), 2.96 (dt, *J* = 4.4, 2.4 Hz, 2H), 2.68 (dd, *J* = 4.0, 1.9 Hz, 2H).

^{13}C NMR (101 MHz, MeOD) δ 166.7, 159.7, 156.1, 138.6, 129.9, 128.6, 127.2, 108.1, 60.3, 59.6, 42.3.

IR (ATR, neat, cm^{-1}): 3169 (s), 1658 (m), 1465 (s), 1031 (m), 1008 (m), 781 (w), 703 (w).

HRMS (EI+/QTOF, m/z) calcd. For $C_{14}H_{14}N_3^+$ $[M+H]^+$ calc.: 224.1182; found: 224.1191.

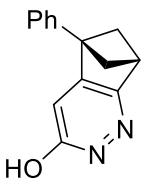

670

2.6.2.10 - Pyridazine 668. Nitrile **669a** (20 mg, 1.0 equiv, 78.3 μmol) and NaOH (50 mg, 16 equiv., 1.25 mmol) were dissolved in a 1:1 mixture of ethylene glycol and water (1.0 mL). The mixture was heated at 120°C for two days. After full conversion of the nitrile **669a** was observed the reaction mixture was cooled, diluted with water (1 mL), and acidified to pH 2 with

concentrated HCl (37% aqueous solution). The aqueous phase was extracted with EtOAc (3 x 5 mL) collecting the organic phases that were dried over $MgSO_4$, filtered, and concentrated *in vacuo*. The residue obtained was re-dissolved in dry acetonitrile (0.783 mL) and a 2M aqueous solution of HCl (117 μL, 3.0 equiv., 1.0 mmol) was added. The mixture was stirred overnight at room temperature. After this period, hydrate hydrazine (4 μL, 1.0 equiv., 78.3 μmol) was added heating at 70°C. After 4 h the formation of the product was observed. The reaction mixture was cooled and diluted with EtOAc (5 mL) and water (5 mL). The organic phase was separated, and the aqueous layer was extracted with EtOAc (3 x 5 mL). Flash chromatography (SiO_2, 9:1 CH_2Cl_2:MeOH) provides the title pyridazine **670** (5.2 mg, 30%) as a brown amorphous solid.[1]

R_f 0.5 (CH_2Cl_2:MeOH 95:5, UV, $KMnO_4$, ninhydrin).

^{1}H NMR (300 MHz, $CDCl_3$) δ 9.80 (s, 1H), 7.55 – 7.30 (m, 3H), 7.23 – 7.09 (m, 2H), 6.32 (s, 1H), 3.33 (td, J = 2.8, 0.8 Hz, 1H), 2.89 – 2.77 (m, 2H), 2.60 (dd, J = 4.2, 1.9 Hz, 2H).

^{13}C NMR (75 MHz, $CDCl_3$) δ 161.6, 159.3, 157.8, 136.5, 129.1, 128.0, 126.2, 117.3, 58.7, 55.7, 40.8.

HRMS (EI+/QTOF, m/z) calcd. For $C_{14}H_{13}N_2O^+$ $[M+H]^+$ calc.: 225.1022; found: 225.1023.

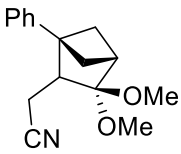

679

2.6.2.11 – Aliphatic nitrile 679. The unsaturated nitrile **669a** (180 mg, 1.0 equiv., 0.70 mmol) was dissolved in ethanol (14 mL). Three cycles

[1] *The full characterization is ongoing.*

of nitrogen and vacuum were performed and Pd/C (75 mg, 0.10 equiv., 10 mol%) was added. The reaction mixture was evacuated and refilled with nitrogen three times before running three cycles of vacuum hydrogen. The mixture was stirred under a hydrogen atmosphere (balloon) at 70°C for three days. After this period, the reaction mixture was filtered over a short pad of celite, and the pad was washed with methanol. The filtrate was concentrated under reduced pressure to yield **679** (175 mg, $P^{\%}$ = 83%,[1] 80%) as an inseparable mixture with **669a** that appears as an amorphous solid.[2]

^{1}H NMR (400 MHz, $CDCl_3$) δ 7.41 – 7.29 (m, 2H), 7.26 (m, 1H), 7.11 – 7.02 (m, 2H), 3.42 (s, 3H), 3.30 (s, 3H), 2.73 (t, *J* = 2.9 Hz, 1H), 2.49 (m, 1H), 2.35 (m, 1H), 2.08 – 1.95 (m, 2H), 1.93 – 1.84 (m, 2H), 1.81 (m, 1H).

HRMS (EI+/QTOF, m/z) calcd. For $C_{16}H_{19}NNaO_2^+$ $[M+Na]^+$ calc.: 280.1308; found: 280.1308.

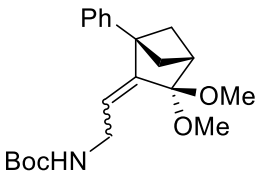

673

2.6.2.12 – Aliphatic nitrile 673. To a solution of **669a** (50 mg, 1.0 equiv., 0.20 mmol), and Boc_2O at 0°C was added $NiCl_2*6H_2O$, in methanol (3.9 mL). Then $NaBH_4$ (89 mg, 12 eq, 2.3 mmol) was added portion-wise.[3] The reaction was stirred at 0°C for 30 min then at room temperature overnight. After this period N1-(2-aminoethyl)ethane-1,2-diamine (23 μg, 1.1 eq, 0.22 mmol) was added in one portion and the reaction mixture was concentrated *in vacuo*. The residue was dissolved in ethyl acetate (4.0

[1] *The main impurity is **669a**.*
[2] *The full characterization is ongoing.*
[3] *Intense black collation appears, strong effervescence observed.*

mL) and washed with a solution of citric acid (4.0 mL, 0.1 M in water) and with sodium bicarbonate (4.0 mL, saturated solution in water). The organic layer was separated from the water phases, dried over Na_2SO_4, filtered, and purified by flash chromatography (SiO_2; 100:0-90:10 *c*-hexanes:EtOAc) to afford **673** as an amorphous brown solid (24 mg, 35%, brsm 67%[1]) along with unreacted **669a** (24 mg).[2]

^{1}H NMR (400 MHz, $CDCl_3$) δ 7.43 – 7.34 (m, 2H), 7.34 – 7.27 (m, 3H), 5.31 (t, J = 6.6 Hz, 1H), 3.48 (s, 6H), 2.99 (t, J = 2.8 Hz, 1H), 2.52 (dt, J = 4.7, 2.5 Hz, 2H), 2.25 – 2.17 (m, 2H).

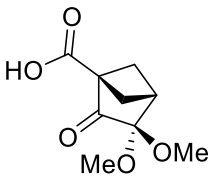

689

2.6.2.13 – Acid 689. Sodium periodate (1.64 g, 15 equiv., 7.68 mmol) was added to a vigorously stirred biphasic solution **659** (119 mg, 1.0 equiv., 0.51 mmol) in a 1:3 mixture of ethyl acetate:water (43 mL) at 4 °C. Then, ruthenium(IV) oxide hydrate (9.4 mg, 0.1 equiv., 51 µmol) was added in a single portion, and the light yellow mixture was slowly warmed to room temperature and stirred overnight. After this period the stirring was stopped, and the resulting biphasic light-yellow mixture was separated and extracted with ethyl acetate (3 x 100 mL). The combined organics were washed with brine (100 mL) and with sodium sulfite (100 mL, saturated aqueous solution), dried on Na_2SO_4, and concentrated under vacuum, obtaining the unreacted **659** (36 mg, 0.15 mmol). The aqueous phases were collected, acidified to pH 2 with a solution of HCl (6 M aqueous), extracted with ethyl acetate (3 x 300 mL), dried over Na_2SO_4,

[1] *Yield based on the recovered starting material.*
[2] *The full characterization is ongoing.*

filtered, and concentrated under vacuum providing the title compound **689** (58 mg, 56%, brsm 86%).[1][2]

^{1}H NMR (400 MHz, $CDCl_3$) δ 3.45 (s, 6H), 2.86 – 2.80 (m, 1H), 2.52 – 2.44 (m, 2H), 2.24 – 2.15 (m, 2H).

[1] *Based on the recovered starting material.*
[2] *The full characterization is ongoing.*

2.6.3.0 - NMR spectra

2.6.3.1 - ^{1}H NMR and ^{13}C NMR of thioacetal 658

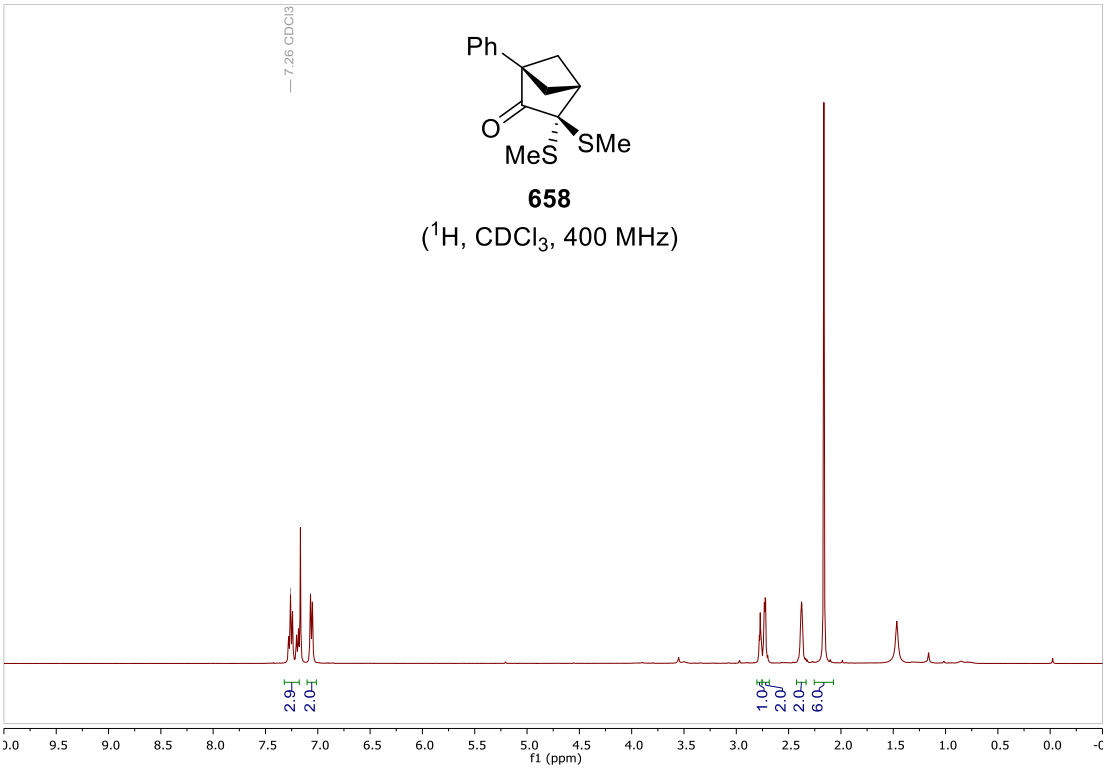

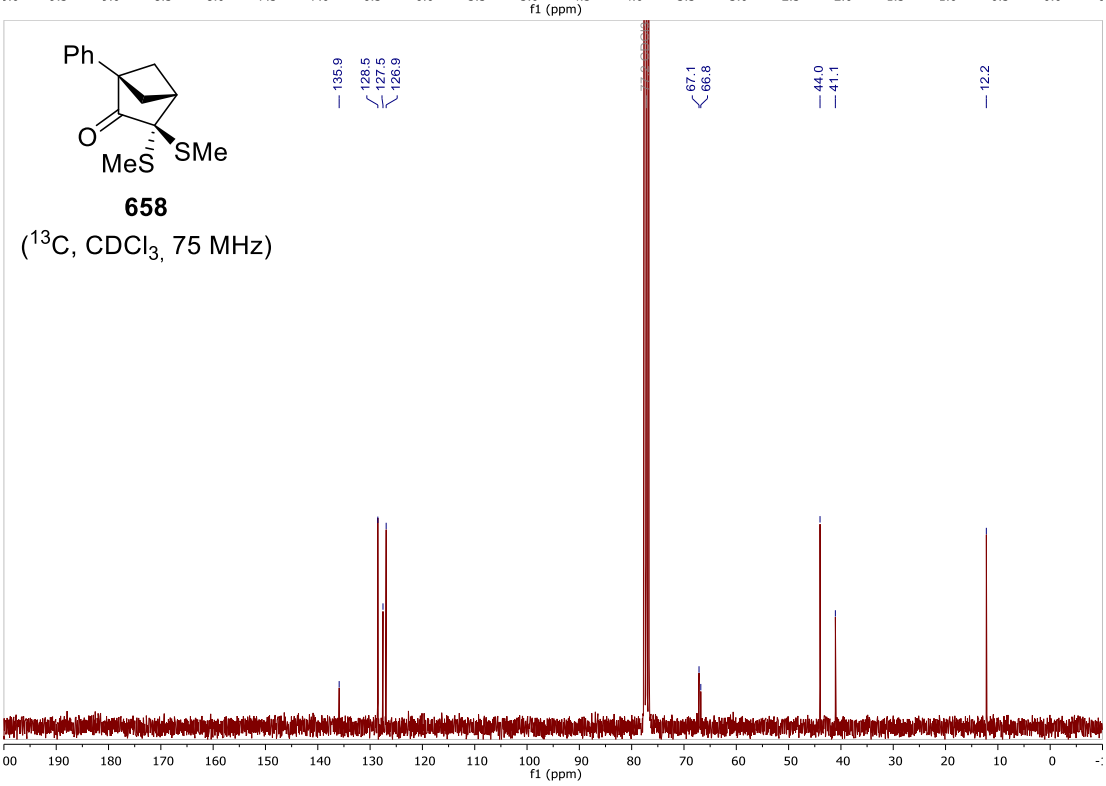

2.6.3.2 - ^{1}H NMR and ^{13}C NMR of acetal 659

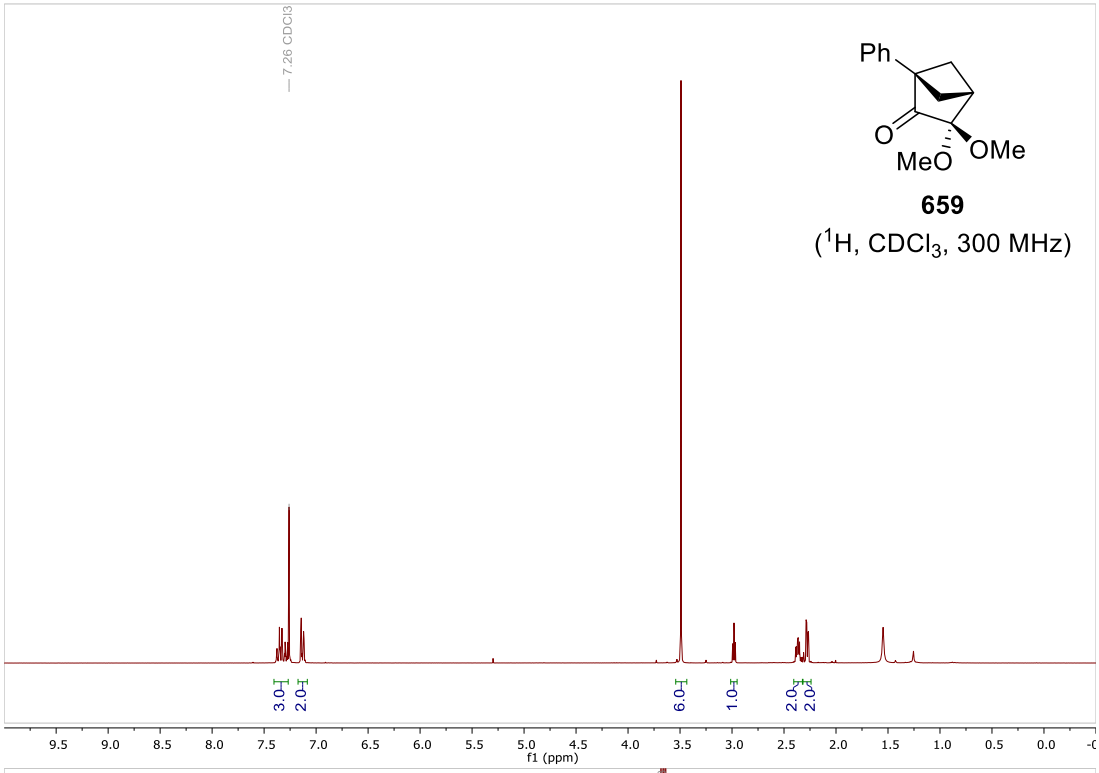

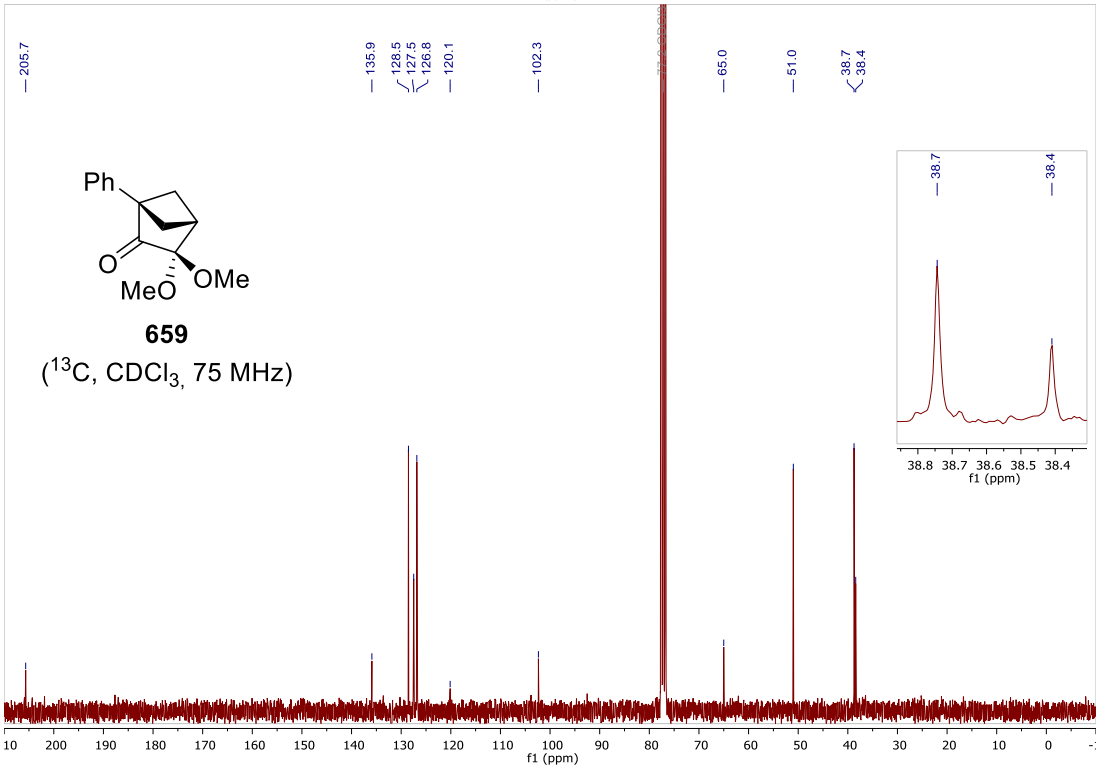

2.6.3.3 – *crude* ^{1}H NMR of the diketone 660

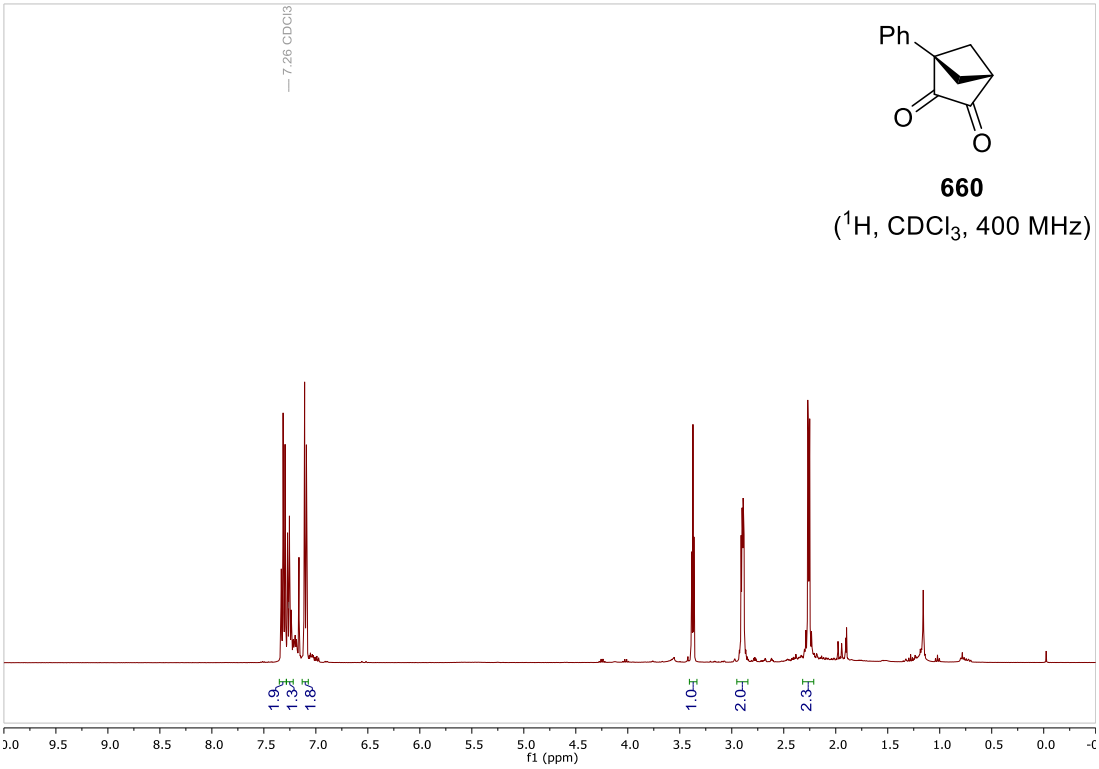

2.6.3.4 - ^{1}H NMR and ^{13}C NMR of the quinoxaline 661

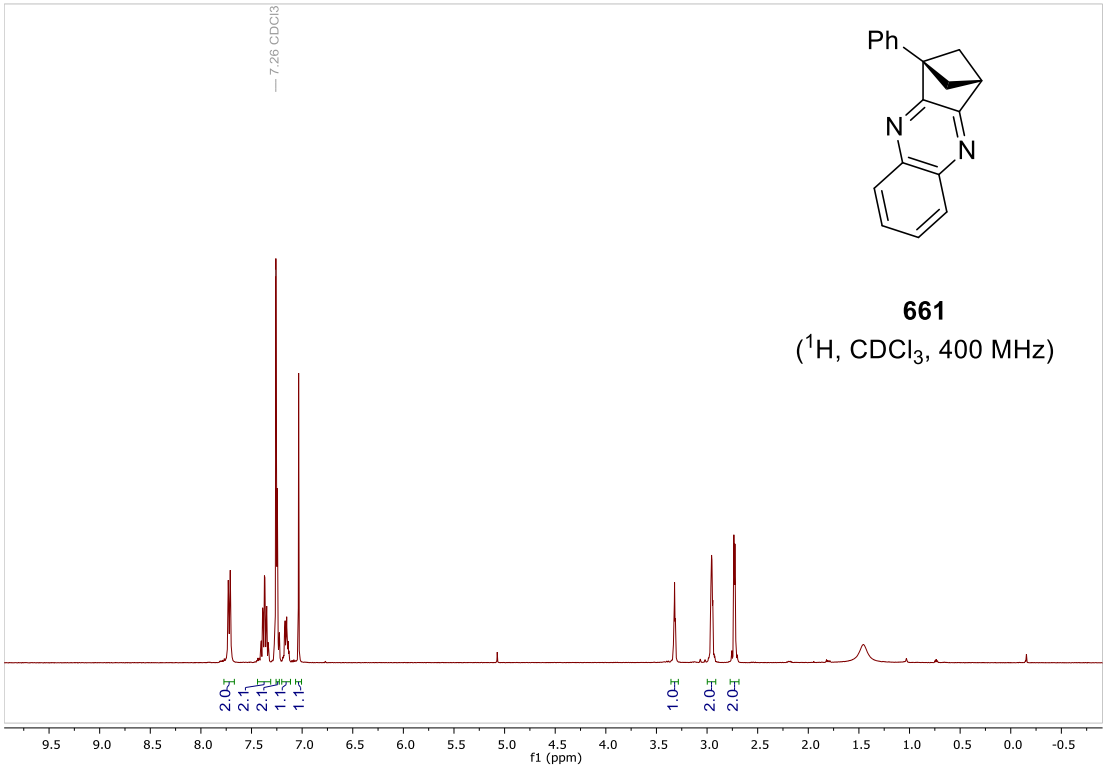

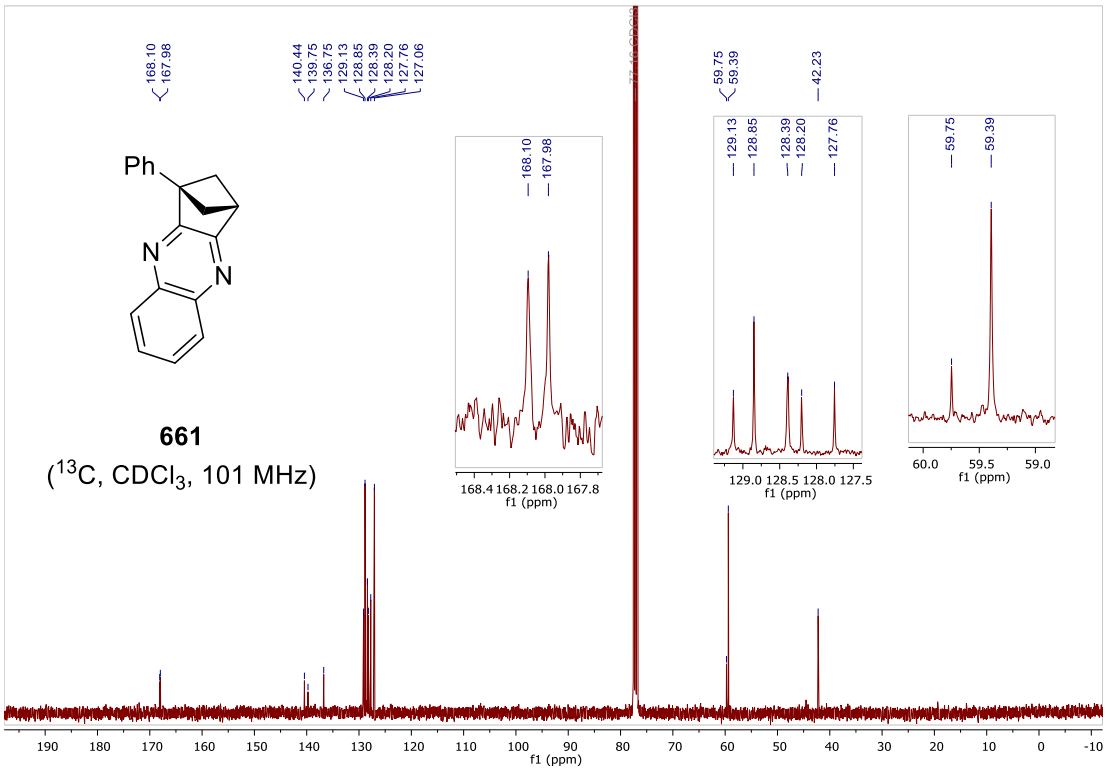

2.6.3.5 - ^{1}H NMR and ^{13}C NMR of imidazole 662

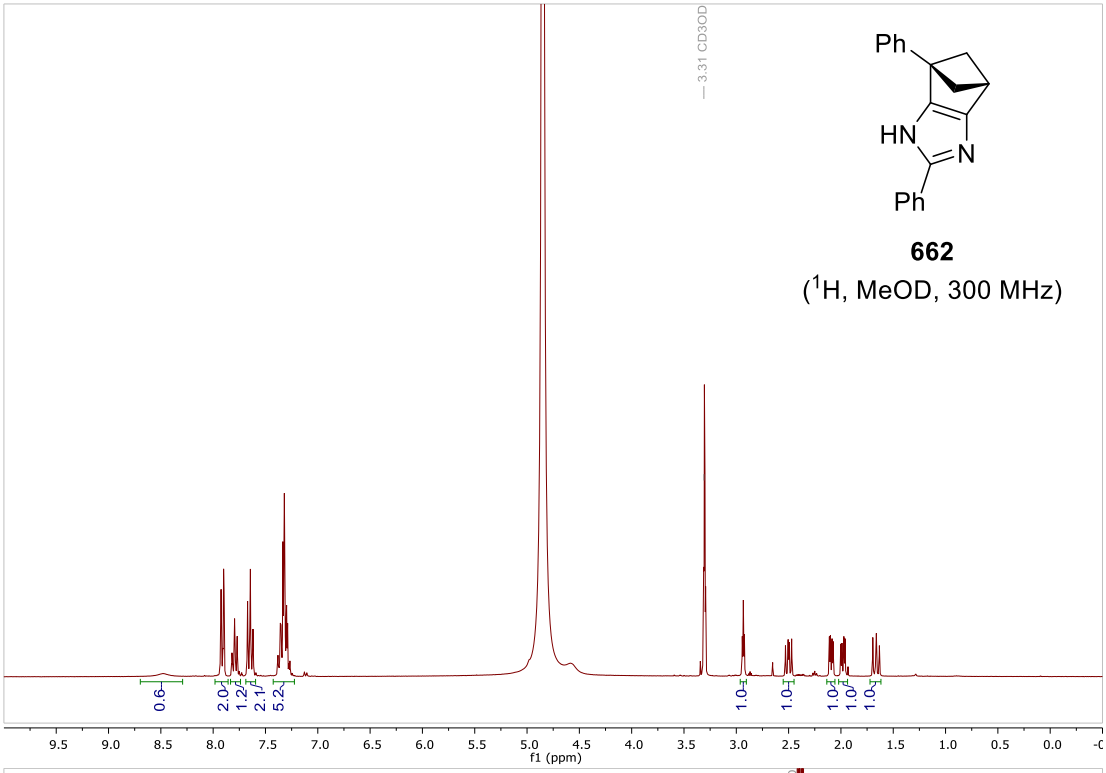

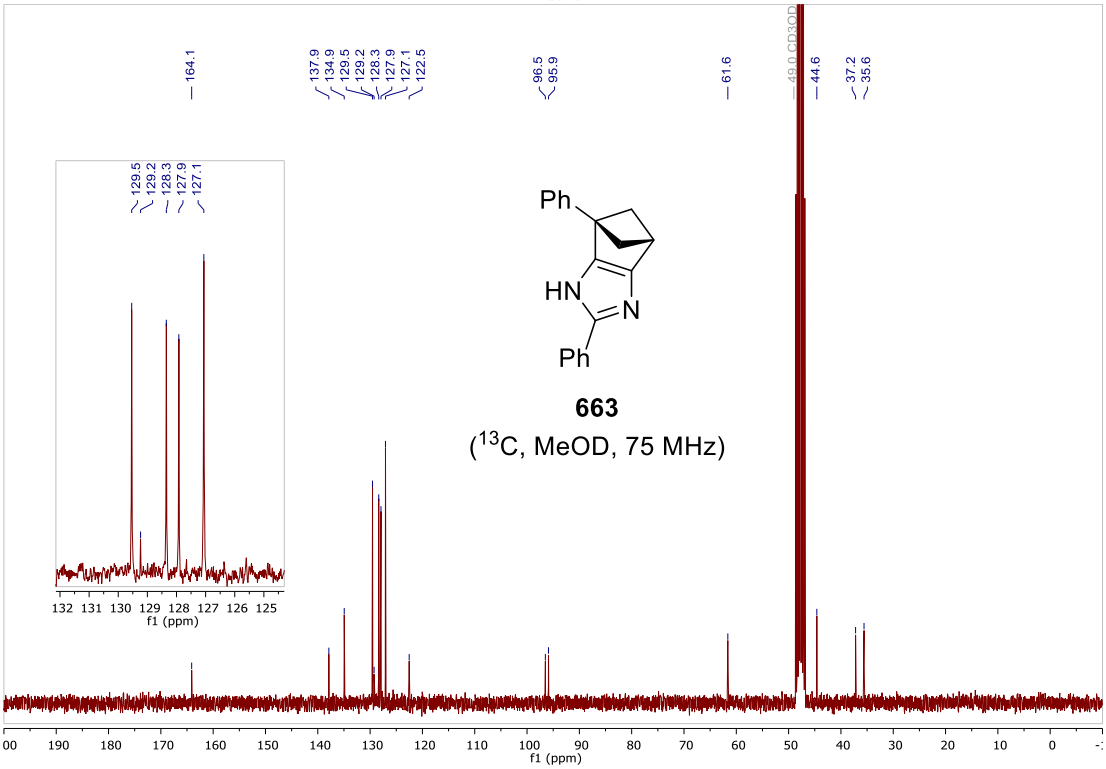

2.6.3.6 - ^{1}H NMR and ^{13}C NMR of imidazole 663

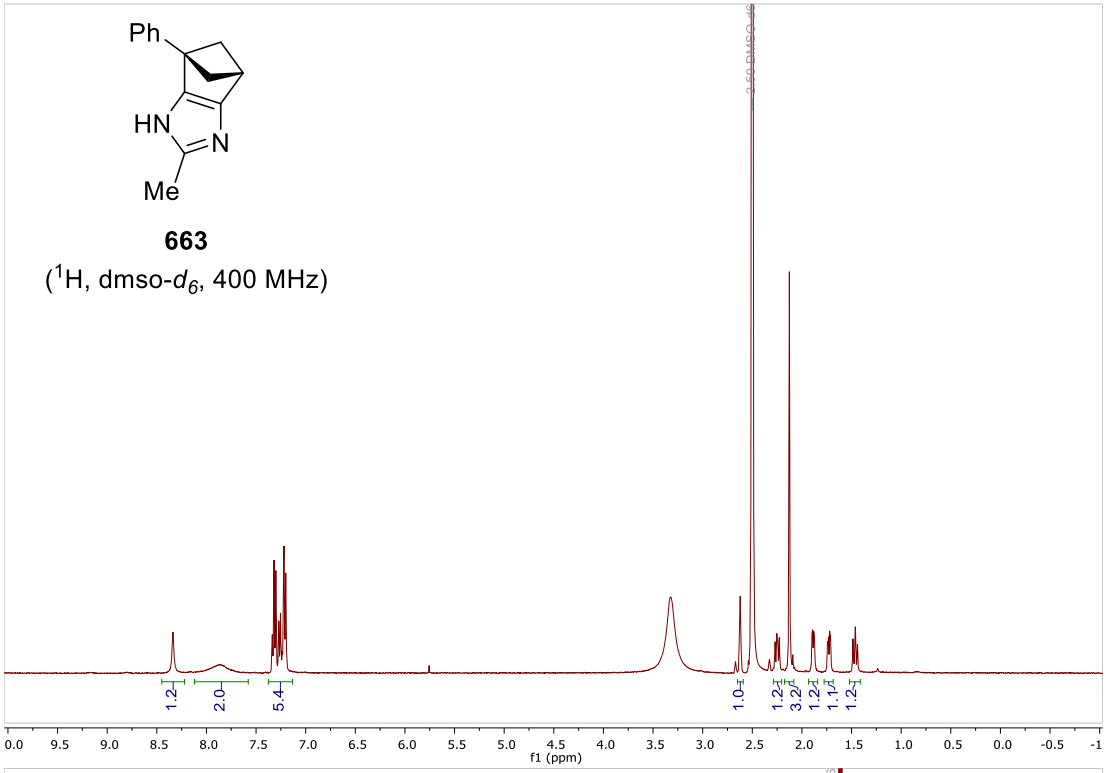

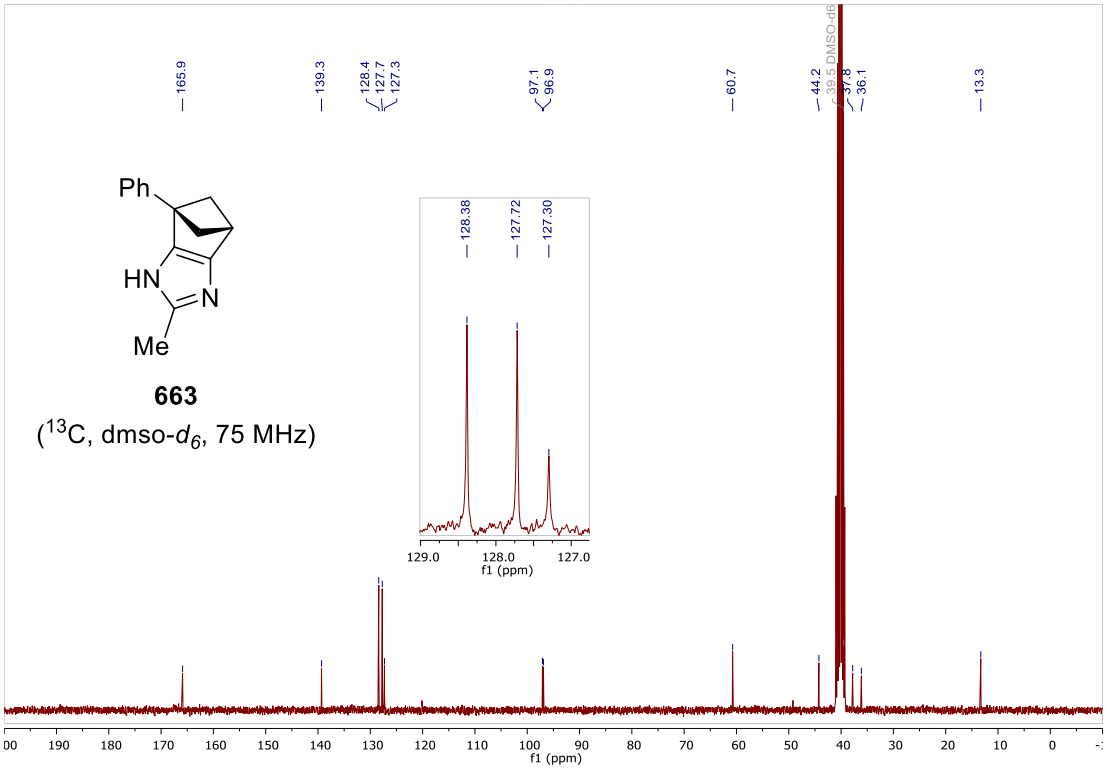

2.6.3.7 - ^{1}H NMR and ^{13}C NMR of nitrile 669a

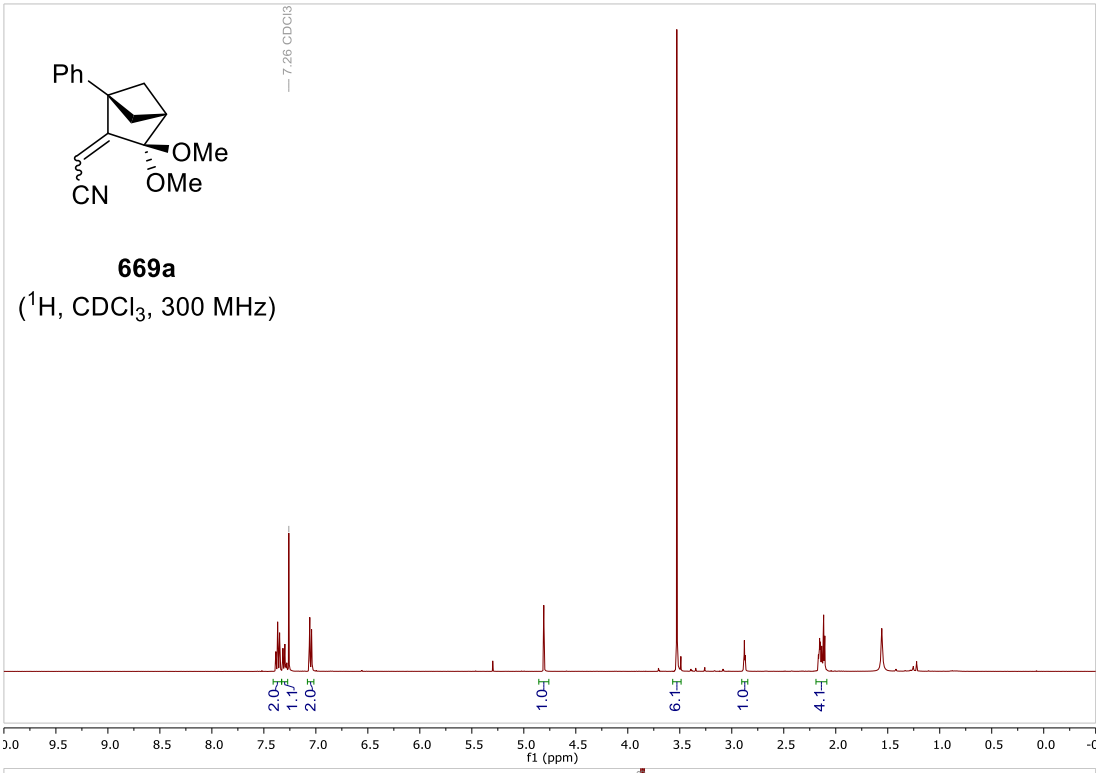

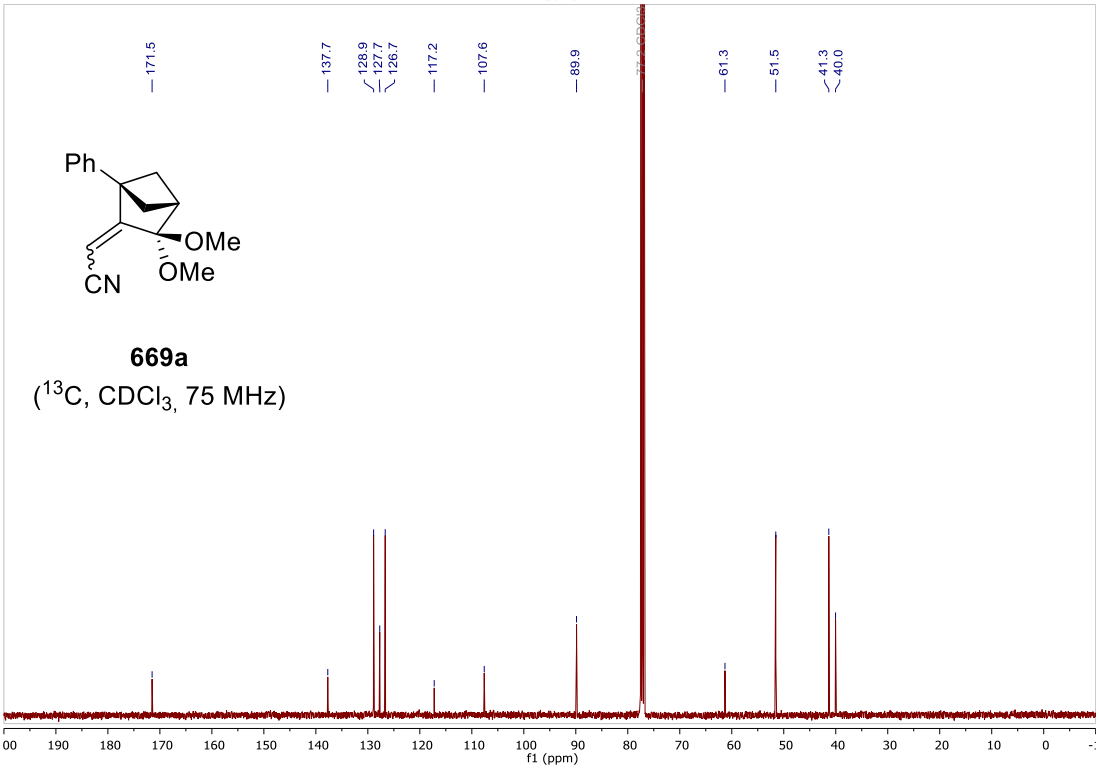

2.6.3.8 - ^{1}H NMR and ^{13}C NMR of nitrile 669b

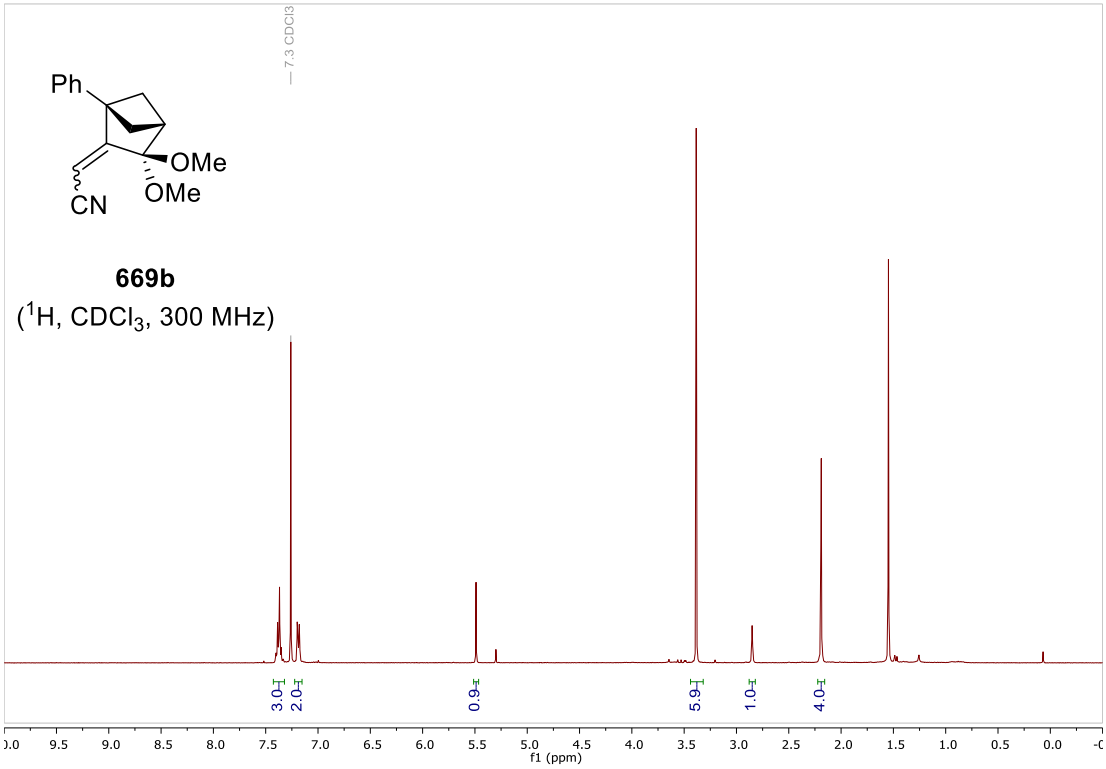

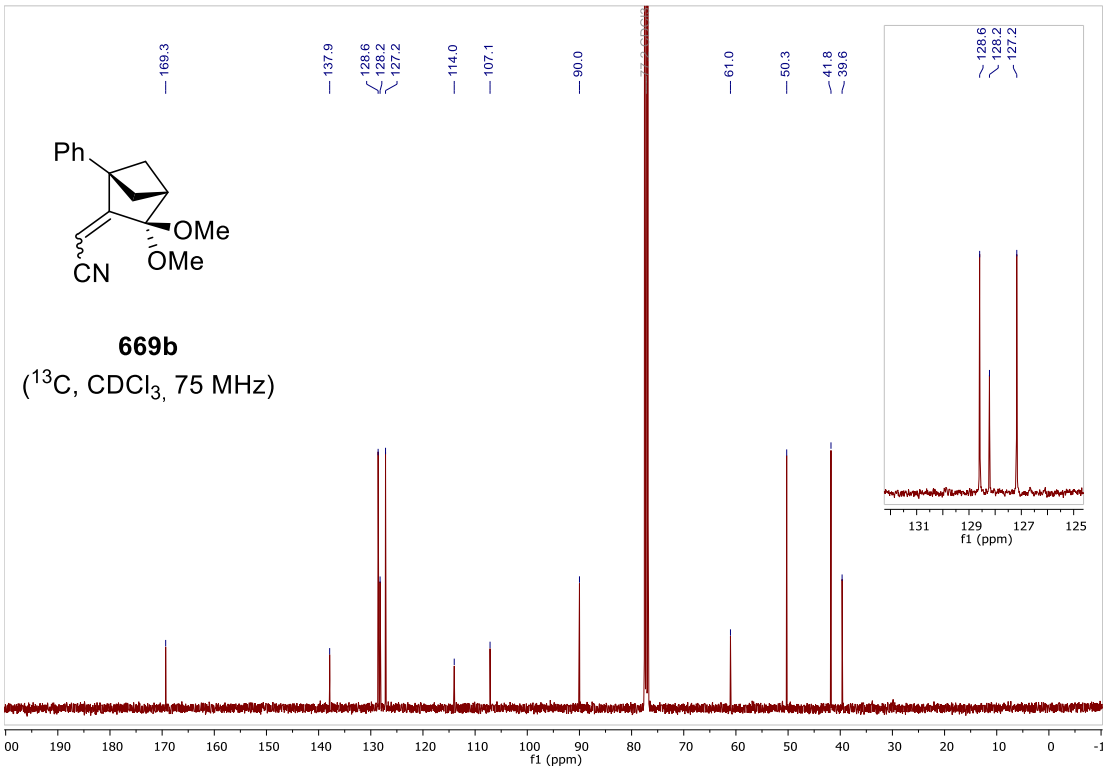

2.6.3.9 - ^{1}H NMR and ^{13}C NMR of nitrile 671

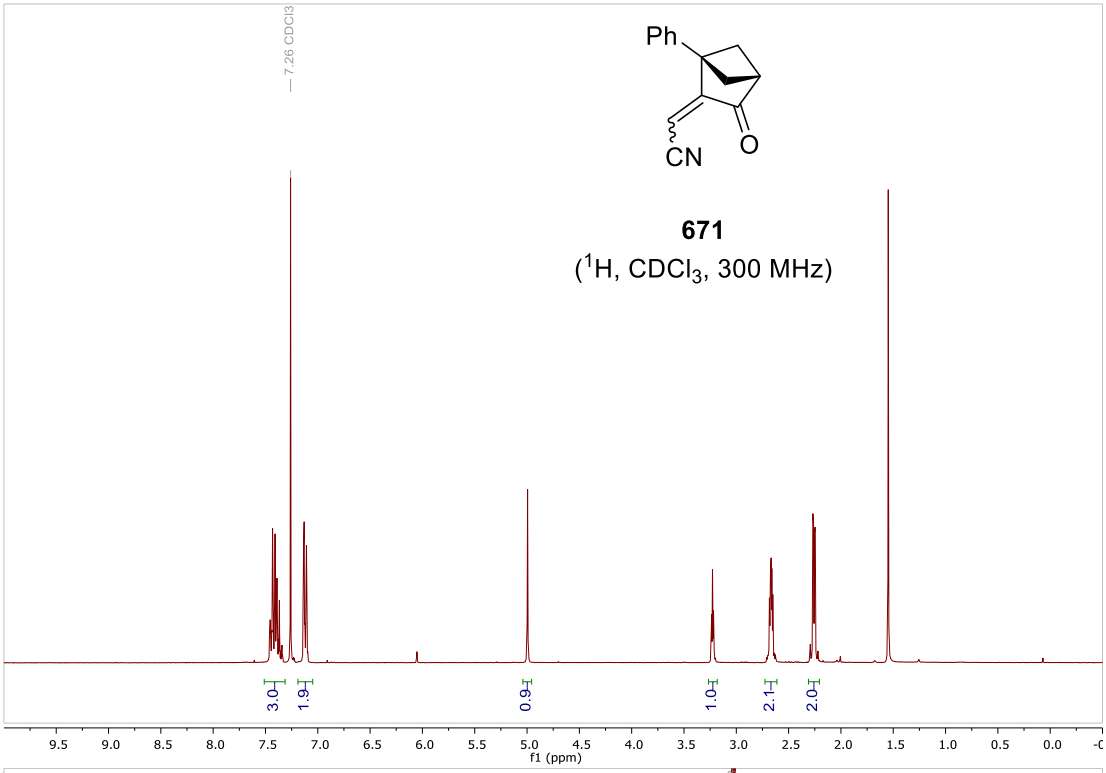

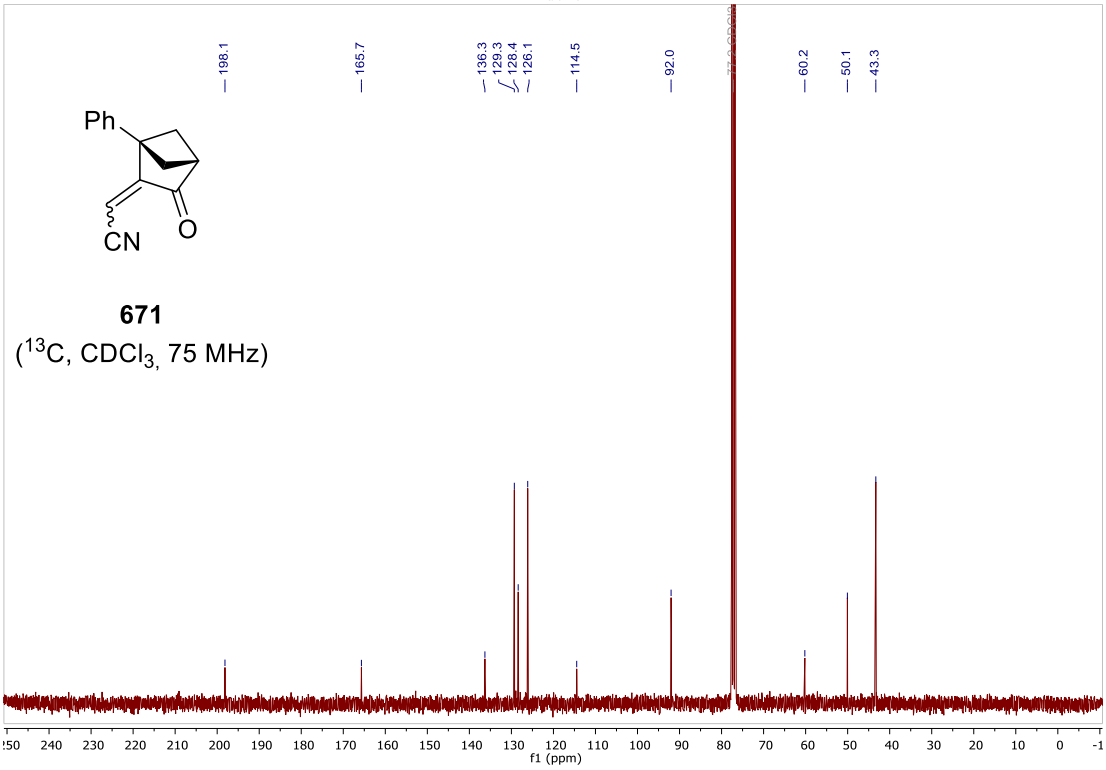

2.6.3.10 - ^{1}H NMR and ^{13}C NMR of pyridazine 672

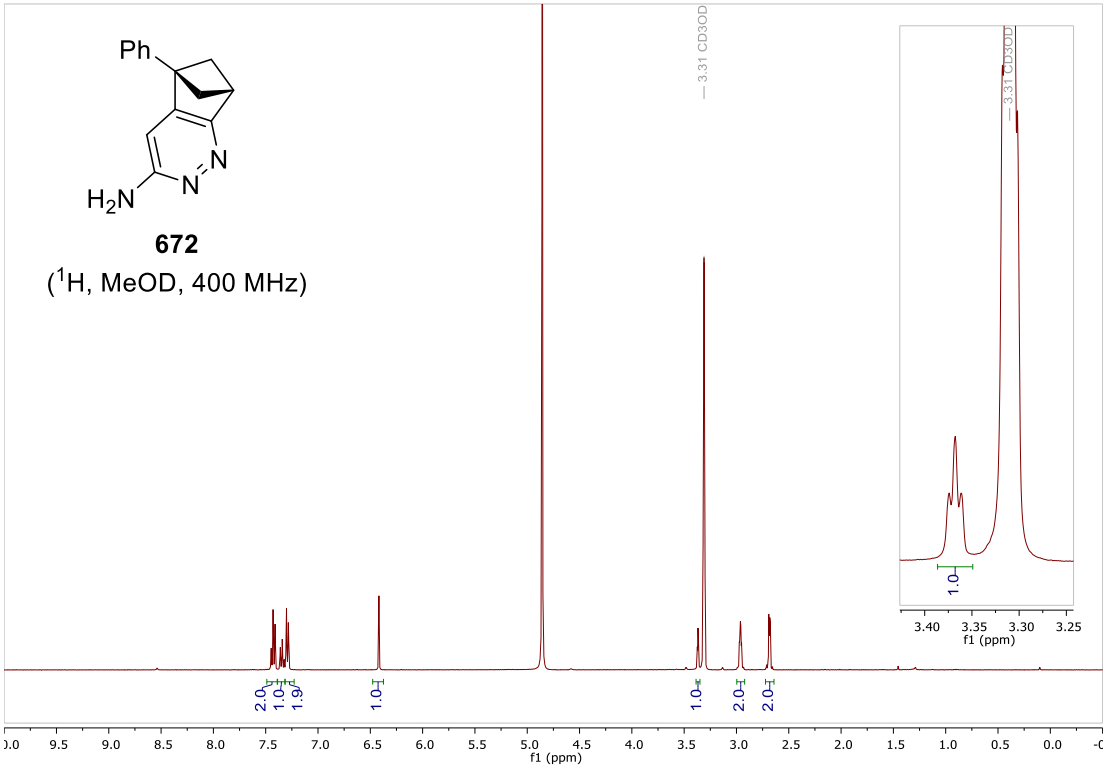

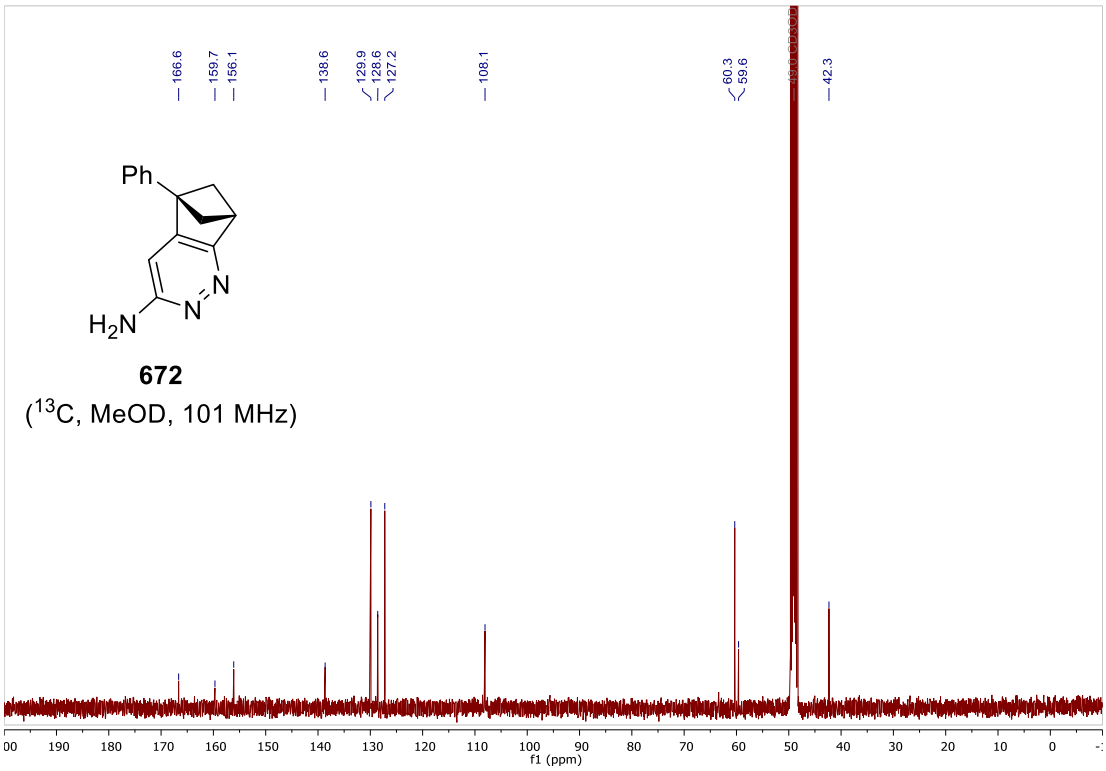

2.6.3.11 - ^{1}H NMR and ^{13}C NMR of pyridazine 670

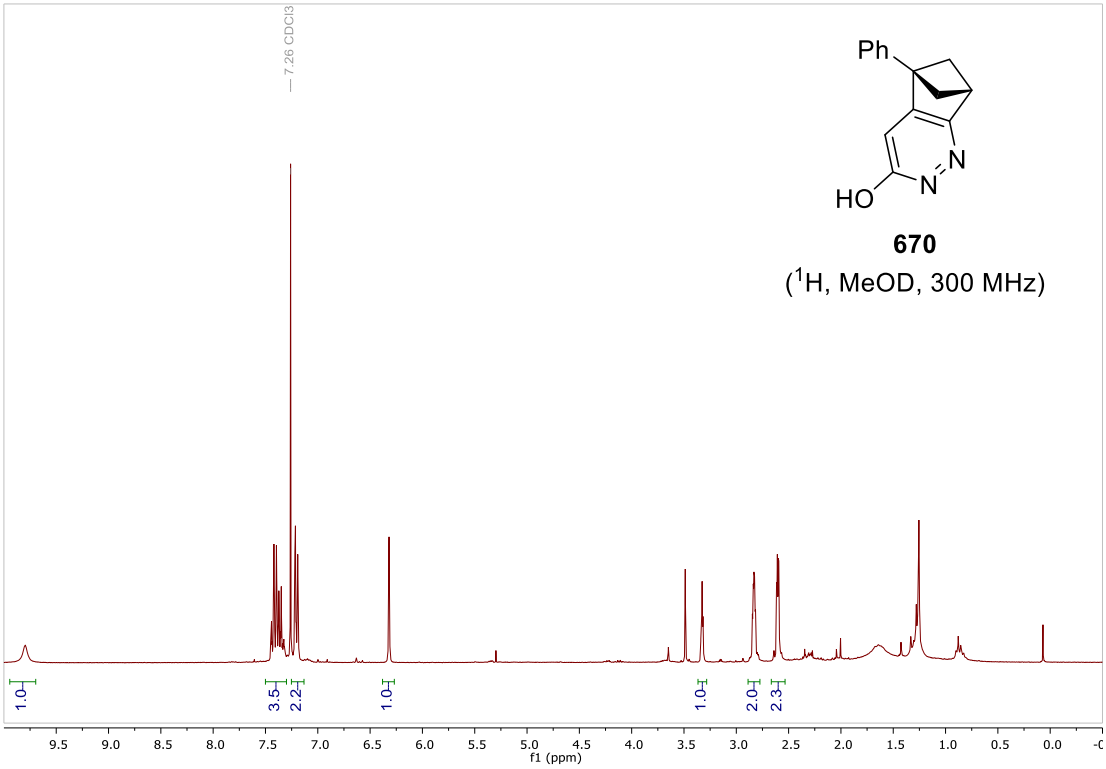

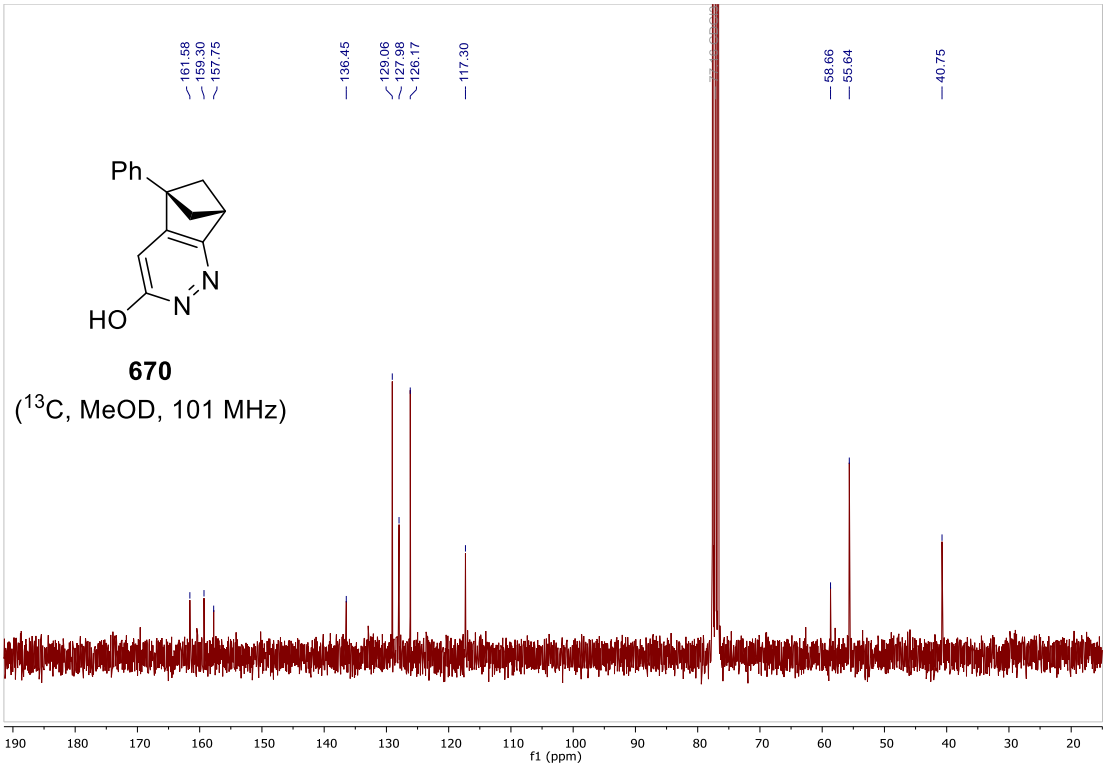

2.6.3.12 - ^{1}H NMR of the aliphatic nitrile 679

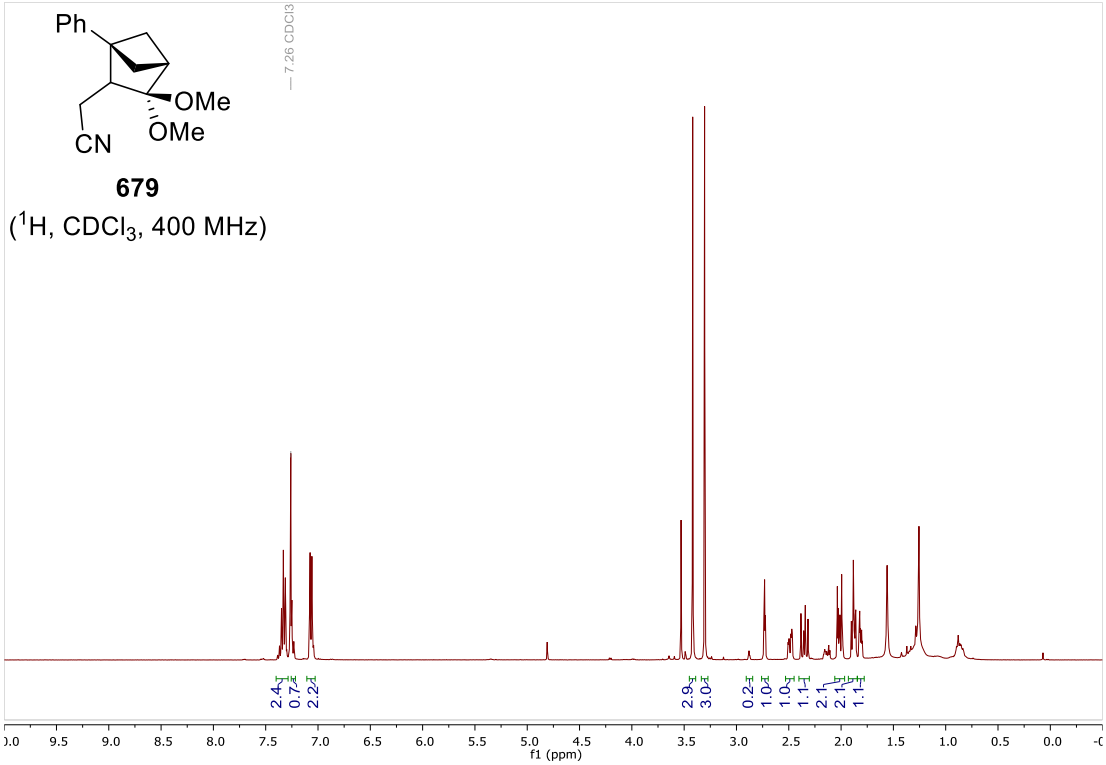

2.6.3.13 - ^{1}H NMR the acid 689

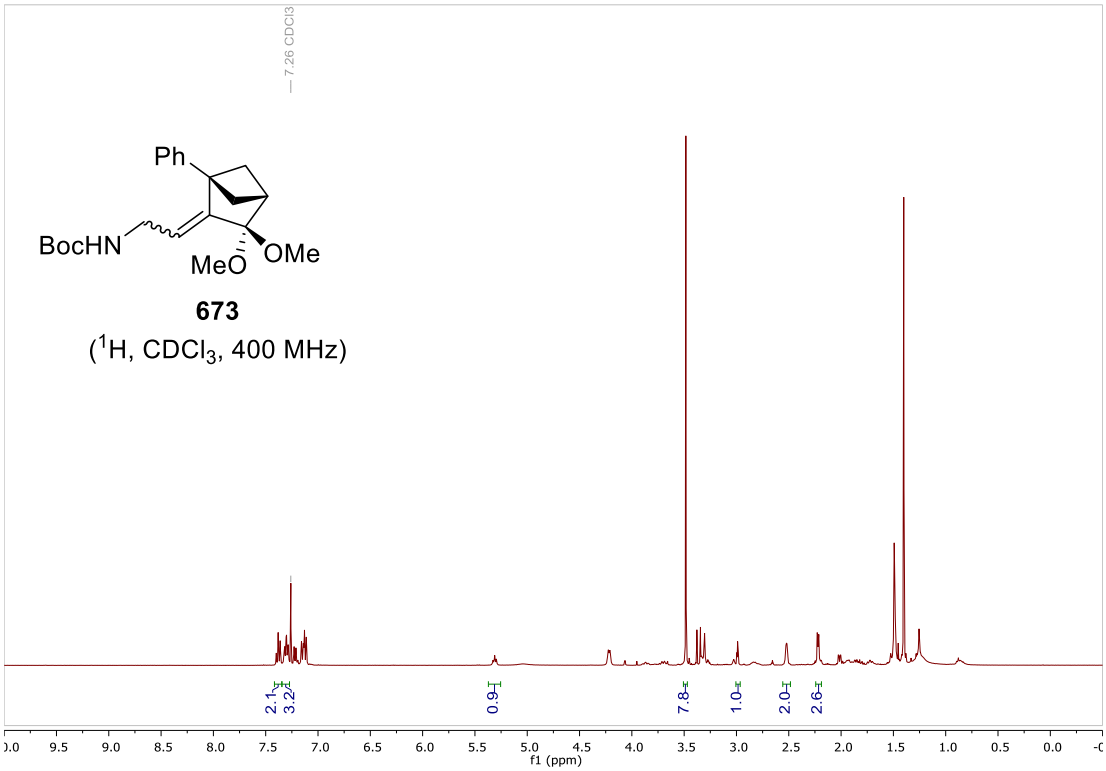

2.6.3.14 - ^{1}H NMR the acid 689